4-2-2024

Fiber distribution and orientation characterization in UHPFRC elements using a magnetic non-destructive testing method

TU Delft Structural Engineering Master Thesis

D.P. Kooreman
4690338

Fiber distribution and orientation characterization in UHPFRC elements using a magnetic non-destructive testing method

by

D.P. Kooreman

In partial fulfilment of the requirements for the degree of

Master of Science
In Civil Engineering

At the Delft University of Technology,
To be defended publicly on Monday February 5th, 2024 at 15:00

Student number:	4690338	
Thesis committee:	dr. M. Luković,	TU Delft, chair
	dr. S.C. Barbosa Nunes,	TU Delft
	prof. dr. ir. E. Schlangen,	TU Delft
	ir. Leon Klerks,	Movares
	Yitao Huang,	TU Delft

An electronic version of this thesis is available at http://repository.tudelft.nl/.

Abstract

Ultra-High Performance Fiber Reinforced Concrete (UHPFRC) is a promising material for different applications such as bridge deck strengthening due to its improved strength and durability properties. Especially the tensile strength and ductility is heavily dependent on the distribution and orientation of the steel fibers within the element. This fiber behaviour can be unpredictable, causing a large scatter in material properties. This scatter is inconvenient for predicting the material properties. The novelty of the material is the main reason that UHPFRC is not included in the Eurocode. Certain countries like Switzerland and France have developed their own UHPFRC norms.

In order to increase the knowledge and understanding of the fiber distribution and orientation, a non-destructive testing method has been developed. Two types of magnetic probes have been developed: the C-shaped ferrite probe and the single ferrite probe. These probes are based on other probes developed at the University of Milan and Porto. The C-shaped ferrite probe is most suitable for measuring the total fiber content and fiber orientation. The single ferrite probe is able to take fiber content measurements closer to the edge making it more efficient for fiber distribution measurements. This can result in a reliable prediction of the peak-tensile strength. The addition of UHPFRC specific design rules and this non-destructive testing method will make UHPFRC and its applications more attractive.

In this research, 27 different UHPFRC plates were cast with the same dimensions of 10x200x200 mm^3. These plates were cast horizontally or vertically with either 1%, 2%, 3% or 4% fiber content. Seven plates were vibrated after casting in order to analyse the influence of vibration. Each fiber content resulted in a relatively homogeneous fiber distribution and random fiber orientation. Horizontal casting of UHPFRC plates usually result in a more homogeneous fiber distribution and more random fiber orientation compared to vertically cast plates. The best distribution and orientation was reached when the elements were not vibrated at all. Vibration can result in severe fiber segregation along the element height and vertical orientation of the fibers. These conclusions hold for longer UHPFRC elements where the element height and the element thickness remains constant.

One of the main pitfalls in this research is the small thickness of the plates. The length of the fibers exceeds the plate thickness, which makes casting very difficult. During casting, fibers will get stuck at the top of the mould, which also influences the results. Moreover, it is important to continuously keep mixing the UHPFRC mixture in order to equally divide the fibers over all plates and to use a mixture that is castable yet not too flowable. High workability mixtures are more prone to fiber segregation.

This page includes the Dutch version of the Abstract

Samenvatting

Ultrahogesterktebeton (UHSB) is een veelbelovend materiaal, geschikt voor vele toepassingen zoals het versterken van een bestaand brugdek, vanwege de hoge materiaalsterkte en duurzaamheid waardoor het materiaal onderhoudsvrij is voor minstens 100 jaar. Vooral de treksterkte en buigzaamheid van het materiaal is sterk afhankelijk van de vezelverdeling en vezelrichting. Het gedrag van de vezels is moeilijk te voorspellen waardoor de materiaalsterkte met grote mate varieert. De onbekendheid met het materiaal is de belangrijkste reden dat de Eurocode nog geen specifieke rekenregels voor UHSB bevat. Sommige landen zoals Zwitserland en Frankrijk hebben hun eigen UHSB normen ontwikkeld.

Om de kennis en het begrip op het gebied van de staalvezels te vergroten is er een niet-destructieve methode ontwikkeld voor UHSB. Twee verschillende sondes zijn ontwikkeld: de C-vormige sonde en een sonde met een enkele kern. Deze sondes zijn gebaseerd op eerder ontwikkelde sondes aan de Universiteit van Milaan en Porto. De C-vormige sonde is geschikt om het vezelgehalte en de vezelrichting te meten. De sonde met een enkele kern is in staat om de vezelverdeling te meten omdat deze dichterbij de rand van het element kan meten. Met deze gegevens kan de maximale treksterkte geschat worden. De toevoeging van UHSB specifieke ontwerpregels en deze niet-destructieve methode zal UHSB en haar toepassingen aantrekkelijker maken.

Voor dit onderzoek zijn er 27 verschillende UHSB plaatjes gestort van 10x200x200 mm^3. Deze plaatjes hebben een vezelgehalte van 1%, 2%, 3% of 4% en zijn óf horizontaal óf verticaal gestort. Zeven van deze plaatjes zijn getrild door middel van een triltafel om de effecten van trillingen op de staalvezels te onderzoeken. Het vezelgehalte leek geen tot weinig effect te hebben op het gedrag van de vezels in de plaatjes. De vezelverdeling en vezelrichting in horizontaal gestorte plaatjes was over het algemeen efficiënter dan in de verticaal gestorte plaatjes. Het trillen van de plaatjes zorgt voor sterke scheiding van de vezelverdeling en het verticaal oriënteren van de vezels. Daarom kunnen de plaatjes beter zonder trillen gestort worden. Deze conclusies gelden ook voor langere elementen met dezelfde hoogte en dikte van de plaatjes.

Eén van de grote valkuilen van dit onderzoek is de smalle dikte van de plaatjes ten opzichte van de stalen vezels. Dit maakt het storten erg lastig doordat vezels vast blijven zitten in de mal. Dit is terug te zien in de resultaten. Daarnaast is het belangrijk om de UHSB mix continu te mixen zodat de vezels gelijk worden verdeeld onder de verschillende plaatjes. Om scheiding van de vezelverdeling te verminderen, moet de USHB mix niet te vloeibaar zijn.

Table of contents

Preface

This thesis discusses the characterization of steel fiber behaviour in Ultra High Performance Fiber Reinforced Concrete (UHPFRC). An experimental research is included concerning thin UHPFRC plates, in which a magnetic non-destructive testing method was used.

My name is Duco Kooreman, I am the main researcher and author of this report. I have finished my Bachelor of Science in Civil Engineering and continued my path with a Master in Structural Engineering. Within my studies, I specialised mostly in concrete. For this project, I worked together closely with Movares, an engineering consultancy based in Utrecht, and the TU Delft.

The main target audience for this Thesis is concrete specialists, UHPFRC specialists in particular, and students and others that are interested in the fiber behaviour in UHPFRC elements or the magnetic non-destructive testing method.

In the process of the making of this Thesis, I have received supervision and help from multiple parties. In particular, I want to thank Movares and my personal supervisor, Leon Klerks, in particular who has supported me throughout the entire process, helped me avoid certain problems and obstacles and critically analyse my choices, planning and result. Moreover, I want to thank Yitao Huang, a PhD student at the TU Delft, who is also specialised in UHPFRC. He helped me during multiple steps of my experimental research and has given me input for my subject specification and my results. I also want to thank Kees van Beek for providing me with the necessary testing method equipment and enabling me to perform my experiments. Finally, I want to thank Mladena Luković and Sandra Nunes, my personal supervisors from the TU Delft. They have helped me to specify my Thesis subject, guided me throughout the process and critically analysed my results in order to improve my final product.

Figure 1: Steel fibers in UHPFRC plate specimen, picture taken by D. Kooreman

1. Introduction

1.1 Problem description

Ultra-High Performance Fiber Reinforced Concrete (UHPFRC) is a promising material with improved material properties compared to other concrete types. The material cannot be categorised as a concrete material or as a steel material (Brühwiler, 2017). The behaviour of the material does not follow general concrete or steel standards so these are not applicable for the design with this material. This self-compacting material is known for its high compressive strength and strong durability.

This material is very suitable for the strengthening of existing structures, bridge decks in particular. This is especially interesting for bridges in the Netherlands since a large number of bridges need heavy maintenance or replacement. Civil structures built after World War 2 have almost reached the end of their design life, which is usually around 50 or 100 years for civil structures. Besides this, the traffic load has increased significantly compared to the 60's or 70's. One of the goals of the TU Delft is to increase the circularity of bridge designs (Cao, 2021). Adding a thin layer of UHPFRC on top of a bridge deck can increase durability and strength enough to extend the service life of the structure.

However, the strength and ductility of UHPFRC is dependent on the fiber distribution and orientation within the element. There are multiple factors that influence the fiber distribution and orientation. These varying factors cause a large scatter in UHPFRC strength properties (Huang, Schlangen, & Lukovic, 2023).

1.2 State-of-the-art

Fiber reinforced concrete exists for quite a significant material but UHPFRC itself is a novel material. The knowledge and experience on UHPFRC differs a lot over the world. Countries like Switzerland, France, the United States of America and Japan have built a significant amount of UHPFRC structures where other countries, such as the Netherlands, stay behind. Figure 2 shows all of the current UHPFRC applications in Switzerland. In the last 5 years, the country has built over 44 UHPFRC structures per year on average which is over 60% of the total amount of UHPFRC structure in Switzerland (EPFL, 2023).

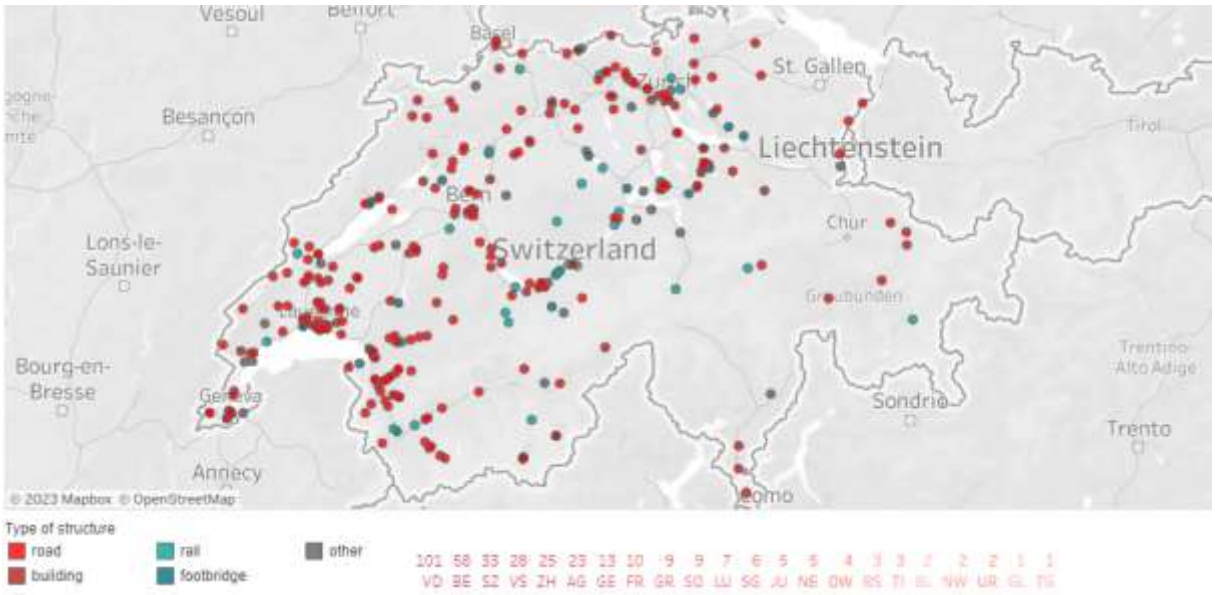

Figure 2: map of UHPFRC applications in Switzerland, source: (EPFL, 2023)

In order to characterize and research the effect of fiber distribution and fiber orientation within UHPFRC elements, a magnetic NDT method has been developed. This method uses a magnetic ferrite probe that can measure the magnetic inductance of the steel fibers. The TU Delft has recently developed two versions of this probe but these have not been used or tested.

1.3 Research goal and scope

The main objective of this MSc Thesis is to characterize the fiber distribution and fiber orientation and find a procedure to improve the reliability of UHPFRC strength properties, using the magnetic ferrite probes developed by the TU Delft. This can be a first step in making UHPFRC a more used building material in countries like the Netherlands.

After an extensive literature research, a number of small UHPFRC plates will be cast in order to calibrate the magnetic probes and research certain influences on the fiber distribution and fiber orientation. These influences will consist of fiber content, casting orientation and vibration time. Measurements will also be performed on larger UHPFRC shear panels and compared to the results of the small plates. In order to validate these results, the effects of edge distance, surface roughness and painted surfaces must be defined. Finally, the magnetic probe measurements will be evaluated by comparing the results to CT scans of the plates.

1.4 Research questions

This MSc Thesis will answer the following research question and sub-questions:

How can the fiber distribution and orientation in UHPFRC elements be characterized and what effects will this have on the design tensile strength and ductility?

- How do the fiber distribution and orientation affect the tensile strength and ductility in UHPFRC elements?
- How is fiber distribution and orientation taken into account in European standards, particularly the French and Swiss standards?
- Does the magnetic NDT method give a reliable prediction of the fiber distribution and fiber orientation and what are the limiting effects of edge distance and surface roughness?
- How do the fiber content, casting orientation and vibration time influence the fiber distribution and fiber orientation?
- What are the differences between measuring on bigger UHPFRC shear panels and smaller plates and how do the results compare?
- What procedure results in the most reliable predicted tensile strength and what recommendations can be given to change current UHPFRC design?

1.5 Methodology

The first step of this thesis is learning about UHPFRC and its properties, the possible applications, fiber distribution and orientation, influences on fiber behaviour and applicability of the magnetic NDT method. This will all be researched and incorporated in an extensive literature report.

Next, in order to be able to use the probe and prove the effectiveness of the probe, the probe has to be calibrated. This calibration is done using multiple UHPFRC plates with varying fiber contents. After calibration is done, the same measurements used for calibration can be used to characterize the fiber distribution and fiber orientation within these plates.

By varying the fiber content, casting orientation and vibration time, the effects of these factors on the fiber distribution and fiber orientation can be determined. These influences result in an optimal procedure that can be used to acquire a UHPFRC element with an efficient and reliable fiber distribution and fiber orientation.

This fiber distribution and fiber orientation can be used to predict the tensile strength of the UHPFRC element which can be compared to values found in destructive testing methods. Based on this comparison, recommendations can be given.

1.6 Report structure

The first two chapters of this Thesis are based on a literature study. Chapter 2 discusses UHPFRC on a material level, properties and applications. The third chapter characterizes the fiber distribution, fiber orientation and the critical factors influencing this distribution and orientation. The chapter also includes testing methods, like the magnetic NDT method used in this MSc Thesis. Moreover, the mechanical properties used in current design calculations are discussed in Chapter 3.

Chapters 4, 5 and 6 are based on the experimental study of this Thesis. The fourth chapter describes the experimental program that is performed for this Thesis. Chapter 5 contains the results which are discussed in Chapter 6: Discussion.

Finally, the report ends with Conclusions, Recommendations and Future research.

2. UHPFRC

This chapter will introduce the material Ultra-High Performance Fiber Reinforced Concrete (UHPFRC) and comment on its interesting properties and behaviour. The comparison is made between UHPFRC and Conventional Concrete (CC). Advantages and disadvantages of UHPFRC are mentioned based on structural, durability, sustainability and financial aspects. This chapter also includes an overview of some UHPFRC applications.

2.1 Introduction UHPFRC

Concrete types are usually classified by their compressive strength and so is UHPFRC. This classification does not take the fiber content into account since the fibers have little influence on the compressive strength. For this reason, the material can be denoted as Ultra-High Performance Concrete (UHPC). CC is characterized by a cylinder compressive strength lower than 40 MPa. The compressive strength of High-Strength Concrete (HSC) is between 40 and 150 MPa. Finally, UHPC is characterized by a compressive strength higher than 150 MPa where some mixtures can even attain a compressive strength over 300 MPa. This is also visually presented in Figure 3, where CC is denoted as NSC (Normal Strength Concrete). The figure also shows that an important reason for this increased compressive strength, is the low water-to-binder ratio (Schlangen, 2021). This will be discussed in detail more in this chapter.

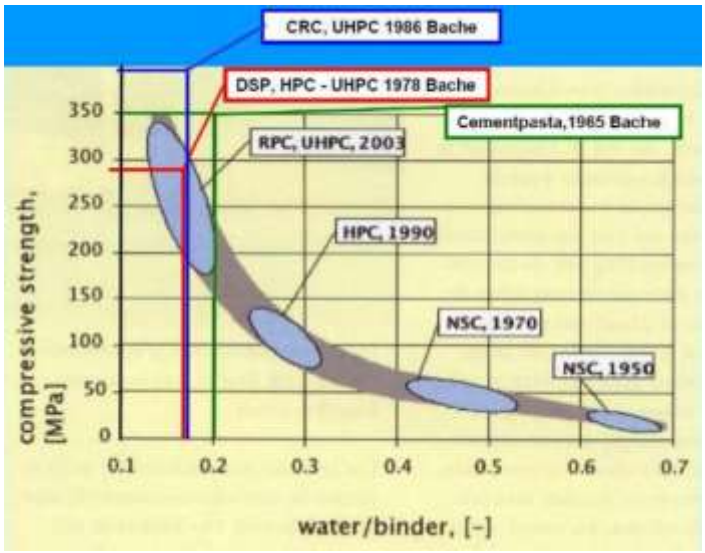

Figure 3: classification of UHPFRC based on compressive strength, source: (Schlangen, 2021)

Figure 4 shows the different composition of UHPFRC compared to CC (based on volume percentage). This shows that UHPFRC uses materials like silica fume, limestone, superplasticizer and fibers. Concrete contains a lot of coarse aggregate, where UHPFRC has no coarse aggregate at all. The fraction of cement and fine aggregates is a lot bigger for UHPFRC. These aspects are also clear when visually inspecting the material in Figure 4. This figure also shows that UHPFRC has a larger packing density and is a more homogeneous material which is discussed more in the rest of this chapter.

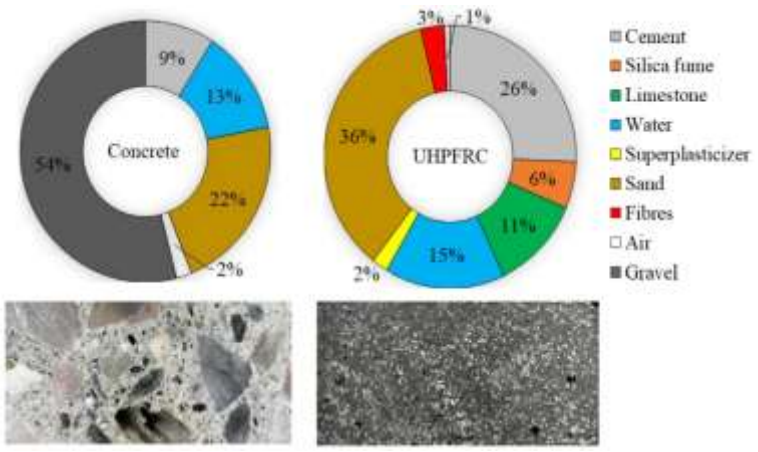

Figure 4: mix proportions and appearance of CC and UHPFRC, source: (Naaman & Wille, 2012)

2.2 Concept behind UHPFRC

2.2.1 Improvement of packing density

In CC, cement is usually the smallest particles with gaps in between these cement particles. However, UHPFRC also contains limestone/quartz/blast furnace slag and silica fume which particles are all smaller than cement particles. These are able to fill the gaps in between the cement particles increasing the compactness of the concrete (Figure 5). Because of this compactness there is more contact area between the aggregate particles. In concrete, stress is transferred via these contact areas. The more contact area, the better stresses can be transferred. It should be noted that this principle only works for compressive stresses and not for tensile stresses. The mechanical principle is shown visually in Figure 6 where the stress transfer paths are more direct. The size propertions of the aggregates result in an improved packing density. Because of this high packing density, the material has a significant increase in compressive strength (Reitsema, 2012).

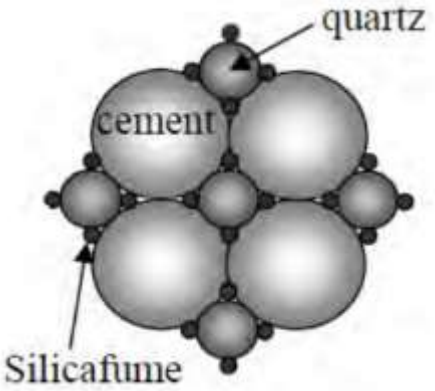

Figure 5: packing and size ratio of cement, quartz and silica fume, source: (Reitsema, 2012)

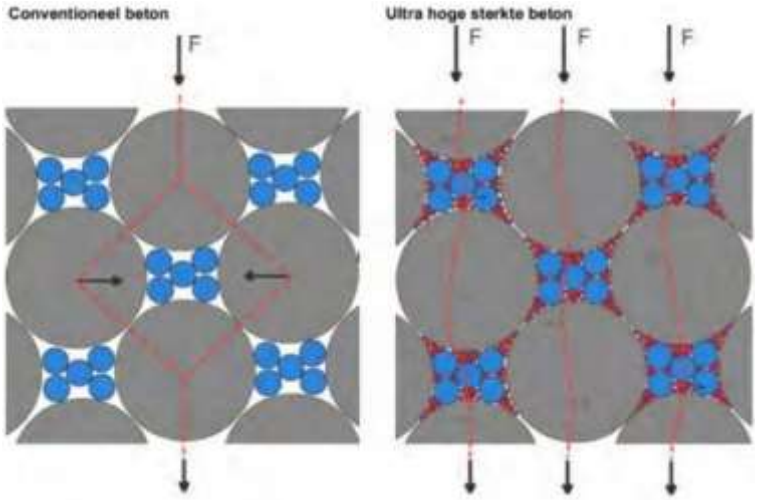

Figure 6: mechanical principal of high compressive strength due to compactness, source: (Reitsema, 2012)

The microstructure of concrete can be improved in lots of ways. For instance, optimizing the particle size curve so there is a more efficient packing of the material and adding more fine powders that can fill the small gaps in between the aggregates (Schlangen, 2021). This optimization can be achieved using packing models by dividing the aggregates into different classes based on their size. These models use a couple of principles: the particle size curve should have as little of a spread as possible around the mean aggregate diameter per class, the ratio between the mean aggregate diameter in each class should be big (preferable bigger than 13:1) and the fine powders should clump as little as possible (Vergoossen, 1999).

2.2.2 Increase in homogeneity

The homogeneity of UHPFRC is better compared to CC due to multiple reasons. For instance, the decrease of the maximum aggregate size results in less variation of the aggregates which means the concrete mix is more homogeneous (Schlangen, 2021). Furthermore, shear and tensile stresses are created at the Interfacial Transition Zone (ITZ) between aggregate and matrix. These stresses can result in crack initiation. These stresses increase along with the aggregate size so by decreasing the maximum aggregate size, there are lower shear and tensile stresses and less risk of cracking. This will also result in less and smaller cracks in the cement matrix. These microcracks can also close again due to the reactive behaviour of the UHPFRC materials (Vergoossen, 1999).

The improvement of the cement matrix is another reason for the increased homogeneity of UHPFRC. An important factor here is the Young's Modulus of the cement paste. This value is equal to or even larger than the Young's Modulus of the aggregates used for UHPFRC. The ratio between the Young's Modulus of aggregate and cement paste is usually around 3/1 for CC but 1/1 for UHPFRC. This difference in Young's Modulus results in a stiff granular skeleton of the aggregates which obstructs the shrinkage of the cement paste during hardening. This leads to more gaps within the concrete which is avoided in UHPFRC by the similar Young's Modulus (Vergoossen, 1999). This large stiff granular skeleton is also caused by the large volume fraction of aggregates in CC. The aggregates in UHPFRC (sand, blast furnace slag and silica fume) on the other hand, will be incorporated in a continuous cement matrix and will not act as a stiff granular skeleton. This will also decrease the amount of shrinkage (Vergoossen, 1999).

The difference in packing density is shown in Figure 7. This is a comparison of the microstructure between CC (left), HSC (middle) and UHPC (right) without steel fibers. In this figure, CC is denoted as OC (Ordinary Concrete). The UHPC specimen has a homogeneous structure while there is a clear difference between aggregate and matrix in the CC specimen. Especially the coarse aggregate is clearly visible while this is missing in the UHPC mix.

Figure 7: comparison (micro)structure of CC, HSC and UHPC, source: (Reitsema, 2012)

2.2.3 Addition of fibers

The addition of fibers is another principal aspect of UHPFRC that gives the material its incredible properties. However, the addition of fibers also has its disadvantages. For example, the steel fibers result in a decrease in packing density. A rigid fiber can get in between grains so the grains are not directly interlocking creating bigger gaps between the grains (See Figure 8). These gaps lead to a worse packing density. The relationship between packing density and fiber content decreases at a more or less constant rate, regardless of the fiber type and aggregate size. (Chu, Jiang, & Kwan, 2019).

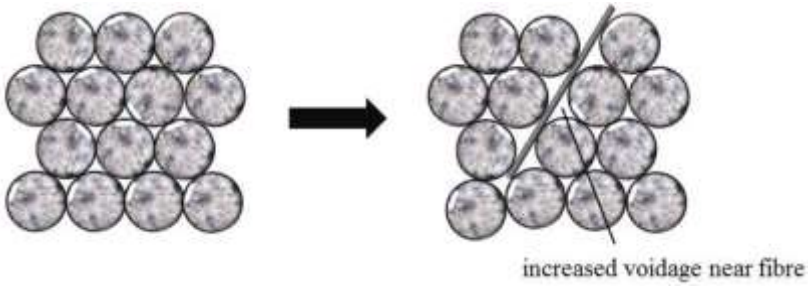

Figure 8: addition of fibers can decrease packing density, source: (Chu, Jiang, & Kwan, 2019)

However, the advantages of fibers outweigh the disadvantages. Where UHPC without fibers has a very brittle behaviour, UHPFRC can deform relatively much before failure and is therefore a far more ductile material. Usually, ductile behaviour is preferred in structural elements over brittle behaviour. Ductile behaviour can experience more deformation without failing. This is also shown in Figure 9 (Memon, Jhatial, Sohu, Lakhiar, & Hussain, 2018).

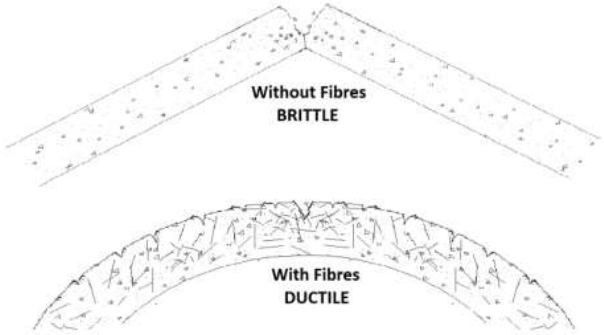

Figure 9: ductile behaviour of UHPFRC due to fibers, source: (Memon, Jhatial, Sohu, Lakhiar, & Hussain, 2018)

The flexural and the tensile strength of UHPC are also improved by the addition of steel fibers. The presence of steel fibers within the concrete element results in a different cracking pattern. In CC, there is usually one big crack that keeps propagating. However, fiber reinforced concrete can result in a finer cracking pattern, with more but smaller cracks. This property depends on the fiber content. The flexural strength can be increased with about 35 to 92 percent (Amoorezaei & Dabbagh, 2022). Flexural tests performed by the TU Delft have also shown the effect of fibers added to a cement paste. As can be seen in Figure 10, a beam tested without fibers had a flexural failure load of 91 kN while the same beam with 0.8% fibers had a flexural failure load of 340 kN and 531 kN for a beam with 1.6% fibers. The figure also shows the cracks present in the beam during failure. The beam without fibers show a small amount of cracks where one specific flexural crack is clearly the cause of the failure. The presence of fibers result in more cracks initiating but these cracks are much smaller causing better ductility and a higher failure load (Reitsema, 2012).

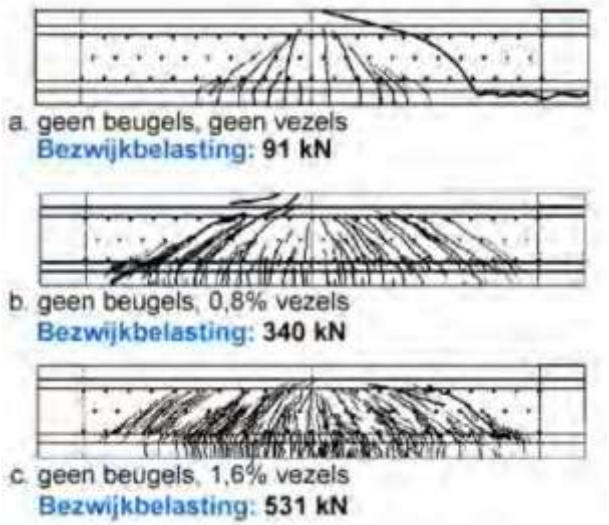

Figure 10: higher failure load due to fiber addition, source: Reitsema, 2012)

The difference between UHPFRC and Normal Strength Concrete (NSC) for the compressive and tensile strength is shown in Figure 11. In this figure, the compressive and tensile constitutive relationship is shown where UHPFRC clearly has a more ductile behaviour. Besides this, the peak strength is also higher for UHPFRC. The addition of fibers is not the only cause for this increase but also other aspects like the increase in packing density and homogeneity (Wu, Oehlers, Rebentrost, & Whittaker, 2009).

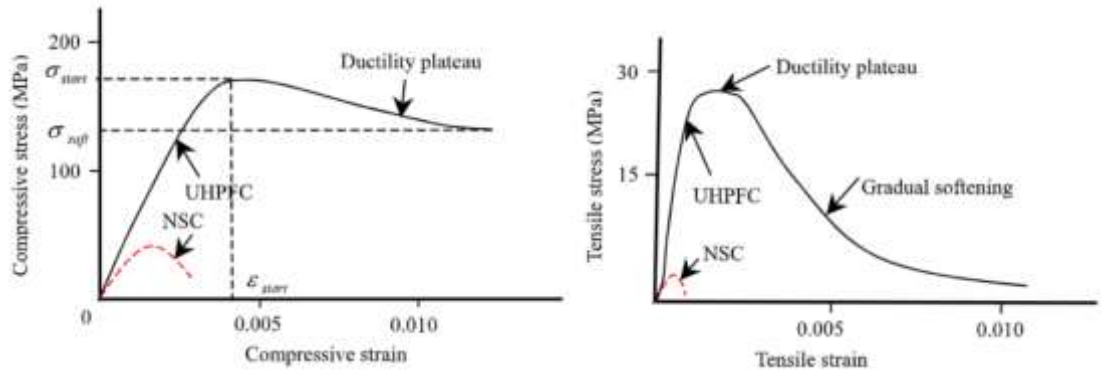

Figure 11: comparison compressive behaviour CC and UHPFRC, source: (Wu, Oehlers, Rebentrost, & Whittaker, 2009)

In an ideal UHPFRC mixture, there are multiple fiber sizes. Fibers with a small length and diameter are more effective for the initial microcracks. Once the cracks are initiated, the small fibers can take over the tensile stresses delaying the further propagation of the cracks. This increases the pre-peak strength of the material. Once a macrocrack is formed, the bigger fibers are more effective. This is shown in Figure 12. These large fibers results in an increase in fracture energy of the material (Schlangen, 2021).

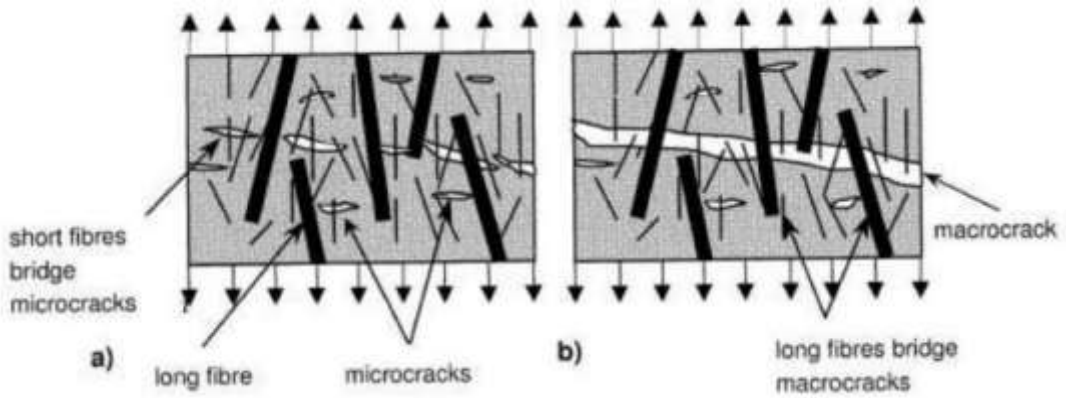

Figure 12: contribution short and long fibers to cracking resistance, source: (Schlangen, 2021)

Moreover, traditional CC elements usually have reinforcement in the form of a steel rebar in order to improve tensile capacity. This reinforcement is not always necessary when using UHPFRC since the fibers also provide tensile strength. The solution with fibers is generally more economical and less prone to corrosion compared to steel reinforcement (Schlangen, 2021).

Another advantage of adding steel fibers to the mixture is the reduction of time-dependent effects like creep and shrinkage. Experimental results show that the presence of fibers can greatly reduce the time-dependent effects. For instance, drying shrinkage can be decreased by more than 100% and the tensile creep can be decreased with 73% after 7 days with ordinary curing. These time-dependent effects for UHPFRC are far more complex than for CC so more research should be conducted but the experimental results show good promise (Garas, Kahn, & Kurtis, 2009). Experimental results also show a decrease of creep in long-term periods. After 360 days, the creep of Fiber Reinforced Concrete (FRC) was reduced by 70% compared to a CC element (Barbos, 2015).

Furthermore, the strength of the cement paste can be higher than the average aggregate strength. This difference in strength has an influence on the cracking of the material. Figure 13a shows the common way of cracking for CC. The cracks will form around the aggregates and through the cement matrix. However, for UHPC in Figure 13b, the cement strength is higher than the strength of the aggregates. This results in a crack through the aggregates instead of the cement matrix. The consequence of this is that cracks in UHPC are less coarse compared to CC. Because of these smooth crack surfaces, the cracks are able to take less stresses. However for UHPFRC, the addition of fibers increase the capacity for transferring stresses after cracking again. That is why UHPFRC is still able to withhold stresses after cracking of the concrete. Moreover, the presence of the fibers will also hinder the formation of a crack. A different crack will form on both sides of the fiber which are usually not alligned perfectly and therefore do not form a continuous crack along the full thickness of the element. This delays the failure of the element and therefore increases the ductility of UHPFRC (Reitsema, 2012).

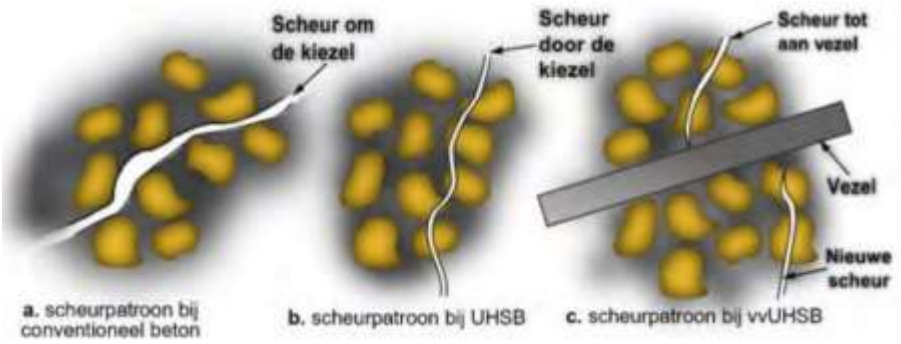

Figure 13: comparison cracking behaviour of CC, UHPC and UHPFRC, source: (Reitsema, 2012)

These advantages of fibers are very promising but only apply if there are enough fibers present in the right direction. That is why it is very important that the fibers are present everywhere throughout an element, thus have a homogeneous distribution (Schlangen, 2021). This also shows the importance of an extensive research on the fiber distribution in UHPFRC elements.

2.3 Mechanical properties

Due to the aspects discussed in Chapter 2.2, UHPFRC reaches significantly better material properties compared to CC. Table 1 gives an overview of some important properties for CC (denoted as NC), High Performance Concrete (HPC) and Ultra-High Performance dura Concrete (UHPdC), which is a commercial brand of UHPFRC. As can be seen from the table, UHPFRC has superior mechanical properties in every single aspect (Tayeh, Aadi, Hilal, & Bakar, 2019).

Table 1: overview of important properties of CC, HPC and UHPFRC, source: (Tayeh, Aadi, Hilal, & Bakar, 2019)

Characteristics	Unit	NC	HPC	UHPdC
Specific Density	kg/m3	2300	2400	2350 – 2450
Cylinder Compressive Strength, fcy	MPa	20 – 50	50 – 100	120 – 160
Cube Compressive Strength, fcc	MPa	20 – 50	50 – 100	130 – 170
Creep Coefficient at 28 days		2 – 5	1 – 2	0.2 – 0.5
Post Cured Shrinkage		1000 – 2000	500 – 1000	< 100
Modulus of Elasticity, Eo	GPa	20 – 35	35 – 40	40 – 50
Poisson's Ratio,		0.2	0.2	0.18 – 0.2
Splitting Cyl. Cracking Strength, ft	MPa	2 – 4	4 – 6	5 – 10
Splitting Cyl. Ultimate Strength, fsp	MPa	2 – 4	4 – 6	10 – 18
Flexural 1st Cracking Strength, fcr,4P	MPa	2.5 – 4	4 – 8	8 – 9.3
Modulus of Rupture, fcf,4P	MPa	2.5 – 4	4 – 8	18 – 35
Rapid Chloride Permeability	coulomb	2000 – 4000	500 – 1000	< 200
Chloride Diffusion Coefficient, Dc	mm2/s	4 – 8x10-6	1 – 4x10-6	0.05 – 0.1x10-6
Carbonation Depth	mm	5 – 15	1 – 2	< 0.1
Abrasion Resistance	mm	0.8 – 1.0	0.5 – 0.8	< 0.03
Water Absorption	%	> 3	1.5 – 3.0	< 0.2

Due to the improved material properties, UHPFRC structures can be designed to be very slender. On one hand, a small thickness can be preferred by architects because it is aesthetically pleasing. On the other hand, it will also decrease the self-weight of the structure. This allows a further decrease in the required material usage. This will be discussed in more detail later. Figure 14 shows the difference between an L-shaped wall made of CC and UHPFRC. Both have similar structural capacity, showing the increased strength of UHPFRC.

Figure 14: comparison L-shaped element CC and UHPFRC, source: (Yu, 2015)

However, the mechanical properties of UHPFRC van differ significantly. The scatter of three properties is shown in Table 2: compressive strength, Young's Modulus and tensile strength. These results were acquired using a UHPFRC mixture with 2% fiber content (Huang, Schlangen, & Lukovic, 2023). The coefficient of variation (CV) is also calculated which magnitude indicates the scatter in the corresponding material property. Clearly, the peak tensile strength has the biggest scatter.

Table 2: statistics of mechanical properties of UHPFRC, source: (Huang, Schlangen, & Lukovic, 2023)

UHPFRC	Cubical compressive strength (MPa)	E-Modulus (GPa)	Peak tensile strength (MPa)
μ	122.4	45.2	9.2
σ	5.1	1.1	2.1
CV	4.2	2.4	22.8

2.3.1 Compression

As discussed in Chapter 2.1, concrete is known for its excellent resistance against compressive loading. Concrete structures are designed and calculations are made based on the concrete compressive strength. These design calculations are usually based on the Eurocode, which includes concrete types with compressive strengths up until 90 MPa. This compressive strength can increase greatly when using UHPFRC. The material has a very dense microstructure making it very compact, resulting in compressive strengths of 150 or 300 MPa in some cases (Schlangen, 2021).

This concrete compressive strength is usually assessed using compressive cylinders or cubes which are smaller than the standard cylinders or cubes used for measuring the compressive strength of CC. This is because of the high difference in compressive strengths. Bigger cylinders would simply require too much load until failure of the specimen.

2.3.2 Tension

For UHPFRC behaviour, tensile performance is one of the most important properties and the structural design with the material requires a reliable indication of the tensile capacity. However, this tensile response is dependent on many parameters. For example: fiber type, fiber content, bond strength, fiber distribution, fiber orientation. In general, there are two different tensile responses possible for UHPFRC: strain-softening and strain-hardening. Figure 15 shows the behaviour of both possibilities under a tensile load. After the elastic domain of the material, the material strength still increases with an increasing strain for the strain-hardening behaviour. On the other hand, for strain-softening, the material strength deteriorates with increasing strain. Strain-hardening is the more preferable behaviour regarding the mechanical performance of the material (Guo, Wang, & Gu, 2022).

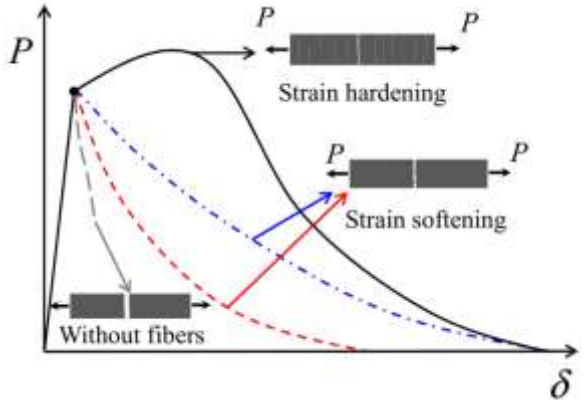

Figure 15: strain-hardening vs strain-softening, source: (Guo, Wang, & Gu, 2022)

The strain-hardening behaviour of UHPFRC can be distinguished in three different parts which can be seen in Figure 16. It should be noted that this graph is not to scale but merely serves the purpose of explaining the tensile behaviour. The first part is the elastic domain (Part I) where the material will have a linear strain in relationship to the stress with the Young's Modulus as the slope gradient. After this part, multiple non-visible micro-cracks will initiate. This part is called the strain-hardening domain (Part II). The Strain-softening domain is determined by the propagation of a single discrete crack. This crack is usually characterised when the crack width reaches half the fiber length. During this process, the stress inside the specimen is concentrated towards this one crack while the other micro-cracks are actually unloaded (Shen & Brühwiler, 2020).

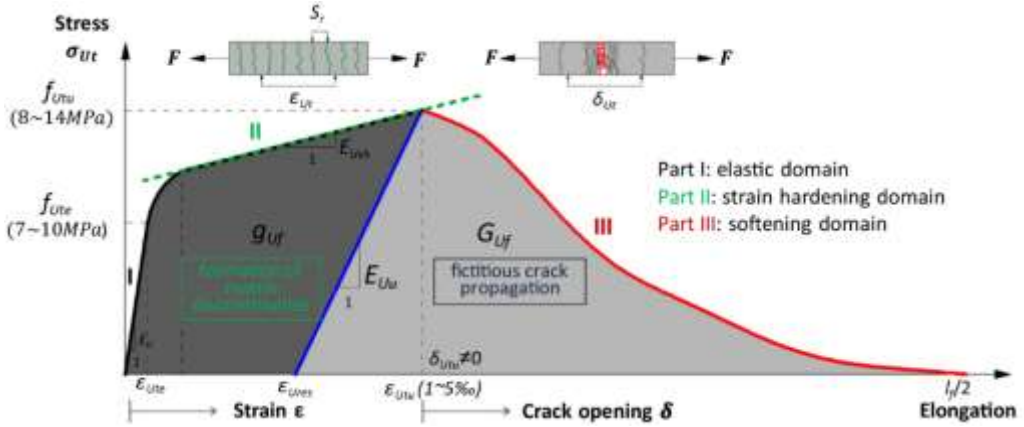

Figure 16: tensile strain-hardening behaviour of UHPFRC element, source: (Shen & Brühwiler, 2020)

The stress-strain relationship of a normal UHPFRC element is simplified in Figure 17. This approximation of the tensile behaviour can be used in calculations and Finite Element Analysis models. In this approximation of the tensile behaviour of UHPFRC, the different domains of the behaviour are assumed as linear with constants indicated in Figure 17. These constants are usually the stress and strain values at the limits of each domain and the slope gradient of the linear graph. The first domain is the elastic domain starting at the origin of the graph where both stress and strain are zero. After reaching the elastic limit stress, f_{Ute}, the strain-hardening domain initiates. This domain ends at the maximum tensile stress that the tensile member can take, also known as the post-cracking peak tensile stress, f_{Utu}. This value is very important for characterizing the tensile behaviour. (Sawicki, Brühwiler, & Denarié, 2022).

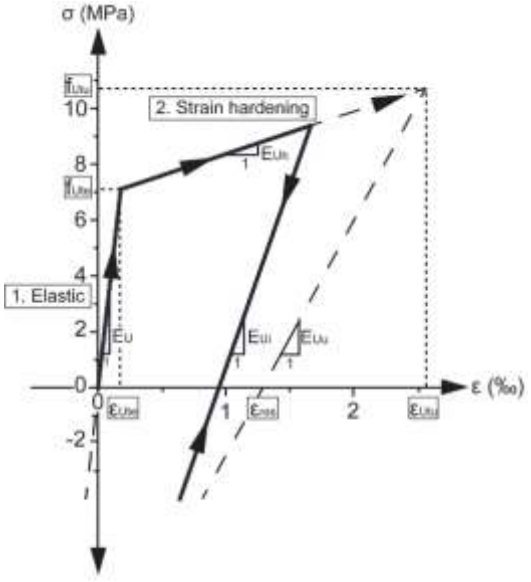

Figure 17: simplified tensile behaviour of UHPFRC, source: (Sawicki, Brühwiler, & Denarié, 2022)

2.3.3 Shrinkage behaviour

Drying shrinkage is one of the biggest contributing factors to the total shrinkage of a concrete element. Since UHPFRC has a very small water-to-cement ratio, the most shrinkage happens during hardening. There is barely any shrinkage on a long-term scale. The amount of shrinkage is dependent on the thermal curing of the material. Without this curing, the shrinkage is around 550 µm/m ($0.55*10^{-3}$), but this can decrease to 0 – 10 µm/m ($0 - 0{,}01*10^{-3}$) by curing the element. So in general, UHPFRC experiences less shrinkage than CC but thermal curing is really helpful to minimize it even more (Reitsema, 2012).

Autogenous shrinkage contributes the most to the total shrinkage of UHPFRC. However, this shrinkage can be reduced by thermal curing or shrinkage reducing agents. However, this is not necessarily needed because of the high tensile strength of UHPFRC (Brühwiler, 2017).

The autogenous shrinkage can also be reduced by adding a coarse aggregate made out of basalt ranging from 2 to 5 mm. This will not reduce the compactness of the material a lot. However, the addition of this coarse aggregate will reduce the homogeneity and therefore, increase the uncertainty of the material properties. For curing at low temperatures, the replacement of silica fume with metakaolin can help decrease the autogenous shrinkage. This effect is much less for curing at high temperatures from 42 degrees Celsius. The use of an expansive additive and a shrinkage reducing additive can also reduce the autogenous shrinkage to almost zero (U.S. Department of Transportation, 2013).

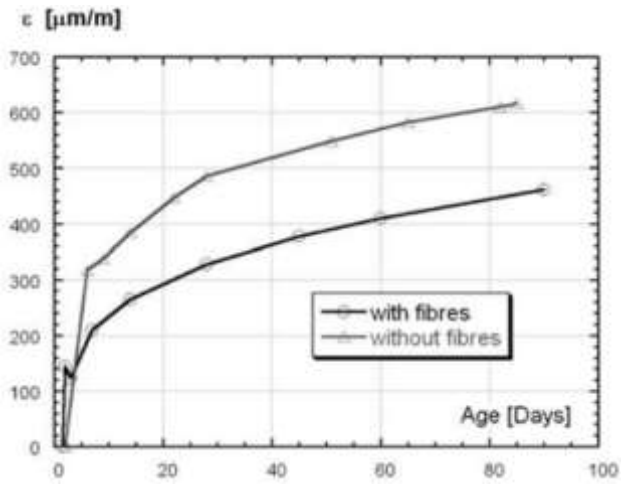

Figure 18: effect of fiber addition on autogenous shrinkage, source: (Tayeh, Aadi, Hilal, & Bakar, 2019)

The addition of fibers to UHPC has a positive effect on the autogenous shrinkage. Figure 18 shows the autogenous shrinkage of UHPC with and without fibers at 20 degrees Celsius over time. Clearly, the shrinkage takes on a much higher value for UHPC than for UHPFRC. This is another reason why the addition of fibers is beneficial (Tayeh, Aadi, Hilal, & Bakar, 2019).

2.3.4 Creep behaviour

Apart from shrinkage, creep is also a time-dependent property. The generalised creep coefficient of UHPC is determined by interpolation of the creep coefficient values of concrete types with a lower compression strength. Figure 19 shows the relationship. For high compressive strengths, the amount of creep is smaller and the creep varies less over time. Also, the difference in the creep coefficient after 28 and 100 days is minimal for high compressive strengths. The creep coefficient of UHPC is estimated to be 0.8, which seems to be relatively accurate, when checking Figure 19. A French brand of UHPFRC called Ductal claims to achieve a creep coefficient of 0.3 (Reitsema, 2012).

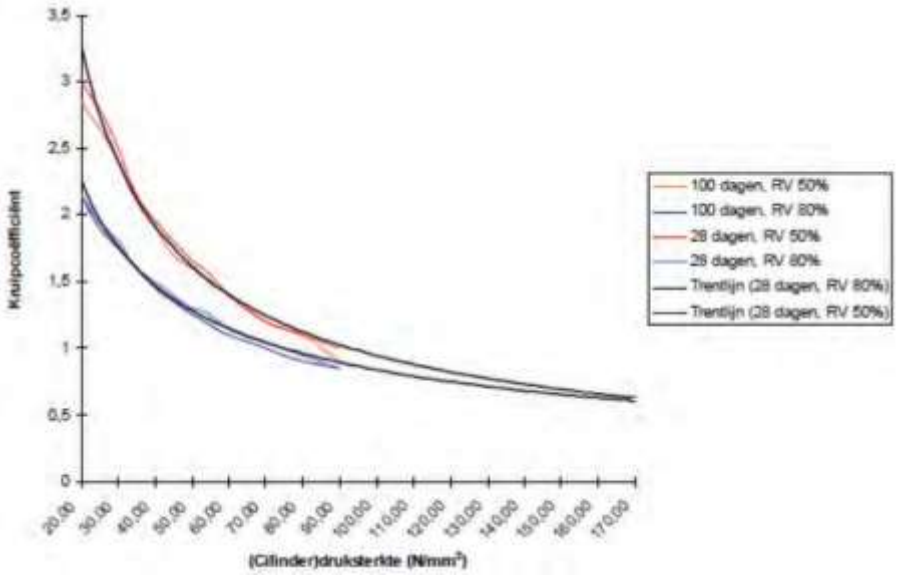

Figure 19: creep coefficient based on compressive strength, source: (Reitsema, 2012)

2.3.5 Fatigue behaviour

Fatigue has more influence for light-weight structures and is therefore more of a risk for UHPFRC elements. Experimental results show that the fatigue resistance of UHPFRC elements is heavily dependent on the fiber type. Long fibers are less active for microcracks than shorter fibers and fatigue cracks are usually microcracks. That is why UHPFRC mixtures with mostly long fibers will have a lower fatigue resistance. Therefore, it is important to check the function of the element and how vulnerable it is against fatigue when choosing the fiber type (Reitsema, 2012).

2.4 Durability properties

UHPFRC is also a very promising material for durability reasons. Table 3 shows some durability aspects denoted with a value for comparison. This shows that UHPFRC is superior in every durability aspect compared to CC or HPC. This is mostly due to its dense microstructure which is discussed more in the following paragraphs.

Table 3: durability indicator values according to AFGC, source: (Reitsema, 2012)

Indicator	Conventional Concrete C30/35	HPC C90/105	UHPFRC C170/200
Total porosity [%]	± 15	± 8	4 - 6
Capillary porosity [%]	± 8	± 5	1.5 – 2.0
Nitrogen permeability [m^3]	10^{16}	10^{17}	< 10^{18}
Chloride-ion diffusion, intrusion depth [mm]	23	8	1
Carbonation depth [mm]	7	4	1.5
Freeze/thaw and salt resistance [g/m^3]	< 1500	150	20/50 (water or heat treatment)

Figure 20, on the next page, also shows the relative parameters of UHPC, HPC and CC for ten different durability aspects with the same conclusion that UHPFRC has superior durability properties for every single aspect (Du, et al., 2021).

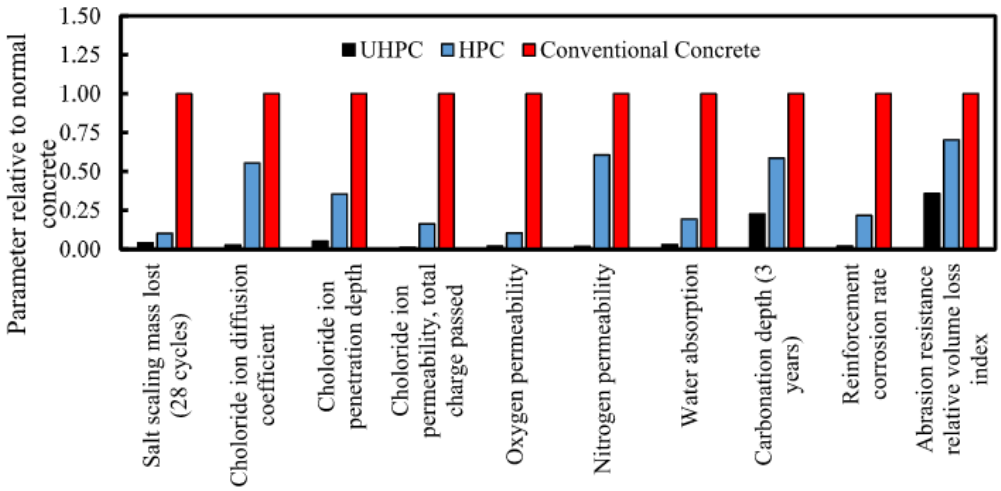

Figure 20: durability parameters of UHPC compared to HPC and CC, source: (Du, et al., 2021)

2.4.1 Permeability

As discussed in chapter 2.2, UHPFRC has a much denser microstructure than CC or HPC which leads to a very low porosity and permeability. The water-to-cement ratio, the use of SCM's, the pore diameter and the pore connectivity are new biggest influences on the permeability (Li, Wu, Shi, Yuan, & Zhang, 2020).

The main cause of deterioration of concrete composite elements is corrosion of the reinforcement. This corrosion occurs if the permeability is high. The corrosion resistance of UHPFRC is extremely good since the permeability is very close to zero (Li, Wu, Shi, Yuan, & Zhang, 2020).

2.4.2 Carbonation

In the presence of sufficient moisture, a chemical reaction between CO_2 in the environment and hydration products in the concrete can take place. $CaCO_3$ forms from this reaction lowering the pH value. The protective oxide layer around the reinforcement will break down in such a low pH environment leading to quicker corrosion. However, as discussed before, a very saturated mixture has a higher porosity and thus faster carbonation. Due to its low w/c-ratio and low water content, the process of carbonation rarely occurs in a UHPFRC element (Li, Wu, Shi, Yuan, & Zhang, 2020).

2.4.3 Freeze-thaw resistance

Freeze-thaw damage when an amount of water enters the concrete and the temperature decreases so the water freezes and expands. This expansion causes tensile stresses in the concrete and might lead to cracking. UHPFRC has a relatively high tensile resistance compared to other concrete types. However, the main reason UHPFRC has a high freeze-thaw resistance is the low permeability and porosity of the material (Li, Wu, Shi, Yuan, & Zhang, 2020).

Multiple researches were done to determine the freeze-thaw resistance of UHPFRC. For instance, Acker and Behloul (Acker & Behloul, 2004) did 300 freeze-thaw cycles on UHPFRC specimen but the specimen showed no degradation. Ahlborn et. al., Piérard et al., and Magureanu et al. had similar results where the latter even showed a higher compressive strength and E-modulus after over 1000 freeze-thaw cycles (U.S. Department of Transportation, 2013).

This was also proven to be true for CC beams strengthened with a UHPFRC jacket in a research by the TU Delft. In this research, thin UHPFRC panels were attached to CC beams using an epoxy resin. This researched showed that using epoxy resin resulted in a better bond strength than other solutions, such as in-situ casting or bolts. The beam was subjected to 30 freeze-thaw cycles and compared to a beam without freeze-thaw on shear resistance. There was a decrease in capacity of 5% which is very small compared to standard CC elements. This shows that the freeze-thaw resistance of UHPFRC is really good. Even thin plates have low enough permeability to avoid water ingress. The epoxy resin also proved to provide sufficient bond strength, even after the freeze-thaw cycles (Huang & Luković, 2022). These UHPFRC panels will be discussed in more detail in Chapter 2.7.3.5.

2.4.4 Chemical/acid attack resistance

Research showed that the strength of UHPFRC specimen immersed in tap and sea water showed even greater values over time compared to the initial strength. This is explained by the continued hydration of the unhydrated cement. However, after 12 months, the compressive strength decreased by 12% due to acid attack. The other properties of UHPFRC after acid attack also decreased but only by 9.2% which is much lower than for other types of concrete. This shows that UHPFRC is a suitable material for harsh environments (Li, Wu, Shi, Yuan, & Zhang, 2020).

2.4.5 Alkali-silica reaction

Once again, because of the low permeability of UHPFRC, the resistance against alkali-silica reaction is also very good and will not form a concern under any curing regime (Li, Wu, Shi, Yuan, & Zhang, 2020). In order for a alkali-silica reaction to happen, there must be free water present. However, this low permeability prevents the presence of this free water and thus decreasing the risk of alkali-silica reactions.

2.4.6 Fire resistance

UHPFRC shows three different stages while exposed to fire. The first stage is at relatively low temperatures (150 to 350 degrees Celsius) which is the initial stabilizing and regaining stage. The strength loss stage ranges from 350 to 800 degrees Celsius. The last stage ranges from 800 degrees Celsius and up. In this stage the UHPFRC loses all of its strength (Li, Wu, Shi, Yuan, & Zhang, 2020).

Figure 21 below shows the decrease in compressive strength over time during a fire. In this graph, RPC stands for Reactive Powder Concrete which is a concrete type somewhere in between UHPC and HPC. OC (Ordinary Concrete) is equivalent to CC. The stronger concrete types experience a bigger decrease in compressive strength. Because of the significantly larger initial compressive strength, the final compressive strength is significantly higher than for CC. The described effect also applies in the case of UHPFRC (Liu & Huang, 2008).

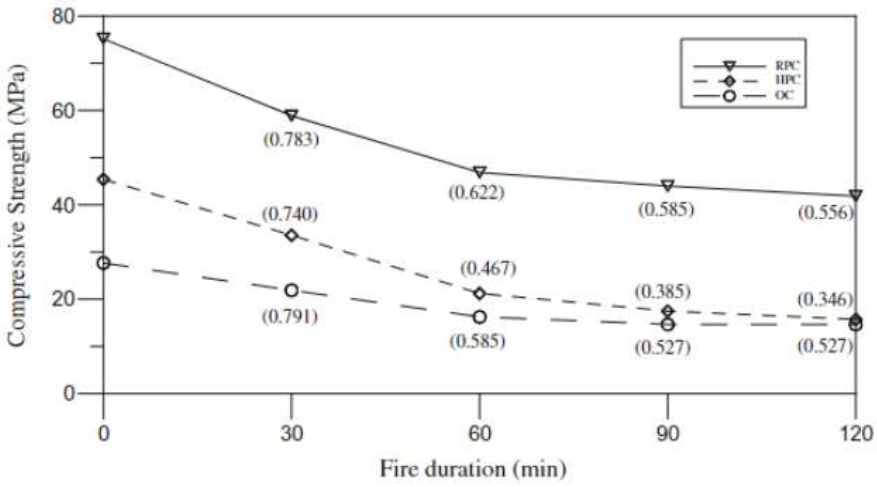

Figure 21: compressive strength under a fire load, source: (Liu & Huang, 2008)

Spalling is one of the bigger problems of UHPFRC under fire conditions. The water present inside the concrete can evaporate and form steam. This steam cannot get out of the concrete due to the dense microstructure resulting in big internal stresses (Reitsema, 2012). There are multiple measurements that can be taken to minimize explosive spalling. For instance, the increase of fiber content in the material or changing the fiber material to polypropylene (Li, Wu, Shi, Yuan, & Zhang, 2020). According to the article by Heinz et al. the optimal steel fiber content is 3.05% to minimize spalling and other fire damage (South Dakota Department of Transportation).

2.4.7 Service life

The superior performance and durability of UHPFRC results in low-maintenance structures. Normal reinforced CC structures usually require maintenance, strengthening or even replacement multiple times during their service life. UHPFRC has the ability to increase the service life because of its good performance. Generally, even under severe environmental circumstances, UHPFRC structures will not need maintenance for a 100 years after construction, which is the average service life of a civil structure. This results in lower costs, which will be discussed later (Huang, Grünewald, Schlangen, & Luković, 2022).

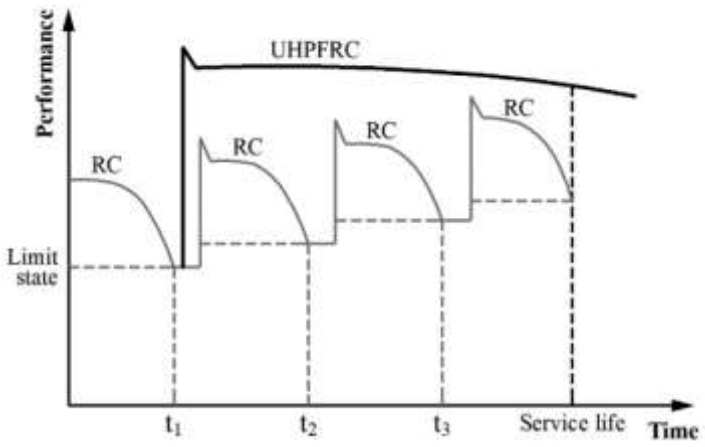

Figure 22: performance over time of UHPFRC strengthening, source: (Denarié, 2005)

2.5 Sustainability properties

2.5.1 Quality

The quality of UHPFRC is dependent on a lot of different aspects but it has the potential to have far greater quality than CC. A couple of these influencing aspects are the water-to-cement ratio, the curing method, the bond strength, the fiber distribution and orientation (Huang, Grünewald, Schlangen, & Luković, 2022). This last two aspects regarding the steel fibers are focussed on in this Master Thesis. The quality control of these aspects is described in detail in Chapter 3.

2.5.2 CO2 footprint

The CO_2 footprint per cubic meter of UHPFRC is significantly higher than CC because of the large amount of cement and the production of steel fibers. However, due to the advantages of UHPFRC, the material usage is far smaller which means the total amount of cement used in a UHPFRC element is still smaller than in a CC element (Toutlemonde & Resplendino, 2014). Furthermore, the service life of the structure is longer. During the use phase of an UHPFRC structure, maintenance or replacement is required less often, also decreasing CO_2 footprint (Huang, Grünewald, Schlangen, & Luković, 2022).

In a previous research, the energy and raw material consumption was determined for a square reinforced column made of UHPFRC and C40/50. The energy and raw material consumption of the UHPFRC column was 74 and 58 percent of the C40/50 column, respectively. For this research, a commercial brand of UHPFRC, Ductal was used (Ahlborn & Kollmorgen, 2004).

In some cases, the fibers provide enough tensile capacity so steel rebars are no longer necessary or can at least be reduced to the minimum reinforcement. In case there is no standard reinforcement, the fiber content should be at least 2% (Reitsema, 2012).

2.5.3 ECI calculation

A quick Environmental Cost Indicator (ECI) calculation was done to find the environmental impact of a cubic meter of UHPFRC compared to CC. For this calculation, the concrete LCA (Life Cycle Analysis) dataset is used from the TU Delft Course CIE4100: Materials and Ecological Engineering (TU Delft CIE4100, 2020). This dataset can be found in Appendix 1.

The mix design of CC is found in the same course as the concrete LCA dataset. This mix design can be found in Table 4 and is supposed to result in a concrete strength class of C55/67 (TU Delft CIE4100, 2020). The mix design for UHPFRC is taken from the standard mix design of a commercial UHPFRC brand Ductal (Akhnoukh & Buckhalter, 2021). These amounts together with the concrete LCA dataset are used to calculate the ECI value for a cubic meter of CC and a cubic meter of UHPFRC. The calculation of these values can also be found in Appendix 1.

Table 4: mix proportions CC and UHPFRC, source: (TU Delft CIE4100, 2020) & (Akhnoukh & Buckhalter, 2021)

Mix ingredient	CC amount [kg/m3]	UHPFRC amount [kg/m3]
CEM I	250	-
CEM III	225	712
Gravel 4-8 mm	1177	-
Sand 0-4 mm	684	1020
Silica fume	-	231
Limestone filler	-	211
Super plasticizer	3.5	30.7
Steel fibers	-	156
Water	160	109

The environmental costs of one cubic meter of CC is €21,17 which becomes €41,24 when adding 123 kg of steel reinforcement. A cubic meter of UHPFRC has an environmental cost value of €51,25 which becomes €60,85 when adding 59 kg of steel reinforcement. UHPFRC needs less reinforcement than CC because of the tensile capacity of UHPFRC, mostly due to the fiber content. The reinforcement weight was calculated using the reinforcement ratio from the experimental data of a PhD Thesis. These reinforcement ratios resulted in a similar structural capacity for both a CC and UHPFRC beam (Sine, 2021).The calculations for the reinforcement weight can also be found in Appendix 1. These reinforcement ratios are taken from the additional strengthening layer alone. The density of the steel bars is taken as 7,850 kg/m^3 (Tosec, 2023).

This means that one cubic meter of R-UPHFRC is more harming to the environment than a cubic meter of RC. Figure 23 shows the ECI value per environmental impact factor. Clearly, the Global Warming Potential (GWP) has the highest contribution to the total ECI value. Apart from this, Acidification Potential and Human Toxicity Potential are the biggest problems. There is not much difference in the ratios between the different materials. For all impact factors, R-UHPFRC has the highest ECI value and CC the smallest.

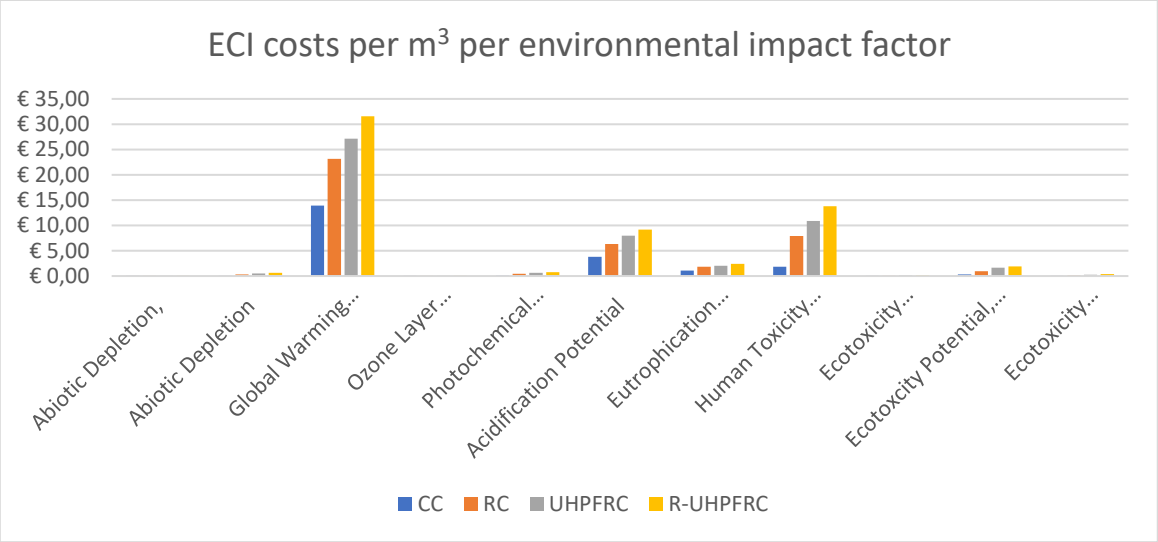

Figure 23: ECI costs per cubic meter per environmental impact factor (TU Delft CIE4100, 2020), as calculated in Appendix 1

However, in general UHPFRC is a more environmental friendly material than CC. This is due to the high strength capacity of UHPFRC. In most applications, the UHPFRC alternative requires a lot less material than the traditional design with CC. That means that even though the ECI value per cubic meter might be higher for UHPFRC, the total ECI value for a real life application can be significantly lower. The ECI calculation including a comparison with traditional strengthening methods has already been done for a real life application, namely The Guillermaux Bridge in Switzerland. The results of this calculation can be found in Chapter 2.7.2.4 which shows that UHPFRC can be a more sustainable material than CC.

2.5.4 Recycling

Studies have been done about the recycling of UHPFRC where the best method seems to be crushing the material into fine 0/3 mm sand and fibers. The latter can be extracted relatively easy using a magnet. The crushed sand consists of aggregate and cement which behaves like a sort of hard sand. The fine particles have a moderate binder effect and the workability of a new concrete mixture barely differs from a fresh mixture. The compressive strength decrease is limited to 10%. This means all the material can be re-used in a new application (Sedran, Durand, & de Larrard, 2009).

2.6 Financial aspects

The Cement Efficiency Factor (CEF) is defined by the compressive strength of the material divided by the amount of cement used for one cubic meter of the material. In this research the CEF for UHPC, HSC and NSC was 0.16, 0.12 and 0.13, respectively. This shows UHPC is more efficient regarding the financial aspects (Aziz & Ahmed, 2012).

2.6.1 Long life span

As described before, the service life of a UHPFRC structure is relatively long compared to a conventional alternative using reinforced CC. This increase in life span is also financially beneficial since more years can pass until the structure needs replacement or rehabilitation (Huang, Grünewald, Schlangen, & Luković, 2022).

2.6.2 Low maintenance

UHPFRC has very good resistance against chemical attack, as described earlier. The risk of carbonation, corrosion, freeze-thaw, alkali-silica reaction, etc is very small which means the element will not be damaged easily. Little to no damage means little to no reparation or at least not frequently. Furthermore, the elements are more slender so there is a smaller surface area and the surface of the element is very smooth due to the fine microstructure. Finally, there is no need for a finishing coat over the element since the UHPFRC has a self-compacting effect (Reitsema, 2012). All these aspects explain the low maintenance and therefore low maintenance costs of the material.

2.6.3 Reduction in material consumption

UHPFRC shows significantly improved material properties compared to CC. The tensile capacity of the UHPFRC can even be taken into account for structural calculations. That is why UHPFRC elements can be a lot more slender than CC element, as discussed before. These slender elements naturally use less building materials. This fact can make the total costs of an UHPFRC alternative still lower than the traditional way with CC (Bertola, Schiltz, Denarié, & Brühwiler, 2021).

2.6.4 Fast construction

The construction phase of a UHPFRC structure is usually a lot smaller than a CC structure. This is due to two main reasons. First of all, the slenderness of UHPFRC elements makes it easier for the elements to be transported. That is why a lot of elements can be prefabricated and assembled on-site. Secondly, the hardening process of UHPFRC is very quick in comparison to CC. CC needs around 28 days before it has developed its characteristic material properties but UHPFRC has usually hardened within a day. This also greatly reduces the construction time and thus costs. Especially since in general, labour costs are far higher than material costs (Bertola, Schiltz, Denarié, & Brühwiler, 2021). Besides this, a structure will have a quicker out-of-use period so the traffic hindrance is decreased. This is also financially advantageous (Huang, Grünewald, Schlangen, & Luković, 2022).

2.6.5 High material costs

Due to the content of steel fibers, high quality additions and high dosage of chemical admixture, the costs of a UHPFRC mix can be relatively high compared to CC. An average cubic meter of UHPFRC can cost about €2300 to €2800. The costs of a cubic meter of CC is almost negligible compared to these numbers, generally around €160 (Akhnoukh & Buckhalter, 2021). This difference is a factor of 16! Of course, these numbers do not take the difference in material usage into account so a complete costs calculation will give a more accurate comparison.

2.7 Applications of UHPFRC

There are already quite some applications of UHPFRC. For example, slender balconies, pedestrian bridges and architectural elements. However, the application in big structural civil structures is still in its early stages, especially in the Netherlands (GWW, 2019). Firstly, this part discusses the use of UHPFRC in the strengthening of bridge decks and existing concrete beams. This is relevant to the problem description, described in Chapter 1. Afterwards, other types of UHPFRC applications will be discussed without going into detail.

2.7.1 General history of UHPFRC applications and Eurocode

Concrete structures in the Netherlands have to satisfy the rules set in Eurocode 2. However, the highest concrete class in this code is C90/105 where UHPFRC has larger strengths. That is one of the reasons the Eurocode does not apply for UHPFRC. Moreover, due to the fibers within the concrete the behaviour of UHPFRC is not characteristic for concrete. The material itself behaves like a composite material of concrete and steel. That is why local standards are developed like the Swiss code (EPFL-Swiss Federal Institute of Technology, 2016) or the French code (AFNOR, 2016). These codes provide methods and calculations to predict the structural behaviour of UHPFRC elements. However, it is not part of the official Eurocode yet so this limits the application in the Netherlands.

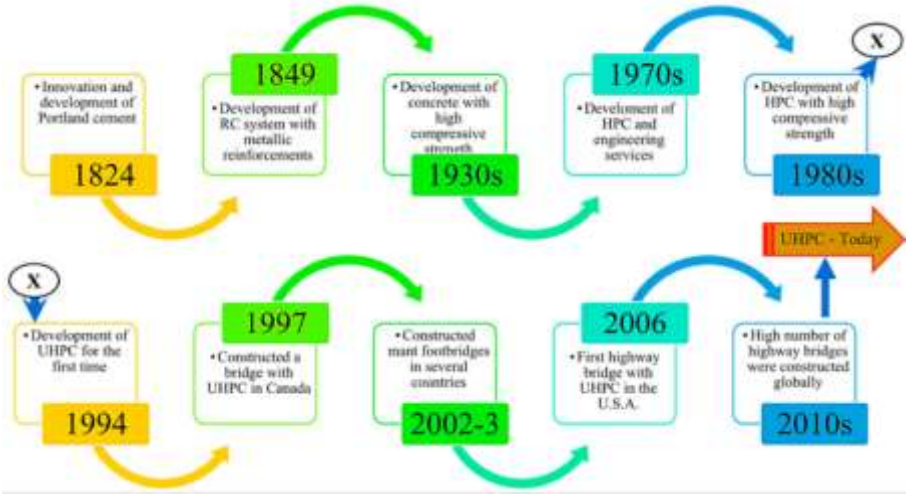

Figure 24: history of UHPFRC applications, source: (Amran, et al., 2022)

As can be seen in Figure 24, the first large scale application using UHPFRC was in 1997 in Sherbrooke, Canada. This pedestrian bridge spanned 60 meters consisting of six prefabricated slab segments supported by a truss structure. UHPFRC was used to fill stainless steel tubes for the bottom chord and diagonals of the bridge (Figure 25). Previously, the maximum compressive strength of concrete was 105 MPa which suddenly increased to 200 MPa for UHPFRC, a huge improvement (Berendsen, 2014).

Figure 25: first large scale application of UHPFRC, source: (Berendsen, 2014)

2.7.2 Bridge deck strengthening

2.7.2.1 The need for bridge deck strengthening

After World War 2, around the 1950's and 1960's, a lot of bridges, tunnels, water locks and viaducts have been built in the Netherlands. Normally, these large civil structures are supposed to have a life span of about 100 years which means it will take another 30 years before the structures need reconstruction. However, these structures were designed based on a traffic load of the 20th century. Over the years, the amount of traffic and therefore traffic loads have increased immensely. This increases the risk of damage or even failure of these structures and decreases the life span. That is why Rijkswaterstaat wants to work on the reconstruction and renovation of these structures in the coming years (Rijkswaterstaat, 2023). Rijkswaterstaat is a part of the Ministry of Infrastructure and Water Management in the Netherlands. They are responsible for designing, constructing, managing and doing maintenance on a lot of Dutch civil structures.

For Rijkswaterstaat, safety is priority number one. That is why the bridges, tunnels, water locks and viaduct are monitored and checked regularly. That is how Rijkswaterstaat knows the state of a structure and when the structure is due for reconstruction or renovation. However, most civil structures built around the 1950's and 1960's have been around for quite some time with an increasing traffic load so errors, emergency repairs and maintenance increases more and more. That is where rehabilitation or strengthening comes into play (Rijkswaterstaat, 2023).

The effects of rehabilitation or repair of the structure depend on the rehabilitation method and the materials used for rehabilitation. In general, rehabilitation is the repair or strengthening of an existing structure in order to upgrade the strength or improve the life span. Rehabilitation of a structure is usually preferred by governments and industry due to the short out-of-use phase, the relatively small traffic hindrance and the solution is financially more beneficial. On top of this, rehabilitation is also environmentally more advantageous since less raw materials are used compared to reconstruction (Huang, Grünewald, Schlangen, & Luković, 2022).

Casting a new layer of CC, specifically in the areas where the largest stresses occur, is one of the most common methods of strengthening nowadays. However, the development of new materials such as UHPFRC result in more rehabilitation alternatives. In this chapter, different rehabilitation alternatives are researched properly and compared against each other (Huang, Grünewald, Schlangen, & Luković, 2022).

2.7.2.2 UHPFRC bridge deck strengthening variants

The main goal of UHPFRC strengthening is to improve the heavily loaded areas of a structure. The specific strengthening method depends on the circumstances. The structural capacity of the structure might be sufficiently high to carry the acting loads but the environmental conditions can be so severe, durability needs improvement. The excellent durability properties of UHPFRC have been mentioned before. In this case, a UHPFRC layer of only 10 to 30 mm is necessary to improve durability. This configuration is called Reinforced Concrete – UHPFRC (RC-U) and is shown on the left of Figure 26. In this configuration, the UHPFRC mostly has a protective function (Sine, 2021).

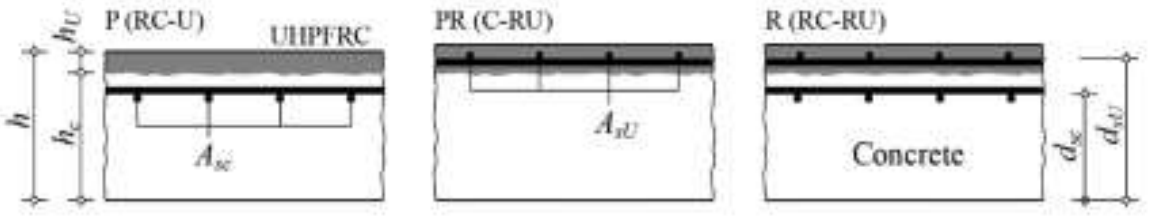

Figure 26: configurations for UHPFRC bridge deck strengthening, source: (Brühwiler, 2017)

For a larger structural capacity, small diameter rebars can be added to the UHPFRC. The existing concrete might already be reinforced, depending on the function of the element. This is the difference between the two other configurations of UHPFRC strengthening, namely Concrete – Reinforced UHPFRC (C-RU) and Reinforced Concrete – Reinforced UHPFRC (RC-RU). For these configurations, the reinforcement cover and the distance to the substrate interface should not be smaller than 10 mm or the diameter of the reinforcement (Sine, 2021). The UHPFRC layer in these configuration is usually 50 to 75 mm (Brühwiler, 2017).

The results of this strengthening method can even have preferable effects when comparing to the replacement of a structure. In a different Master Thesis research, a reinforced CC slab was strengthened with a UHPFRC top layer and compared to a new reinforced CC slab. This was a direct comparison of the structural effects between rehabilitation and renovation. By adding a UHPFRC layer with a thickness of 38 mm, the maximum load increased by 41%. Besides this, the UHPFRC layer contributes a lot to the durability of the slab decreasing its environmental vulnerability (Garner, 2011).

2.7.2.5 Examples of application

The Chillon viaducts in Switzerland were built in the 1960s and consist of two parallel highway bridges of reinforced CC. Each bridge carries one direction and has post-tensioned box girders of variable height. The bridge consists of segments spanning between 92 and 104 m with a total length of over 2 km. In 2012, early signs of an alkali-aggregate reaction were spotted in the concrete. This reaction can lead to a big decrease of the concrete strength and therefore lead to unsafety of the structure. That is why a top layer of UHPFRC embedded with steel rebars was cast. This protects the concrete from water ingress thus hindering the alkali-aggregate reaction. Moreover, the structural resistance and stiffness increased and the out-of-use period was relatively short (Brühwiler, et al., 2015).

Figure 27: Chillon viaducts in Switzerland, source: (Brühwiler, et al., 2015)

For the design of the strengthened structure, the future effects of the alkali-aggregate reaction had to be taken into account. That is why the assumption was made that the CC had lost 50% of its compressive strength. The UHPFRC layer was designed to have a thickness of 40 mm with transversal reinforcement with a concrete cover of 16 mm (Figure 28). The design was checked in Ultimate Limit State (ULS) for bending moment resistance, shear resistance and fatigue resistance using similar calculations as for the composite beams and slabs. This design was also tested numerically using a Non-Linear Finite Element Analysis (NLFEA). This numerical method investigated tensile stresses due to time-dependent effects and the deformation of the deck under high wheel loads. Representative elements of the Chillon viaduct have also been tested experimentally confirming the effectiveness of the strengthening method (Brühwiler, et al., 2015).

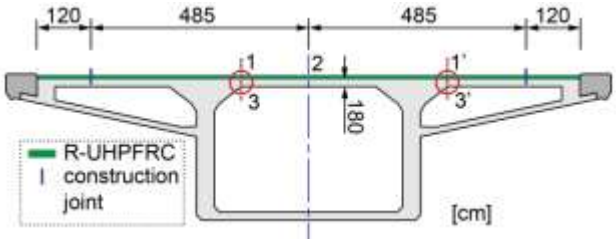

Figure 28: design of UHPFRC strengthening Chillon viaducts, source: (Brühwiler, et al., 2015)

There are multiple other examples of UHPFRC bridge deck strengthening: a road bridge deck in Vuarrens (France), a building slab in Geneva (Switzerland), a bridge deck including sidewalks in Montreux (Switzerland) and the Chandelard bridge near Lausanne (Switzerland). All these slabs were strengthened with a 30 mm thick UHPFRC layer on top. This layer mostly has a durability function but also contributes to the bridge strength and stiffness (Moreillon & Menétrey, 2013).

2.7.3 Other applications

2.7.3.1 UHPFRC columns

As follows from experimental values, the maximum axial force on a UHPC column is on average 3.85 times higher than the same column using CC. This behaviour can be seen in Figure 29, where CC is denoted as NSC. It should be noted that this is uniaxial compression behaviour. As mentioned earlier, steel fibers barely contribute to the compressive strength meaning there would be no reason to use UHPFRC instead of UHPC. However, the fibers add more ductility, both for tension and compression. In reality, a column can buckle or have an eccentrical load resulting in additional bending moment and therefore tensile stresses. Because of this, the tensile behaviour of the UPHFRC is also relevant showing the significance of fibers. Especially fibers at the edges of the column contribute a lot to the additional bending moment resistance since the strains and stresses are the biggest here (Schmidt, Fehling, Glotzbach, Fröhlich, & Piotrowski, 2012).

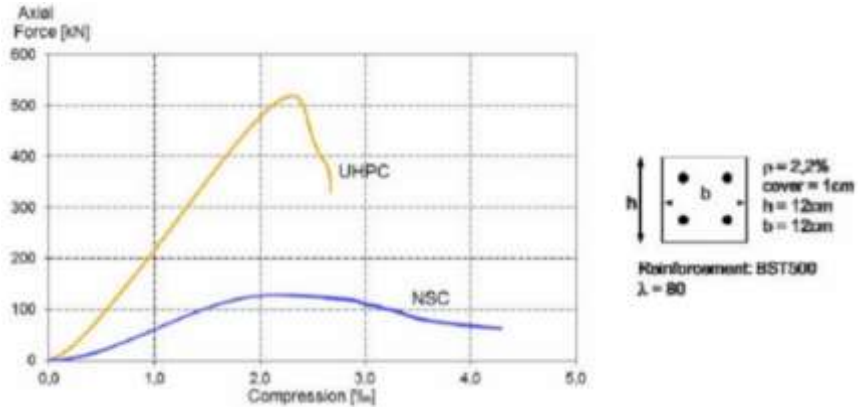

Figure 29: structural behaviour of UHPFRC and CC column, source: (Schmidt, Fehling, Glotzbach, Fröhlich, & Piotrowski, 2012)

An example of reinforced UHPFRC columns can be found at the La République Bridge in Montpellier, France. The columns, also known as bridge piers, consist out of UHPFRC and steel tendons. The columns are relatively slender which results in an aesthetically pleasing design. The column design and a picture of the final bridge can be found in Figure 30 (Riciotti, Pastor, Hajar, & Bernardi, 2017).

Figure 30: column design of La République Bridge, source: (Riciotti, Pastor, Hajar, & Bernardi, 2017)

UHPFRC can also be used for strengthening around an existing column, in the form of a jacket. The UHPFRC jacket is only applied in specific areas of the column where the highest loads occur or the damage is present. For instance, Figure 31 shows a realistic example of UHPFRC strengthened bridge columns. The UHPFRC jacket is placed around the column where plastic hinges might occur. Experiments proved that this solution showed better performance, energy dissipation and reduced the damage due to plastic hinges (Alsomiri, Jiang, & Liu, 2021). A real life example can be found in Canada and was built in 2014. UHPFRC strengthening was specifically chosen here for its seismic performance, corrosion resistance and spalling resistance (Kennedy, Habel, & Fraser, 2015).

Figure 31: UHPFRC strengthened column bridge in Canada, source: (Kennedy, Habel, & Fraser, 2015)

2.7.3.2 Thin slabs / floors

The structural application of UHPFRC thin floors without conventional reinforcement is possible due to the strong properties of UHPFRC. However, this application is scarcely used. The general thickness of these floor is about 40 to 60 mm.

An example of a thin UHPFRC slab is the deck of the Seonyu footbridge in Seoul, South Korea. The deck of this bridge consisted of 30 mm thick slabs which is considered very thin. Of course, the acting loads on a footbridge are also relatively small compared to other bridge types so that is why this realisation was possible. Figure 32 shows the footbridge along with two local bending failure modes of the deck (Spasojevic, Redaelli, & Muttoni, 2009).

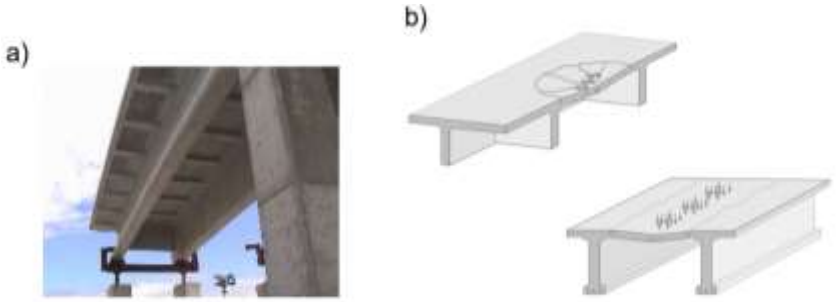

Figure 32: thin deck of Seonyu footbridge, source: (Spasojevic, Redaelli, & Muttoni, 2009)

A toll station in Millau, France, also has a thin UHPFRC slab as a roof. The curved roof has an area of 98 by 28 meters divided over 54 separate slabs. Prestressed beams are used to connect the slabs using an epoxy adhesive. A big challenge for this project was designing the roof against thermal loading causing relatively high tensile stresses. The toll station can be seen in Figure 33 (Berendsen, 2014).

Figure 33: thin roof of toll station in Millau, source: (Berendsen, 2014)

2.7.3.3 Industrial floors

Industrial floors can often have harsh environmental conditions and get damaged from heavy equipment or building materials. This damage can lead to inefficiency of the workplace, uncomfortable usage and damage of more equipment. That is why it is important to repair the floor in case of damage. One of the most important factors is the out-of-use period of the floor. UHPC is a fast hardening material with high early age strength. Combined with the great ductility of UHPC, the material is ideal for this application. A UHPC industrial floors is usually combined with a steel reinforcement net to prevent cracking and increase ductility (Vastmans Frank betonvloeren, 2019).

Figure 34: industrial UHPFRC floor at waste recycling sorting plant, source: (Buitelaar, 2018)

However, a steel reinforcement mesh cannot be used in very slender floors whereas UHPFRC does not always require a steel reinforcement net due to the presence of fibers. Moreover, the usage of steel fibers is significantly cheaper than a reinforcement mesh (Vastmans Frank betonvloeren, 2019). This is why fiber reinforced concrete is attractive for industrial floors. However, in the Netherlands these floors are usually no UHPFRC floors due to the lack of UHPFRC design rules. An example of a UHPFRC industrial floor is depicted in Figure 34. This is a floor at a waste recycling sorting plant with very harsh environmental conditions (Buitelaar, 2018).

2.7.3.4 Joints between decks

The high ductility property is one of the reasons why UHPFRC can be especially suitable for a semi-stiff joint application. For instance, the connection between precast bridge deck panels. This joint has to transfer bending moment, shear and tensile forces for which UHPFRC has relatively high resistance.

An example of a UHPFRC bridge deck joint can be found in America. For example, a UHPFRC construction joint was applied between precast bridge deck panels on the I-81 in Syracuse, New York. Figure 35 shows the transverse connection detail between the adjacent panels. This construction joint consists solely of UHPFRC with a reinforcement rebar connection all elements. Another advantage of UHPFRC is that the tension development length is very small in UHPFRC compared to CC. This is why the rebar embedded in UHPFRC can have a much shorter length (U.S. Department of Transportation, 2014).

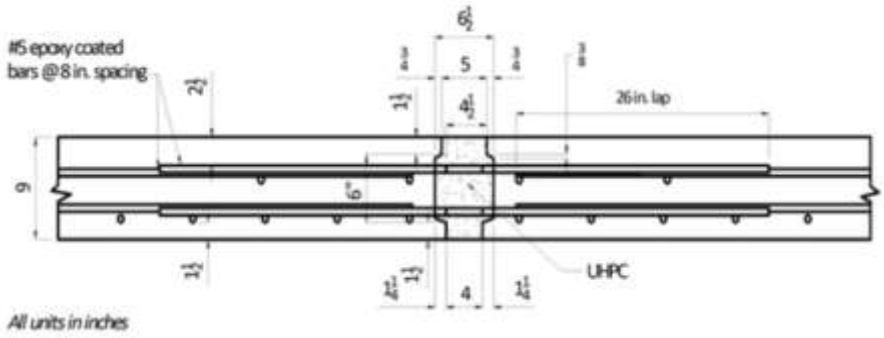

Figure 35: transverse connection between bridge deck panels of I-81 bridge in New York, source: (U.S. Department of Transportation, 2014)

For another bridge in America, a UHPFRC slab has been applied to connect two different girders above a bridge pier. UHPFRC was used here to repair a leaky joint, provide deck continuity and to have a long-lasting seal. The design and realisation can be found in Figure 36 (Graybeal, 2017).

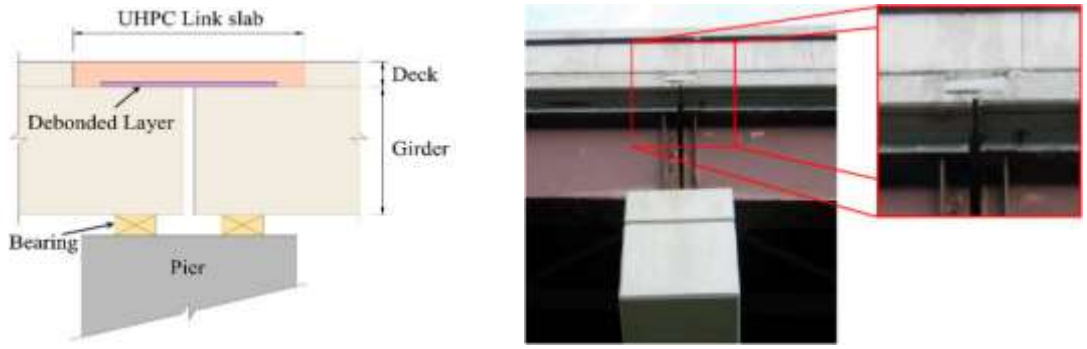

Figure 36: design and realisation of UHPFRC connection slab, source: (Graybeal, 2017)

2.7.3.5 Composite beams and slabs

There are multiple types of composite beams and slabs using UHPFRC. One of the most common are reinforced CC beams/slabs with a UHPFRC layer on top. This top layer might be either in tension or compression for a hogging or sagging bending moment, respectively. Because of the very high compressive strength of UHPFRC, the top layer will contribute a lot to the sagging bending moment capacity. On the other hand, hogging bending moment capacity will also improve compared to CC since the tensile strength of UHPFRC can be taken into account for calculations. This type of composite beams and slabs is similar to UHPFRC beam strengthening, which was discussed before.

A different TU Delft research by PhD Candidate Yitao Huang researches the shear behaviour of reinforced concrete beams strengthened with UHPFRC panels (see Figure 37). These panels have the following dimensions: 1400x200x10 mm^3. The shear panels contain no stirrups and are attached to the side of the existing reinforced concrete beam for the purpose of increasing the shear force resistance. Instead of stirrups, 13 mm long steel fibers are added with a diameter of 0.2 mm diameter. The fiber content is 2%. The research distinguished multiple solutions to attach the shear panels to the concrete beam, like epoxy resin, casting in-situ and steel bolts (Huang, Gu, Mustafa, Grünewald, & Luković, 2023). A possible hypothesis during this research was severe segregation of the steel fibers within the panels. This would be an issue since certain areas would have less fibers and thus have a smaller tensile resistance and ductility. This is a practical example where the characterization of the steel fiber behaviour can benefit the development and understanding of UHPFRC. The research in this thesis will also assess the fiber behaviour in these shear panels. The material composition and mixing procedure that was used to cast these shear panels will also be used in the experimental research of this thesis. This is described in Chapter 4.

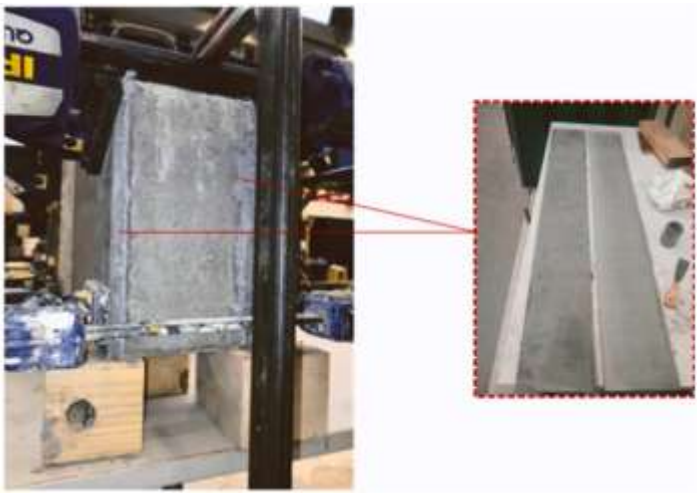

Figure 37: precast concrete beam strengthened with UHPFRC panels, source: (Huang, Gu, Mustafa, Grünewald, & Luković, 2023)

2.7.3.6 UHPFRC water lock gates

A water lock gate can also experience big out-of-plane loads which it has to resist in order to fulfil its function. The strong properties of UHPFRC and its low permeability makes it an interesting material for this function. A water lock gate made of C53/65 concrete needs a thickness of 450 mm where the same water lock gate made of UHPFRC only needs 200 mm on average (Cement, 2013).

In the Netherlands, the first concrete water lock gates in the world were built in 2010. This was an alternative solution to the common steel water lock gates. Even though the present reinforcement is strong enough to carry the acting load, steel fibers are included to ensure enough ductility and durability. The required thickness of the water lock gates was only 100 mm (Cement, 2010).

Figure 38: UHPFRC water lock gate construction, source: (Cement, 2013)

2.7.3.7 UHPFRC balconies

Most CC balconies have a thickness of about 220 mm (Betonhuis). Due to the strong properties of UHPFRC, a balcony can become much more slender. Some UHPFRC contractors even claim they can cast balcony slabs with a thickness of 50 mm (Hi-Con, 2023).

Figure 39: UHPFRC balconies in Utrecht (a) and Delft (b), source: (Hi-Con, 2023)

The design of the balconies is done using the Eurocode and the officially approved changes to the Eurocode by Hi-Con. Hi-Con is a company which focusses on UHPFRC projects, also within the Netherlands. In the Netherlands, they have designed slender balconies, facades, pedestrian bridges and cycling bridges. Examples of slender balconies can be found in Utrecht (Figure 39a), Arnhem, Amsterdam, Bilthoven and Delft (Figure 39b). The balconies in Utrecht in Figure 39a have a thickness of 70 mm and have a cantilever length of 3 meters. This shows the extreme strength of these balconies. The approved document allows Hi-Con to use a compressive strength of 110 MPa for their design and a smaller concrete cover of 10 mm. It is not allowed to use the fibers as structural reinforcement but it is necessary to provide ductility and a minimum tensile strength. The fiber distribution and orientation is checked manually by casting a slab in 45 degrees and cutting beams from the slab (Hi-Con, 2023). It is questionable if this method is representative for actual applications.

2.7.3.8 Example road bridge using only UHPFRC

The first road bridge made of UHPFRC was built in Switzerland in November 2020 (Figure 40). The bridge consists of two lanes and has a span of 25 meters. There are four UHPFRC precast T-shaped girders with a varying height between 0.75 m at the supports and 1.25 at mid-span. The element thickness of the girders are greatly reduced compared to CC girders. On top of the girders, a 50 mm thick layer was cast in-situ to obtain a monolithic structure with semi-flexible joints. On-site construction only took 1 week before traffic could use the bridge. This is a huge financial advantage making the total costs significantly lower than a CC alternative (Brühwiler, 2022).

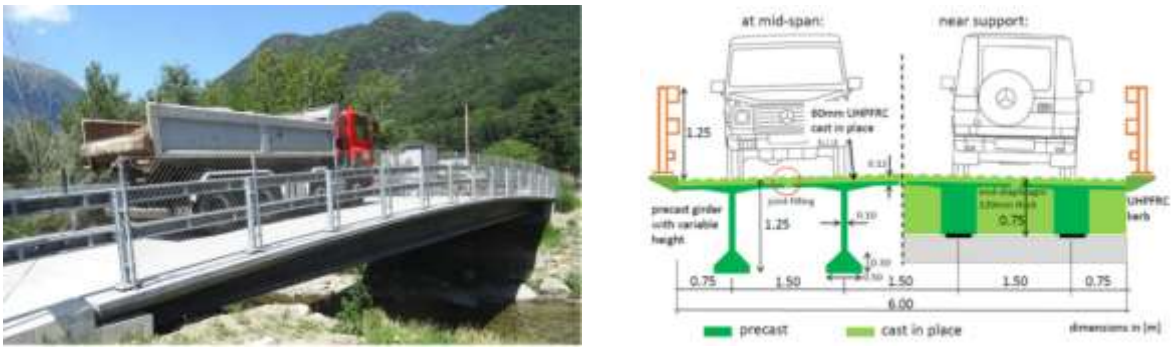

Figure 40: Swiss road bridge using precast and in situ UHPFRC, source: (Brühwiler, 2022)

3. Fiber distribution and orientation

This chapter first discusses quality control and the design codes for UHPFRC elements. The chapter also discusses UHPFRC testing methods, like the magnetic NDT method used in this MSc Thesis. Afterwards, a description of the fiber distribution and orientation is given, some of the major influences on these factors are defined and the desired fiber distribution and orientation is described.

3.1 Design codes

In order to standardise UHPFRC applications and give UHPFRC designs more validation and substantiation, multiple recommendations and norms have been written. These norms are usually nationally applied so exclusively written and used by one specific country. For instance, the French have developed a code compatible with Eurocode 2 and use it as a national addition to this Eurocode. Japan has introduced recommendations for High Performance Fiber Reinforced Concrete in 2004 which mainly focusses on design and construct. Switzerland has also built many UHPFRC structures by applying its own UHPFRC specific norm. In the USA and Canada, technical recommendations about UHPFRC have been released where the American Concrete Institute (ACI) has also introduced a norm called “structural design of UHPFRC” (Sine, 2021).

The French and Swiss standard are of the most interest for applications in the Netherlands. One of the reasons for this is that both standards are developed within Europe. Moreover, the French standard is the only standard that is directly compatible to Eurocode 2 and is basically an UHPFRC addition to the Eurocode. The Swiss code, on the other hand, is the only standard that provides specific standards regarding UHPFRC strengthened structures. These are the two standards that will be discussed with the most detail. Afterwards, the effect of the varying fiber distribution and orientation on the design in the Japanese and Australian guidelines will be discussed.

3.1.1 Swiss guidelines

The Swiss code for UHPFRC design mostly contains calculations using rules of thumb and general design values for specific situations. In order to validate the usage of UHPFRC for these applications, a couple of tests should be performed according to the Swiss code. An overview of these tests can be found in Table 5.

Table 5: overview of tests in Swiss code in order to validate UHPFRC application, source: (EPFL-Swiss Federal Institute of Technology, 2016)

Type of test		Initial tests		Periodic quality tests		Suitability tests		Quality tests	
Responsible		Supplier of UHPFRC		Supplier of UHPFRC		Contractor		Contractor	
Test method	Reference		Frequency		Frequency		Frequency		Frequency
Workability	Section C.4	X	5 years	X	every production day	X	A	X	C
Compressive strength	Section C.1	X		X	all the 50 m³, at least 1 time per production week	X	A	X	D
Modulus of elasticity	Section C.1	X							
Tension by bending test	Appendix E	X		X	all the 150 m³	X	B	X	E
Tensile test	Appendix D	X		X	all the 1000 m³				
Impermeability	Section C.3	X							
Ability to be cast on sloping ground	Section C.5	X[1)]				X[1)]	A		
Bond strength by pull-off	Section C.6					X	A	X	D
Shrinkage	Section C.7	X							
Creep	Section C.7	X							

X: test to be performed
1) only if the UHPFRC is declared able to be cast on sloping ground
A: 1 time before each execution
B: 1 time before each execution, or if the volume of UHPFRC to cast exceeds 50 m³
C: 1 time per casting. During each delivery by the mixer lorry for specialized casting (slope> 5 % or casting with a machine)
D: at least 1 time per execution or all the 50 m³ of casted UHPFRC
E: at least 1 time per execution or all the 300 m³ of casted UHPFRC

Some of the calculations from the Swiss code are specifically developed for strengthening applications. Most of these calculations are only suitable for specific applications. The code also includes the description and requirements for multiple tests assessing flexural, shear or punching shear strength (EPFL-Swiss Federal Institute of Technology, 2016). The specific calculations will not be included in this Thesis.

The design strength in the Swiss standard is determined by estimating the tensile strength disregarding the effects of fiber orientation and distribution. These effects can negatively influence the tensile strength. This is why the standard includes a safety factor of 0.835 which is used to decrease the design tensile strength. According to this standard, the most commonly used UHPFRC type has a standard tensile strength of 7.0 MPa. Including the safety factor, results in a design tensile strength of 5.85 MPa. The standard also acknowledges the magnetic inductance method to be a reliable method of estimating the tensile strength. (Islam, Zhang, & Jin, 2022). This method will be discussed later.

3.1.2 French guidelines

The French have produced multiple recommendations considering UHPFRC that comply with the Eurocode. Three main documents have been produced as national additions to the Eurocode. NF P 18-710 is a design standard focusing on the design of UHPFRC structures (Toutlemonde, Bernardi, Brugeaud, & Simon, 2004). The design calculation methods used in these recommendations are based on many material tests and are usually very conservative (Berendsen, 2014). The product standard focusing on UHPFRC specification, performance, production and conformity is called NF P 18-470 which distinguishes Type S UHPFRC for structural applications and Type A or Z UHPFRC for non-structural architectural applications like facades. Lastly, NF P 18-451 has been produced focusing on the execution of UHPFRC applications (Toutlemonde, Bernardi, Brugeaud, & Simon, 2004).

3.1.2.1 Constitutive tensile law

The French recommendations distinguishes the tensile behaviour between Strain-softening and strain-hardening using classes T1, T2 and T3. Class T1 is the behaviour of UHPFRC in case of Strain-softening under direct tension. Limited strain-hardening happens for Class T2 specimen and significant strain-hardening happens for Class T3. This classification is dependent on the post-cracking strength (f_{ctf}) divided by the orientation factor K compared to the tensile limit of the elastic domain.

There is also a difference in the French recommendations for the tensile behaviour between thick and thin members. A thin member is defined by a thickness smaller or equal to three times the longest fiber length present in the element. Elements with a bigger thickness are considered thick (AFNOR, 2016).

3.1.2.2. Fiber orientation factor

The French Standard was the first standard to incorporate a fiber orientation factor K. The fiber orientation design factor in the French Standard is better defined than in the Swiss standard. In the French standard to factors are used: K_{global} and K_{local}. These factors are determined by the ratio between the strength of lab cast specimen and mock-up specimen. The factors have the goal of taking the difference in fiber orientation of the cast specimen and the actual application into account. This means mock-up tests are required for the calculation of the material (Islam, Zhang, & Jin, 2022).

The global factor is used for calculation of larger areas like the shear resistance of a slab. Local defects will not have a big influence on global properties. Besides this, a local factor exists to calculate stress distributions in very localized areas like the prestressing stresses at an anchor (Islam, Zhang, & Jin, 2022). The standard generally uses a value of 1.25 and 1.75 for K_{global} and K_{local}, respectively (AFNOR, 2016).

3.1.3 Japanese guidelines

The Japanese guidelines for UHPFRC also acknowledges the problem of segregation and varying orientation of the steel fibers. In the guidelines, it is recommended to place the fibers using tremie pipes or buckets. Continuous placement of the fibers is very important. Areas where multiple placements of fibers merge are avoided as much as possible as this will result into weak points of the UHPFRC element (Uchida, Niwa, Yoshihiro, & Katagiri, 2005).

The tensile strength of UHPFRC is obtained using a splitting tensile test with cylindrical specimen. The mean value of these destructive tests was 11.7 MPa with a standard deviation of 1.3 MPa. For safety reasons, the Japanese guidelines use a characteristic tensile strength of 8.8 MPa in their UHPFRC design (Uchida, Niwa, Yoshihiro, & Katagiri, 2005).

3.1.4 Australian guidelines

The Australian national standard includes three fiber orientation factors, K_s, k_{3Dt} and k_{3Db}. The factor K_s is a fiber orientation casting bias factor which is taken as a constant of 0.64, which is, for instance, used for shear design calculations. This factor is based on a 2D fiber orientation. The other two factors are three-dimensional orientation factors. These factors are variables dependent on the average fiber length and the specimen size (Islam, Zhang, & Jin, 2022).

3.2 Testing methods

Multiple properties to indicate the quality and strength of the UHPFRC can be measured, similar to normal concrete. The workability can be measured by the flow of the mixture using the cone slump-flow test. Also the initial and final setting time can be observed which are heavily influenced by temperature curing. The compressive strength can also be measured by using a modified version of the ASTM C39 standard testing method. UHPFRC has a way higher compressive strength than CC so the failure load is higher meaning the machinery has to provide more force. A different solution is using smaller cube samples than for CC. This is still representative for the material property because UHPFRC is much more homogeneous than CC due to its relatively small particles (U.S. Department of Transportation, 2013).

However, UHPFRC also shows to have a significant tensile capacity which can be measured using multiple tests like a dog-bone tensile test or a flexural 3-point bending test. However, this tensile strength is highly dependent on the fiber content/distribution and the orientation of the fibers. The fiber distribution and orientation might be optimal for the dog-bone specimen but that does not guarantee that the actual UHPFRC element will have the same distribution and orientation. This results in a significant amount of uncertainty and thus variety in tensile strength and ductility.

For the behaviour of UHPFRC, specific codes, described in Chapter 3.1, have simplified the stress-strain diagram. The actual tensile behaviour also depends on other factors like the distribution and orientation of the steel fibers. This given fact increases the uncertainty of the tensile behaviour for design calculations. This shows the relevance of decreasing the uncertainty in fiber distribution and orientation. Most designs with UHPFRC are based on a homogeneous fiber distribution and random fiber orientation. However, this is not always a reliable assumption for UHPFRC (Boulekbache, Hamrat, Chemrouk, & Amziane, 2010).

3.2.1 Destructive testing methods

Especially the tensile and flexural behaviour are dependent on the fiber distribution and orientation. A proper quality control test method to determine this fiber distribution and orientation is vital to gain more knowledge about the material and thus increase the reliability of applications. If UHPFRC behaviour can be predicted more accurately, designs can be optimised with a lot of benefits in aesthetic, financial, practical and sustainable areas.

In the past, the only existing methods to determine fiber distribution were destructive methods. The most common one is crushing or sawing a UHPFRC specimen and counting the fibers by hand. Manual counting will consume a lot of man hours and is therefore time-consuming and expensive. Also, the specimen is no longer usable after testing so the method is also non-sustainable. This is the case for all destructive testing methods. The problem of this destructive testing method is that it does not account for the fiber orientation. This method only gives information about the amount of fibers, thus the fiber content.

Another destructive testing method is a pull-off test, performed according to ASTM D4541-02. For this test, a cylindrical specimen is taken from the structure by a diamond or carbide-tipped core drill. After this the necessary load is measured to pull out the sample. Figure 41 shows the process of the method and the resulting cylindrical residues. This test is not able to predict the fiber content or fiber orientation (South Dakota Department of Transportation).

Figure 41: cylindrical specimens taken for destructive testing, source: (South Dakota Department of Transportation)

The most widely used destructive testing of concrete, measures the strength properties directly. For a compressive strength test, a standard 150 x 150 x 150 mm^3 compressive cube can be used. However, compressive machines usually have insufficient strength to crush a large UHPFRC cube. Due to the homogeneous mix of UHPFRC, it is allowed to use smaller cubes. The most common UHPFRC compressive cubes are 100 x 100 x 100 mm^3 where the loading area is a factor 2,25 smaller. This result is still representative because of the small aggregates and homogeneous mixture of UHPFRC (Kusumawardaningsih, Fehling, & Ismail, 2015).

The tensile strength of UHPFRC can be measured using a flexural bending test. This can be done using a 400 x 100 x 100 mm^3 beam under three-point bending. The measured flexural strength should be equal to the tensile strength if the material was fully homogeneous. There are some small imperfections in every UHPFRC beam but in general the material is quite homogeneous so this assumption can be made (Jiao, et al., 2022).

There is more direct way to measure the tensile strength of UHPFRC, by casting dog-bone specimen for multiple fiber contents. These dog-bones are exposed to a tensile force until the specimen fail. A dog-bone shape is used so the failure zone is relatively well determined, which is the thinner section of the specimen. The maximum tensile load at failure divided by the thin area of the dog-bone will be the tensile strength which is heavily dependent on the fiber content, distribution and orientation (Huang, Schlangen, & Lukovic, 2023).

3.2.2 Non-destructive testing methods

3.2.2.1 Translucent fluid

One method of studying fiber distribution and orientation is by using a translucent fluid. For instance, a Carbopol-based fluid can be used, which is a translucent polymer. It turned out that the yield stress of the hardened fluid, has a relationship with the fiber orientation. The relationship is shown in Figure 43 where the orientation factor is on the vertical axis. This factor indicates how many fibers are orientated perpendicular to the cross-section. This means the lower the yield stress of the translucent fluid, the better the fiber orientation. The difference can also be seen in Figure 42 where the left image (a) is made with a Carbopol-based fluid with a yield stress of 25 Pa and the right image (b) with a yield stress of 70 Pa. The fiber distribution in the former is much better compared to the latter (Boulekbache, Hamrat, Chemrouk, & Amziane, 2010).

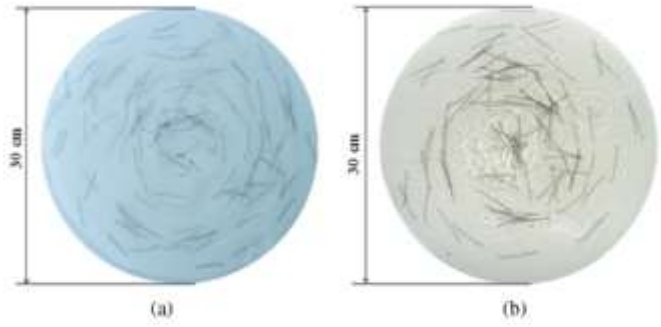

Figure 42: fiber orientation in Carbopol-based fluids with different yield stress, source: (Boulekbache, Hamrat, Chemrouk, & Amziane, 2010)

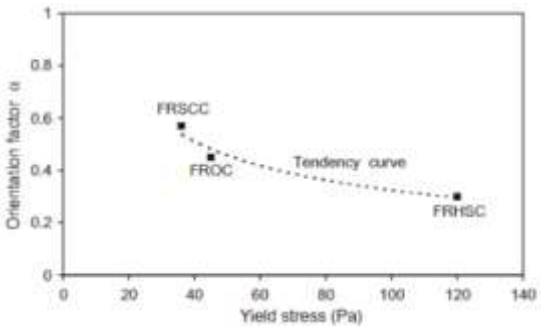

Figure 43: relationship yield stress and fiber orientation, source: (Boulekbache, Hamrat, Chemrouk, & Amziane, 2010)

3.2.2.2 Open coaxial transmission line

Another method of predicting the fiber content in a concrete mix is by using an open-ended coaxial probe. This probe sends an electromagnetic wave propagating in a transmission line like a regular coaxial cable. The reflection of this wave happens when the transmission line suddenly ends in an open circuit. The analysis of this reflected wave can give information about the material. Measurements with this probe showed a correlation between the fiber content and the phase differences in the measured reflection coefficient. This coefficient is related to the degree in which the wave will weaken when inside the specimen. This testing method is not suitable for industrial applications, since it was noted that the moduli showed saturation after the average range of dosages (Torrents, Juan-García, Patau, & Aguado, 2009).

Figure 44: Experimental setup of open coaxial transmission line, source: (Torrents, Juan-García, Patau, & Aguado, 2009)

3.2.2.3 Electrical resistivity methods

This NDT method is also developed for determining fiber orientation. To determine this property, this method used the electrical properties of the steel fibers. By measuring the resistivity, the general fiber orientation can be predicted. The whole method is based on the identification of the axes with the maximum and minimum resistivity. The fibers are mostly orientated perpendicular to the axis with the maximum resistivity, at local scale. The testing method is validated with a couple of slabs where the axis of maximum resistivity is locally determined at multiple spots in the slab. Both slabs also have a different casting position and thus a different fiber orientation pattern. The results can be seen in Figure 45 where it is clear that the fiber orientation can be determined relatively well since it is perpendicular to the axis of maximum resistivity, the arrows in the figure (Lataste, Behloul, & Breysse, 2008).

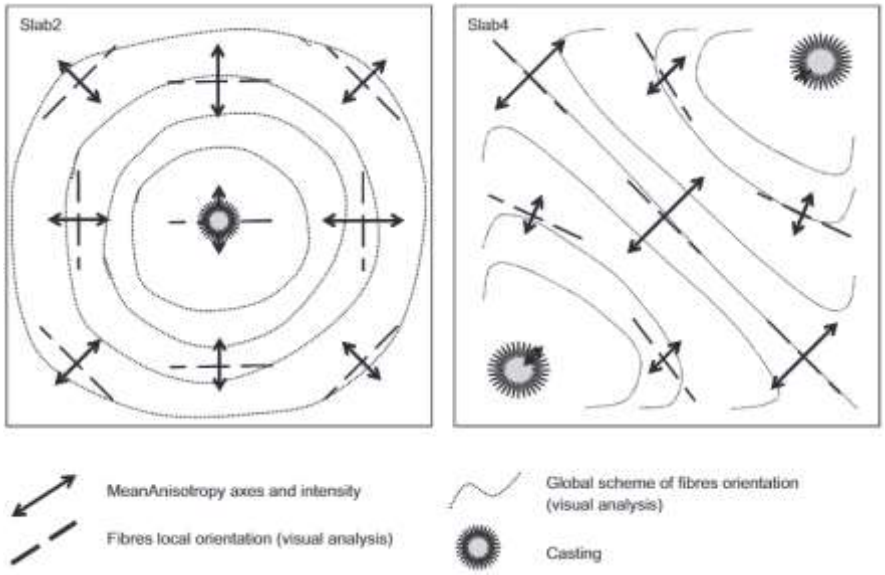

Figure 45: fiber orientation for different plates with different casting patterns, source: (Lataste, Behloul, & Breysse, 2008)

3.2.2.4 CT scan

The CT-scanner is mostly known for its contribution to the medical field. However, it can also help indicating the fiber distribution and orientation by scanning UHPFRC elements instead of human bodies. The scanner differs from a regular X-ray machine, by emitting not one X-ray beam but a series of X-ray beams. These beams go through a certain object, in this case a UHPFRC sample, showing the information of a singular 2D cross-section. All of the 2D images can be used to obtain a 3D image of the contents of the sample, showing the fiber distribution in a far more detailed manner than a single X-ray machine ever could. However, the issue of this method is the high costs and the limitation of element size that the CT-scanner can fit (Ruan & Poursaee, 2019).

3.2.2.5 Magnetic probe

The magnetic probe method is a NDT method for measuring both fiber content, fiber distribution and fiber orientation in UHPFRC specimen. The standard magnetic probe consists of a U-shaped ferrite core with a single copper wire around both core legs. This probe can be used to measure the inductance measured through the UHPFRC and the inductance through air. The inductance value through the UHPFRC sample increases along with the fiber content V_f and is influenced by the fiber orientation. The inductance is at its maximum when the direction of the probe legs is aligned with the fibers and at its minimum when the fibers are perpendicular to the axis of the magnetic field (Nunes S. , Pimentel, Sine, & Mokhberdoran, 2021). The next part will discuss this method in more detail.

3.3 Magnetic probe

3.3.1 Theory

This method is based on measuring the inductance through air and through a UHPFRC sample, completing a magnetic circuit with the probe. This inductance is defined as the amount of magnetic flux produced for a given electric current (Nunes, Pimentel, & Carvalho, 2016). One of the main parameters for this measuring method is the magnetic permeability which is defined as the inductance through the UHPFRC sample divided by the inductance through air. This parameter represents how easy it is to create a magnetic field within a measured object. It is much easier to create a magnetic field within a magnetic sample than through air or concrete. However, due to the ferromagnetic properties of the steel fibers, the magnetic circuit will be formed easier so the magnetic permeability will increase.

3.3.2 Evolution of probe

3.3.2.1 First magnetic probe development by TU Milan

In 2010, research for a non-destructive testing method started at the Technical University in Milan. The main goal of this research was to find a non-destructive method that gives information about the fiber size, concentration and orientation. They started experimenting with a magnetic probe, which was the first iteration of the magnetic probe. Figure 46 shows this first iteration along with a simulation of the magnetic flux caused by the probe (Faifer, Ottoboni, Toscani, & Ferrara, 2010).

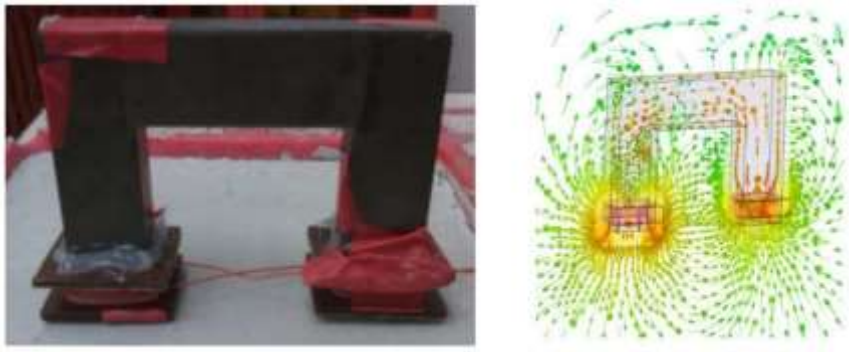

Figure 46: first iteration of magnetic probe and magnetic flux, source: (Faifer, Ottoboni, Toscani, & Ferrara, 2010)

The results from this magnetic probe showed that the higher the concentration of fibers, the higher the inductance results. Moreover, the probe also showed potential to measure the fiber orientation. The difference in magnetic inductance between perpendicular directions became higher if the probe was orientated along the average fiber orientation. This showed that the method had potential to measure both the fiber concentration and orientation (Mokhberdoran, 2020).

In 2011, the research team made two adjustments to the magnetic probe: a different magnetic circuit of the probe was used and there were wire windings placed on the top part of the coil increasing the amount of turns in the windings by 38 turns. The resulting iteration of the magnetic probe can be seen in Figure 47. This magnetic probe had similar results as the iteration before but gained higher inductance values due to the higher number of wire turns (Faifer, Ottoboni, Toscani, & Ferrara, 2010).

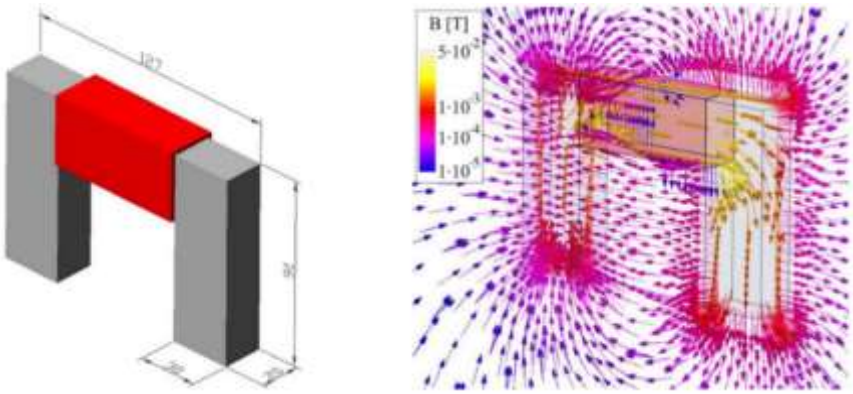

Figure 47: later iteration of magnetic probe and magnetic flux, source: (Faifer, Ottoboni, Toscani, & Ferrara, 2010)

3.3.2.2 Magnetic probe development by the University of Porto

The research team of both the Civil Engineering and Electrical Engineering faculties of the University of Porto had a couple of different goals. First of all, they wanted to develop a non-destructive testing method to measure the inductance not only on cubic or cylindrical specimen but also on thin plates made of UHPFRC. Furthermore, they also wanted to find a way to accurately predict the fiber content and orientation based on the measured inductances. The team was also able to develop a set-up that could align the fibers in a preferential direction. The developed magnetic probe consisted of a U-shaped ferrite core with a single copper wire coil around both legs of the core. The first iteration of the magnetic probe by the team in Porto can be seen on the left of Figure 48. On the right of Figure 48 the newer version of the magnetic probe is shown (Nunes, Pimentel, & Carvalho, 2016).

Figure 48: newer versions of the magnetic probe, source: (Nunes, Pimentel, & Carvalho, 2016)

3.3.2.3 Magnetic probe development by TU Delft

In order to do magnetic NDT measurements and do more research on the fiber behaviour within UHPFRC elements, the TU Delft has developed two different ferrite probes of their own. The C-shaped ferrite probe can be seen on the far right of Figure 49. This probe is very similar to the last iteration of the C-shaped ferrite probe from the University of Porto. However, this probe has more coil windings around each leg. The TU Delft has also created a single ferrite magnetic probe, shown on top of the wooden object in Figure 49. The effectiveness and benefits of this single ferrite probe compared to the C-shaped ferrite probe will be researched in this thesis. Both of these probes have not been used or tested yet. That is the reason why these probes first need to be calibrated. This will be explained later.

Figure 49: ferrite probes by TU Delft, photos taken by D. Kooreman

3.3.3 Calculations

One of the most important parameters of this method is the ratio between the measured inductance through the UHPFRC sample and the inductance through air. This air inductance should always be the same since air has no magnetic properties. This air inductance is considered as the reference / base value of the probe measurements. This value is different for different types of probe.

$$\mu_{r,i} \approx \frac{L_{UHPFRC,i}}{L_{air}} \quad (1)$$

$\mu_{r,i}$ = relative magnetic permeability [-]
$L_{UHPFRC,i}$ = inductance measured through the UHPFRC material [H]
L_{air} = inductance measured through the air / reference value [H]

By measuring in two perpendicular directions, the average relative magnetic permeability can be determined which is used to determine the fiber content and fiber orientation factor ρ_{ij}. The formulas for these parameters can be found below. In the formula for the fiber content, the calibration constant k_v is used which must be determined. In previous research, a relationship was found between the values of k_v and the thickness of the UHPFRC specimen. However, in order to use this formula, the factor $k_{v,ref}$ must be determined first experimentally, using a reference thickness of 50 mm (Nunes S. , Pimentel, Sine, & Mokhberdoran, 2021). This allows the comparison for different element sizes.

$$\mu_{r,mean} = \frac{1}{2}\left(\mu_{r,i} + \mu_{r,j}\right) \quad (2)$$

$$V_f = \frac{\mu_{r,mean}-1}{k_v} \quad (3)$$

$$\frac{k_v}{k_{v,ref}} = \sqrt{\frac{1-e^{-0.0642h_U}}{1-e^{-0.0642h_{U,ref}}}} \quad (4)$$

$$\rho_{ij} = \left(\rho_i - \rho_j\right) = \frac{\mu_{r,i}-\mu_{r,j}}{2\left(\mu_{r,mean}-1\right)} \; with \; i \perp j \quad (5)$$

$\mu_{r,mean}$ = average relative magnetic permeability between directions i and j [-]
$\mu_{r,i}$ = relative magnetic permeability in directions i [-]
$\mu_{r,j}$ = relative magnetic permeability in directions j [-]
V_f = fiber content by volume percentage [%]
k_v = angle between V_f and $\mu_{r,mean}$ / calibration constant [-]
$k_{v,ref}$ = k_v value corresponding to a UHPFRC element thickness of 50 mm [-]
h_U = thickness of UHPFRC element [mm]
$h_{U,ref}$ = reference thickness of UHPFRC element = 50 mm [mm]
ρ_{ij} = orientation indicator [-]

Formulas 1 through 5 are all found in previous literature, along with the corresponding parameters (Nunes S. , Pimentel, Sine, & Mokhberdoran, 2021).

The relationship between the fiber orientation factor and the mean fiber orientation angle differs slightly for different fiber contents. The relationship is defined by the formulas underneath along with a visual representative graph in Figure 50. This graph shows there is a slight difference in the orientation factor for fibers for angles of 0 and 90 but these differences are almost negligible (Li, Xia, Chin, & Jones, 2020).

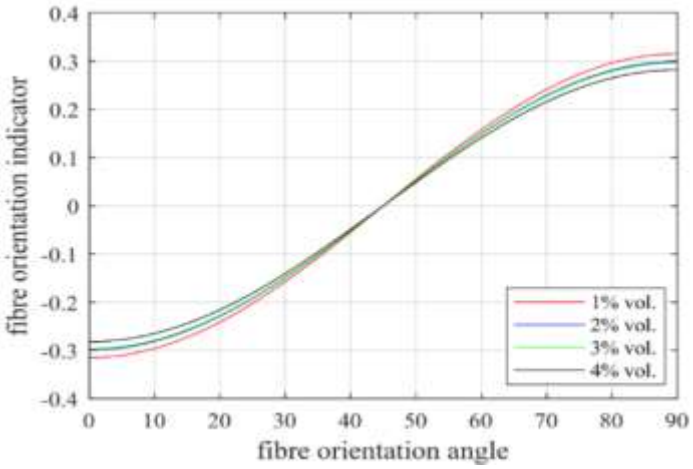

Figure 50: fiber orientation indicator versus angle for different fiber contents, source: (Li, Xia, Chin, & Jones, 2020)

The fiber orientation factor, α_0, and the fiber efficiency factor, α_1, have to be determined for the calculation of the post-cracking tensile strength. The orientation factor is defined as the probability of a fiber to intersect a planar surface perpendicular to a certain direction. Its value can differ between 0 and 1 where the value becomes 1 if all fibers are orientated perpendicular to the surface so θ = 0. The efficiency factor contains a number of phenomena but the most relevant is the dependency between the pull-out force and the angle of the fiber with regard to the fracture surface. Research has shown that fibers up to an angle of 60 degrees still have an effect on the pull-out capacity (Nunes S. , Pimentel, Ribeiro, Milheiro-Oliveira, & Carvalho, 2017).

$$\alpha_{0,i} = k_\alpha(\rho_i - \rho_j) + \alpha_{0,iso} \; with \; i \perp j \tag{6a}$$

$$\alpha_{0,j} = -k_\alpha(\rho_i - \rho_j) + \alpha_{0,iso} \; with \; i \perp j \tag{6b}$$

$$\alpha_{0,iso} = \begin{cases} \frac{2}{\pi}, & \frac{h_U}{l_f} \to 0 \; (2D \; distribution) \\ \left[\frac{2}{\pi}; 0.5\right], & in \; between \; 2D \; and \; 3D \\ 0.5, & \frac{h_U}{l_f} \to \infty \; (3D \; distribution) \end{cases} \tag{7}$$

$$\alpha_{1,i} = \begin{cases} 1.686\sqrt{\alpha_{0,i}} - 0.406, & \alpha_{0,i} < 0.70 \\ 1.0, & \alpha_{0,i} \geq 0.70 \end{cases} \tag{8}$$

$\alpha_{0,i}$ = fiber orientation factor in direction i	[-]
$\alpha_{1,i}$ = fiber efficiency factor in direction i	[-]
k_α = calibration constant determined by image analysis	[-]
$\alpha_{0,iso}$ = fiber orientation factor corresponding to fiber isometry	[-]
h_U = thickness of UHPFRC element	[mm]
l_f = length of steel fibers	[mm]

The constant k_α must be determined by some form of cross-section analysis, using specimens with different fiber contents and a wide variety of fiber orientations. This constant changes when using a different fiber type or a different probe. In a previous research, a value of 1.85 was found for this value so this can be used as a reference. The value of $\alpha_{0,iso}$ is dependent on the ratio of the element thickness and the fiber length. (Nunes S. , Pimentel, Ribeiro, Milheiro-Oliveira, & Carvalho, 2017). A different research found an average value of 0.6 for the orientation and efficiency factor multiplied. This value can be used if the fibers are moderately aligned along loading direction (Abrishambaf,

Pimentel, & Nunes, A meso-mechanical model to simulate the tensile behaviour of ultra-high performance fibre-reinforced cementitious composites, 2019).

All these factors can be used to predict the tensile strength of UHPFRC. For this calculation, the bond shear stress slip relationship is approximated by a rigid-plastic law and the assumption is made that the average pull-out length is a quarter of the fiber length. The formula below describes the tensile strength based on the orientation factor, the efficiency factor, the fiber content, the fiber length, the fiber diameter and the equivalent bond strength τ_f. This formula also includes the fiber factor, discussed in Chapter 5.2.7. The equivalent bond strength can be experimentally measured with a pull-out test and depends on both the matrix and the fibers (Nunes S. , Pimentel, Sine, & Mokhberdoran, 2021). In another research, this bond strength value was found to be 11.1 MPa (Abrishambaf, Pimentel, & Nunes, 2017).

$$f_{Utu,i} = \tau_f \alpha_{0,i} \alpha_{1,i} V_f \frac{l_f}{d_f} \quad (9)$$

$f_{Utu,i}$ = UHPFRC tensile strength in direction I [MPa]
τ_f = equivalent fiber-to-matrix bond strength [MPa]
$\alpha_{0,i}$ = fiber orientation factor in direction i [-]
$\alpha_{1,i}$ = fiber efficiency factor in direction i [-]
V_f = fiber content by volume percentage [%]
l_f = length of steel fibers [mm]
d_f = diameter of steel fibers [mm]

Formulas 6 through 9 are all found in previous literature, along with the corresponding parameters (Nunes S. , Pimentel, Sine, & Mokhberdoran, 2021).

3.3.4 Sensitivity of distribution and orientation measurements

3.3.4.1 Fiber distribution

The measured inductance increases for a higher fiber content in the measured area. This increase of the inductance with the fiber content is shown in Figure 51a and 51b. The relationship between the mean relative magnetic permeability and the fiber content is also given by formula in Figure 51b. This formula includes the parameter k_v and a constant of 1. This k_v parameter, which represents the slope of the relationship, has to be calibrated before the results can be interpreted. The constant of 1 can be explained logically. If the fiber content is 0%, there are no fibers present which means the sample consists of concrete matrix only. This matrix has no magnetic properties, just like air, which means the measured inductance value will have the same value as the reference value. This results in an average magnetic

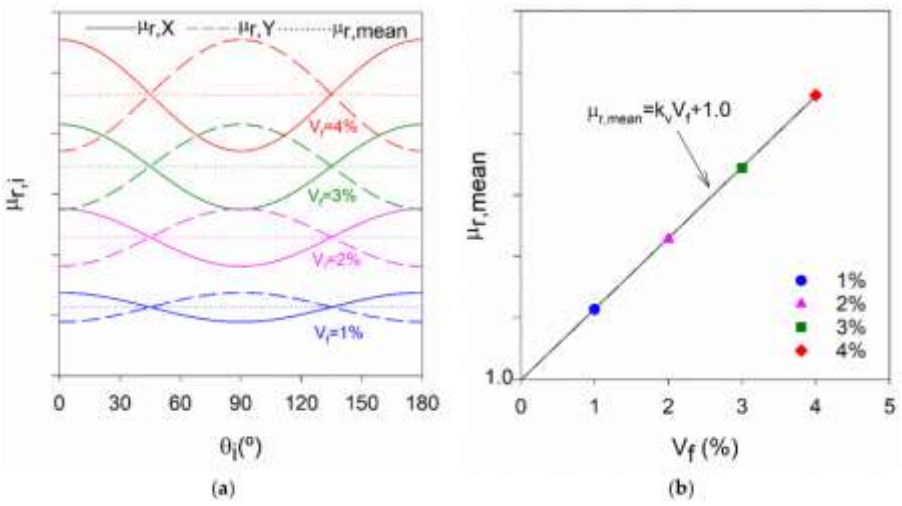

Figure 51: variation of relative inductance with measuring angle and fiber content, source: (Nunes S. , Pimentel, Sine, & Mokhberdoran, 2021)

permeability of 1.0 (Nunes S. , Pimentel, Sine, & Mokhberdoran, 2021).

Table 6 below shows the results of a magnetic probe measurement calibration. For these results, the NDT methods was applied on 150x150 mm^2 UHPFRC plates with a thickness of 25 or 30 mm. Multiple elements had been cast with different fiber contents. The fiber content in volume percentage is denoted in Table 6 by V_f. This research noted that the k_v value increases with the length of the fibers and the thickness of the element, which is to be expected (Sine, 2021).

Table 6: data from UHPFRC specimen and determined kv values, source: (Sine, 2021)

Ref.	h_U [mm]	l_f [mm]	d_f [mm]	V_f [%]	k_v [-]
DEWST1	25	9-12 [a])	0.175	0.5	4.12
				1.5	
				3.0	
DEWST2	30	13	0.2	1.0	4.68
				2.0	
				3.0	
				4.0	
DEWST3	25	10	0.175	1.0	3.90
				2.0	
				3.0	
				4.0	

The amount of fiber segregation over the element thickness can also influence the value of k_v. In Figure 52, HRk plates are horizontally cast plates without forced fiber orientation, HOk are horizontally cast plates with forced orientation and VRk are vertically cast plates without force orientation. Figure 52 showed that plate type HRk showed significant fiber segregation towards the bottom. This affects the factor in the linear relationship between V_f and $\mu_{r,mean}$, which is k_v. The other plate types have a mean value of 4.16 while the HRk plates have a mean value of 5.37 (Sine, 2021). This also shows that a more constant and reliable fiber distribution can result in a far more reliable prediction of the material properties.

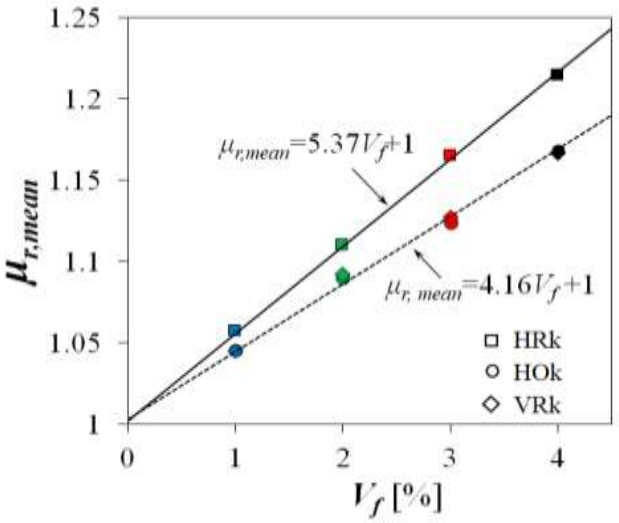

Figure 52: mean relative inductance and fiber content relationships with different k_v values, source: (Sine, 2021)

3.3.4.2 Fiber orientation

For the fiber orientation, a thin sheet of plastic can be prepared with a line every 15 degrees. This is done so the magnetic probe can be aligned with these lines and the inductance can be measured every 15 degrees (Figure 53a). This results in a graph like in Figure 53b. The inductance value becomes higher if the magnetic probe is aligned in the same direction as the fibers. Figure 53b clearly has the highest inductance values for an angle of 0 degrees. This means that more fibers are aligned with this angle of zero degrees (Sine, 2021). The exact orientation parameters can also be calculated using the formulas given when explaining the magnetic NDT method.

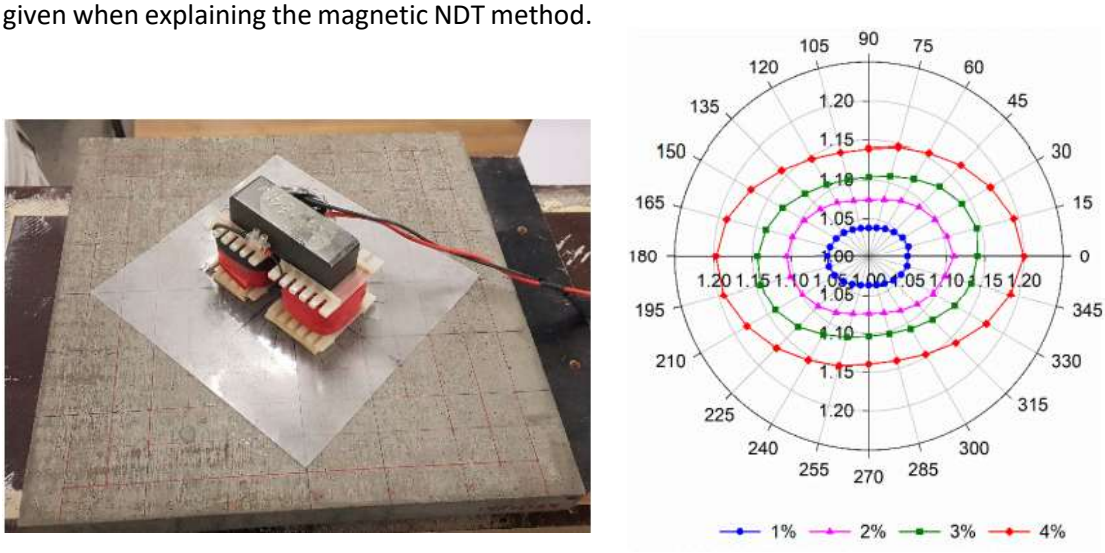

Figure 53: inductance measurement set-up every 15 degrees and orientation results, source: (Sine, 2021)

With this information gathered, the local fiber distribution and orientation is known and can be used to determine the global and local behaviour of this element. A visual representation of a possible fiber distribution and fiber orientation can be seen in Figure 54a and Figure 54b for an area of 800 by 900 mm. Figure 54a shows the fiber orientation in a grid of 50 mm where a similar semi-circle like in the previous figure is given at each point of the plate. Figure 54b shows the fiber content over the entire plate. It is clear that there is segregation in this plate since the top left corner has a significantly higher fiber content than the rest of the plate (Sine, 2021).

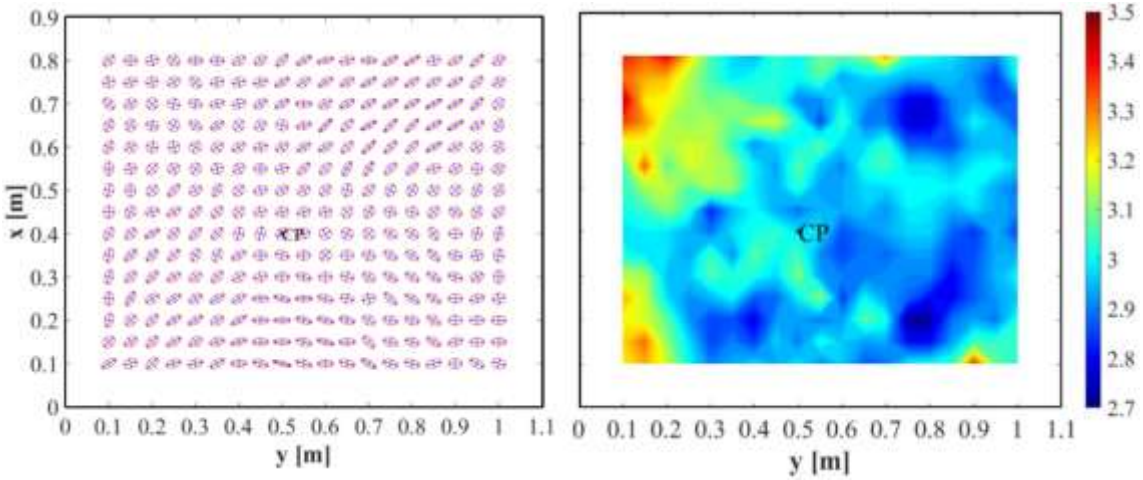

Figure 54: fiber orientation and distribution measured in UHPFRC plate, source: (Sine, 2021)

3.3.4.3 Effective depth of magnetic probe

The effective testing depth of this magnetic NDT method is approximated using experimental data. By placing acrylic plates between the magnetic probe and the UHPFRC specimen, the distance between the probe and the specimen was increased. For multiple thicknesses of the acrylic plates in between, the magnetic permeability was measured. This value was used in the formula below for μ_1 and the magnetic permeability when placing the probe directly on the specimen is denoted as μ_0. The values of 1 in this formula are representative for the magnetic inductance of air (Li, Xia, Chin, & Jones, 2020).

$$AF_t = \frac{\mu_t - 1}{\mu_0 - 1} \times 100\% \quad (10)$$

AF_t = attenuation factor for probe distance t [-]
μ_t = relative magnetic permeability for probe distance t [-]
μ_0 = relative magnetic permeability for probe directly on specimen [-]

This testing was done using UHPFRC specimen with 2% and 2.5% volume of fibers. For each fiber content, two points were measured so four points in total. The results can be found in Table 7 and Figure 55. This data shows that the attenuation factor drops below 10% for depths greater than 24 mm which shows that fibers this far away barely have any effect on the measured relative magnetic permeability. That is why it was concluded that the effective depth of the magnetic probe is around 24 mm. This value is only valid for the specific probe used. (Li, Xia, Chin, & Jones, 2020).

Table 7: attenuation factor measurements using different fiber contents and distances from probe, source: (Li, Xia, Chin, & Jones, 2020)

t (mm)	2% vol.—A	2% vol.—B	2.5% vol.—A	2.5% vol.—B
0	100%	100%	100%	100%
2	75%	72%	77%	73%
4	57%	54%	57%	58%
8	40%	39%	39%	40%
12	23%	23%	24%	26%
15	19%	19%	16%	19%
17	14%	15%	13%	15%
20	10%	13%	12%	12%
24	6%	7%	7%	6%
32	3%	2%	4%	4%
36	3%	3%	3%	3%

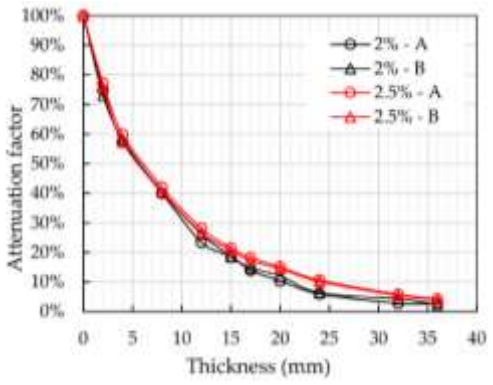

Figure 55: attenuation factor for different distances from probe, source: (Li, Xia, Chin, & Jones, 2020)

The effect of specimen thickness on the k_v value has also been researched in previous researched, as defined in Formula 4. For this research, instead of 50 mm, 100 mm was taken as the reference thickness. The result can be found in Figure 56 where the value of 1 on the y-axis is reached at the reference thickness (Nunes S. , Pimentel, Sine, & Mokhberdoran, 2021). As can be seen in the figure, this relationship is not dependent on the fiber content but it might differ per probe type. That is why it is not advised to use this relationship for different probe types.

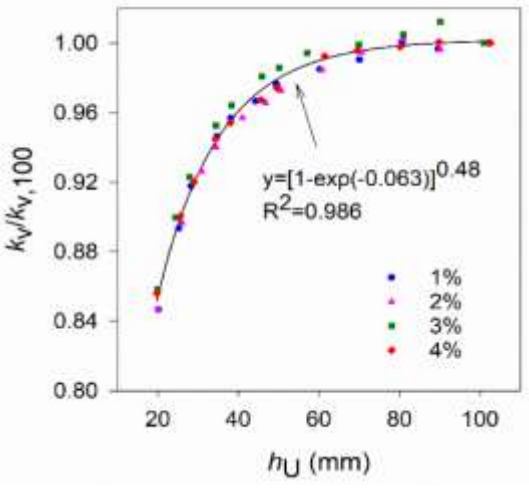

Figure 56: Relationship k_V value and thickness, source: (Nunes S. , Pimentel, Sine, & Mokhberdoran, 2021)

3.3.4.4 Edge effect

The so-called “edge effect” takes place when the probe is placed to closely to the edge of a UHPFRC element. The created magnetic field from the probe extends over a certain area outside of the probe. The inductance value becomes higher if there are more fibers in this measurement area. If the probe is placed at the edge of a UHPFRC element, there will be a part of the measurement area where there is no UHPFRC present, meaning there are no fibers with ferromagnetic properties. This will result in a decrease of the inductance value: the edge effect.

Previous study has found that the used C-shaped ferrite probe had a minimum edge distance of 100 mm. After the plate was reduced to 200 x 200 mm, the inductance value started dropping quickly. The results are shown in Figure 57 where the ratio of the inductance decrease and the specimen size decrease was considered on the right y axis. This result shows a clear decrease for specimen sizes smaller than 20 cm. That is why the edge distance of 100 mm was found to be the minimal edge distance for the given probe type in order to minimize the edge effect (Nunes S. , Pimentel, Sine, & Mokhberdoran, 2021).

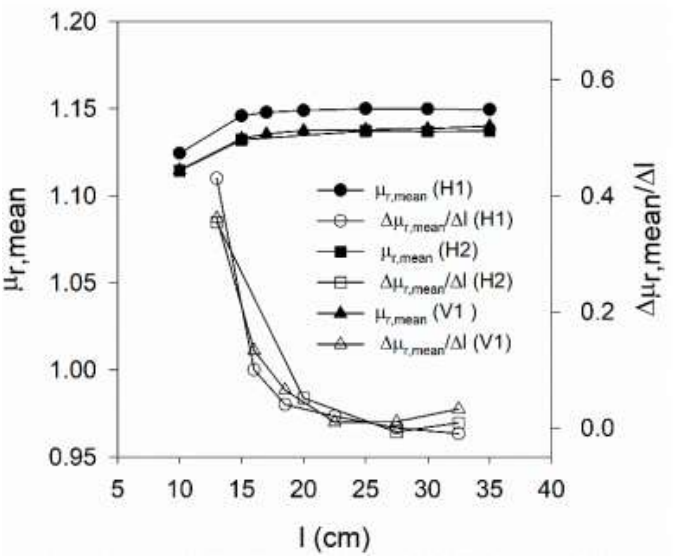

Figure 57: variation of $\mu_{R,mean}$ with specimen size l, source: (Nunes S. , Pimentel, Sine, & Mokhberdoran, 2021)

3.4 Characterization of fiber distribution and orientation

3.4.1 Fiber distribution

Multiple methods have been proposed by researchers to quantify the fiber distribution where most try to quantify the amount of fiber segregation. For instance, the formula below can be used to calculate the degree of segregation along the height of the UHPFRC element h_U. In this formula, the value z refers to the distance of the fiber to the top of the element. This means the fibers will be distributed symmetrically in the midplane for a segregation degree of 0.5 (Sine, 2021).

$$\xi_{seg} = \frac{1}{h_U N_f} \sum_{i=1}^{N_f} z_i \qquad (11)$$

ξ_{seg} = degree of segregation [-]
h_u = height of UHPFRC element [mm]
N_f = number of fibers [-]
z_i = distance of fiber to the top of the element [mm]

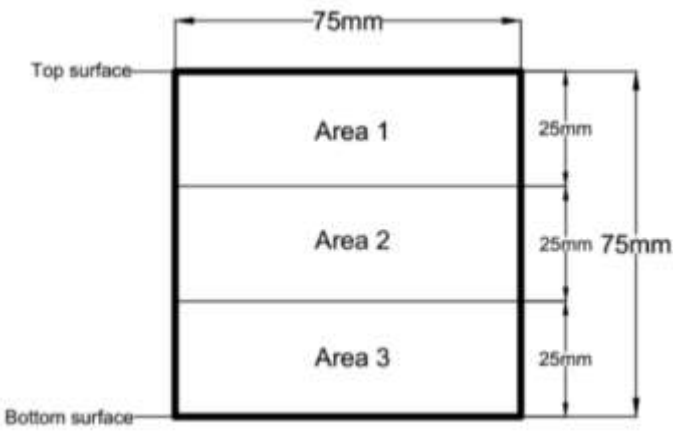

Figure 58: areas in specimen to determine sedimentation, source: (Li, Xia, & Galobardes, 2018)

Another parameter describing the amount of segregation is the sedimentation ratio. This is the ratio between the number of fibers in the bottom and top part of the specimen. Figure 58 shows a general UHPFRC sample. In this figure, Area 1 is the top region of the element and Area 3 is the bottom region. As mentioned, the sedimentation ratio is a simple ratio determined by the formula below. Usually, the value of the sedimentation ratio exceeds 1 since fibers tend to agglomerate to the bottom of the specimen (Li, Xia, & Galobardes, 2018).

$$Sedimentation\ ratio = \frac{N_{f,Area\,3}}{N_{f,Area\,1}} \quad (12)$$

Both these segregation factors are not very suitable for the magnetic NDT method since the NDT method does not quantify the number of fibers. This research will assess the fiber distribution along the plane of the plate and not over the thickness.

3.4.2 Fiber orientation

Normally in an environment without restrictions, a fiber can freely rotate in all three dimensions. This is defined in a spherical coordinate system instead of an orthogonal system. In this case, an orientation needs to be defined. A direction in the three-dimensional space is defined by the azimuth and the elevation (see Figure 59) (Sine, 2021).

However, depending on the application, the fiber orientation might be restricted. For instance, fiber movement within a thin plate is restricted in the direction of the thickness. This means the elevation will tend more towards 0° than 90°. This case can be simplified as a two-dimensional problem where the only variable is the azimuth (Sine, 2021). Using this information, the amount of fibers in a certain direction can be measured. Figure 60 is an example of the results from measuring the fiber orientation of 4 specimen with different fiber contents. For this experiment, the measurement was done every 15° (Nunes S. , Pimentel, Sine, & Mokhberdoran, 2021).

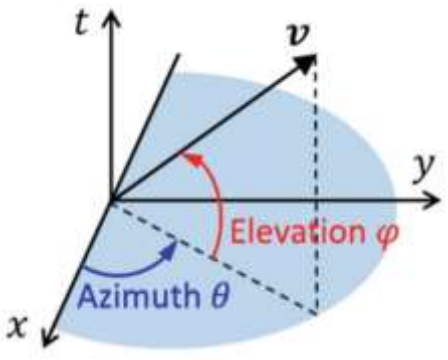

Figure 59: Spherical coordinates for fiber orientation, source: (Bhandari & Babar, 2018)

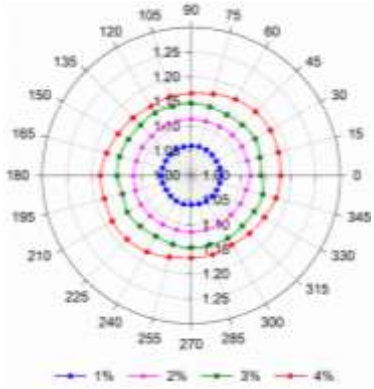

Figure 60: Example fiber orientation in 2D for thin UHPFRC plate, source: (Nunes S. , Pimentel, Sine, & Mokhberdoran, 2021)

3.5 Influences on fiber distribution and orientation

3.5.1 Workability

Fiber distribution and orientation is directly influenced by the workability, also known as flowability or rheology. This flowability must be controlled within a certain spectrum. If the concrete mix is very fluid, the fibers have a lot of mobility and will move easily under the effects of light external vibration. This effect might lead to fiber segregation. A stiff concrete mix, on the other hand, has a high risk of fiber conglomeration. The fibers can clump together limiting the movement of the fibers. This also happens if the fiber content is too high. In this case, a homogeneous fiber distribution will be much less probable and the difference in local effects will be significant. The effect of a stiff concrete mix proved to be bigger and more negative than for a fluid mix (Boulekbache, Hamrat, Chemrouk, & Amziane, 2010).

In previous research, the effects of cement content and fiber content on the relative slump flow was researched. For three different cement contents, a linear relationship was found between the relative slump flow and the fiber content, which is shown in Figure 61. For the mixtures UHPC1, UHPC2 and UHPC3 a cement content of 875 kg/m^3, 612 kg/m^3 and 699 kg/m^3 was used, respectively. The water content and amount of superplasticizer was kept constant. A higher cement content resulted in less workability. This research uses three fiber types: straight steel fibers, hooked end steel fibers and polypropylene fibers. (Yu, 2015).

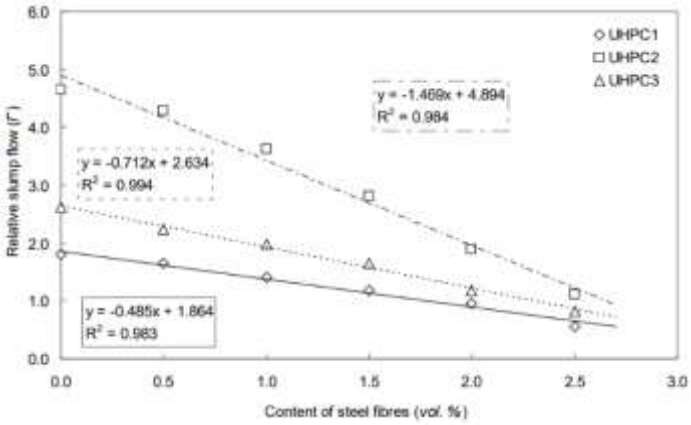

Figure 61: Slump flow vs fiber content for different cement contents, source: (Yu, 2015)

A different research wanted to find the relationship between the slump flow diameter and the fiber factor. The fiber factor is a combination of the fiber content and the slenderness of the used fibers, which can be seen on the x-axis of Figure 62. In this research, the fiber length remains 13 mm and the fiber diameter 0.2 mm. This means the fiber factor has a linear relationship with the fiber content. A relationship was found consisting of 3 different regions. The first region had a constant relationship from a fiber factor of 0 up to 1. Between a fiber factor of 1 and 2, the relationship is slightly decreasing linearly. After a fiber factor of 2, the flow diameter decreases a lot quicker due to fiber agglomeration. This is also shown in Figure 62 (Nunes, 2017). Another research mentions that a flow diameter exceeding 265 mm might lead to fiber segregation. (Nunes S. , Pimentel, Sine, & Mokhberdoran, 2021).

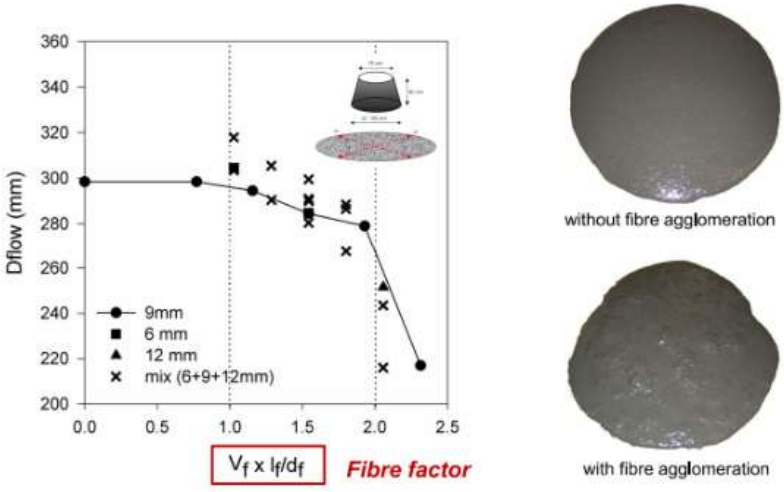

Figure 62: flow diameter vs fiber factor, source: (Nunes, 2017)

There are three different reasons that the addition of steel fibers decrease the workability of the UHPFRC mixture. One of which is the relatively high surface area to volume ratio. Due to the elongated shape of the steel fiber the surface area to volume ratio is much higher than that of other mix materials like the aggregates. This increased surface area results in bigger cohesive forces between the fibers and the matrix decreasing the workability. The decrease in workability is also caused by the stiffness of the steel fibers. The stiff fibers can push apart particles larger than the fiber length changing the structure of the granular skeleton. The final reason can be the shape of the steel fibers. Some fibers have hooked ends or have a sinusoidal shape to increase the anchorage between fiber and concrete matrix. However, this also increases the friction and thus decreases the mixtures workability. The second reason can be eliminated by using a small fiber length and the last reason can be eliminated by only using straight fibers. So when using short and straight steel fibers, the only cause for a decrease in workability is the bigger cohesive forces (Yu, 2015).

A different research also noted that the adequate viscosity is required to align the fibers properly. The study showed that high viscosity and low yield stress result in the best fiber alignment. It should be noted, however, that high viscosity can reduced the velocity of the UHPFRC casting flow. In this case fibers might not align as well with the flow direction and the fibers might get entangled (Islam, Zhang, & Jin, 2022).

3.5.2 Mould dimensions

The dimensional limits of the casting mould, the walls, will also influence the fiber orientation. This is called the “wall effect”. It generally only occurs when the distance of the fiber to the wall is less than half the fiber length. Fibers tend to align with the direction of the wall because of the physical barrier that the wall forms. Furthermore, the flow velocity is much smaller at the wall than away from the wall due to shear resistance of the wall. This will also cause the fibers to align with the direction of the mould walls (see Figure 63) (Boulekbache, Hamrat, Chemrouk, & Amziane, 2010).

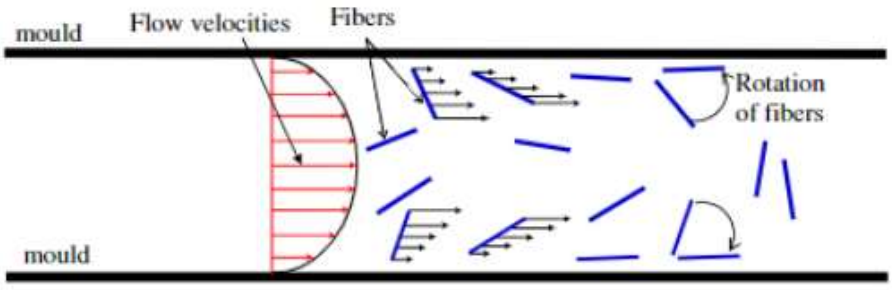

Figure 63: wall effect for fibers in narrow mould, source: (Boulekbache, Hamrat, Chemrouk, & Amziane, 2010)

The influence of this wall effect depends on the dimensions of the mould. The effect is much more significant for small-scaled elements so it also contains an additional size-effect. Figure 64 shows that the percentage of an element affected by the wall effect, the wall effect zone, is much bigger for narrow moulds. For a very narrow flow channel, the middle zone without the wall effect is so thin that the fibers will still orientate relatively well in the direction of the mould wall (Akeed, et al., 2022).

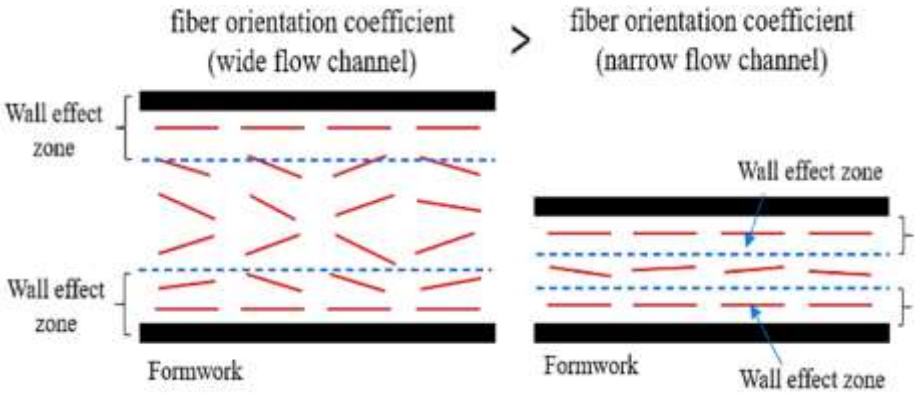

Figure 64: wall effect for fibers in wide and narrow flow channel, source: (Akeed, et al., 2022)

The same principle holds for the fiber length. Longer fibers are more vulnerable to the wall effect when the mould dimensions are smaller than the fiber length. Figure 65a shows this effect visually where it is shown that short fibers are also influenced by the addition of longer fibers. This way, the short fibers will also tend to orientate more horizontally. Figure 65b shows the same mould but now there are only short fibers present in the mixture. The wall effect is still present here but outside of the wall effect zone, the short fibers have a more random orientation (Yu, Spiesz, & Brouwers, 2014).

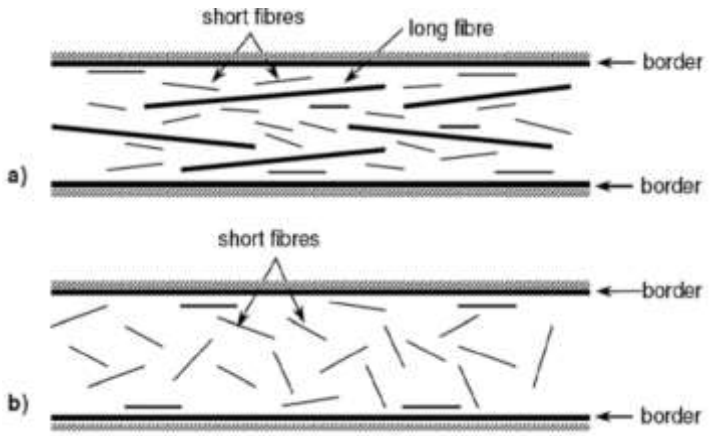

Figure 65: wall effect for short and long fibers, source: (Yu, Spiesz, & Brouwers, 2014)

3.5.3 Mould orientation

There are also multiple configurations in which a mould can be positioned during casting. A slab can be placed vertically and horizontally when casting. Horizontal casting is the most used method but plates will likely have a rough surface resulting in an uneven plate thickness. This can be solved by polishing but this will cost more time and money. On the other hand, placing the mould in a vertical position guarantees a constant plate thickness. Gravity will have more influence on the specimen because the gravity works parallel to the plane of the plate. This might lead to a worse fiber distribution since more fibers will move to the bottom of the plate. This is also influenced a lot by the flowability of the mixture (Nunes S. , Pimentel, Sine, & Mokhberdoran, 2021). The difference in casting orientation for this research is shown in Chapter 4.

Figure 66 below shows an example of a UHPFRC 0.03x0.85x1.10 m^3 plate cast in vertical positioning. The ovals in the figure represent the main fiber orientation at that point. The casting was done from one side of the mould. In general, most fibers seem to orientate vertically along with the direction of the flow. However, near the bottom of the plate, more fibers are orientated horizontally. This could possibly be explained by the wall effect (Sine, Pimentel, Nunes, & Mokhberdoran, 2020)

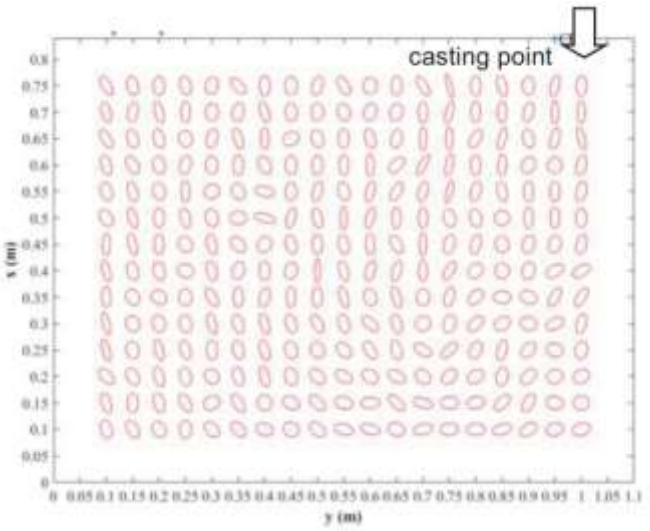

Figure 66: fiber orientation in UHPFRC plate cast vertically, source: (Sine, Pimentel, Nunes, & Mokhberdoran, 2020)

3.5.4 Casting flow type

The way the concrete mix flows within a mould has a big influence on the orientation and distribution of fibers. As depicted in Figure 67a, a simple straight confined flow direction can lead to a shear flow where most fibers will align with the flow direction. For a converging flow direction, the fibers tend to have more of an angle when the flow size decreases giving a very high fiber alignment along the flow direction. On the other hand, a diverging flow will result in a very low fiber alignment along the flow direction. The fibers tend to orientate more perpendicular to the flow direction for a diverging flow. Similar to Figure 67a, Figure 67d shows a straight flow. However, now the flow is not confined at the edges so the end forms more of an arch, also known as a fountain flow. Such a flow can also cause the fibers to align perpendicular to the flow direction. The radial flow in Figure 67e has the same effect where fibers align perpendicular to the flow direction (Kang & Kim, 2011).

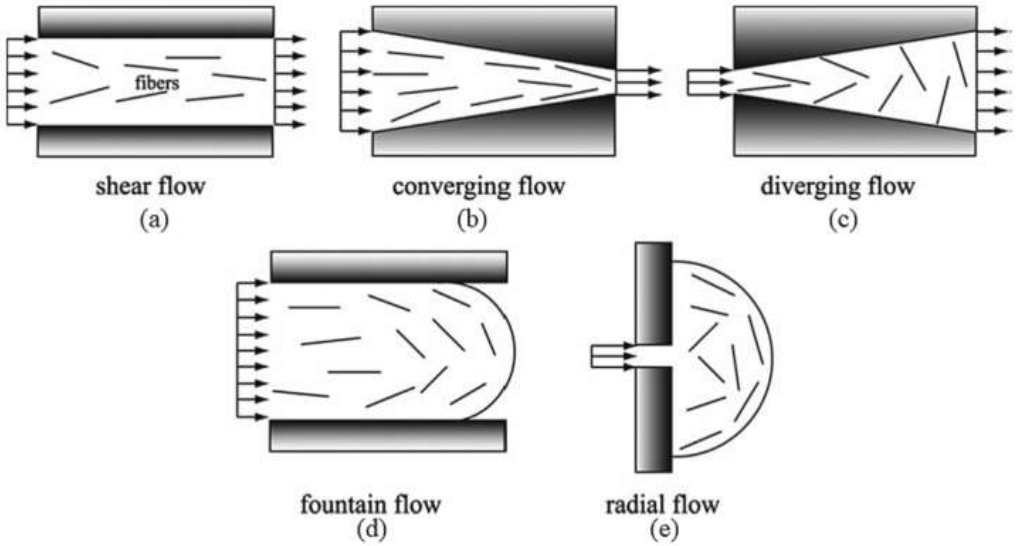

Figure 67: fiber orientation behaviour for different flow types, source: (Islam, Zhang, & Jin, 2022)

3.5.5 Casting placement

Research has also been done about the location of casting relative to the mould. When casting from one of the edges of the mould, a shear flow or fountain flow will take place towards one direction. Usually a mould will confine the flow direction so the fibers will orientate in the direction of the flow. For a beam this is usually the principal stress direction so this is beneficial for the bending moment capacity. On the other hand, casting at mid-span can disturb the fiber orientation meaning the flexural capacity will be less compared to casting from the sides (Yang, Joh, & Kim, 2010).

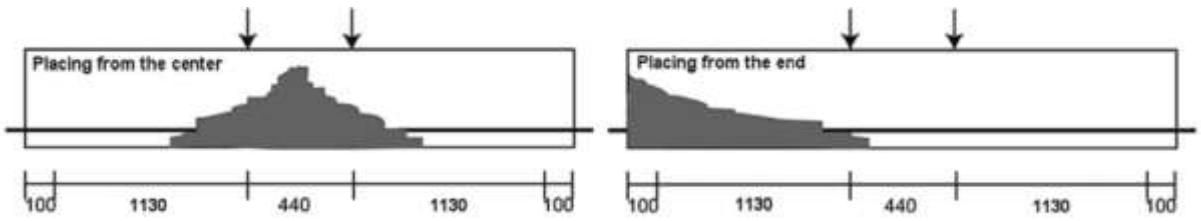

Figure 68: fiber distribution for casting at the center and at the end, source: (Yang, Joh, & Kim, 2010)

Fiber orientation when casting a circular slab have also been investigated for different casting placements. Casting in the middle of the slab generally results in fibers aligning perpendicular to the radius of the slab (A in Figure 69). Casting from the edges of the slab causes fibers to align along the radius of the slab (B in Figure 69). Finally, casting at random places also results in a random fiber orientation (C in Figure 69) (Barnett, Lataste, Parry, Millard, & Soutsos, 2009).

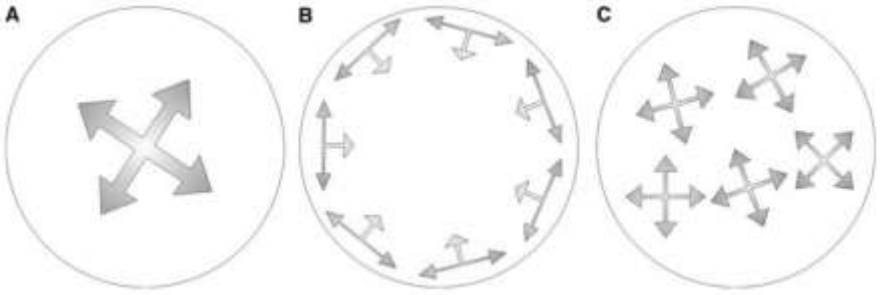

Figure 69: fiber orientation for different casting methods, source: (Barnett, Lataste, Parry, Millard, & Soutsos, 2009)

The difference in casting from the center and casting from the end of an element is also tested experimentally. Figure 70 shows an image analysis of two different casting placements. Figure 70a shows the cross-section of an UHPFRC element when casting from the center of the element. Figure 70b shows the same but for casting from the end of the element. The latter shows a higher number of fibers while the fiber content is the same. This is because the fibers are orientated perpendicular to the cross-section, because of the casting placement. This is a familiar concept when manually counting the fibers. The higher the amount of fibers counted, the more perpendicular the orientation of the fibers to the cross-section. This also explains why the fibers in Figure 70b are all singular points since this is the cross-section of the fibers. Figure 70a, on the other hand, shows less fibers where some fibers can be seen as longer lines indicating a different fiber orientation.

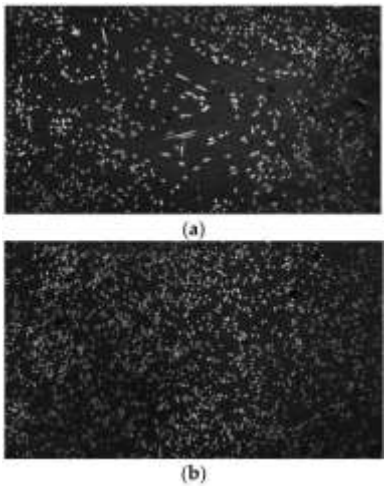

Figure 70: fiber orientation for casting from the center (a) and casting from the end (b), source: (Choi, Kang, Lee, Koh, & Ryu, 2016)

3.5.6 Fiber type

UHPFRC elements with different fiber lengths were also tested to find the effect of fiber length. In this research, three different lengths were used: 13 mm, 16.3 mm and 19.5 mm. The fiber length had little effect on the fiber distribution but a significant influence on the fiber orientation. The shorter fibers had more tendency to align along with the flow direction than longer fibers. However, the wall effect was more present for the longer fibers (Yoo, Kang, & Yoon, 2014).

The shape of the fiber is also a very important variable in the determination of the tensile strength of UHPFRC. A lot of fiber shapes exist, each with a different pull-out force value. The pull-out mechanism of a fiber can be divided up in five different phases.

1. Elastic or plastic deformation of the fiber
2. Debonding between fiber and concrete matrix
3. Friction of fiber pull-out
4. Pulling the fiber shape in a more straight form
5. Breaking of the fiber

Figure 71 shows the pull-out load of a fiber versus the pull-out slip for three different fiber shapes: a hooked fiber, a corrugated fiber and a straight fiber. The hooked fiber attains the highest pull-out load (Akeed, et al., 2022). This is mostly due to the high friction of fiber pull-out and the strong force necessary to pull the fiber into a straight form (phase 3 and 4 of the fiber pull-out) (Reitsema, 2012).

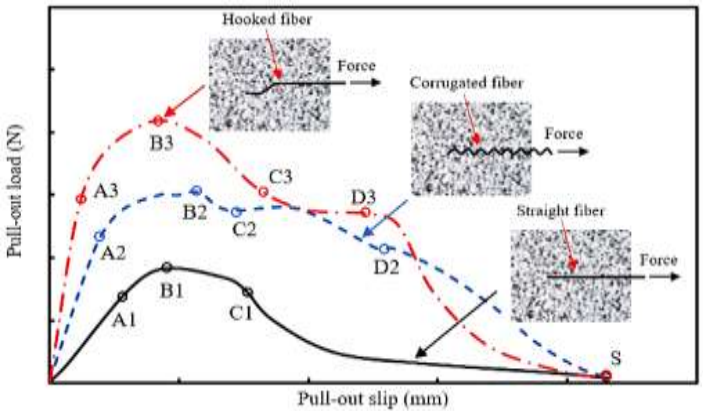

Figure 71: fiber pull-out load versus slip for different fiber shapes, source: (Reitsema, 2012)

One of the most important parameters to define the fiber type is the fiber factor which is defined by the fiber content multiplied by the aspect ratio of the fibers. The aspect ratio quantifies the slenderness of the fiber and is calculated by dividing the fiber length by the fiber diameter. The fiber factor mostly influences the tensile and flexural capacity of UHPFRC elements. The higher the fiber factor, the higher the strength (Yazici, Inan, & Tabak, 2006).

3.5.7 Vibration of the element

Vibration of UHPFRC elements on a vibration table causes sedimentation of steel fibers meaning the fibers will have segregation towards the bottom. The exact determination of the effects of vibration have been quantified by calculating the sedimentation ratio, as defined in Formula 12. In this experiment 6 UHPFRC prisms were cast without vibration and 6 UHPFRC prisms were cast on a vibration table and vibrated for 15 minutes at 50 Hz frequency. As can be seen in Table 8, the sedimentation ratio of increases from 1.098 to 1.236 due to this vibration. This is an increase of 12.5%.

Table 8: sedimentation ratio with and without vibration of specimen, source: (Li, Xia, & Galobardes, 2018)

Specimen Number	Tested Inductance(mH)	Number of fibres	Sedimentation ratio
3% Vibrated top	20.088	665	1.236
3% Vibrated bottom	20.654	804	
3% Non-vibrated top	19.990	695	1.098
3% Non-vibrated bottom	20.573	750	

Another research on UHPFRC from 2022 applies a novel double-axis vibration mixing technology. It is claimed that this vibration technology improves the fiber distribution and reduce the standard deviation of fiber orientation. The concrete matrix without fibers is first vibrated for three minutes before adding the fibers. After the fibers are added, the mixture is vibrated for one more minute. It should be noted that a UHPFRC mixture was used with a relatively small water-to-cement ratio of 0.16 (Zheng, Zhou, Nie, Luo, & Huang, 2022).

3.5.8 Alignment using electro-magnetic field

The fiber orientation can be influenced manually using a uniform magnetic field where the magnetic properties of the fibers will result in a tendency of the fibers to rotate in the direction of this magnetic field. If all tensile stresses in the element have the same orientation, the efficiency of the steel fibers is at a maximum. It is important that the magnetic field is uniform over the entire specimen. If this is not the case, the fibers will concentrate towards the spot with higher induction of the magnetic field and the fiber distribution will be influenced. Figure 72 shows a set-up that can be used to orientate the steel fibers. The result of this orientation method can be seen in Figure 73 where Figure 73a shows the steel fibers after using the method and Figure 73b shows the steel fiber orientation without the method. In the 3D case, the fiber orientation factor can increase from a mean of 0.50 to 0.90, increasing the possible efficiency of the fibers (Mu, Li, Qing, Lin, & Zhao, 2016).

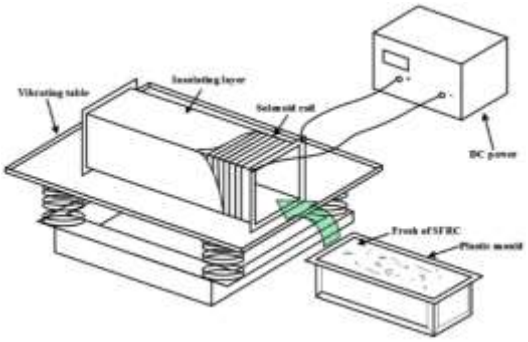

Figure 72: electro-magnetic field set up to orientate steel fibers, source: (Mu, Li, Qing, Lin, & Zhao, 2016)

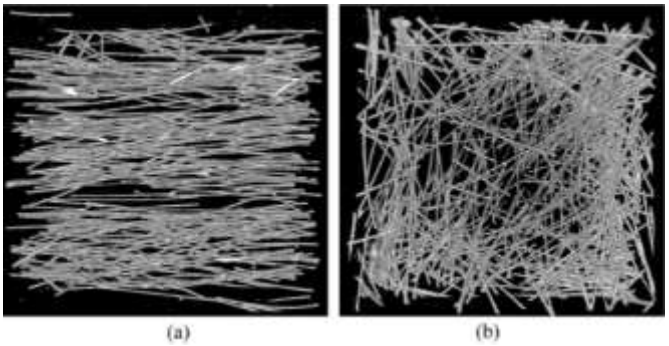

Figure 73: steel fiber orientation with and without electro-magnetic field, source: (Mu, Li, Qing, Lin, & Zhao, 2016)

This method is more difficult in practice since the elements are usually much bigger than in experimental research. However, it is possible to orientate fibers in the edges of elements. Since these areas have the biggest internal forces, the method can still be beneficial (Kloft, Ledderose, & Stümmler, 2021).

3.6 Beneficial fiber distribution and orientation

3.6.1 Fiber distribution

Experiments have shown that the distribution of fibers along the cross section of an element is vital for the tensile behaviour of UHPFRC. If an element is uniformly loaded in tension, a uniform fiber distribution is favoured. However, if an element is eccentrically loaded, an additional bending moment will occur causing additional tensile stresses on one side of the element. In this case, it is beneficial to have more fibers on the tensile side. This is also the case for a UHPFRC element under flexural loading (Akeed, et al., 2022).

However, usually a homogeneous distribution is preferred since this will decrease the difference in local tensile behaviour. If fibers are concentrated in one area, this area will have a strong tensile strength but other areas will have a relatively small resistance. By obtaining a homogeneous fiber distribution, all areas are similarly strong and the global strength will increase (Akeed, et al., 2022).

3.6.2 Fiber orientation

Figure 74 shows the relationship between the mean fiber orientation angle and the tensile strength. In this figure, f_{Ute} represents the first-crack strength and f_{Utu} the tensile peak strength. These figures show that the tensile strength is the greatest when the fibers are aligned with the direction of the tensile stress. By orienting the fibers in the direction of the tensile stress, the tensile capacity of the fibers can reduce further propagation of the crack. At this point, the concrete matrix will have no more contribution to the tensile capacity of the specimen which will be fully taken by the steel. However, the problem in practice is that the direction of the stress varies. That is why a randomly orientated fiber pattern can be advantageous (Tran, Shen, Sorelli, Ftima, & Brühwiler, 2023).

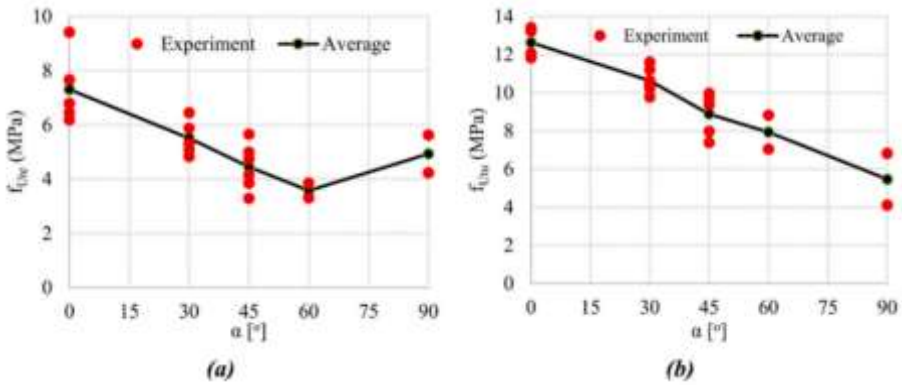

Figure 74: relationship between mean fiber orientation and tensile parameters, source: (Tran, Shen, Sorelli, Ftima, & Brühwiler, 2023)

3.6.2.1 Orientation in thick plates

When a UHPFRC plate is relatively thick, the fibers are able to rotate freely, allowing the fibers to have a significant elevation. When the plate thickness is more than the fiber length, it is theoretically possible for the fibers to be orientated vertically so they are perpendicular to the acting stresses ($\phi=90^o$). As discussed in Chapter 3.1.2.1, the French UHPFRC standard considers a plate to be thick for a thickness greater than three times the fiber length.

3.6.2.2 Orientation in thin plates

The most drastic change in fiber efficiency happens when a fiber angle exceeds 30 degrees relative to the stress direction. The fiber efficiency is the least when a fiber is orientated perpendicular to the tensile stress (Akeed, et al., 2022).

This is exactly where a thin plate can be useful. When a plate has a thickness smaller than the fiber length, the fibers will be physically unable to have an out-of-plane orientation. Actually, previous experiments have shown that the fibers tend to orientate much more horizontally, within the preferred 30 degrees rotation ($\phi\leq30^o$). This is also caused by the wall-effect, which was previously discussed. That means the fiber orientation around one axis is almost fixed and there are only two more orthogonal axis that need to be accounted for. Fiber orientation in thin plates is almost a 2D problem (Akeed, et al., 2022).

In this 2D fiber plane, the same principal holds. The fibers are most efficient if they are orientated in the same direction as the tensile stresses. This direction of the tensile stresses is completely dependent on the stress distribution in the element and therefore the specific application. Slender beams only have stresses orientated in the direction of the beam while bigger beams or even slabs can have stresses in all directions. In these cases, a dominant fiber orientation might have a negative effect on the elements strength. So the preferred fiber orientation can also be a completely random orientation in all directions, depending on the application (Akeed, et al., 2022).

4. Experimental program

This chapter describes the experimental research program in this Master Thesis. The experimental program is described including the preparation, the methodology and the measurements.

4.1 Preparation

4.1.1 Materials

For UHPFRC, the exact amount of materials has to be more precise than for CC. All ingredients must have the correct proportion in order to achieve the high strengths necessary. Table 9 contains the composition of the UHPFRC mix used for testing at the TU Delft. All components are quantified as mass per cubic meter of UHPFRC.

All the mix materials can be divided into five categories: powders, aggregates, fibers, water and superplasticizer. The powders consist of cement, silica fume and blast furnace slag. These powders all have their own purpose(s). All of the powders increase the packing density of the material since they can fill the gaps between the aggregates, as discussed in Chapter 2.

The aggregates category consist of different sand types since UHPFRC does not contain large aggregates. The sand types are categorized by their particle size. These particle sizes are indicated in Table 9. This means that all of the sand particles have a diameter between 0.125 and 1.00 mm. There are no aggregates present with a diameter larger than 1 mm which is one of the reasons why the material is so homogeneous.

The benefits of adding steel fibers to the mixture have been extensively discussed in Chapter 2. The same steel fibers were used that were used for the larger shear panels, described in Chapter 2.7.3.5. These fibers are 13 mm in length and 0.2 mm in diameter.

There is a very limited amount of water used in UHPFRC which is one of the factors causing the high strengths of the material. The water-to-cement ratio of this mixture is around 0.25. However, this low water content has negative consequences for the workability. This is the reason superplasticizer is added to the mixture. Superplasticizer significantly improves the flow of the cement paste which makes the material easier to work with.

Table 9: mix material composition for a UHPFRC mixture with 2% fiber content

Component	Weight kg/m3
CEM I 52,5 R	800.4
CEM I 42,5	69.6
Blast furnace slag	104.4
Silica fume	43.8
Water	219.945
Superplasticizer	26.6
Sand 0,5-1,0	529.1
Sand 0,25-0,5	318.7
Sand 0,125-0,25	213.3
Steel Fibers	156.25

4.1.2 Mixing procedure

The mixing procedure is quite specific. In order to compare the results to the larger shear panels, the same procedure is applied that was used for the shear panels. The first step is mixing all dry materials. The ingredients should be added to a large mixing container starting with the material with the largest particles (the most coarse sand) and ending with the silica fume which has the smallest particles. After stirring these dry materials for 30 seconds, 90% of the water is added and mixed once again for 30 seconds. The remaining 10% of the water is combined with the superplasticizer which is then also added to the mixture. This should be mixed for another 2 minutes and 30 seconds. Finally, the steel fibers are added gradually while mixing after every addition of fibers. After the last fibers are added to the mixture, the mixture is mixed for another minute. After this, the mixture is ready for casting.

4.2 Research plan

The main influences that are researched in this Thesis are the casting direction, duration of vibration, workability of the fresh mixture and fiber content. The casting direction is distinguished in horizontal and vertical orientation (Figure 75). The amount of vibration is distinguished in 0 minutes, 1 minute, 2 minutes, 3 minutes and 5 minutes. The vibration is applied using a vibration table. A vibration needle is normally used for vibration in conventional concrete but the packing density of UHPFRC is too high for the needle to penetrate. That is why a vibration table is used for UHPFRC which vibrates the entire plate including mould. The workability changes due to the different fiber contents, which differs between 1%, 2%, 3% and 4%. In total, 27 plates are produced and measured. An overview of all plates can be found in Table 10 where all plate types have been given a designation.

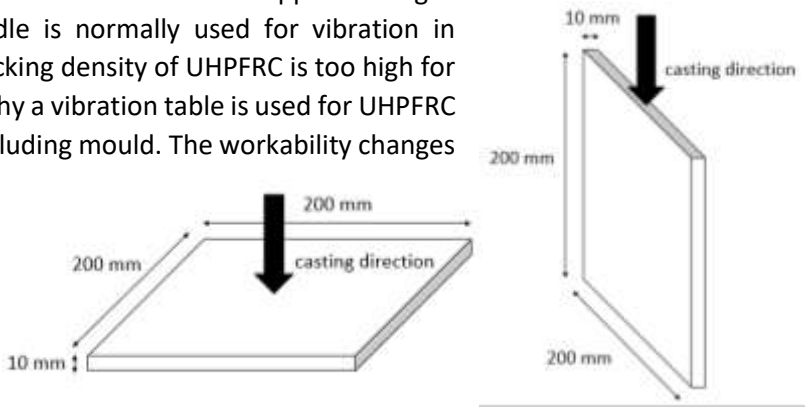

Figure 75: horizontal casting (left) and vertical casting (right)

The first letter in this designation defines horizontal (H) or vertical (V) casting. This letter is followed by a number defining the fiber content percentage. If the plate is not vibrated, the designation ends with either an A or a B indicating the first and second plate, since two plates are made for every configuration. There is one exception: the 2% fiber content plates without vibration have been cast twice meaning there are four horizontally cast plates and four vertically cast plates. This was done to ensure a reliable comparison to the vibrated plates, since these all have a 2% fiber content. For vibrated plates, the third indicator is the letter V followed by a number indicating the amount of minutes it was vibrated. The designation then ends again with an A or a B distinguishing the first and second plate cast under the same circumstances and procedure.

Table 10: overview and designation of all plates

Casting orientation	Vibration time	1%	2%	3%	4%
Horizontal	0 min 0 min	H1A + H1B	H2A + H2B H2A2 + H2B2	H3A + H3B	H4A + H4B
Vertical	0 min 0 min 1 min 2 min 3 min 5 min	V1A + V1B	V2A + V2B V2A2 + H2B2 V2V1A V2V2A + V2V2B V2V3A + V2V3B V2V5A + V2V5B	V3A + V3B	V4A + V4B

For the casting of these plates, wooden moulds are made with the inside dimensions of 200x200x10 mm^3. In total, two horizontal moulds are made and four vertical moulds. After casting, the material needs at least one day before demoulding is possible.

The dimensions of the plate are chosen for multiple reasons. The used fiber length is 13 mm which is bigger than the plate thickness. This was done in order to approximate a 2D fiber orientation, as described in Chapter 3.6.2.2. Theoretically, a 13 mm long fiber is able to rotate 50 degrees within a 10 mm thick plate. However, due to the wall effect this is very unlikely. As described in Chapter 3.5.2, the wall effect generally occurs if the fiber distance from the edge is less than half the fiber length. This will definitely be the case. Another reason to choose this plate thickness is to allow better comparison to the larger shear panels which have the following dimensions: 1400x200x10 mm^3. The only different dimension is the specimen length.

The horizontally cast plates will have a rough side (top of plate) and a smooth side (bottom of plate). According to previous research (Nunes S. , Pimentel, Sine, & Mokhberdoran, 2021), magnetic probe measurements might not be reliable for a plate with high surface roughness. This surface roughness effect will be tested for two different horizontal plates.

4.3 Measurements

4.3.1 Workability

Immediately after mixing, the workability of the fresh UHPFRC mixture was assessed by performing a slump flow test. Generally for UHPFRC, a Hägermann cone is used which is a smaller version of the Abrams cone. The dimensions of the Hägermann cone can be found in Figure 76a with a total volume of 0.34 L. Normally, this type of cone is used to test the workability of mortars. Since UHPFRC has no coarse aggregates, the material behaves like a mortar which is why the Hägermann cone is suitable. After the cone is filled with the fresh UHPFRC mix, the cone is lifted from a smooth surface. After the UHPFRC mix spread out, the maximum diameter of the circle is measured, denoted as d_1. The diameter is also measured orthogonal to the direction of d_1, which is denoted as d_2 (Figure 76b). The mean diameter is then used to calculate the UHPFRC relative slump flow, for which the formula can be found below (Yu, 2015).

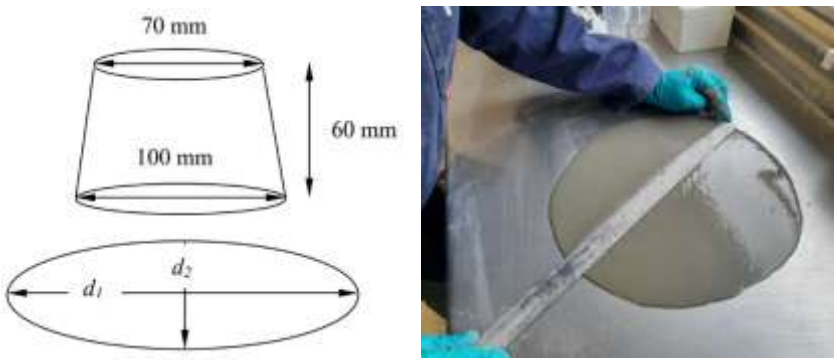

Figure 76: dimensions Hägermann cone (a) and measurement of slump flow test (b), source: (Yu, 2015) and picture taken by D. Kooreman

$$d = \frac{d_1 + d_2}{2} \quad (13)$$

$$Flow\ \Gamma_{p/m} = \left(\frac{d}{d_0} - 1\right)^2 \quad (14)$$

d = mean flump diameter [mm]
d_0 = largest diameter of Hägermann cone = 100 mm [mm]
d_1 = largest flump diameter [mm]
d_2 = largest flump diameter perpendicular to d_1 [mm]
$\Gamma_{p/m}$ = concrete relative slump flow [-]

4.3.2 Characterization external effects

4.3.2.1 Edge effect

Experiment

The edge effect needs to be checked to make sure the measurements at 50 mm from the edge give a reliable result. This is checked by sequentially removing 10 mm of material from the edge of two different plates. After each removal, the inductance is measured in the middle of the plate. This measurement was carried out for both the single ferrite probe and the C-shaped ferrite probe in the same direction. Once the inductance starts dropping quickly, the edge effect is taking place and the minimum edge distance is known. This process is repeated 6 times until the probe is only 30 mm from the edge of the plate (see Figure 77).

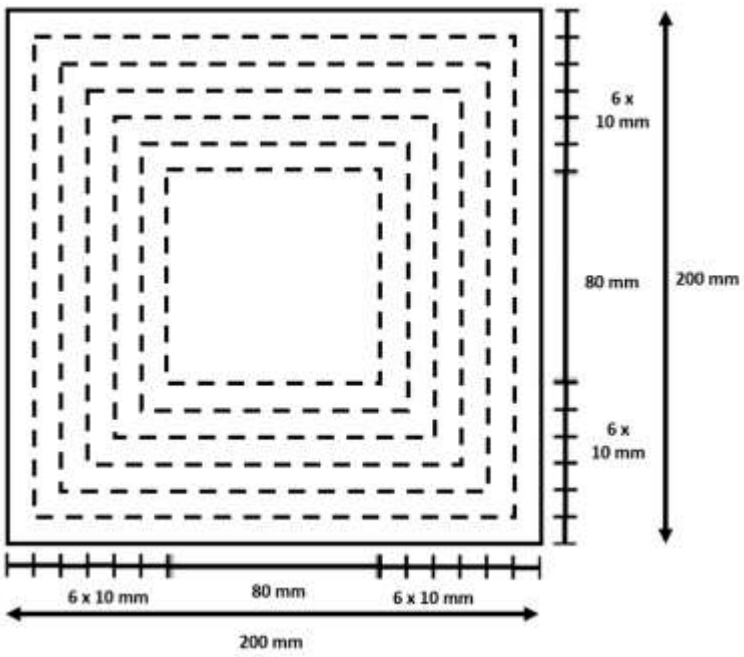

Figure 77: testing method for the edge effect of the used probes

Results

The results of this experiment can be found in Figure 78. The edge distance is determined using the same method as in previous research, shown in Figure 57 in Chapter 3.3.4.4. For each measurement, the change in mean relative inductance is divided by the change in specimen length. As described in the experiment, the decrease in specimen size is 20 mm every time.

The right figure shows that the measurements using the C-shaped ferrite probe start decreasing significantly after a specimen size of 160 mm and decreases even more for a specimen length smaller than 120 mm. This is why the minimum edge distance for the C-shaped ferrite probe is determined as 80 mm. The inductance values from the single ferrite probe start decreasing in a later stage and start decreasing significantly after a specimen size of 100 mm. That means the minimum edge distance for the single ferrite probe is 50 mm, which allows this probe type to take reliable measurements closer to the edge.

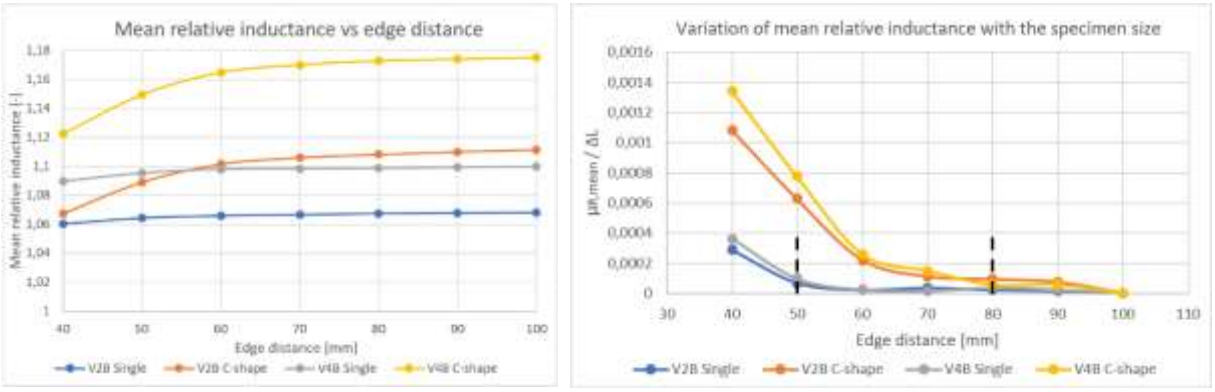

Figure 78: relationship edge distance with relative fiber content (left) and mean relative inductance (right)

4.3.2.2 Element size effect

Most tests of this experimental programme are performed on relatively small plates of 200 x 200 mm which might not be representative of larger real-life applications because of the small size. That is why the results from the small plates are compared and validated with the results of a larger UHPFRC element. As mentioned in Chapter 2.7.3.5, these elements are produced by TU Delft PhD Candidate Yitao Huang. This research uses a significant amount of both horizontally and vertically cast shear panels. For this research, two vertically cast shear panels and two horizontally cast shear panels are assessed. The dimensions of these shear panels are 1400 x 200 x 10 mm^3 which is the same height and thickness as the small plates cast in this research. However, the length is 7 times longer than that of the small plates. All shear panels have been vibrated for 15 minutes (Huang, Schlangen, & Lukovic, 2023).

Similar to the small plates, the shear panels will be measured using the single ferrite probe and the C-shaped ferrite probe. The single ferrite probe measures the fiber content every 50 mm in the vertical direction and every 100 mm in longitudinal direction. This will result in the fiber distribution. The C-shaped ferrite probe measures the fiber orientation every 200 mm along the length of the shear panel. This is also shown in Figure 79. Unlike the small plates, these measurements are done every 45 degrees, in order to decrease the amount of measurements.

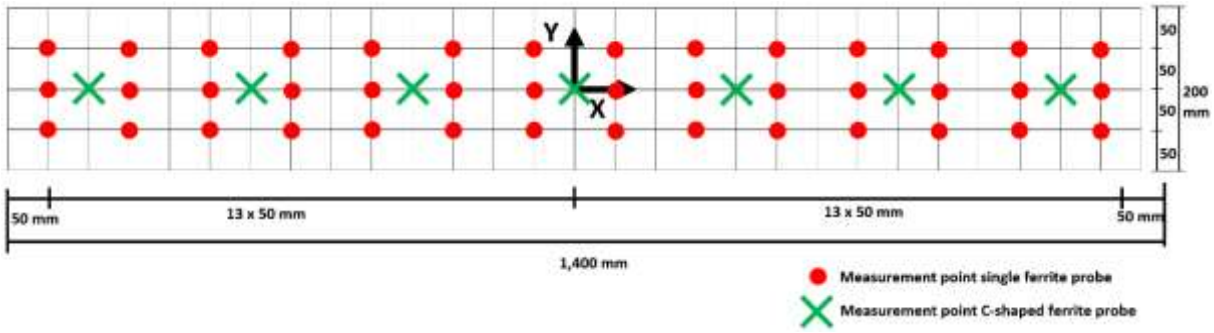

Figure 79: Measurement points for large shear panels

4.3.2.3 White paint effect

For the experimental testing of UHPFRC shear panels, PhD Candidate Yitao Huang has painted his panels using white paint with small black dots so he is able to monitor the displacement of the panels by tracking the black dots (Huang, Schlangen, & Lukovic, 2023). However, this paint layer might have a significant influence on the data results. That is why the effect of the paint layer has to be checked.

For each fiber content percentage, one plate is painted white. For each plate, the C-shaped ferrite probe will be used to measure the inductance every 45 degrees. These results can be compared to the results found previously without the paint. Figure 80 displays a measurement on one of the painted plates. If the difference in the results with and without paint is significant, the measurements for the shear panels can be adjusted based on the found paint layer effect. If the difference is insignificant, the measurements on a painted surface are considered to be reliable.

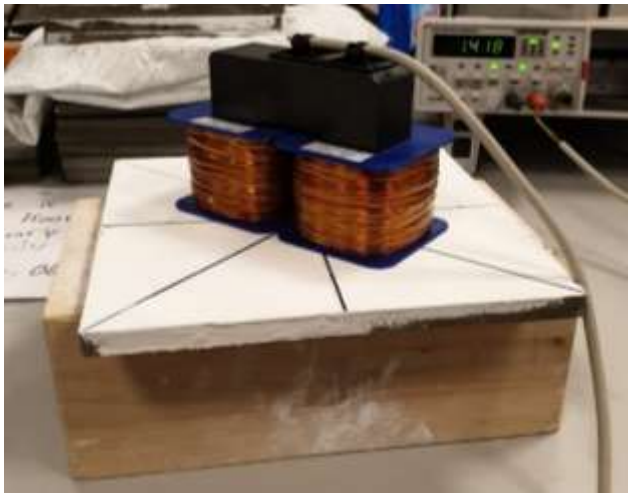

Figure 80: C-shaped ferrite probe measurement on painted plate, picture taken by D. Kooreman

As described, four different plates have been tested for the paint effect: V1B, V2A, V3A and V4A. For every single measurement, the inductance value decreased due to the paint layer. However, the decrease deviates between different fiber contents. The inductance values were used to approximate the fiber content, using the found k_v values from the plates without any paint. The results can be found in Table 11. As can be seen, the decrease is quite small for lower fiber contents but increases for higher fiber contents. The maximum decrease in the approximated fiber content is 0.13% for the 4 percent fiber content plate. This is considered to be insignificant. The average deviation of the inductance values themselves is also given in Table 11.

Table 11: fiber content estimation and deviation with and without paint layer

		V1B	V2A	V3A	V4A
V_f	No paint	0.92%	1.94%	2.79%	3.92%
	With paint	0.89%	1.90%	2.68%	3.79%
Av. deviation	Approx. V_f	0.02%	0.04%	0.11%	0.13%

4.3.2.4 Surface roughness effect

For all horizontally cast plates, the rough side gives smaller inductance values as result. The inductance was expected to decrease for higher surface roughness, as was found in previous research (Nunes S. , Pimentel, Sine, & Mokhberdoran, 2021). The effect of this surface roughness is tested on two different plates: H1B and H3B. By sanding down the rough side, this side can also be smoothened. When repeating the measurements, the values might change and approximate the values from the smooth side more.

In this research, two different influences were found that increase the surface roughness. The plates were covered with a thin sheet of plastic after casting. Two horizontally cast plates with 2% fiber content were covered with the sheet too early. The mixture stuck to the plastic causing a lot of surface roughness. This was the case for the left plate in Figure 81 where the wrinkles of the plastic sheet are visible on the casting surface. The right plate in Figure 81 was covered correctly and has a relatively smooth surface. Another notable influence was the fiber content. For the largest fiber content of 4%, there was a lot more surface roughness due to steel fiber sticking out of the casting surface. This complicated performing the inductance measurements.

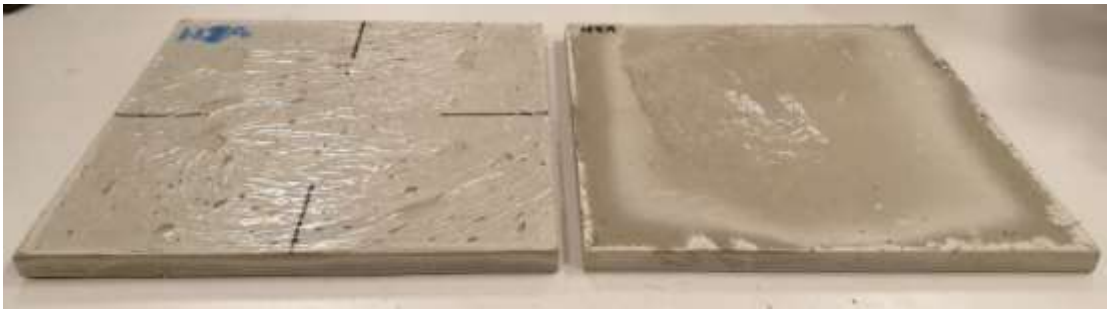

Figure 81: surface roughness of plate H2A (left) and H3A (right)

Plates with a lot of surface roughness, like plate H2A, had too many defects to sand down properly. That is why the effect of surface roughness is tested on plates H1B and H3B. As was expected, the value increases after smoothening the surface. However, this difference is very little. As can be seen in Appendix 4, the average relative increase of the inductance values only increases with about 2%. A possible explanation of this result is a wrong method of smoothening. The surface was smoothened using a sanding machine with sanding paper. This sanding paper might not be strong enough to sand down UHPFRC including the steel fibers. The surface did feel a lot smoother after using the machine but there were still some inconsistencies. This could be interesting for future research.

4.3.3 Fiber distribution

The single ferrite probe was used to determine the fiber distribution over in-plane dimensions of the plate. This probe type allows measurements closer to the edge of the plate without much influence from the edge effect. The measurement was done in a square matrix every 25 mm. A schematic overview of the measurements can be found in Figure 82. In this overview, a measurement is done at every red dot. All measurements have a minimum edge distance of 50 mm. This edge distance is verified in Chapter 4.3.5.1.

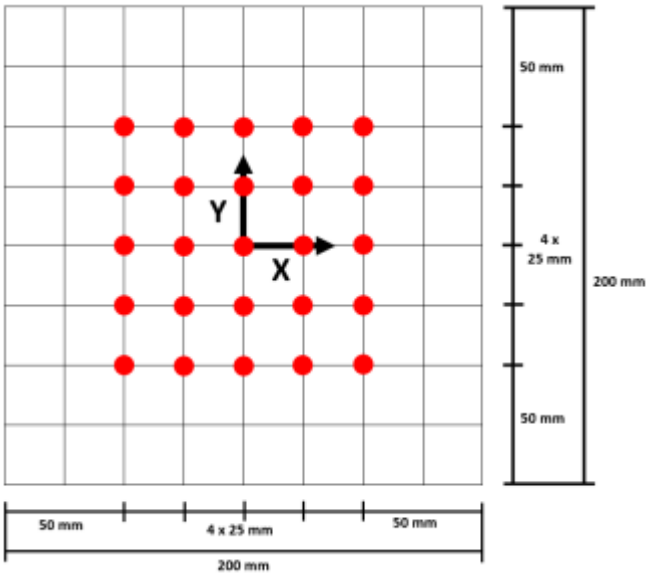

Figure 82: distribution measurement points using the single ferrite probe

Because of the rectangular shape of the magnetic core in the single ferrite probe and the asymmetrical coil windings around it, each measurement point needs to be measured in both orthogonal directions. This means each point results in two inductance values. This is done to eliminate the influence of fiber orientation. After measuring these values, the average relative magnetic permeability can be calculated which can be used to determine the fiber content, as described in Chapter 3.3.4.1. This local fiber content gives an indication of the fiber distribution.

4.3.4 Fiber orientation

For the fiber orientation, the C-shaped ferrite probe is used. Similar to the method in Chapter 3.3.4.2, the inductance is measured every 15 degrees (Figure 83a). The inductance is measured over the full 360 degrees which is the same position as the starting angle, 0 degrees (Figure 83b). This means 25 measurements are performed for every plate. Opposite directions should, in theory, give the same inductance values. For example, an angle of 60 degrees should give the same value as 240 degrees since the probe is orientated in the same direction, only rotated by 180 degrees. A slight change in the inductance value can be explained by measurement errors, either from the probe itself or human error. For instance, the angle of the probe might not be perfectly aligned to the line on the plastic sheet. After measuring multiple plates with different fiber contents, the k_v constant has to be approximated for both probe types, before the result can be interpreted.

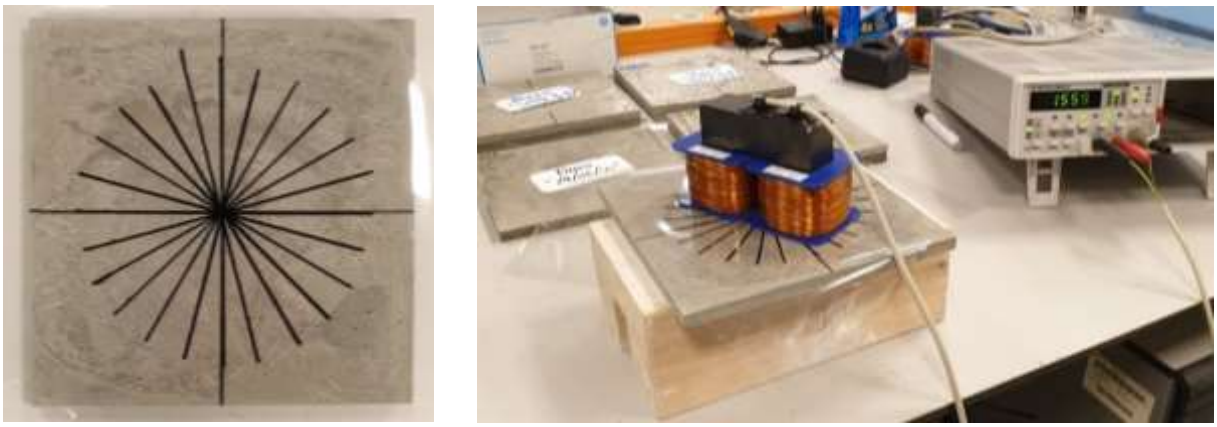

Figure 83: plastic sheet with angles of 15 degrees (a) and C-shaped ferrite probe measurements (b), pictures taken by D. Kooreman

4.3.5 CT scan

For the validation of the probe measurements, a CT scan is performed on ten different plates with fiber contents of 1%, 2% and 3%. Plate V2V5A was also scanned because this plate experienced the most fiber segregation. These CT scan images can be analysed and compared to the results from the inductance measurements in order to evaluate on the effectiveness of both probes to determine the fiber distribution.

Normally, a CT scanner will emit a series of X-ray beams that go through the plate, resulting in multiple slices through the material, multiple cross-sections. However, the plates in this research only have a thickness of 10 mm, which is too thin to make slices (Ruan & Poursaee, 2019). That is why a X-ray photo must be made of the plate. This will limit the accuracy of the fiber content measurement, since it is now a single 2D image while fiber content is a 3D percentage. In the 2D image, fibers can be aligned or overlapping so the a lot of actual fiber area can be missing. Also, because this is a 2D image, the 2D area percentage will be significantly larger than the actual fiber content percentage. When a fiber is visible in the image, it means that somewhere over the thickness of the plate, there is a fiber present. However, the fiber is not present over the entire thickness of the plate in this location.

In order to process the CT scan image, a greyscale imaging method must be applied. This method can distinguish the fibers among the matrix and calculate the area percentage of fibers. For this method, the computer tool ImageJ has been used (ImageJ, 2024).

The quality of the image of the full plates is not good enough to apply greyscale imaging. Usually, the largest difference in fiber content is over the height of the plate. That is why the plate was divided into three equal parts: top, middle and bottom. Each of this parts was photographed using the CT scanner in the center of the plate. This is also visualised in Appendix 6. Figure 84 shows the CT scan setup for a singular plate fixed in a Styrofoam block that fixes the plate vertically.

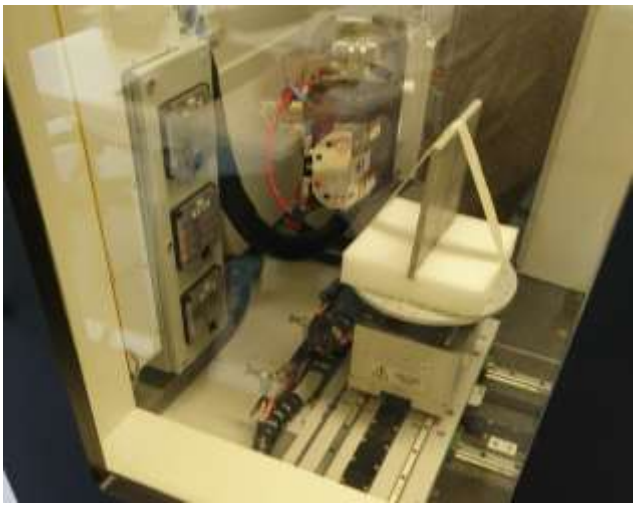

Figure 84: CT scan of UHPFRC plate, picture taken by D. Kooreman

By increasing the brightness, the contrast and the sharpness of the image, the fibers can be distinguished using grey-scale imaging in each part of the plate.

5. Results and discussion

This chapter contains all the results found in the experimental research. Most of the data and other results are found in the Appendices but this chapter contains the important results with corresponding data and figures that are needed to make conclusions about the research.

5.1 Workability

Table 12 shows the results of the slump-flow tests, as previously discussed. The mixture with a fiber content of 1% has the biggest flow diameter and the mixture with 4% fibers the smallest. Two measurements in Table 12 are marked red to indicate that these values were not used for the comparison. The 4% fiber content mixture was left out because the material did not behave as a fluid but showed extreme fiber conglomeration. All the fibers clumped together as a solid, as can be seen in Figure 85. That is why this slump value should not be used for comparison. The mixture 2% vibr B is also not included in the plot since this slump flow value was obtained by performing the test 10 minutes after mixing. UHPFRC hardens very quickly so this explains the decrease in slump flow. The relative slump flow is calculated using Formula 13 and 14.

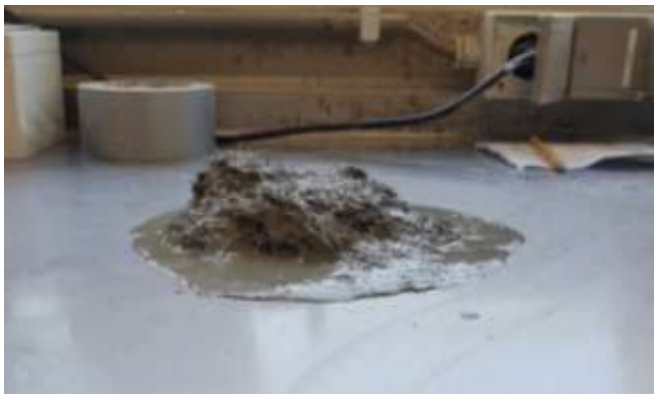

Figure 85: fiber conglomeration of 4% fiber content mixture, picture taken by D. Kooreman

Table 12: slump-flow results for mixtures with different fiber contents

	Fiber factor	d_1 [mm]	d_2 [mm]	d [mm]	Relative slump flow
0%	0.00	347	340	343.5	5.93
1%	0.65	344	334	339.0	5.71
2% B	1.30	313	319	316.0	4.67
2% vibr A	1.30	315	315	315.0	4.62
2% vibr B	1.30	315	294	304.5	4.18
3%	1.95	304	273	288.5	3.55
4%	2.60	198	195	196.5	0.93

The UHPFRC flow diameter gathered during previous research was shown in Figure 62. This research resulted in a relationship consisting of three different sections (Nunes, 2017). Figure 86 shows the found relationship in this research combined with the found relationship in Figure 62. For both results, the same three sections can be distinguished. The bounds of the three sections are similar. The constant section of the relationship ends at a fiber factor of 0.8 and the slightly decreasing section ends at a fiber factor of 1.9. For fiber factors of 1.9 or higher, the workability decreases significantly.

As mentioned in Chapter 3.5.1, a previous research has found that fiber segregation might occur for UHPFRC mixtures with a flow diameter that exceeds 265 mm (Nunes S. , Pimentel, Sine, & Mokhberdoran, 2021). All reliable slump-flow measurements resulted in a larger flow diameter than this given limit. Thus the workability of the mixture might result in a certain amount of fiber segregation within the plates.

The main difference between the two results is the magnitude of the diameter flow for smaller values of the fiber factor. The constant section found in this research consists of a diameter flow of 340 mm but previous research found a value of 300 mm. This can be explained by a deviation in other mix materials. Figure 61 showed that the cement content can also significantly influence the workability flow. That could explain why the magnitude of the diameter flow is bigger in this research. In conclusion, the found data points seems to compare well to previous research.

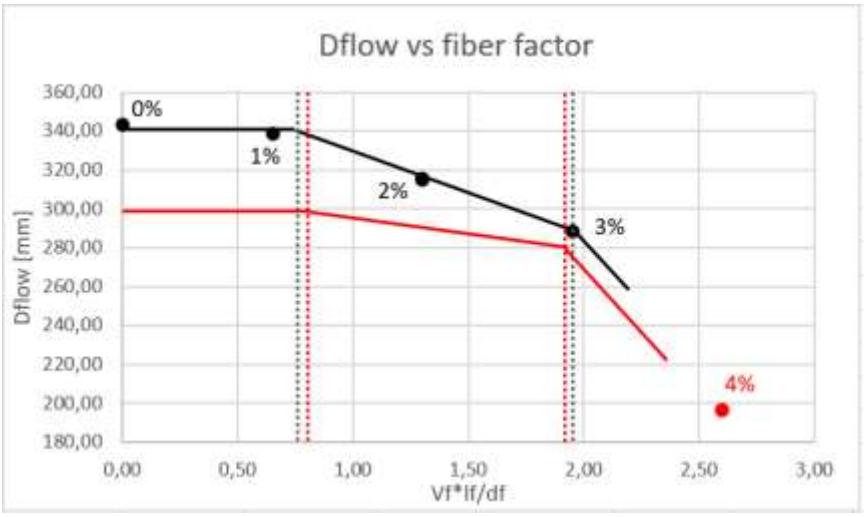

Figure 86: workability comparison between this research and previous findings (Nunes, 2017)

5.2 Mass density

The mass of every plate was measured to calculate the average density of the plates using the dimensions of 200x200x10 mm^3. It is important to note that this plate volume can vary so the results might not be fully accurate. Especially the volume of the horizontally cast plates can differ since these plates do not have a constant thickness. The results can be found in Table 13. The density increases for a higher fiber content. It should be noted that some plates from the same UHPFRC mixture have a very different mass. For instance, the mass of plate V2B is 6.5% greater than the mass of plate H2A.

The difference in mass can be explained by a different amount of fibers. A mixture with 2% fibers should results in multiple plates with the same average fiber content but the fiber content can differ slightly between the individual plates. This can happen due to multiple reasons. One of the reasons can be fiber segregation in the mixing container, resulting in a higher fiber content for the plates cast from the material at the bottom of the mixing container.

Table 13: mass and density of plates with different fiber contents

	H_a [g]	H_b [g]	V_a [g]	V_b [g]	Average [g]	Av. density [kg/m3]
1%	1064.0	1035.0	1030.4	1045.5	1043.7	2609.3
2%	1030.9	1037.0	1080.3	1097.9	1062.9	2657.3
2% B	1071.7	1053.2	1062.3	1069.9		
3%	1067.4	1062.1	1081.4	1108.8	1079.9	2699.8
4%	1117.1	1079.7	1099.3	1107.9	1101.1	2752.5

An important aspect to notice is the difference between horizontal and vertical casting. For vertical casting, the plate thickness is fixed which means the volume of the plate cannot differ much from the 400 cm^3 mould volume. However, this thickness is no longer fixed for horizontally cast plates. These plates can thus have a smaller or larger volume. This results in a different mass density than was calculated. This should be kept in mind when assessing the results.

By taking the average of all plates cast from the same mixture, the average plate mass and the fiber content are linearly correlated. This is to be expected. A trendline fits the average values very well resulting in a fitting parameter, R^2, of 0.998, which can be seen in Figure 87. The origin of the trendline is 1025 g which corresponds to an average density of 2560 kg/m^3. This is the theoretical density of this UHPC mixture without fibers. UHPC mass density values from previous research, ranged from 2511 to 2530 kg/m^3 (Arafa, Shihada, & Karmout, 2010). This is close to the found value in this research. The difference between the results can be explained by different quantities of the mix materials. For instance, the other research only used 600 kg/m^3 of cement where this research used 870 kg/m^3.

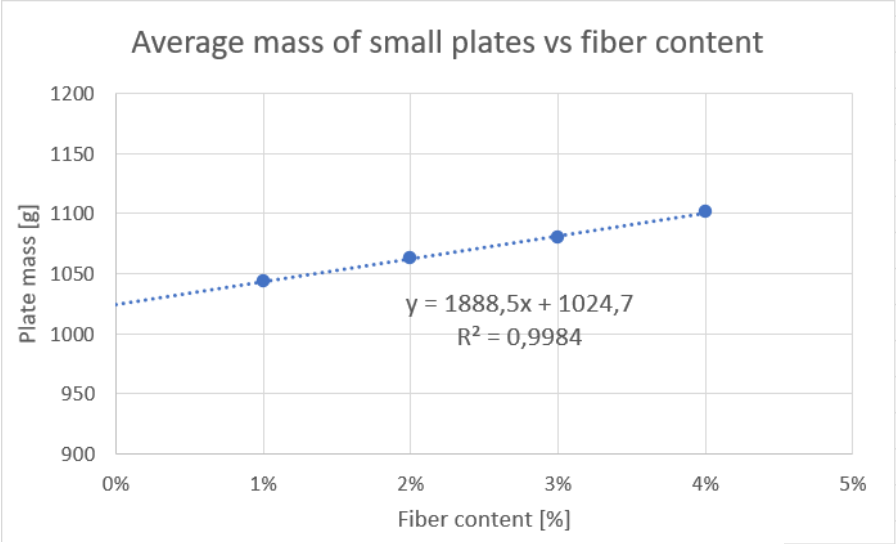

Figure 87: average mass of small plates vs fiber content

5.3 Fiber distribution

This part describes the measurement results using the single ferrite probe. This probe was mainly used to measure the local fiber content, thus the fiber distribution.

5.3.1 Determination k_V value

For every probe type and every specimen thickness, the k_v constant has a different value. As discussed in Chapter 3.3.4.1, this is a calibration constant that indicates the relationship between the relative mean magnetic permeability and the fiber content. The k_V constant differs for different element thicknesses. Since the same thickness of 10 mm is used for every measured element in this Thesis, the k_v value will remain the same per probe type. All of the measurement values obtained with the single ferrite probe can be found in Appendix 2. The air inductance was measured frequently and differed slightly between 372.0 mH and 372.3 mH. However, the average was 372.2 mH, which is taken as the reference value. Every point plotted in Figure 88 is the average of the mean relative magnetic permeability measured in each point of the plate, indicated in Figure 82 in Chapter 4.3.3. The linear relationship was determined using Excel which uses the method of least squares. The found slope value, which is the k_V value, was 2.6082. All single ferrite core measurements are performed on the smooth side of the plates so all measurements should follow the same curve.

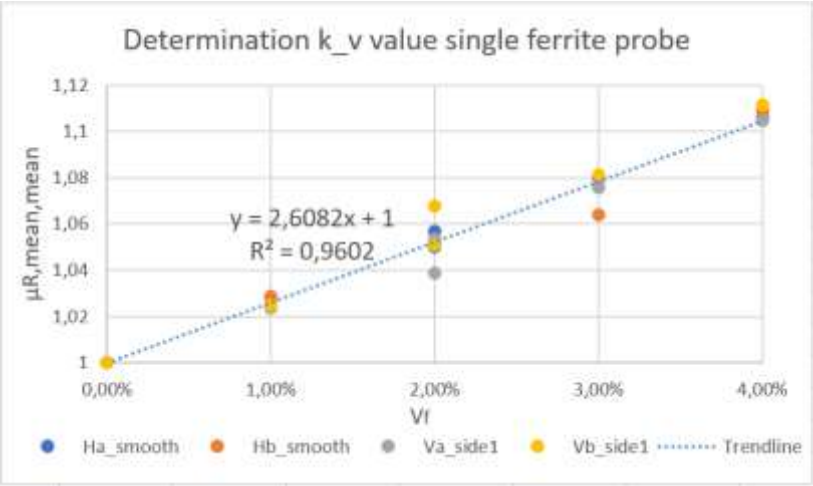

Figure 88: determination kv value of single ferrite probe for t=10 mm

It can be noted that most plates are very close to the found trendline except for two results for the 2% fiber content plates and one result for the 3% fiber content plates. Despite these measurements, the fitting parameter, R^2, has a value of 0.9602 which is relatively good. These results can be caused by human error during casting. For instance, the fibers might not have been distributed well enough during the mixing process or the fibers might have already experienced segregation in the mixing container. This results in a higher fiber content of the mix in the bottom of the container thus plates with higher fiber content that were cast with this part of the mix. However, the average fiber content of all plates cast with the 2% fiber content mixture will still be 2%. When the trendline is plotted through the average points of each fiber content, the fitting parameter becomes 0.99 which is excellent.

One might notice that the 2% fiber content plates have twice the amount of data points as the other percentages. This is simply because the 2% plates without vibration have been cast twice, as described in Chapter 4. Twice the amount of plates results in twice the amount of data points.

The theory and Figure 88 shows that the inductance increases for a higher fiber content. The 2% fiber content plates seem to have the biggest spread in data points. Plate V2B resulted in a higher mean relative inductance value which makes sense since this plate also has the biggest mass and likely has the highest fiber content of all 2% plates. The trendline that determines the k_V value goes through the average value of the points, as is intended. The actual mean fiber content of plate V2B can be determined by moving horizontally from the point until the trendline is reached. When moving down from this intersection point, the actual fiber content of 2.60% is found. This is significantly higher than 2% fiber content showing how big the influence of human error can be. In practice, someone with more expertise will cast the elements so there is less difference in fiber content between the different plates. However, this research focusses on the local fiber distribution within the plates.

5.3.2 Results fiber content

The local fiber content measurements can all be found in Appendix 2 along with the calculated fiber contents and the contour graphs for all plates.

Plate V3A seems to have severe fiber segregation, as can be seen in Figure 89, where the top contour plot represents plate V3A. In this plot, the difference between the minimum and maximum fiber content is 2,58%. This value is so large compared to other 3% fiber content plates that the plate is considered as non-reliable. It is unclear why this plate has significantly more fiber segregation compared to other plates. A possible reason can be the small thickness of the plate compared to the fiber length. For comparison, Figure 89 also presents a contour plot of plate H4A, which has an average amount of fiber segregation, compared to all plates. For this plate, the difference in minimum and maximum fiber content is only 0,93% showing the difference in fiber segregation.

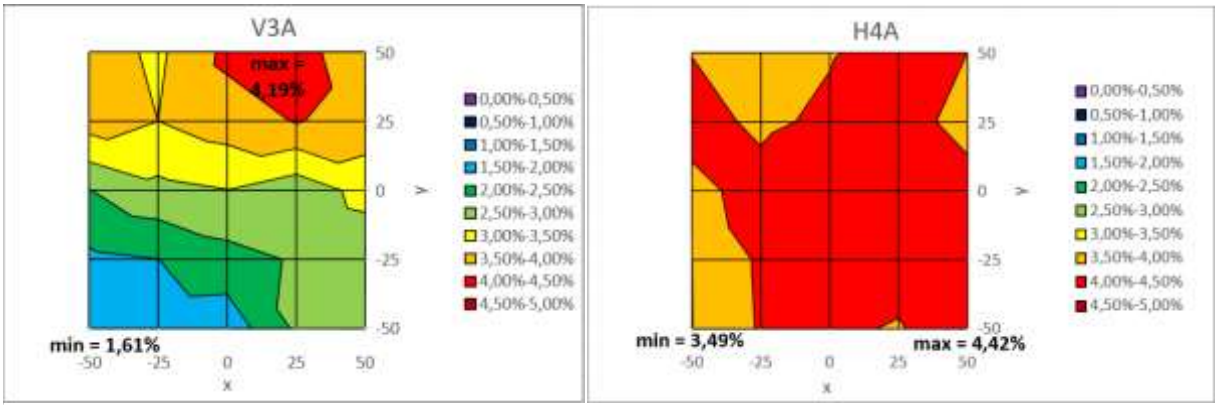

Figure 89: fiber content contour plots of plate V3A and H4A

When comparing the contour fiber distribution plots of different fiber contents in Appendix 2, the difference in minimum and maximum fiber content within a singular plate is interesting. For larger fiber contents, this difference significantly increases. On average, the difference of the 1% fiber content plates is only 0.38% fiber content. The mean difference in minimum and maximum fiber content for the 2% and 3% fiber content plates is 0.71% and 1.05%, respectively. However, for the 4% fiber content plates this value is 1.20%, which shows a clear correlation between the fiber content and the homogeneousness of the fiber distribution. The variation in the fiber content increases for larger fiber contents.

5.3.3 Results casting orientation

Figure 90 shows the contour plots of the plates with the highest segregation for horizontal and vertical casting, H3A and V2B, disregarding plate V3A. The other contour plots can be found in Appendix 2. The presented plates are the plates with the least homogeneous fiber distribution. V2B has a more significant fiber segregation where the most fibers are at the top.

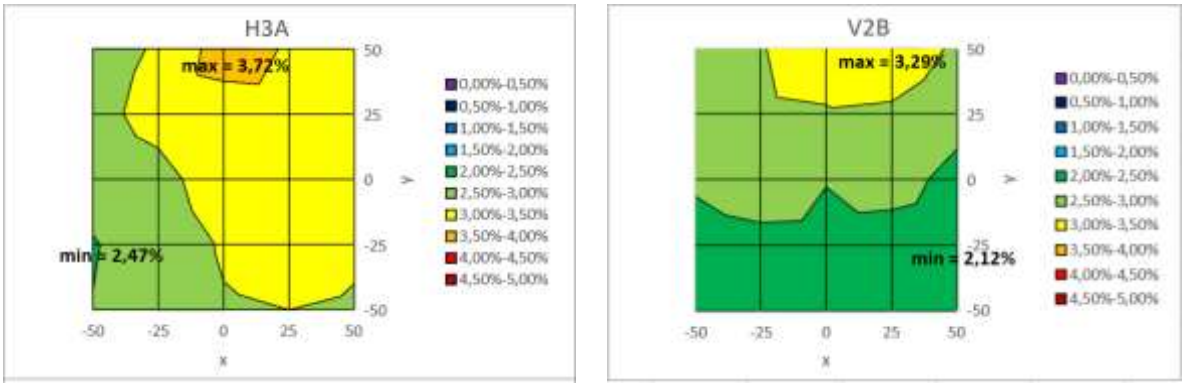

Figure 90: fiber distribution contour plot for plates H3A and V2B

The segregation towards the top of the plate is unexpected since the fibers have a higher mass density than the rest of the mix materials. This is likely caused by the small plate thickness of 10 mm compared to the fiber length of 13 mm. The fibers get stuck at the top of the mould and cannot shift downwards. Vibrating the plates might prevent this from happening.

These results show that on average, horizontal casting results in a more homogeneous local fiber distribution than vertical casting. The mean difference in minimum and maximum fiber content within the horizontally cast plates is 0.69% where it is 1.08% for the vertically cast plates. There are two main aspects that can cause this difference in local fiber distribution quality. For the vertically cast plates, gravity works in the direction of the plate allowing the relatively heavy steel fibers to shift in this direction. Also, the plate thickness is smaller than the applied fiber length. This can cause fibers to get stuck at the top of the mould which is likely the cause of the fiber distribution of plate V3A and plate V2B (Figure 89 and Figure 90, respectively). In conclusion, with regard to the local fiber distribution, horizontal casting seems to lead to a more homogeneous and therefore preferable distribution.

5.3.4 Results vibration

As described in Chapter 4, a number of 2% fiber content plates are vibrated to determine how the vibration affects the fiber distribution. The results can be found in Figure 91 where the distribution graphs on the far left are vibrated for 2 minutes, the middle graphs for 3 minutes and the graphs on the far right for 5 minutes. The difference between the different vibration times is clear.

First of all, the results show that vibrating the plates prevents the fibers from getting stuck at the top of the mould. By vibrating the plates, the fibers actually move downwards causing segregation in the opposite direction. After vibrating for 3 minutes or more, there are barely any steel fibers left at the top of the plate. The purple area in the contour plots represent a fiber content between 0 and 0.5%. This area increases along with the vibration time. A larger area with a low fiber content at the top means an area in the bottom with an even higher fiber content. This means that the fiber content must increase quickly over a short height. This causes the relatively small height of the colour bands in the contour graphs for 5 minutes vibration. In general, the longer the vibration time, the stronger the fiber segregation within the plate.

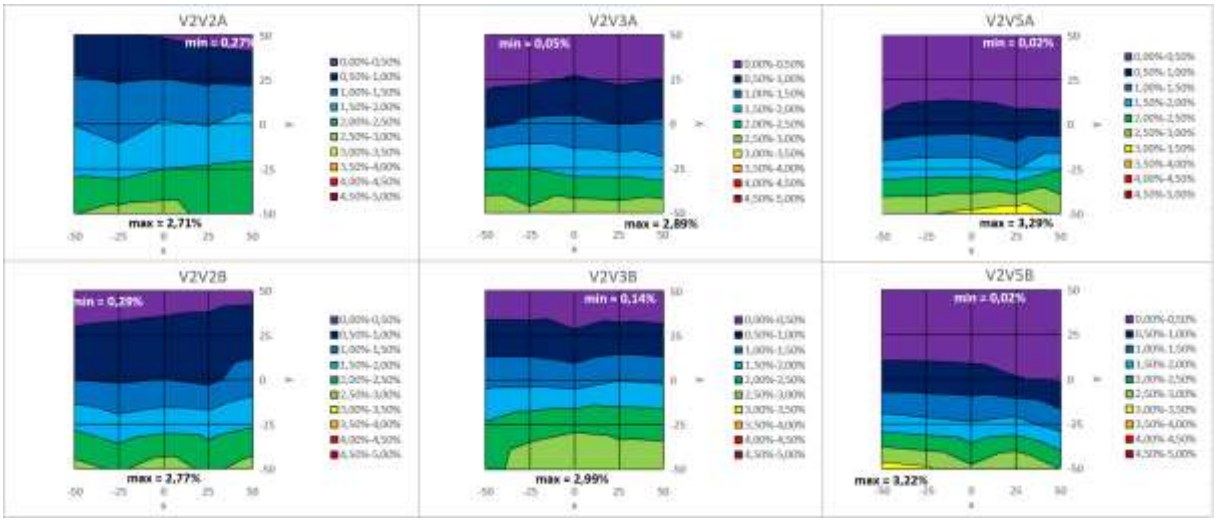

Figure 91: fiber distribution contour plots for plates with a vibration time of 2 min, 3 min and 5 min

5.4 Fiber orientation

The next part describes the measurement results using the other probe type, the C-shaped ferrite probe. This probe was mainly used to measure global fiber content and fiber orientation.

5.4.1 Determination k_v value

The k_v value was also determined for the C-shaped ferrite probe. The distribution measurements with a single ferrite probe were only performed on the smoother side of all plates. However, these measurements were performed on both sides including the rough casting surface of the horizontally cast plates. The surface roughness from these sides causes a clear decrease in the measured inductance value which is why a distinction is made between the results on the smooth sides of the plates and the rough sides. This was also done in previous researches (Nunes S. , Pimentel, Sine, & Mokhberdoran, 2021).

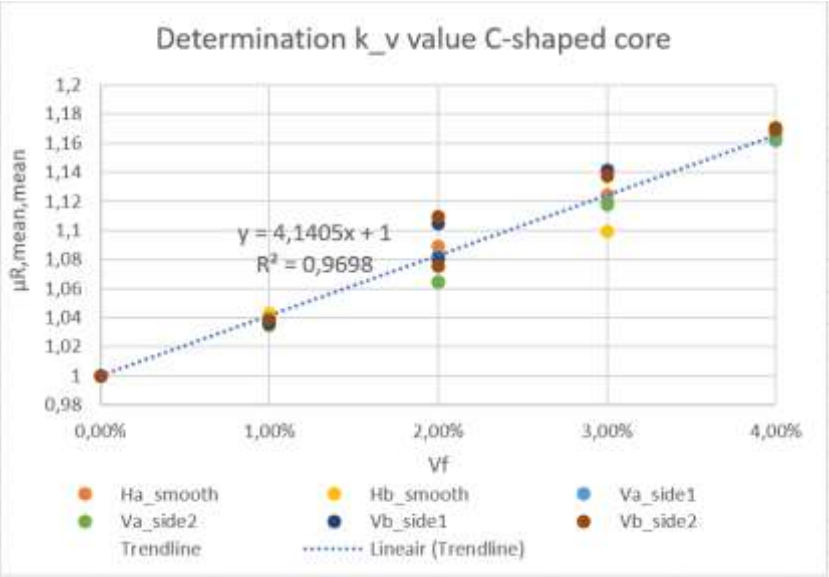

Figure 92: determination k_v value of C-shaped probe for 10 mm thickness

As shown in Figure 92 and 93, the difference between the smooth and rough sides is significant. The k_V value is 4.1405 for the smooth sides and 2.4927 for the rough sides. This value is much higher compared to the single ferrite core. For both k_v values, the fitting parameter of the trendline is relatively well.

For the C-shaped ferrite probe the air inductance value differed between 1.363 H and 1.364 H with an average value of 1.363 H. This reference value is very reliable and only deviates 1 mH at most. The absolute value of this deviation is bigger than for the single ferrite but the relative value is smaller since the absolute value of the air inductance is also larger for the C-shaped ferrite probe.

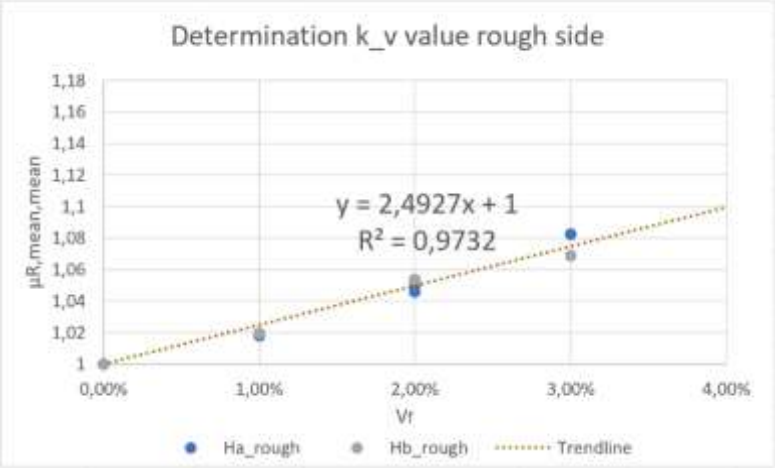

Figure 93: determination k_v value of C-shaped ferrite probe for casting surfaces

Similar to the measurements using the single ferrite probe in Figure 88, the results for the plates with 1% and 4% fiber content are well approximated by the trend line. For the C-shaped ferrite probe, there are again some measurements that deviate from the found trendline for plates with 2% and 3% fiber content. Once again, it should be noted that the trend line does approximate the average of the different plates. The fitting parameter is still relatively good, 0.9698 for the smooth sides and 0.9732 for the rough sides. Figure 93 can also be used to estimate the real fiber content of every plate by moving horizontally from a data point to the found trendline. For plate V2B, this results in an actual fiber content of 2.60%, just like for the single ferrite probe. This verifies the theory that the single ferrite core can give a good estimation of the fiber content. This reasoning also supports the theory that the difference in mass between the different plates can be caused by a varying fiber content.

5.4.2 Results fiber content

As expected, the plates with a higher fiber content return the highest inductance values. Figure 94 combines all the measurements obtained using the C-shaped ferrite probe. Every circle represents one plate side with a measurement every 15 degrees. This figure plots the relative inductance minus 1 in order to see the differences more clearly. Since the relative inductance of air is equal to one the increase in relative inductance is plotted in the radial direction.

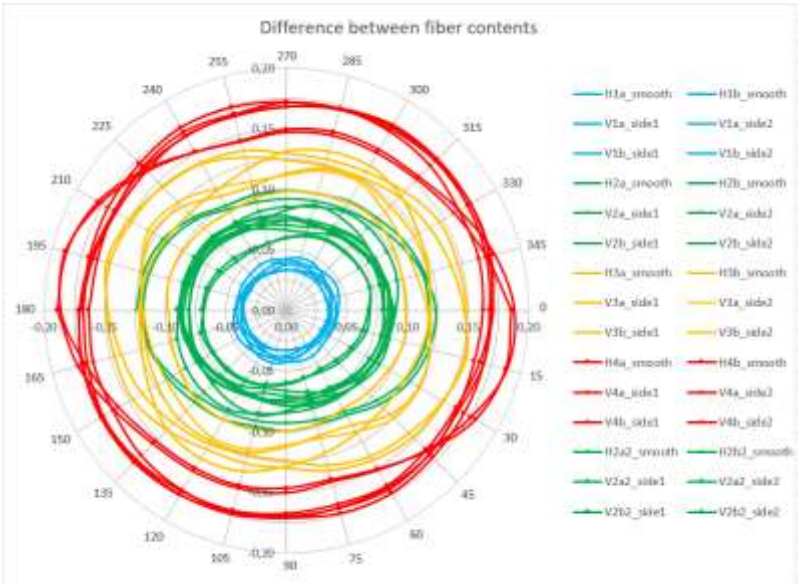

Figure 94: $\{\mu_r - 1\}$ plot for all plates without vibration, measured every 15 degrees

The average relative inductance for both V2B sides is 1.107 which corresponds to a fiber content of 2.58%. This is bigger than plate H3B where the average relative inductance on the smooth side was 1.099 responding to a fiber content of 2.39%. This is the reason that two green curves (V2B_side1 and V2B_side 2) in Figure 94 exceed a yellow curve (H3B_smooth). This is actually also visible in Figure 92 where the dark red and dark blue dot (V2B_side1 and V2B_side 2) on the 2% fiber content line have a higher value than the yellow dot (H3B_smooth) on the 3% fiber content line.

Table 14: orientation indicator ρij for small plates without vibration

V_f	Plate	Orientation $\rho_{ij,max}$ [-]	Average [-]
1	H1A	0.038	0.054
1	H1B	0.034	
1	V1A	0.052	
1	V1B	0.091	
2	H2A	0.077	0.089
2	H2B	0.060	
2	V2A	0.079	
2	V2B	0.117	
2	H2A2	0.069	
2	H2B2	0.088	
2	V2A2	0.114	
2	V2B2	0.108	
3	H3A	0.110	0.076
3	H3B	0.048	
3	V3A	0.054	
3	V3B	0.094	
4	H4A	0.033	0.050
4	H4B	0.017	
4	V4A	0.117	
4	V4B	0.035	

Table 14 contains the calculated values for the orientation indicator $\rho_{ij,max}$, defined by Formula 5. The direction resulting in the largest orientation indicator is taken for the comparison of the different fiber orientation plots. Figure 95 contains the values of the orientation factor in a graph with the fiber content on the x-axis. There is no clear correlation. All orientation indicator values remain relatively small for each fiber content. This indicates that the fiber orientation is relatively random. As discussed before, this is generally advantageous in UHPFRC elements so the tensile strength is similar in all directions.

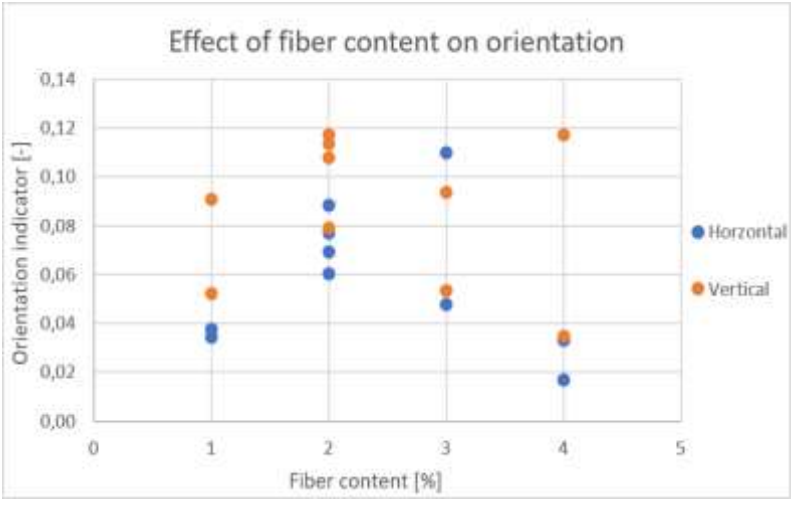

Figure 95: orientation indicator for different fiber contents

5.4.3 Results casting orientation

The orientation factor values from Table 14 are also assessed to determine the casting orientation effect. The average orientation factor of the horizontally cast plates is 0.057 and 0.086 for the vertically cast plates. This difference is not very significant since both values are relatively low. Figure 96 shows the fiber orientation for plates H3A and V4A which are the plates with the least random fiber orientation for both horizontal and vertical casting. H3A and V4A correspond to an orientation factor of 0.110 and 0.117, respectively. The fiber orientation of V4A is slightly more orientated than for H3A since the ellipse is slightly more narrow.

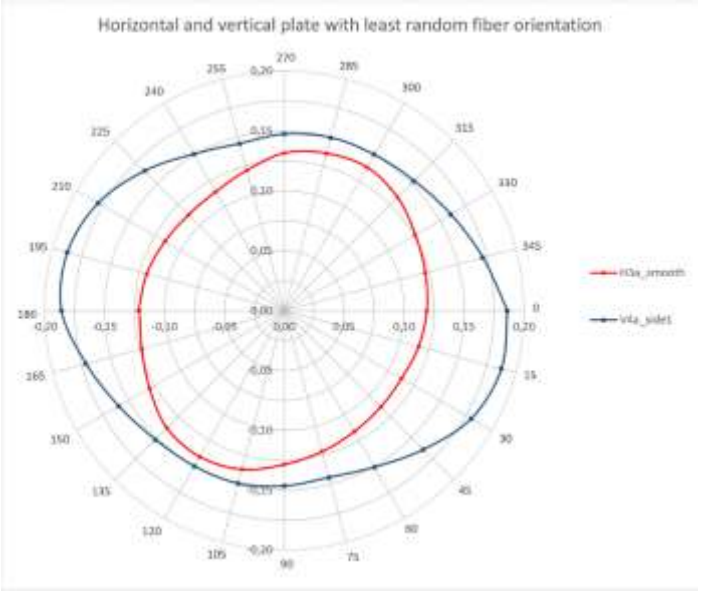

Figure 96: {μr – 1} plot for plates H3A and V4A

The average orientation factor of the horizontally and vertically cast plates is 0.057 and 0.086, respectively. In the total range of possible values for the orientation factor (between 0 and 1), this is no significant difference. The plots in Figure 96 are obtained by subtracting the relative air inductance of 1 meaning the actual fiber orientation has a very circular shape. On average, horizontal casting seems to be slightly preferable over vertical casting regarding the fiber orientation. However, statistically speaking, this could also be an coincidence since this result was obtained using 20 different plates. In any case, the difference between the casting orientation is relatively small.

5.4.4 Results vibration

The fiber orientation results for the vibrated plates are presented in Figure 97. It is remarkable that the longer the plate is vibrated, the smaller the measured inductance values are. This makes sense since the measurements are taken in the middle of the plate. Distribution measurements show that the fibers move to the bottom of the mould when vibrated meaning the local fiber content in the centre of the plate will decrease along with the vibration time. Less fibers results in a lower inductance value. Thus vibration can result in a sever underestimation of the fiber content. This is the reason why it is better to estimate the fiber content with the single ferrite core probe, since this probe can take measurements closer to the edge. However, for larger and more practical applications, the C-shaped ferrite probe is more suitable.

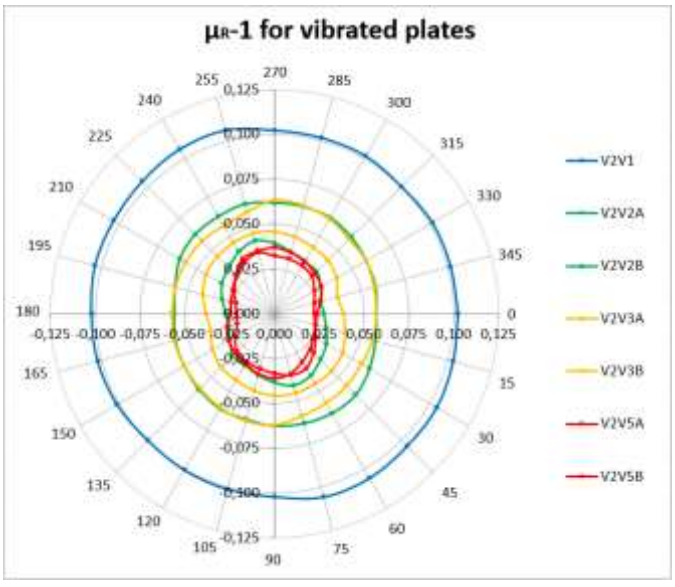

Figure 97: {μ_r – 1} plots for vibrated plates

Figure 98 also shows that the shape of the fiber orientation changes by vibrating. Plate V2V1 has only been vibrated for one minute and has a relatively circular shape. Plates with a longer vibration time like plate V2V5A tend to have a vertical orientation. This happens because a fiber will experience the least resistance when it is rotated in the direction of movement so the direction of gravity. This difference is shown in Figure 98. Once again, this measurement was performed in the middle of the plates where fibers are moving downwards during vibration of the element. In the bottom part of the plate, the fibers will settle and rotate more horizontally. This is why orientation measurements can be unreliable when the specimen is vibrated.

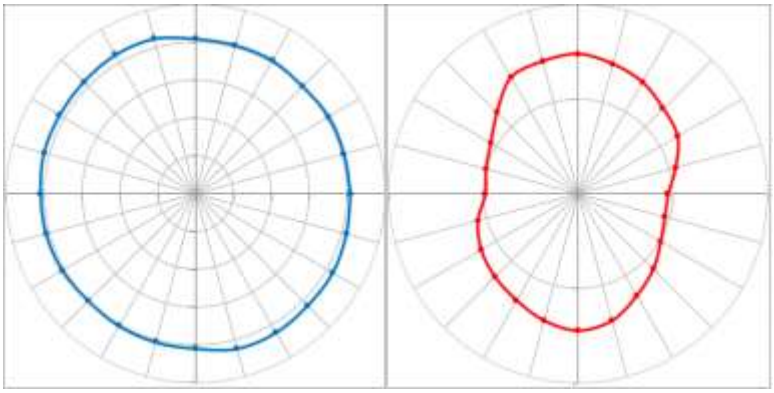

Figure 98: {μr – 1} plots for plate V2V1 (left) and plate V2V5A (right)

5.7 Large shear panels

As described in Chapter 4.3.2.2, four different shear panels have been measured using the magnetic non-destructive testing method. This is done for comparison to the small plate results and to validate the findings.

5.7.1 Horizontally cast panels

The horizontally cast panels have a relatively good fiber distribution and orientation compared to the vertically cast panels. The distribution of both panels is shown in Figure 99 where all fiber content measurements remain within the bounds of 1% and 2%. This value is relatively low since the panels were cast using a 2% fiber content mixture. It is unclear what caused this difference. Chapter 4.3.2 shows that the surface roughness from the casting surface and the addition of a white paint layer both have little influence on the inductance values. However, both these effects are relatively small so the measurements on the painted shear panels are expected to be reliable. These measurements show that horizontal casting also results in a reliable fiber distribution for larger UHPFRC elements. The fiber segregation within the horizontally cast panels is insignificant.

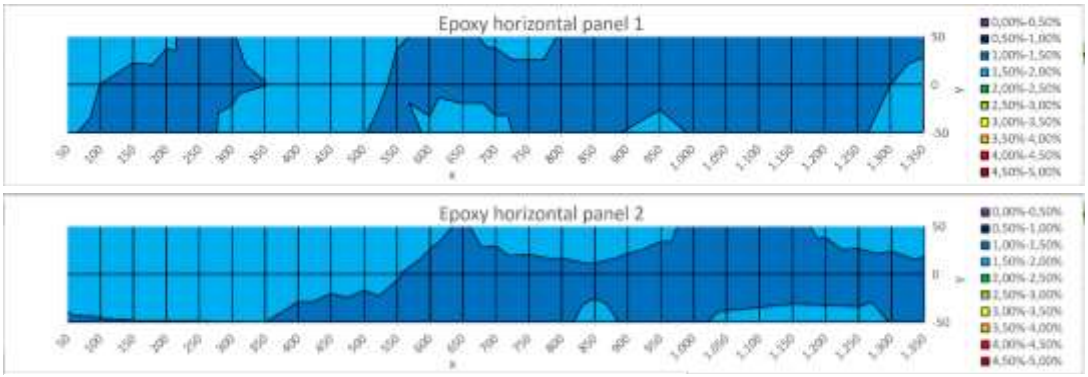

Figure 99: fiber distribution of horizontally cast panels 1 (top figure) and 2 (bottom figure)

The fiber orientation is shown in Figure 100 where the majority of the measured points approached a circular and thus random fiber orientation. This was also one of the findings for the small plates that were horizontally cast. Because the segregation is not severe for the horizontally cast plates, the measurements in the middle of the plate (y=0) can estimate the fiber content relatively well. These values have an average of about 2% which was the original intended fiber content for these panels.

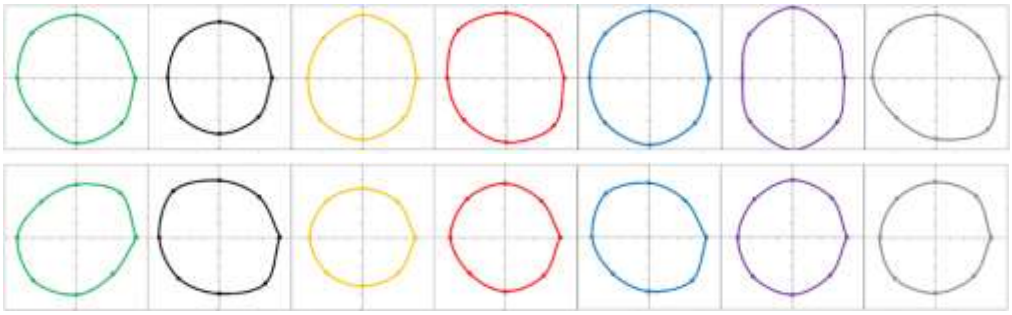

Figure 100: {$\mu_r - 1$} plots of horizontally cast panels 1 (top figure) and 2 (bottom figure)

5.7.2 Vertically cast panels

The results from the two vertically cast shear panels can be found in Figures 101 and 102. Both panels have a similar fiber distribution and orientation. Severe segregation occurs towards the bottom of the panel, which is to be expected after vibrating for a long time. It is notable that both panels have one bottom corner with a very low fiber content as well. The rest of the bottom part of the shear panels is high in fiber content.

Figure 102 shows the fiber orientation at multiple locations on the panels. The magnitude of this fiber orientation shape is the largest at locations with a large fiber content. For instance, in panel 1, the fiber content is highest around x = 500 mm. This is exactly where one of the measurements has been done using the C-shaped ferrite probe, namely the third one. The third measuring point resulted in the largest magnitude of fiber orientation measurements. This is in line with the results from the small plates. All measurements show a preferential vertical orientation, similar to the small plates that were vibrated for a long time. Once again, this measurement will likely be unreliable due to the long vibration and thus heavy fiber segregation.

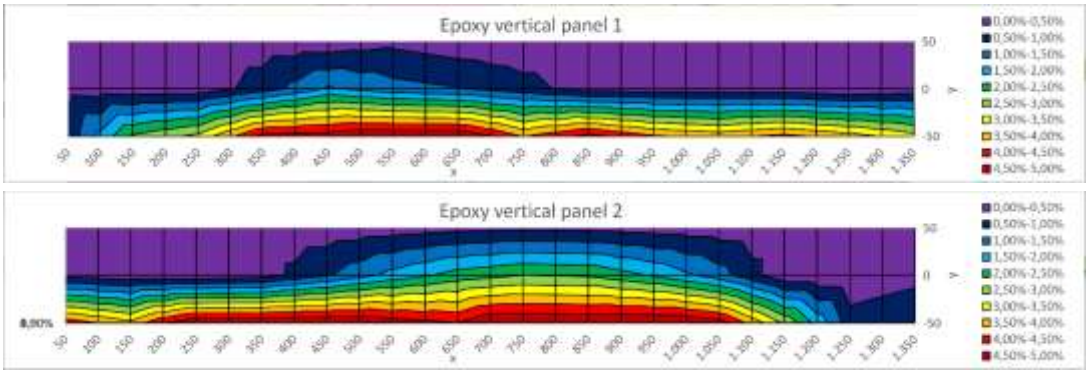

Figure 101: fiber distribution of vertically cast panels 1 (top figure) and 2 (bottom figure)

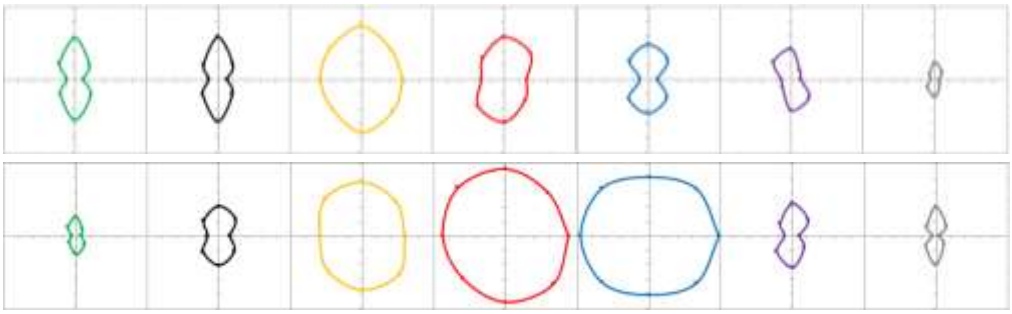

Figure 102: {$\mu_r - 1$} plots of vertically cast panels 1 (top figure) and 2 (bottom figure)

5.8 CT scan

As described in Chapter 4.3.5, a CT scan has been used to X-ray ten different UHPFRC plates. The resulting images of all full 10 plates can be found in Appendix 6. When comparing these to the fiber content contour plots, the results seem to match quite well. The fiber area percentage is approximated using the greyscale imaging tool ImageJ (ImageJ, 2024). Firstly, an overview is given of the fiber contents derived from the magnetic NDT method.

5.8.1 Fiber content from NDT method

In this research, 20 different UHPFRC plates were cast without vibrating the plates. The average fiber content of each plate was estimated using measurements from the single ferrite probe and the C-shaped ferrite probe. An overview of these results can be found in Table 15. These measurements show that the difference in fiber content is significant between plates cast from the same mixture. This is most likely caused by fiber segregation within the UHPFRC mix before casting. However, the average fiber content of all plates cast from the same mixture approximates the intended fiber content rather well. This proves that both probe types can give a reliable prediction of the fiber content in case there is a small amount of segregation. A large amount of segregation can lead to an underestimation of the global fiber content, which was seen for the vibrated plates. This effect is more significant for the C-shaped probe, since this probe type has a stronger "edge effect".

For example for plate V2V5A, the magnetic NDT measurements resulted in an approximated fiber content of 1.14% and 0.73% for the single ferrite probe and the C-shaped ferrite probe, respectively. The actual fiber content should be around 2% since the mixture it was cast with contained this fiber content. Because of the heavy fiber segregation within the plate, the fiber content is significantly underestimated. This is the reason that the vibrated plates are not included in Table 15.

Table 15: estimation of fiber content in all non-vibrated plates

		Fiber content			
	Weight [g]	By single ferrite probe [%]	Average [%]	By C-shaped ferrite probe [%]	Average [%]
H1A	1064.0	1.08	1.01	0.95	0.93
H1B	1035.0	1.10		1.03	
V1A	1030.4	0.90		0.85	
V1B	1045.5	0.95		0.90	
H2A	1030.9	1.93	2.02	1.94	2.00
H2B	1037.0	1.97		1.98	
V2A	1080.3	2.05		1.97	
V2B	1097.9	2.59		2.59	
H2A2	1061.7	2.19		2.15	
H2B2	1043.2	1.97		1.92	
V2A2	1052.3	1.47		1.56	
V2B2	1059.9	1.95		1.90	
H3A	1067.4	3.04	2.89	3.00	2.91
H3B	1062.1	2.44		2.40	
V3A	1081.4	2.96		2.86	
V3B	1108.8	3.12		3.37	
H4A	1117.1	4.04	4.15	4.02	4.06
H4B	1079.7	4.20		4.15	
V4A	1099.3	4.03		3.96	
V4B	1107.9	4.31		4.11	

5.8.2 Fiber content: NDT method vs CT scan

First of all, the CT scan was performed on the entire plate. However, these images contained a lot of shading from the edges of the plate. That is why three separate photos are taken at the center of the plate for greyscale analysis and a quick numerical comparison. This process is described and shown in Appendix 6. For the visual comparison, the full plate images were used.

Figure 103, on this page and the next, is a side-by-side view of the contour plots and CT scan images of three different plates. Plates H1A, H3A and V2V5A are chosen as an example since the NDT method showed that these plates differ significantly in fiber distribution. Since the NDT measurements have been performed 50 mm from the edge, the measured area has been highlighted in red.

Fortunately, the CT scan images generally confirm the magnetic probe measurements. The image of plate H1A clearly has a much smaller fiber content than plate H3A. Moreover, the distribution seems slightly more homogeneous. For plate H3A, the top right quarter seems to contain the most fibers where the bottom left seems to contain the least. This is also somewhat reflected in the contour plot from the NDT method. As was expected, the CT scan of plate V2V5A shows that severe fiber segregation has occurred in the plate. The top part of the plate barely contains any fibers, since all have sunk to the bottom. It is interesting to notice that two cracks have occurred at the top of the plate. This shows the brittle behaviour of the material in the absence of fibers.

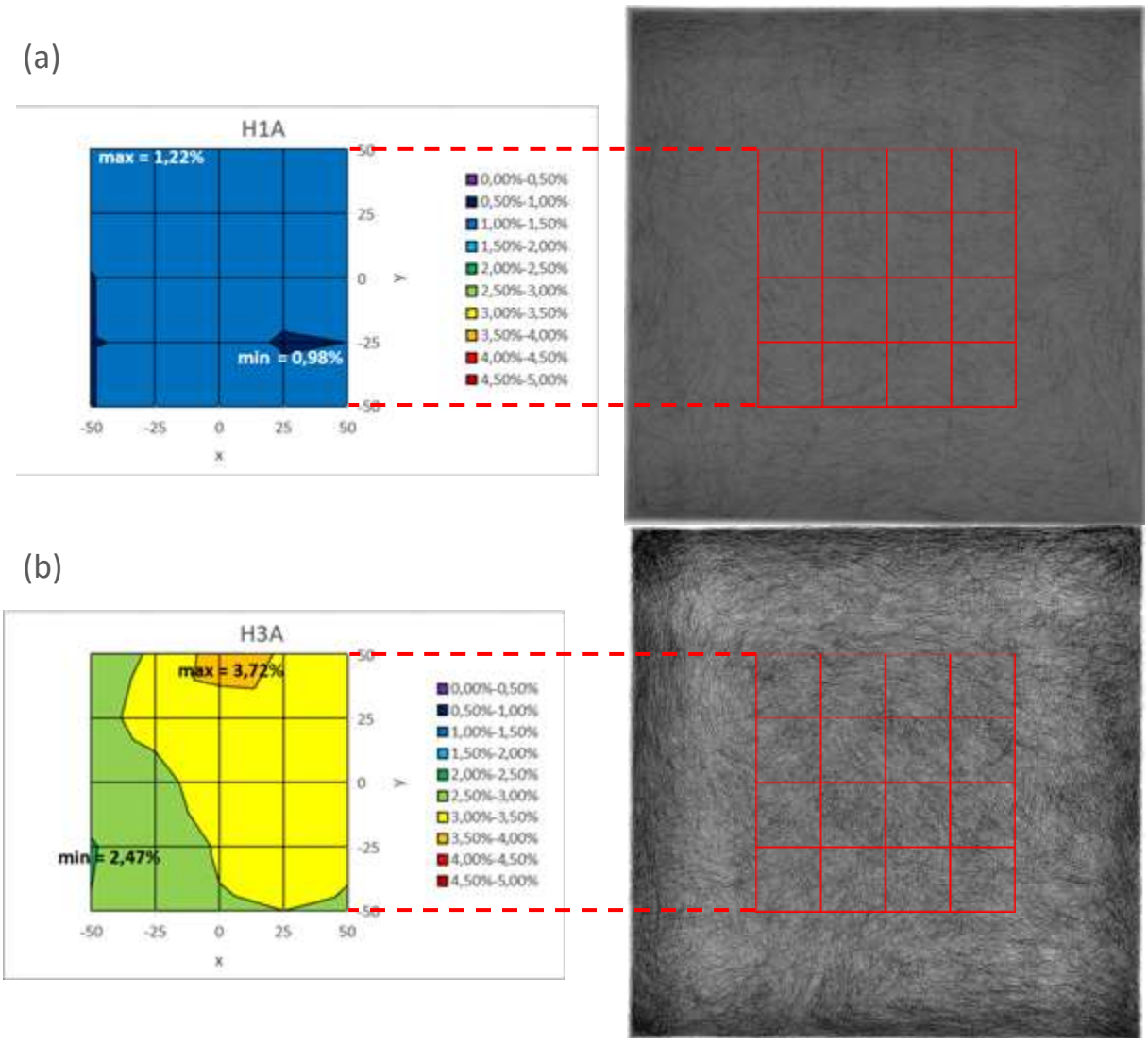

Figure 103: side-by-side comparison contour plot NDT method and CT scan for plates H1A (a), H3A (b) and V2V5A (c)

(c)

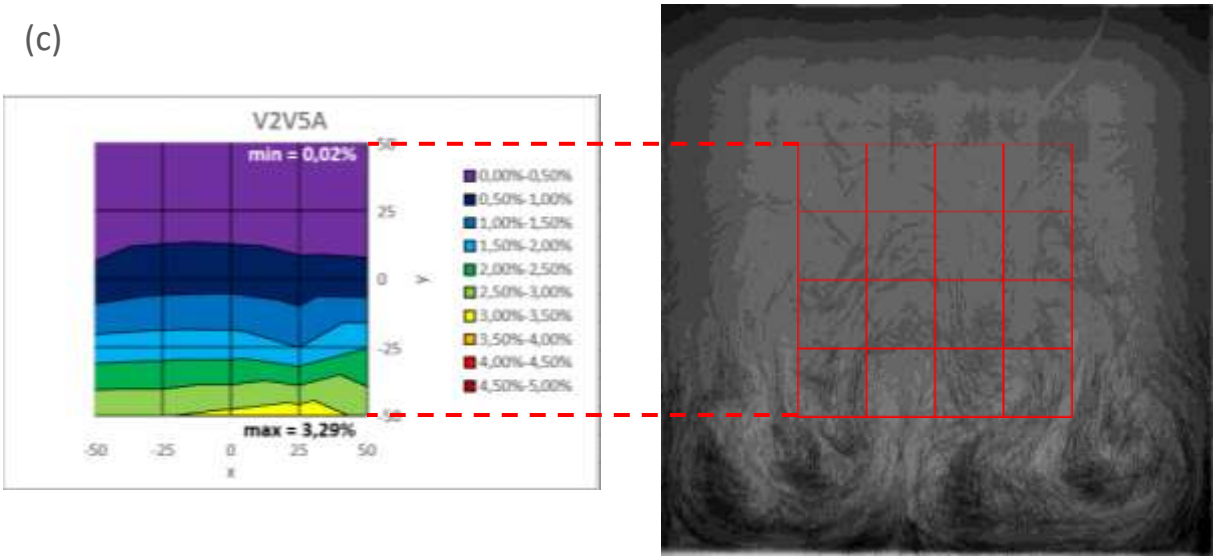

Continuation Figure 103: side-by-side comparison contour plot NDT method and CT scan for plates H1A (a), H3A (b) and V2V5A (c)

Table 16, on the next page, contains the area percentages of the fibers in the 2D CT scan image in each part of the plate. This is compared with the found fiber contents using the NDT method on the right side of Tabel 17. It is important to note that the area percentages were determined in the center of all plates, as described in Appendix 6.

Immediately, it is notable that the area percentage has a much larger value than the fiber content. This phenomenon occurs because the CT scan image is a 2D projection of a 3D scenario. The thickness of the plate is not taken into account by the area percentage. When a fiber is visible in the CT scan image, the area percentage will include this fiber. However, the fiber is not present over the entire thickness of the plate. This is why the magnitude of the percentage is much larger for the area percentage of fibers.

On the other hand, when fibers are overlapped, there is a certain area that is not taken into account. This is the area where the fibers cross, which is marked white in Figure 104. For a perfect 3D approximation of the fiber content, this area should be included twice in the area. Instead, the greyscale imaging tool will not distinguish the individual fibers and analyse this area as a singular point. However, this effect is significantly less dominant than the effect mentioned in the last paragraph.

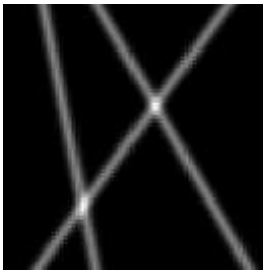

Figure 104: fibers overlapping in greyscale

This is why the area percentage is not a good representation of the fiber content which is a 3D parameter. However, the area percentage and the fiber content are correlated. This can also be seen in Table 16 where the contour plots, found with the single ferrite probe, are shown. In general, the area percentage of fibers is larger in the part of the plate with the largest fiber content. Plate V2V5A has the most severe fiber segregation which also follows from the area percentages. At the top, there is only 1.5% of fiber area percentage and at the bottom, there is 61%. In conclusion, even though there is not a direct relationship between the fiber area percentage and the fiber content, there is a clear correlation between the two.

Table 16: estimated fiber content using CT scan image and the NDT method

H1A	%Area	Single ferrite probe
top	33.2%	1.08%
center	30.9%	
bottom	28.6%	
H1B		
top	32.8%	1.10%
center	31.5%	
bottom	33.6%	
V1A		
top	26.6%	0.90%
center	32.0%	
bottom	31.5%	
H2A2		
top	49.6%	2.19%
center	41.0%	
bottom	38.5%	
H2B2		
top	42.8%	1.97%
center	41.7%	
bottom	40.2%	
V2A2		
top	36.4%	1.47%
center	37.1%	
bottom	31.4%	
V2B2		
top	40.9%	1.95%
center	41.3%	
bottom	42.1%	
H3A		
top	51.4%	3.04%
center	46.1%	
bottom	47.0%	
V3B		
top	50.1%	3.12%
center	48.8%	
bottom	45.7%	
V2V5A		
top	1.5%	1.14%
center	15.1%	
bottom	61.0%	

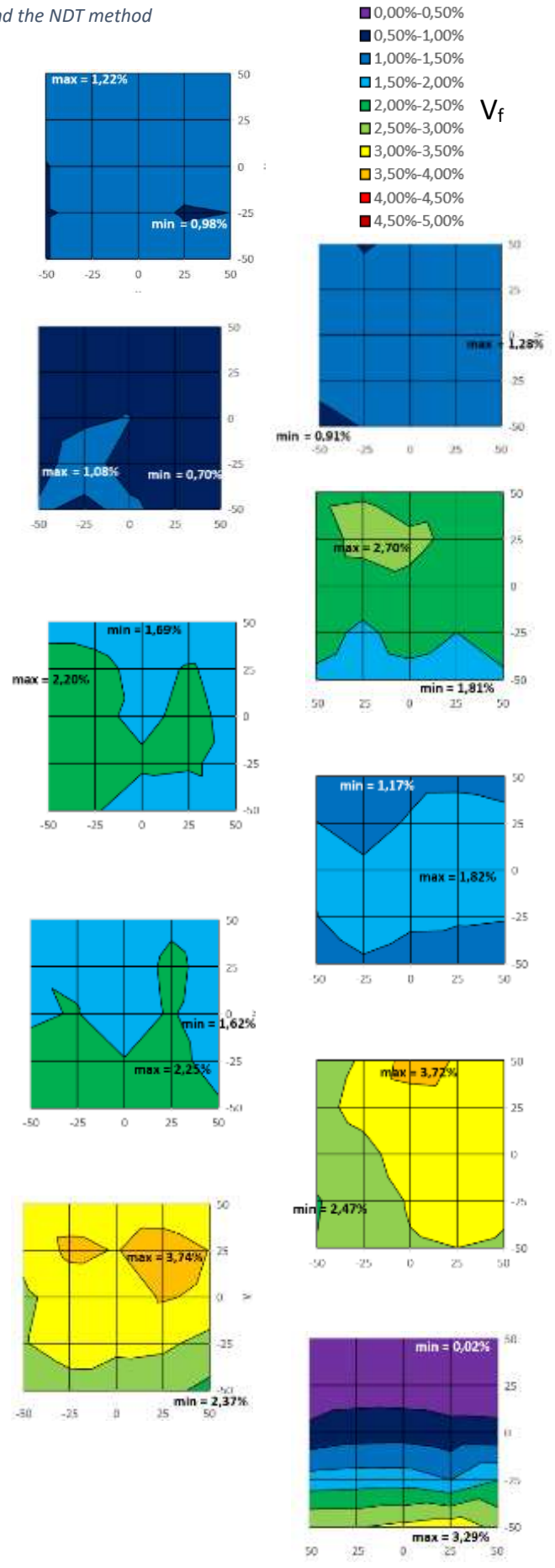

5.9 Influence on estimation of tensile strength

In this part, the peak-tensile strength used for design calculations is estimated for both the Swiss code, the French code and using the results from this research. These results are compared in order to show the possible benefit of the non-destructive magnetic testing method.

5.9.1 Peak-tensile strength used for calculations

Switzerland

As discussed in Chapter 3.1.1, the Swiss design code applies a standard value of 7.0 MPa for the UHPFRC tensile strength. This value is based on a perfectly random fiber distribution and a homogeneous fiber distribution. For safety reasons, this value is decreased using a safety factor of 0.835 resulting in a design tensile strength of 5.85 MPa.

France

The French standard destructively measures the peak-tensile strength of multiple UHPFRC elements for a certain mixture with a certain fiber content. The average value of these elements is taken as the peak-tensile strength where a large safety factor, the K-factor, is introduced to account for a poor fiber distribution and orientation. For local defects, this K-factor is 1.75. As shown in Table 2, the average tensile strength for UHPFRC elements with 2% fiber content was 9.20 MPa. This means that the used peak-tensile strength in design calculations will be 5.25 MPa, including the safety factor.

5.9.2 Peak-tensile strength from this research

The peak-tensile strength can be estimated using data from this research. In order to be able to compare the results to the previous calculations, only the 2% fiber content plates are regarded. For these plates, the orientation factor ranged between 0.06 and 0.12. A k_α factor of 1.85 is assumed and a $\alpha_{0,iso}$ factor of 0.62 follows from the ratio of 10/13 between the element thickness and fiber length. Using Formula 6 results in a α_0 range between 0.731 and 1.462. Because this range is larger than 0.70, Formula 8 results in a α_1 factor of 1. It is assumed that a professional technician with more expertise will not have a significant difference in fiber content between the different elements. However, the local fiber content can still differ within an element. Plate V2B has the least homogeneous fiber distribution of all the 2% fiber content plates and ranges between 2.12% and 3.29%. This is a range of 1.17% which is 0.585% from the average. That is why the maximum range for the local fiber content has been taken from 1.42% to 2.59% which is ±0.585% from 2%. By assuming a bond strength τ_f of 11.1 MPa, found in previous research (Abrishambaf, Pimentel, & Nunes, 2017), Formula 9 can give an estimation of the peak-tensile strength. This value ranges between 7.49 and 13.66 MPa. For safety reasons, the worst case scenario is assumed meaning the peak-tensile strength for design calculations will be 7.49 MPa.

These quick calculations show one of the possible advantages of this newly developed non-destructive testing method. Compared to the Swiss and French code, the design peak-tensile strength can increase by 28.0% and 42.7%, respectively. For this result, the UHPFRC elements were cast by someone with very little experience with concrete casting or steel fibers. The tensile strength can increase more and become more reliable if the elements are cast by an expert technician, preferably with experience using steel fibers.

6. Conclusions

This research started with an extensive literature research on UHPFRC, European guidelines and influence of and on fiber distribution and orientation. For the experimental part of the research, 27 UHPFRC plates with different fiber contents, different casting orientations and different vibration times were cast. First of all, these plates were used to calibrate the two magnetic probes used in this research. Three influences on the fiber distribution and fiber orientation were analysed: fiber content, casting orientation and vibration time. Larger UHPFRC shear panels are also analysed and compared to the results of the small plates. In order to validate these results, the effects of edge distance, surface roughness and painted surfaces are defined. Finally, ten different plates are scanned using a CT scan. The images, resulting from this scan, are compared to the NDT method results for quality control. In the next part, all research questions of this thesis will be answered.

How do the fiber distribution and orientation affect the tensile strength and ductility in UHPFRC elements?

The fiber distribution and orientation have a strong influence on the tensile strength and ductility of UHPFRC elements. In general, the tensile strength and ductility is larger for larger fiber contents which is the main reason for adding fibers. The fiber distribution should be as homogeneous as possible to ensure large global tensile strength and ductility. This means there should be very little variation in the local fiber distribution. Local defects can cause a significant decrease of the tensile strength and ductility and might cause local failure.

The optimal fiber orientation is dependent on the direction of the stresses in the element. In general, fibers that are aligned with the stress orientation add most to the tensile strength and ductility. In practice, most structural elements experience stress in multiple directions. In that case a random orientation results in the most optimal solution.

How is fiber distribution and orientation taken into account in current European guidelines, particularly the French and Swiss standards?

At this point in time, there are no UHPFRC specific rules included in Eurocode EN 1992-1-1 (NEN, 2020). Switzerland and France have their own national code for using UHPFRC. The Swiss national code determines the peak-tensile strength by assuming a random fiber orientation and a homogeneous fiber distribution. This value is then decreased by a certain safety factor. The French national code determines the average peak-tensile strength of UHPFRC elements experimentally. This average value is decreased using a safety factor as well.

Does the magnetic NDT method give a reliable prediction of the fiber distribution and fiber orientation and what are the limiting effects of edge distance and surface roughness?

Both the single ferrite probe and the C-shaped ferrite probe are able to reliably estimate the actual fiber content. The probe measurements become significantly less reliable in case of heavy fiber segregation. The single ferrite probe is able to measure closer to the edge compared to the C-shaped ferrite probe but is not suitable for measuring fiber orientation. Surface roughness can negatively influence the measurements so it is advised to measure the smooth side of the plate.

How do the fiber content, casting orientation and vibration time influence the fiber distribution and fiber orientation?

- Larger fiber contents can result in more variation of the fiber distribution, resulting in a less homogeneous material. Fiber content does not have a clear influence on the fiber orientation. Even mixtures with heavy fiber agglomeration during the slump-flow test, can result in a relatively homogeneous fiber distribution and a random fiber orientation.
- Generally, horizontal casting resulted in a more homogeneous fiber distribution than vertical casting. This result is leastwise valid for the plate geometry used in this research. The influence of the casting direction on the fiber orientation was relatively small for the conditions tested under this research.
- Vibrating the specimen leads to severe fiber segregation. The fibers tend to orientate vertical when they are moving downwards and settle in a horizontal orientation at the bottom of the plate.

What are the differences between measuring on bigger UHPFRC shear panels and smaller plates and how do the results compare?

The results from the shear panels are very similar to the small plates. The vertically cast panels experienced severe fiber segregation and the fibers accumulated at the bottom of the mould because the panels were vibrated for a long time. The fiber distribution and orientation in the horizontally cast panels was relatively efficient compared to the vertically cast panels.

What procedure results in the most reliable predicted tensile strength and what recommendations can be given to change current UHPFRC design?

In order to achieve the most homogeneous fiber distribution and random fiber orientation, it is advised to cast the UHPFRC elements horizontally. Vertical casting can also be efficient as well as long as the element is not vibrated, particularly for more fluid mixtures. An advantage of vertical casting is the constant thickness of the plate. The fiber content can be determined based on the necessary strength and ductility of the element.

This non-destructive magnetic inductance method can be used to determine the fiber content and orientation factor. These factors can give a reliable estimation of the concrete strength. UHPFRC designs can become more efficient using this method. Moreover, this method can be used as quality control of cast elements to check the fiber distribution and orientation.

How can the fiber distribution and orientation in UHPFRC elements be characterized and what effects will this have on the design tensile strength and ductility?

In order to perform non-destructive measurement on UHPFRC specimen, the TU Delft has developed two magnetic testing probes, a single ferrite probe and a C-shaped ferrite probe. Using the ferromagnetic properties of the steel fibers within the UHPFRC specimen, these probes are able to measure the inductance which can be used to predict the tensile strength of the material. This strength property is heavily dependent on the fiber distribution and the fiber orientation.

The fiber distribution is determined by performing local fiber content measurements, using the single ferrite probe. A contour plot including the local fiber content measurements can help visualise where the weak regions of the UHPFRC element are. The fiber orientation is determined using the C-shaped ferrite probe. The fiber orientation factor can be used to compare fiber orientations at different locations of a UHPFRC element. For this research, the fibers in most elements were orientated randomly.

The estimation of the peak-tensile strength of UHPFRC elements is dependent on the orientation factor and the local fiber content. The standard Eurocode mentions that the code is only applicable for concrete types with a compressive strength of under 90 MPa which UHPFRC exceeds. France and Switzerland have their own UHPFRC specific codes to determine the tensile strength. This determination includes a significant safety factor. The design tensile strength gathered from this research is significantly higher compared to the design tensile strength from these codes.

Figure 105: magnetic NDT method measurements with C-shaped ferrite core, picture taken by Y. Huang

7. Recommendations

From personal experience during this research and the measurements using the magnetic probe types, a number of useful recommendations can be given for students extending this research or engineering companies that consider using UHPFRC in their design.

One of the important steps in this research is finding the right procedure in order to obtain a relatively homogeneous fiber distribution and relatively random fiber orientation. For this research, this was horizontal casting with as little vibration as possible. These conclusions can be used in projects but it is important that this result might not be valid for different UHPFRC elements and different UHPFRC mix proportions. The thickness of the element was smaller than the applied fiber length which influences the results due to the wall effect. This should be kept in mind when designing a structure with UHPFRC.

The results from the measurements on both sides of the vertically cast UHPFRC plates were very similar, unlike for the horizontally cast plates. This difference is caused by the surface roughness of these plates on the casting side. This surface roughness can result in unreliable and varying measurements. That is why it is recommended to perform the probe measurements on the smooth side of the UHPFRC elements.

During casting of the UHPFRC elements, the casting bucket needs to be continuously mixed so the fibers do not get distributed unevenly among the different elements. This could also be done using a concrete mixer where the material will keep getting mixed. This will also increase the reliability of the UHPFRC tensile strength and ductility.

The C-shaped ferrite probe was used to gather information about the fiber orientation. This is possible due to the shape of the probe, unlike the single ferrite probe. The used probe from the TU Delft only consists of a single rectangular core. The dimensions of the core's cross-section were almost equal to each other which decreases the effect of fiber orientation. Theoretically, if the cross-section was a perfect square, there would be no difference between the inductance measurement in x direction and in y direction. This would halve the amount of measurements. The probe can be optimized more by using a circular ferrite core causing the influences of fiber orientation to be negligible in all directions.

For the UHPFRC plates in this research, a minimum tensile strength of 7.49 MPa was found using the calculation model found in previous research (Nunes S. , Pimentel, Sine, & Mokhberdoran, 2021). This value cannot be used as a general strength property for UHPFRC. This method would require a safety factor again which diminishes the usefulness of the non-destructive testing method. The proposed method consists of taking measurements on certain UHPFRC elements so the fiber behaviour within that specific element is known and the material properties can directly be determined based on this information. This will likely require more time which must be taken into account. However, as discussed, the usage of UHPFRC is advantageous for some applications due to the increase in strength, ductility and durability.

8. Future research

More viscous concrete matrix
The slump-flow tests resulted in flow diameters exceeding the 265 mm limit found in previous research. This research claims the mixture is prone to fiber segregation if this limit is exceeded. For future research, it can be interesting to change the mix proportions in order to decrease the workability and assess the results on the fiber behaviour.

Increase element thickness
An important aspect of the scope of this research is the limitation of the element thickness. For this research, the element thickness was smaller than the used fiber length. This research could be replicated with "thick" UHPFRC elements, as defined by the French UHPFRC code as elements with a thickness greater than three times the fiber length. The influences of fiber content, casting orientation and vibration might be different for "thick" elements.

Increase element size
If the resources are available, larger UHPFRC elements can be cast so the elements are more representative for real-life applications. In this case, measurements can also be taken further apart in order to research the influence of measurement distance better. It is also interesting to cast larger plates with the same dimension ratios as the plates in this research. When the measurements are taken at the same points, relative to the small plates in this research, the difference in fiber segregation and orientation can be researched.

Workability over time
In Chapter 5.1, the workability results for each UHPFRC mixture were presented. The workability flow diameter of mixture 2% vibr B was not taken into account when assessing the workability. For this mixture, the slump flow test was performed 10 minutes after mixing which resulted in a decrease of 11 mm in the diameter flow compared to other 2% fiber content mixtures. This decrease in workability over time could be interesting to analyse, since it might have consequences for real-life applications.

2D CT scan correction
As mentioned in Chapter 5.8.2, the fiber content cannot be approximated for plates with a small thickness. It might be possible to accurately approximate the fiber content by finding a reliable relationship between the 2D area percentage and the 3D fiber content percentage.

Appendix

Appendix 1: Excel ECI calculation

Concrete LCA dataset with all multiplication factors:

Impact category		Material / Process Type	Abiotic De	Abiotic De	Global War	Ozone Lay	Photocher	Acidificatio	Eutrophica	Human Tox	Ecotoxicity	Ecotoxicity	Ecotoxicity
			non fuel (/	fuel (ADf)	(GWP)	(ODP)	(POCP)	(AP)	(EP)	(HT)	(FAETP)	(MAETP)	(TETP)
Unit			kg Sb eq	kg Sb eq	kg CO2 eq	kg CFC-11	kg C2H4 e	kg SO2 eq	kg PO43- e	kg 1,4-DB	kg 1,4-DB	kg 1,4-DB	kg 1,4-DB eq
	Monetary value / impact categor		0,16	0,16	0,05	30	2	4	9	0,09	0,03	0,0001	0,06
Raw materials:		Unit:											
CEM I NL		Cement	kg	6,70E-07	5,70E-04	8,20E-01	5,20E-09	2,10E-04	2,70E-03	3,60E-04	5,00E-02	6,90E-04	5,10E+00	6,80E-04
CEM IIIA NL		Cement	kg	6,70E-07	7,70E-04	4,40E-01	5,40E-09	1,20E-04	1,50E-03	1,70E-04	3,30E-02	4,40E-04	7,30E+00	4,50E-04
CEM IIIB NL		Cement	kg	6,50E-07	8,00E-04	3,00E-01	5,20E-09	9,00E-05	1,00E-03	1,00E-04	2,70E-02	3,40E-04	7,80E+00	3,60E-04
Blast Furnace Slag (GGBFS)		Pozzolan / filler	kg	7,60E-10	1,70E-04	1,90E-02	1,10E-09	1,00E-06	5,80E-06	1,40E-06	3,60E-03	4,60E-06	2,00E+00	2,70E-06
Fly ash from coal		Pozzolan / filler	kg	8,50E-10	2,30E-05	3,30E-03	2,60E-10	1,20E-06	1,50E-05	3,50E-06	6,70E-04	2,10E-05	2,10E-01	7,40E-06
Silica fume		Pozzolan / filler	kg	4,80E-09	3,90E-05	5,20E-03	3,90E-10	1,60E-06	1,40E-05	3,30E-06	1,50E-03	3,00E-05	3,20E-01	4,80E-05
Limestone powder NL		Filler	kg	1,90E-08	2,40E-04	3,20E-02	2,40E-09	9,70E-06	8,60E-05	1,80E-05	8,40E-03	1,80E-04	2,00E+00	7,40E-05
Sand, river 0-4 mm NL		Aggregate Fine - primary	kg	1,30E-09	2,00E-05	2,90E-03	3,10E-10	2,30E-06	1,80E-05	4,20E-06	1,90E-03	3,10E-05	2,00E-01	1,10E-05
Sand, sea 0-4 mm NL		Aggregate Fine - primary	kg	3,40E-09	7,40E-05	1,10E-02	1,30E-09	1,00E-05	7,90E-05	1,80E-05	8,00E-03	1,30E-04	7,40E-01	2,30E-05
Sand, crushed 0-4 mm NL		Aggregate Fine - primary	kg	1,90E-08	6,90E-05	9,00E-03	5,70E-10	3,10E-06	2,90E-05	6,10E-06	4,30E-03	5,40E-05	5,50E-01	3,20E-05
Granulate, crushed recycled 0-4 mm		Aggregate Fine - secondary	kg	5,10E-10	1,40E-05	2,00E-03	3,00E-10	6,90E-07	3,00E-06	5,20E-07	3,30E-04	1,60E-05	1,00E-01	2,80E-06
Gravel, river >4 mm NL		Aggregate Coarse - secondary	kg	1,20E-10	7,10E-06	1,10E-03	1,70E-10	3,60E-07	1,40E-06	2,30E-07	1,60E-04	8,40E-06	5,20E-02	7,00E-07
Gravel, sea >4 mm NL		Aggregate Coarse - primary	kg	3,10E-09	7,20E-05	1,10E-02	1,30E-09	1,00E-05	7,90E-05	1,80E-05	7,90E-03	1,30E-04	7,30E-01	2,00E-05
Gravel, crushed >4 mm NL		Aggregate Coarse - primary	kg	3,10E-09	4,30E-05	6,20E-03	6,80E-10	7,10E-06	5,70E-05	1,30E-05	1,70E-02	8,90E-05	4,40E-01	1,70E-05
Granulate, crushed recycled >4 mm		Aggregate Coarse - secondary	kg	7,70E-10	7,00E-06	1,10E-03	1,10E-10	8,30E-07	6,70E-06	1,50E-06	7,20E-04	1,10E-05	6,80E-02	5,60E-06
Expanded clay - light weight aggregate		Aggregate - primary	kg	1,30E-07	2,10E-03	3,10E-01	3,90E-08	1,50E-04	2,30E-03	1,40E-04	2,40E-01	1,90E-02	1,30E+02	6,30E-03
Plasticizer - water reducer		Chemical Admixture	kg	0,00E+00	2,20E-03	3,90E-01	2,20E-07	8,90E-04	1,00E-02	1,60E-03	1,10E-01	6,60E-03	1,70E+01	2,60E-04
Super plasticizer - high range water red		Chemical Admixture	kg	0,00E+00	8,10E-03	7,20E-01	9,60E-08	1,40E-03	9,70E-03	4,60E-04	8,20E-02	3,00E-02	9,10E+00	3,60E-04
Pigment white (titanium dioxide)		Pigment	kg	9,70E-06	3,80E-02	4,50E+00	7,70E-07	2,40E-03	3,60E-02	2,60E-03	1,40E+00	3,10E-02	2,70E+02	1,70E-02
Pigment black (carbon black)		Pigment	kg	1,50E-06	1,10E-02	6,70E-01	3,70E-07	2,40E-04	1,90E-03	1,80E-04	3,10E-01	1,00E-02	2,70E+01	7,20E-04
Pigment (red)		Pigment	kg	1,60E-07	1,30E-03	1,50E-01	2,30E-08	3,80E-05	1,90E-04	3,10E-05	3,80E-02	3,40E-04	6,00E+00	1,80E-04
Tap water		Water	kg	2,60E-10	2,70E-06	3,40E-04	1,60E-11	1,10E-07	8,00E-07	1,40E-07	8,30E-05	1,30E-06	2,20E-02	1,50E-06
Surface / well water		Water	kg	0,00E+00	0,00E+00	0,00E+00	0,00E+00	0,00E+00	0,00E+00	0,00E+00	0,00E+00	0,00E+00	0,00E+00	0,00E+00
Steel rebar		Reinforcement	kg	1,10E-06	1,30E-02	1,50E+00	6,00E-08	1,20E-03	5,10E-03	7,00E-04	5,50E-01	1,80E-02	5,00E+01	2,70E-02
Steel fibres		Reinforcement	kg	3,50E-06	1,40E-02	1,90E+00	9,00E-08	1,30E-03	6,10E-03	8,30E-04	6,10E-01	2,80E-02	6,20E+01	2,90E-02
Steel (zinc coated)		Metal	kg	7,20E-08	1,30E-02	2,60E+00	0,00E+00	1,00E-03	3,30E-03	4,00E-04	1,20E-02	1,10E-03	4,70E-05	6,20E-04
Steel (Stainless steel)		Metal	kg	1,50E-04	3,30E-02	4,50E+00	2,40E-07	2,30E-03	2,40E-02	2,40E-03	7,70E+01	8,20E-02	3,70E+02	1,10E-01
Plastic/polymer fibres		Reinforcement	kg	4,40E-07	3,60E-02	2,40E+00	3,00E-08	2,30E-03	8,30E-03	8,30E-04	2,80E+01	1,90E-02	3,30E+01	2,60E-03

Calculations reinforcement weight

$$\rho_{sc,CC} = \frac{A_s}{A_c} = \frac{n_{bars} * 0.25\pi D^2}{b_c h_{c,add}} = \frac{4 * 0.25\pi * 10^2}{400 * 50} = 0.0157 = 1.57\%$$

$$m_{s,CC} = \rho_{sc,CC} * 1\ m^3 * \rho_s = 0.0157 * 1 * 7{,}850 = 123.25\ kg$$

$$\rho_{sc,U} = \frac{A_s}{A_U} = \frac{n_{bars} * 0.25\pi D^2}{b_U h_U} = \frac{3 * 0.25\pi * 8^2}{400 * 50} = 0.0075 = 0.75\%$$

$$m_{s,U} = \rho_{sc,U} * 1\ m^3 * \rho_s = 0.0075 * 1 * 7{,}850 = 58.88\ kg$$

ECI calculation Conventional Concrete (CC)

Impact category	Material / Process Type			Abiotic De	Abiotic Dep	Global Wa	Ozone Lay	Photochen	Acidificati	Eutrophica	Human To	Ecotoxicity	Ecotoxicity	Ecotoxicity	Terrestrial
				non fuel (A	Fuel (ADF)	(GWP)	(ODP)	(POCP)	(AP)	(EP)	(HT)	(FAETP)	(MAETP)	(TETP)	
Unit				kg Sb eq	kg Sb eq	kg CO2 eq	kg CFC-11	kg C2H4 eq	kg SO2 eq	kg PO42- e	kg 1,4-DB	kg 1,4-DB	kg 1,4-DB	kg 1,4-DB eq	
	Monetary value / impact category equivalent in Euro:			0,16	0,16	0,05	30	2	4	9	0,09	0,03	0,0001	0,06	
		Units:													**Total Euro**
Raw materials:															
CEM I NL	Cement	250	kg	2,68E-05	2,28E-02	1,03E+01	3,90E-05	1,05E-01	2,70E+00	8,10E-01	1,13E+00	5,18E-03	1,28E-01	1,02E-02	€ 15,16
CEM IIIA NL	Cement		kg	0,00E+00	0,00E+00	0,00E+00	0,00E+00	0,00E+00	0,00E+00	0,00E+00	0,00E+00	0,00E+00	0,00E+00	0,00E+00	€ 0,00
CEM IIIB NL	Cement	225	kg	2,34E-05	2,88E-02	3,38E+00	3,51E-05	4,05E-02	9,00E-01	2,03E-01	5,47E-01	2,30E-03	1,76E-01	4,86E-03	€ 5,28
Blast Furnace Slag (GGBFS)	Pozzolan / filler		kg	0,00E+00	0,00E+00	0,00E+00	0,00E+00	0,00E+00	0,00E+00	0,00E+00	0,00E+00	0,00E+00	0,00E+00	0,00E+00	€ 0,00
Fly ash from coal	Pozzolan / filler		kg	0,00E+00	0,00E+00	0,00E+00	0,00E+00	0,00E+00	0,00E+00	0,00E+00	0,00E+00	0,00E+00	0,00E+00	0,00E+00	€ 0,00
Silica fume	Pozzolan / filler		kg	0,00E+00	0,00E+00	0,00E+00	0,00E+00	0,00E+00	0,00E+00	0,00E+00	0,00E+00	0,00E+00	0,00E+00	0,00E+00	€ 0,00
Limestone powder NL	Filler		kg	0,00E+00	0,00E+00	0,00E+00	0,00E+00	0,00E+00	0,00E+00	0,00E+00	0,00E+00	0,00E+00	0,00E+00	0,00E+00	€ 0,00
Sand, river 0-4 mm NL	Aggregate Fine - primary	684	kg	1,42E-07	2,19E-03	9,92E-02	6,36E-06	3,15E-03	4,92E-02	2,59E-02	1,17E-01	6,36E-04	1,37E-02	4,51E-04	€ 0,31
Sand, sea 0-4 mm NL	Aggregate Fine - primary		kg	0,00E+00	0,00E+00	0,00E+00	0,00E+00	0,00E+00	0,00E+00	0,00E+00	0,00E+00	0,00E+00	0,00E+00	0,00E+00	€ 0,00
Sand, crushed 0-4 mm NL	Aggregate Fine - primary		kg	0,00E+00	0,00E+00	0,00E+00	0,00E+00	0,00E+00	0,00E+00	0,00E+00	0,00E+00	0,00E+00	0,00E+00	0,00E+00	€ 0,00
Granulate, crushed recycled 0-4 mi	Aggregate Fine - secondary		kg	0,00E+00	0,00E+00	0,00E+00	0,00E+00	0,00E+00	0,00E+00	0,00E+00	0,00E+00	0,00E+00	0,00E+00	0,00E+00	€ 0,00
Gravel, river >4 mm NL	Aggregate Coarse - secondary	1177	kg	2,26E-08	1,34E-03	6,47E-02	6,00E-06	8,47E-04	6,59E-03	2,44E-03	1,69E-02	2,97E-04	6,12E-03	4,94E-05	€ 0,10
Gravel, sea >4 mm NL	Aggregate Coarse - primary		kg	0,00E+00	0,00E+00	0,00E+00	0,00E+00	0,00E+00	0,00E+00	0,00E+00	0,00E+00	0,00E+00	0,00E+00	0,00E+00	€ 0,00
Gravel, crushed >4 mm NL	Aggregate Coarse - primary		kg	0,00E+00	0,00E+00	0,00E+00	0,00E+00	0,00E+00	0,00E+00	0,00E+00	0,00E+00	0,00E+00	0,00E+00	0,00E+00	€ 0,00
Granulate, crushed recycled >4 mm	Aggregate Coarse - secondary		kg	0,00E+00	0,00E+00	0,00E+00	0,00E+00	0,00E+00	0,00E+00	0,00E+00	0,00E+00	0,00E+00	0,00E+00	0,00E+00	€ 0,00
Expanded clay - light weight aggre	Aggregate - primary		kg	0,00E+00	0,00E+00	0,00E+00	0,00E+00	0,00E+00	0,00E+00	0,00E+00	0,00E+00	0,00E+00	0,00E+00	0,00E+00	€ 0,00
Plasticizer - water reducer	Chemical Admixture		kg	0,00E+00	0,00E+00	0,00E+00	0,00E+00	0,00E+00	0,00E+00	0,00E+00	0,00E+00	0,00E+00	0,00E+00	0,00E+00	€ 0,00
Super plasticizer - high range wate	Chemical Admixture	3,5	kg	0,00E+00	4,54E-03	1,26E-01	1,01E-05	9,80E-03	1,36E-01	1,45E-02	2,58E-02	3,15E-03	3,19E-03	7,56E-05	€ 0,32
Pigment white (titanium dioxide)	Pigment		kg	0,00E+00	0,00E+00	0,00E+00	0,00E+00	0,00E+00	0,00E+00	0,00E+00	0,00E+00	0,00E+00	0,00E+00	0,00E+00	€ 0,00
Pigment black (carbon black)	Pigment		kg	0,00E+00	0,00E+00	0,00E+00	0,00E+00	0,00E+00	0,00E+00	0,00E+00	0,00E+00	0,00E+00	0,00E+00	0,00E+00	€ 0,00
Pigment (red)	Pigment		kg	0,00E+00	0,00E+00	0,00E+00	0,00E+00	0,00E+00	0,00E+00	0,00E+00	0,00E+00	0,00E+00	0,00E+00	0,00E+00	€ 0,00
Tap water	Water	160	kg	6,66E-09	6,91E-05	2,72E-03	7,68E-08	3,52E-05	5,12E-04	2,02E-04	1,20E-03	6,24E-06	3,52E-04	1,44E-05	€ 0,01
Surface / well water	Water		kg	0,00E+00	0,00E+00	0,00E+00	0,00E+00	0,00E+00	0,00E+00	0,00E+00	0,00E+00	0,00E+00	0,00E+00	0,00E+00	€ 0,00
Steel rebar	Reinforcement		kg	0,00E+00	0,00E+00	0,00E+00	0,00E+00	0,00E+00	0,00E+00	0,00E+00	0,00E+00	0,00E+00	0,00E+00	0,00E+00	€ 0,00
Steel fibres	Reinforcement		kg	0,00E+00	0,00E+00	0,00E+00	0,00E+00	0,00E+00	0,00E+00	0,00E+00	0,00E+00	0,00E+00	0,00E+00	0,00E+00	€ 0,00
Steel (Zinc coated)	Metal		kg	0,00E+00	0,00E+00	0,00E+00	0,00E+00	0,00E+00	0,00E+00	0,00E+00	0,00E+00	0,00E+00	0,00E+00	0,00E+00	€ 0,00
Steel (Stainless steel)	Metal		kg	0,00E+00	0,00E+00	0,00E+00	0,00E+00	0,00E+00	0,00E+00	0,00E+00	0,00E+00	0,00E+00	0,00E+00	0,00E+00	€ 0,00
Plastic/polymer fibres	Reinforcement		kg	0,00E+00	0,00E+00	0,00E+00	0,00E+00	0,00E+00	0,00E+00	0,00E+00	0,00E+00	0,00E+00	0,00E+00	0,00E+00	€ 0,00
Total euro				€ 0,00	€ 0,06	€ 13,92	€ 0,00	€ 0,16	€ 3,79	€ 1,06	€ 1,83	€ 0,01	€ 0,33	€ 0,02	€ 21,17

ECI calculation Reinforced Concrete (RC)

Impact category	Material / Process Type			Abiotic De	Abiotic Dep	Global Wa	Ozone Lay	Photochem	Acidificatio	Eutrophica	Human To	Ecotoxicity	Ecotoxicity	Ecotoxicity	Potential	Terrestrial
				non fuel (A	fuel (ADf)	(GWP)	(ODP)	(POCP)	(AP)	(EP)	(HT)	(FAETP)	(MAETP)	(TETP)		
Unit				kg Sb eq	kg Sb eq	kg CO2 eq	kg CFC-11	kg C2H4 eq	kg SO2 eq	kg PO42- e	kg 1,4-DB e	kg 1,4-DB e	kg 1,4-DB e	kg 1,4-DB eq		
	Monetary value / Impact category equivalent in Euro:			0,16	0,16	0,05	30	2	4	9	0,09	0,03	0,0001	0,06		
Raw materials:		Unit:														**Total Euro**
CEM I NL	Cement	250	kg	2,68E-05	2,28E-02	1,03E+01	3,90E-05	1,05E-01	2,70E+00	8,10E-01	1,13E+00	5,18E-03	1,28E-01	1,02E-02		€ 15,16
CEM IIIA NL	Cement		kg	0,00E+00	0,00E+00	0,00E+00	0,00E+00	0,00E+00	0,00E+00	0,00E+00	0,00E+00	0,00E+00	0,00E+00	0,00E+00		€ -
CEM IIIB NL	Cement	225	kg	2,34E-05	2,88E-02	3,38E+00	3,51E-05	4,05E-02	9,00E-01	2,03E-01	5,47E-01	2,30E-03	1,76E-01	4,86E-03		€ 5,28
Blast Furnace Slag (GGBFS)	Pozzolan / filler		kg	0,00E+00	0,00E+00	0,00E+00	0,00E+00	0,00E+00	0,00E+00	0,00E+00	0,00E+00	0,00E+00	0,00E+00	0,00E+00		€ -
Fly ash from coal	Pozzolan / filler		kg	0,00E+00	0,00E+00	0,00E+00	0,00E+00	0,00E+00	0,00E+00	0,00E+00	0,00E+00	0,00E+00	0,00E+00	0,00E+00		€ -
Silica fume	Pozzolan / filler		kg	0,00E+00	0,00E+00	0,00E+00	0,00E+00	0,00E+00	0,00E+00	0,00E+00	0,00E+00	0,00E+00	0,00E+00	0,00E+00		€ -
Limestone powder NL	Filler		kg	0,00E+00	0,00E+00	0,00E+00	0,00E+00	0,00E+00	0,00E+00	0,00E+00	0,00E+00	0,00E+00	0,00E+00	0,00E+00		€ -
Sand, river 0-4 mm NL	Aggregate Fine - primary	684	kg	1,42E-07	2,19E-03	9,92E-02	6,36E-06	3,15E-03	4,92E-02	2,59E-02	1,17E-01	6,36E-04	1,37E-02	4,51E-04		€ 0,31
Sand, sea 0-4 mm NL	Aggregate Fine - primary		kg	0,00E+00	0,00E+00	0,00E+00	0,00E+00	0,00E+00	0,00E+00	0,00E+00	0,00E+00	0,00E+00	0,00E+00	0,00E+00		€ -
Sand, crushed 0-4 mm NL	Aggregate Fine - primary		kg	0,00E+00	0,00E+00	0,00E+00	0,00E+00	0,00E+00	0,00E+00	0,00E+00	0,00E+00	0,00E+00	0,00E+00	0,00E+00		€ -
Granulate, crushed recycled 0-4 mi	Aggregate Fine - secondary		kg	0,00E+00	0,00E+00	0,00E+00	0,00E+00	0,00E+00	0,00E+00	0,00E+00	0,00E+00	0,00E+00	0,00E+00	0,00E+00		€ -
Gravel, river >4 mm NL	Aggregate Coarse - secondary	1177	kg	2,26E-08	1,34E-03	6,47E-02	6,00E-06	8,47E-04	6,59E-03	2,44E-03	1,69E-02	2,97E-04	6,12E-03	4,94E-05		€ 0,10
Gravel, sea >4 mm NL	Aggregate Coarse - primary		kg	0,00E+00	0,00E+00	0,00E+00	0,00E+00	0,00E+00	0,00E+00	0,00E+00	0,00E+00	0,00E+00	0,00E+00	0,00E+00		€ -
Gravel, crushed >4 mm NL	Aggregate Coarse - primary		kg	0,00E+00	0,00E+00	0,00E+00	0,00E+00	0,00E+00	0,00E+00	0,00E+00	0,00E+00	0,00E+00	0,00E+00	0,00E+00		€ -
Granulate, crushed recycled >4 mm	Aggregate Coarse - secondary		kg	0,00E+00	0,00E+00	0,00E+00	0,00E+00	0,00E+00	0,00E+00	0,00E+00	0,00E+00	0,00E+00	0,00E+00	0,00E+00		€ -
Expanded clay - light weight aggre	Aggregate - primary		kg	0,00E+00	0,00E+00	0,00E+00	0,00E+00	0,00E+00	0,00E+00	0,00E+00	0,00E+00	0,00E+00	0,00E+00	0,00E+00		€ -
Plasticizer - water reducer	Chemical Admixture		kg	0,00E+00	0,00E+00	0,00E+00	0,00E+00	0,00E+00	0,00E+00	0,00E+00	0,00E+00	0,00E+00	0,00E+00	0,00E+00		€ -
Super plasticizer - high range wate	Chemical Admixture	3,5	kg	0,00E+00	4,54E-03	1,26E-01	1,01E-05	9,80E-03	1,36E-01	1,45E-02	2,58E-02	3,15E-03	3,19E-03	7,56E-05		€ 0,32
Pigment white (titanium dioxide)	Pigment		kg	0,00E+00	0,00E+00	0,00E+00	0,00E+00	0,00E+00	0,00E+00	0,00E+00	0,00E+00	0,00E+00	0,00E+00	0,00E+00		€ -
Pigment black (carbon black)	Pigment		kg	0,00E+00	0,00E+00	0,00E+00	0,00E+00	0,00E+00	0,00E+00	0,00E+00	0,00E+00	0,00E+00	0,00E+00	0,00E+00		€ -
Pigment (red)	Pigment		kg	0,00E+00	0,00E+00	0,00E+00	0,00E+00	0,00E+00	0,00E+00	0,00E+00	0,00E+00	0,00E+00	0,00E+00	0,00E+00		€ -
Tap water	Water	160	kg	6,66E-09	6,91E-05	2,72E-03	7,68E-08	3,52E-05	5,12E-04	2,02E-04	1,20E-03	6,24E-06	3,52E-04	1,44E-05		€ 0,01
Surface / well water	Water		kg	0,00E+00	0,00E+00	0,00E+00	0,00E+00	0,00E+00	0,00E+00	0,00E+00	0,00E+00	0,00E+00	0,00E+00	0,00E+00		€ -
Steel rebar	Reinforcement	123,25	kg	2,17E-05	2,56E-01	9,24E+00	2,22E-04	2,96E-01	2,51E+00	7,76E-01	6,10E+00	6,66E-02	6,16E-01	2,00E-01		€ 20,07
Steel fibres	Reinforcement		kg	0,00E+00	0,00E+00	0,00E+00	0,00E+00	0,00E+00	0,00E+00	0,00E+00	0,00E+00	0,00E+00	0,00E+00	0,00E+00		€ -
Steel (Zinc coated)	Metal		kg	0,00E+00	0,00E+00	0,00E+00	0,00E+00	0,00E+00	0,00E+00	0,00E+00	0,00E+00	0,00E+00	0,00E+00	0,00E+00		€ -
Steel (Stainless steel)	Metal		kg	0,00E+00	0,00E+00	0,00E+00	0,00E+00	0,00E+00	0,00E+00	0,00E+00	0,00E+00	0,00E+00	0,00E+00	0,00E+00		€ -
Plastic/polymer fibres	Reinforcement		kg	0,00E+00	0,00E+00	0,00E+00	0,00E+00	0,00E+00	0,00E+00	0,00E+00	0,00E+00	0,00E+00	0,00E+00	0,00E+00		€ -
Total euro				€ 0,00	€ 0,32	€ 23,16	€ 0,00	€ 0,46	€ 6,31	€ 1,83	€ 7,93	€ 0,08	€ 0,94	€ 0,22		€ 41,24

ECI calculation Ultra-High Performance Fiber Reinforced Concrete (UHPFRC)

Impact category		Material / Process Type			Abiotic De	Abiotic Dep	Global Wa	Ozone Lay	Photochen	Acidificati	Eutrophica	Human To	Ecotoxicity	Ecotoxicity	Ecotoxicity	Potential, Terrestrial
					non fuel (A	fuel (ADF)	(GWP)	(ODP)	(POCP)	(AP)	(EP)	(HT)	(FAETP)	(MAETP)	(TETP)	
Unit					kg Sb eq	kg Sb eq	kg CO2 eq	kg CFC-11	kg C2H4 ec	kg SO2 eq	kg PO42- e	kg 1,4-DB e	kg 1,4-DB e	kg 1,4-DB e	kg 1,4-DB eq	
		Monetary value / impact category equivalent in Euro:			0,16	0,16	0,05	30	2	4	9	0,09	0,03	0,0001	0,06	
				Unit:												Total Euro
Raw materials:																
CEM I NL		Cement	kg		0,00E+00	0,00E+00	0,00E+00	0,00E+00	0,00E+00	0,00E+00	0,00E+00	0,00E+00	0,00E+00	0,00E+00	0,00E+00	€ 0,00
CEM IIIA NL		Cement	kg		0,00E+00	0,00E+00	0,00E+00	0,00E+00	0,00E+00	0,00E+00	0,00E+00	0,00E+00	0,00E+00	0,00E+00	0,00E+00	€ 0,00
CEM IIIB NL		Cement	kg	712	7,40E-05	9,11E-02	1,07E+01	1,11E-04	1,28E-01	2,85E+00	6,41E-01	1,73E+00	7,26E-03	5,55E-01	1,54E-02	€ 16,70
Blast Furnace Slag (GGBFS)		Pozzolan / filler	kg		0,00E+00	0,00E+00	0,00E+00	0,00E+00	0,00E+00	0,00E+00	0,00E+00	0,00E+00	0,00E+00	0,00E+00	0,00E+00	€ 0,00
Fly ash from coal		Pozzolan / filler	kg		0,00E+00	0,00E+00	0,00E+00	0,00E+00	0,00E+00	0,00E+00	0,00E+00	0,00E+00	0,00E+00	0,00E+00	0,00E+00	€ 0,00
Silica fume		Pozzolan / filler	kg	231	1,77E-07	1,44E-03	6,01E-02	2,70E-06	7,39E-04	1,29E-02	6,88E-03	3,12E-02	2,08E-04	7,39E-03	6,65E-04	€ 0,12
Limestone powder NL		Filler	kg	211	6,41E-07	8,10E-03	3,38E-01	1,52E-05	4,09E-03	7,26E-02	3,42E-02	1,60E-01	1,14E-03	4,22E-02	9,37E-04	€ 0,66
Sand, river 0-4 mm NL		Aggregate Fine - primary	kg	1020	2,12E-07	3,26E-03	1,48E-01	9,49E-06	4,69E-03	7,34E-02	3,86E-02	1,74E-01	9,49E-04	2,04E-02	6,73E-04	€ 0,46
Sand, sea 0-4 mm NL		Aggregate Fine - primary	kg		0,00E+00	0,00E+00	0,00E+00	0,00E+00	0,00E+00	0,00E+00	0,00E+00	0,00E+00	0,00E+00	0,00E+00	0,00E+00	€ 0,00
Sand, crushed 0-4 mm NL		Aggregate Fine - primary	kg		0,00E+00	0,00E+00	0,00E+00	0,00E+00	0,00E+00	0,00E+00	0,00E+00	0,00E+00	0,00E+00	0,00E+00	0,00E+00	€ 0,00
Granulate, crushed recycled 0-4 mm		Aggregate Fine - secondary	kg		0,00E+00	0,00E+00	0,00E+00	0,00E+00	0,00E+00	0,00E+00	0,00E+00	0,00E+00	0,00E+00	0,00E+00	0,00E+00	€ 0,00
Gravel, river >4 mm NL		Aggregate Coarse - secondary	kg		0,00E+00	0,00E+00	0,00E+00	0,00E+00	0,00E+00	0,00E+00	0,00E+00	0,00E+00	0,00E+00	0,00E+00	0,00E+00	€ 0,00
Gravel, sea >4 mm NL		Aggregate Coarse - primary	kg		0,00E+00	0,00E+00	0,00E+00	0,00E+00	0,00E+00	0,00E+00	0,00E+00	0,00E+00	0,00E+00	0,00E+00	0,00E+00	€ 0,00
Gravel, crushed >4 mm NL		Aggregate Coarse - primary	kg		0,00E+00	0,00E+00	0,00E+00	0,00E+00	0,00E+00	0,00E+00	0,00E+00	0,00E+00	0,00E+00	0,00E+00	0,00E+00	€ 0,00
Granulate, crushed recycled >4 mm		Aggregate Coarse - secondary	kg		0,00E+00	0,00E+00	0,00E+00	0,00E+00	0,00E+00	0,00E+00	0,00E+00	0,00E+00	0,00E+00	0,00E+00	0,00E+00	€ 0,00
Expanded clay - light weight aggre		Aggregate - primary	kg		0,00E+00	0,00E+00	0,00E+00	0,00E+00	0,00E+00	0,00E+00	0,00E+00	0,00E+00	0,00E+00	0,00E+00	0,00E+00	€ 0,00
Plasticizer - water reducer		Chemical Admixture	kg		0,00E+00	0,00E+00	0,00E+00	0,00E+00	0,00E+00	0,00E+00	0,00E+00	0,00E+00	0,00E+00	0,00E+00	0,00E+00	€ 0,00
Super plasticizer - high range wate		Chemical Admixture	kg	30,7	0,00E+00	3,98E-02	1,11E+00	8,84E-05	8,60E-02	1,19E+00	1,27E-01	2,27E-01	2,76E-02	2,79E-02	6,63E-04	€ 2,83
Pigment white (titanium dioxide)		Pigment	kg		0,00E+00	0,00E+00	0,00E+00	0,00E+00	0,00E+00	0,00E+00	0,00E+00	0,00E+00	0,00E+00	0,00E+00	0,00E+00	€ 0,00
Pigment black (carbon black)		Pigment	kg		0,00E+00	0,00E+00	0,00E+00	0,00E+00	0,00E+00	0,00E+00	0,00E+00	0,00E+00	0,00E+00	0,00E+00	0,00E+00	€ 0,00
Pigment (red)		Pigment	kg		0,00E+00	0,00E+00	0,00E+00	0,00E+00	0,00E+00	0,00E+00	0,00E+00	0,00E+00	0,00E+00	0,00E+00	0,00E+00	€ 0,00
Tap water		Water	kg	109	4,53E-09	4,71E-05	1,85E-03	5,23E-08	2,40E-05	3,49E-04	1,37E-04	8,14E-04	4,23E-06	2,40E-04	9,81E-06	€ 0,00
Surface / well water		Water	kg		0,00E+00	0,00E+00	0,00E+00	0,00E+00	0,00E+00	0,00E+00	0,00E+00	0,00E+00	0,00E+00	0,00E+00	0,00E+00	€ 0,00
Steel rebar		Reinforcement	kg		0,00E+00	0,00E+00	0,00E+00	0,00E+00	0,00E+00	0,00E+00	0,00E+00	0,00E+00	0,00E+00	0,00E+00	0,00E+00	€ 0,00
Steel fibres		Reinforcement	kg	156	8,74E-05	3,49E-01	1,48E+01	4,21E-04	4,06E-01	3,81E+00	1,17E+00	8,56E+00	1,31E-01	9,67E-01	2,71E-01	€ 30,48
Steel (Zinc coated)		Metal	kg		0,00E+00	0,00E+00	0,00E+00	0,00E+00	0,00E+00	0,00E+00	0,00E+00	0,00E+00	0,00E+00	0,00E+00	0,00E+00	€ 0,00
Steel (Stainless steel)		Metal	kg		0,00E+00	0,00E+00	0,00E+00	0,00E+00	0,00E+00	0,00E+00	0,00E+00	0,00E+00	0,00E+00	0,00E+00	0,00E+00	€ 0,00
Plastic/polymer fibres		Reinforcement	kg		0,00E+00	0,00E+00	0,00E+00	0,00E+00	0,00E+00	0,00E+00	0,00E+00	0,00E+00	0,00E+00	0,00E+00	0,00E+00	€ 0,00
Total euro					€ 0,00	€ 0,49	€ 27,15	€ 0,00	€ 0,63	€ 8,00	€ 2,01	€ 10,89	€ 0,17	€ 1,62	€ 0,29	€ 51,26

ECI calculation Reinforced Ultra-High Performance Fiber Reinforced Concrete (R-UHPFRC)

Impact category	Material / Process Type			Abiotic De	Abiotic Dep	Global Wa	Ozone Lay	Photochen	Acidificati	Eutrophica	Human To	Ecotoxicity	Ecotoxicity	Ecotoxicity	Potential, Terrestrial	
				non fuel (A	fuel (ADF)	(GWP)	(ODP)	(POCP)	(AP)	(EP)	(HT)	(FAETP)	(MAETP)	(TETP)		
Unit				kg Sb eq	kg Sb eq	kg CO2 eq	kg CFC-11	kg C2H4 eq	kg SO2 eq	kg PO42- e	kg 1,4-DB e	kg 1,4-DB e	kg 1,4-DB e	kg 1,4-DB eq		
	Monetary value / impact category equivalent in Euro:			0,16	0,16	0,05	30	2	4	9	0,09	0,03	0,0001	0,06		
Raw materials:		Unit:														**Total Euro**
CEM I NL	Cement	kg		0,00E+00	0,00E+00	0,00E+00	0,00E+00	0,00E+00	0,00E+00	0,00E+00	0,00E+00	0,00E+00	0,00E+00	0,00E+00	0,00E+00	€ 0,00
CEM IIIA NL	Cement	kg		0,00E+00	0,00E+00	0,00E+00	0,00E+00	0,00E+00	0,00E+00	0,00E+00	0,00E+00	0,00E+00	0,00E+00	0,00E+00	0,00E+00	€ 0,00
CEM IIIB NL	Cement	kg	712	7,40E-05	9,11E-02	1,07E+01	1,11E-04	1,28E-01	2,85E+00	6,41E-01	1,73E+00	7,26E-03	5,55E-01	1,54E-02		€ 16,70
Blast Furnace Slag (GGBFS)	Pozzolan / filler	kg		0,00E+00	0,00E+00	0,00E+00	0,00E+00	0,00E+00	0,00E+00	0,00E+00	0,00E+00	0,00E+00	0,00E+00	0,00E+00	0,00E+00	€ 0,00
Fly ash from coal	Pozzolan / filler	kg		0,00E+00	0,00E+00	0,00E+00	0,00E+00	0,00E+00	0,00E+00	0,00E+00	0,00E+00	0,00E+00	0,00E+00	0,00E+00	0,00E+00	€ 0,00
Silica fume	Pozzolan / filler	kg	231	1,77E-07	1,44E-03	6,01E-02	2,70E-06	7,39E-04	1,29E-02	6,86E-03	3,12E-02	2,08E-04	7,39E-03	6,65E-04		€ 0,12
Limestone powder NL	Filler	kg	211	6,41E-07	8,10E-03	3,38E-01	1,52E-05	4,09E-03	7,26E-02	3,42E-02	1,60E-01	1,14E-03	4,22E-02	9,37E-04		€ 0,66
Sand, river 0-4 mm NL	Aggregate Fine - primary	kg	1020	2,12E-07	3,26E-03	1,48E-01	9,49E-06	4,69E-03	7,34E-02	3,86E-02	1,74E-01	9,49E-04	2,04E-02	6,73E-04		€ 0,46
Sand, sea 0-4 mm NL	Aggregate Fine - primary	kg		0,00E+00	0,00E+00	0,00E+00	0,00E+00	0,00E+00	0,00E+00	0,00E+00	0,00E+00	0,00E+00	0,00E+00	0,00E+00	0,00E+00	€ 0,00
Sand, crushed 0-4 mm NL	Aggregate Fine - primary	kg		0,00E+00	0,00E+00	0,00E+00	0,00E+00	0,00E+00	0,00E+00	0,00E+00	0,00E+00	0,00E+00	0,00E+00	0,00E+00	0,00E+00	€ 0,00
Granulate, crushed recycled 0-4 mi	Aggregate Fine - secondary	kg		0,00E+00	0,00E+00	0,00E+00	0,00E+00	0,00E+00	0,00E+00	0,00E+00	0,00E+00	0,00E+00	0,00E+00	0,00E+00	0,00E+00	€ 0,00
Gravel, river >4 mm NL	Aggregate Coarse - secondary	kg		0,00E+00	0,00E+00	0,00E+00	0,00E+00	0,00E+00	0,00E+00	0,00E+00	0,00E+00	0,00E+00	0,00E+00	0,00E+00	0,00E+00	€ 0,00
Gravel, sea >4 mm NL	Aggregate Coarse - primary	kg		0,00E+00	0,00E+00	0,00E+00	0,00E+00	0,00E+00	0,00E+00	0,00E+00	0,00E+00	0,00E+00	0,00E+00	0,00E+00	0,00E+00	€ 0,00
Gravel, crushed >4 mm NL	Aggregate Coarse - primary	kg		0,00E+00	0,00E+00	0,00E+00	0,00E+00	0,00E+00	0,00E+00	0,00E+00	0,00E+00	0,00E+00	0,00E+00	0,00E+00	0,00E+00	€ 0,00
Granulate, crushed recycled >4 mm	Aggregate Coarse - secondary	kg		0,00E+00	0,00E+00	0,00E+00	0,00E+00	0,00E+00	0,00E+00	0,00E+00	0,00E+00	0,00E+00	0,00E+00	0,00E+00	0,00E+00	€ 0,00
Expanded clay - light weight aggre	Aggregate - primary	kg		0,00E+00	0,00E+00	0,00E+00	0,00E+00	0,00E+00	0,00E+00	0,00E+00	0,00E+00	0,00E+00	0,00E+00	0,00E+00	0,00E+00	€ 0,00
Plasticizer - water reducer	Chemical Admixture	kg		0,00E+00	0,00E+00	0,00E+00	0,00E+00	0,00E+00	0,00E+00	0,00E+00	0,00E+00	0,00E+00	0,00E+00	0,00E+00	0,00E+00	€ 0,00
Super plasticizer - high range wate	Chemical Admixture	kg	30,7	3,58E-02	1,11E+00	8,84E-05	8,60E-02	1,19E+00	1,27E-01	2,27E-01	2,76E-02	2,79E-02	6,63E-04			€ 2,83
Pigment white (titanium dioxide)	Pigment	kg		0,00E+00	0,00E+00	0,00E+00	0,00E+00	0,00E+00	0,00E+00	0,00E+00	0,00E+00	0,00E+00	0,00E+00	0,00E+00	0,00E+00	€ 0,00
Pigment black (carbon black)	Pigment	kg		0,00E+00	0,00E+00	0,00E+00	0,00E+00	0,00E+00	0,00E+00	0,00E+00	0,00E+00	0,00E+00	0,00E+00	0,00E+00	0,00E+00	€ 0,00
Pigment (red)	Pigment	kg		0,00E+00	0,00E+00	0,00E+00	0,00E+00	0,00E+00	0,00E+00	0,00E+00	0,00E+00	0,00E+00	0,00E+00	0,00E+00	0,00E+00	€ 0,00
Tap water	Water	kg	109	4,53E-09	4,71E-05	1,85E-03	5,23E-08	2,40E-05	3,49E-04	1,37E-04	8,14E-04	4,25E-06	2,40E-04	9,81E-06		€ 0,00
Surface / well water	Water	kg		0,00E+00	0,00E+00	0,00E+00	0,00E+00	0,00E+00	0,00E+00	0,00E+00	0,00E+00	0,00E+00	0,00E+00	0,00E+00	0,00E+00	€ 0,00
Steel rebar	Reinforcement	kg		0,00E+00	0,00E+00	0,00E+00	0,00E+00	0,00E+00	0,00E+00	0,00E+00	0,00E+00	0,00E+00	0,00E+00	0,00E+00	0,00E+00	€ 0,00
Steel fibres	Reinforcement	kg	156	8,74E-05	3,49E-01	1,48E+01	4,21E-04	4,06E-01	3,81E+00	1,17E+00	8,56E+00	1,31E-01	9,67E-01	2,71E-01		€ 30,48
Steel (Zinc coated)	Metal	kg		0,00E+00	0,00E+00	0,00E+00	0,00E+00	0,00E+00	0,00E+00	0,00E+00	0,00E+00	0,00E+00	0,00E+00	0,00E+00	0,00E+00	€ 0,00
Steel (Stainless steel)	Metal	kg		0,00E+00	0,00E+00	0,00E+00	0,00E+00	0,00E+00	0,00E+00	0,00E+00	0,00E+00	0,00E+00	0,00E+00	0,00E+00	0,00E+00	€ 0,00
Plastic/polymer fibres	Reinforcement	kg		0,00E+00	0,00E+00	0,00E+00	0,00E+00	0,00E+00	0,00E+00	0,00E+00	0,00E+00	0,00E+00	0,00E+00	0,00E+00	0,00E+00	€ 0,00
Total euro				€ 0,00	€ 0,49	€ 27,15	€ 0,00	€ 0,63	€ 8,00	€ 2,01	€ 10,89	€ 0,17	€ 1,62	€ 0,29		€ 51,26

Appendix 2: Fiber distribution results small plates

This Appendix contains the different fiber distributions gathered in this Thesis. First of all, the distributions with different fiber contents are presented from a 1% to 4%. Afterwards, the fiber distribution of the vibrated plates are presented. The contour colours represent the local fiber content which value is given in the legend. For each distribution, the minimum and maximum local fiber content is added to the figure in the spot where the value occurs.

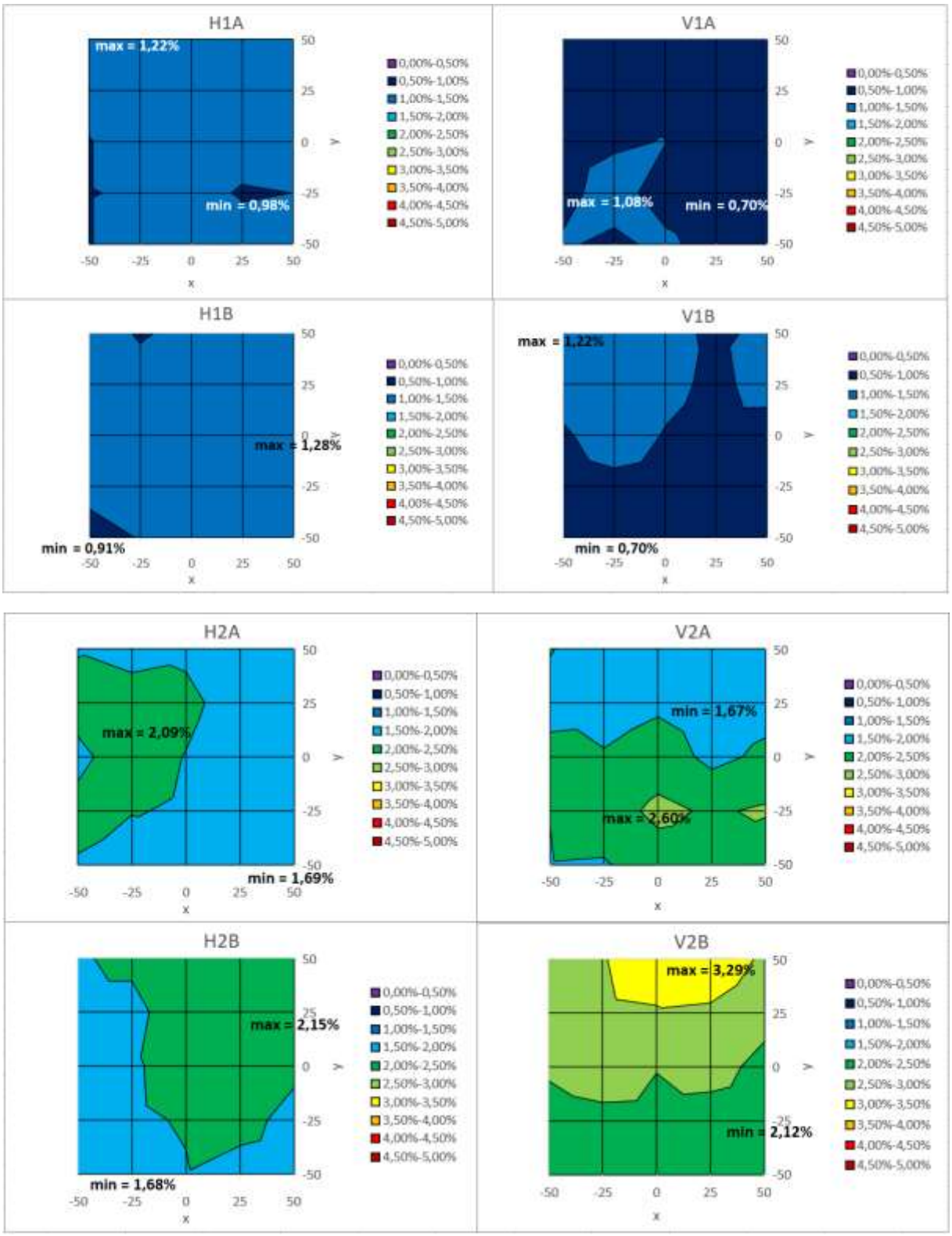

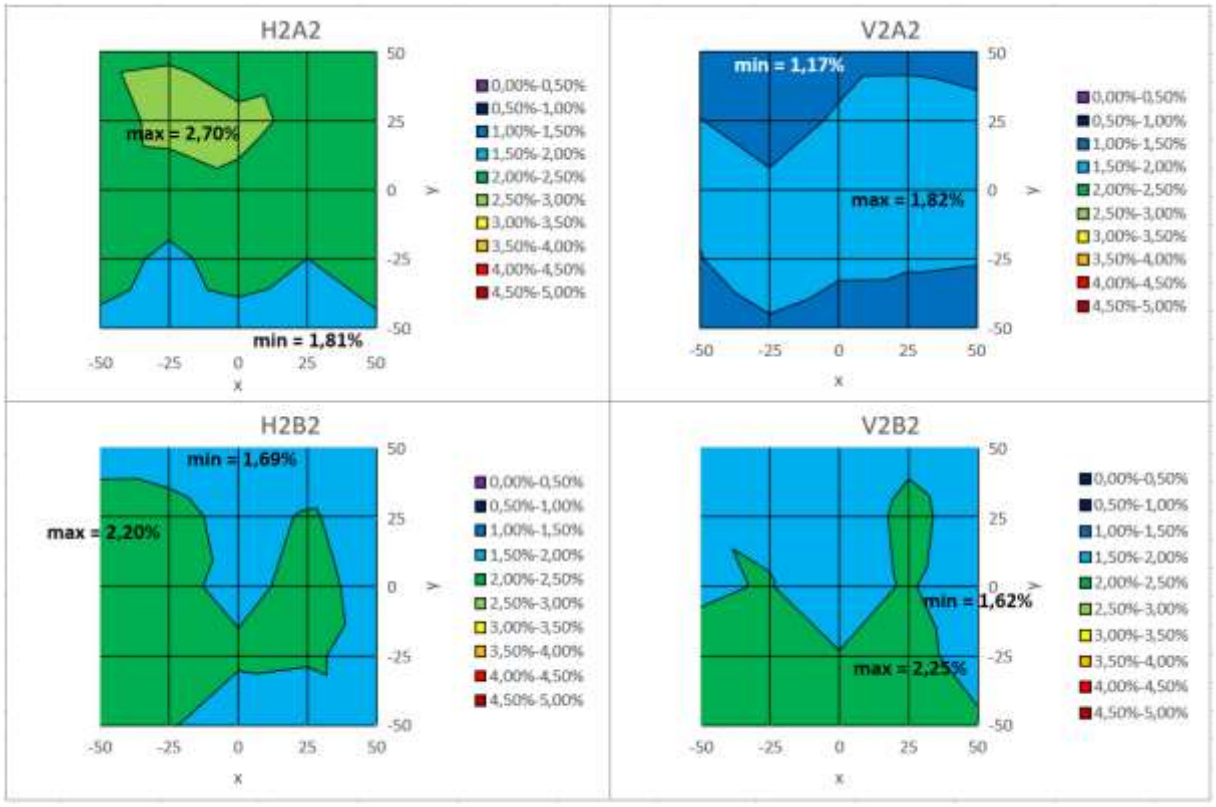
H2A2
max = 2,70%
min = 1,81%
V2A2
min = 1,17%
max = 1,82%
H2B2
min = 1,69%
max = 2,20%
V2B2
min = 1,62%
max = 2,25%
0,00%-0,50%
0,50%-1,00%
1,00%-1,50%
1,50%-2,00%
2,00%-2,50%
2,50%-3,00%
3,00%-3,50%
3,50%-4,00%
4,00%-4,50%
4,50%-5,00%
x
y

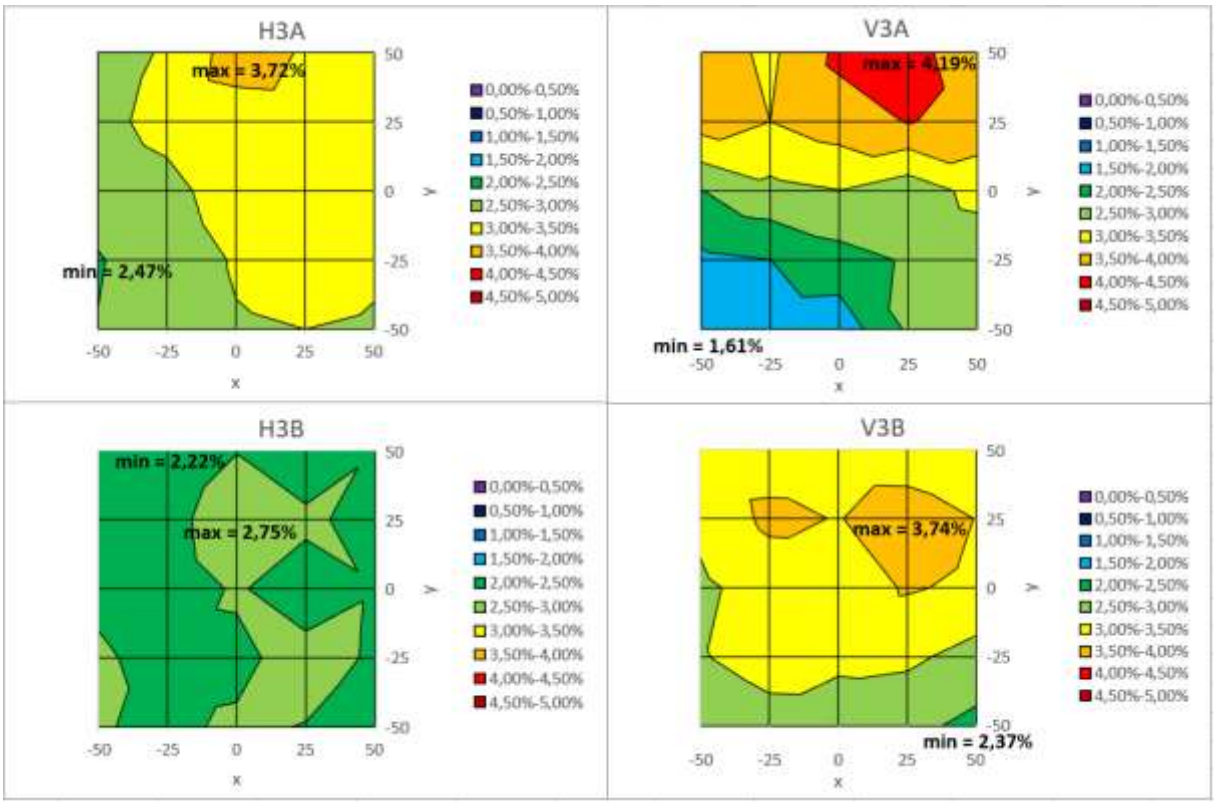
H3A
max = 3,72%
min = 2,47%
V3A
max = 4,19%
min = 1,61%
H3B
min = 2,22%
max = 2,75%
V3B
max = 3,74%
min = 2,37%
0,00%-0,50%
0,50%-1,00%
1,00%-1,50%
1,50%-2,00%
2,00%-2,50%
2,50%-3,00%
3,00%-3,50%
3,50%-4,00%
4,00%-4,50%
4,50%-5,00%
x
y

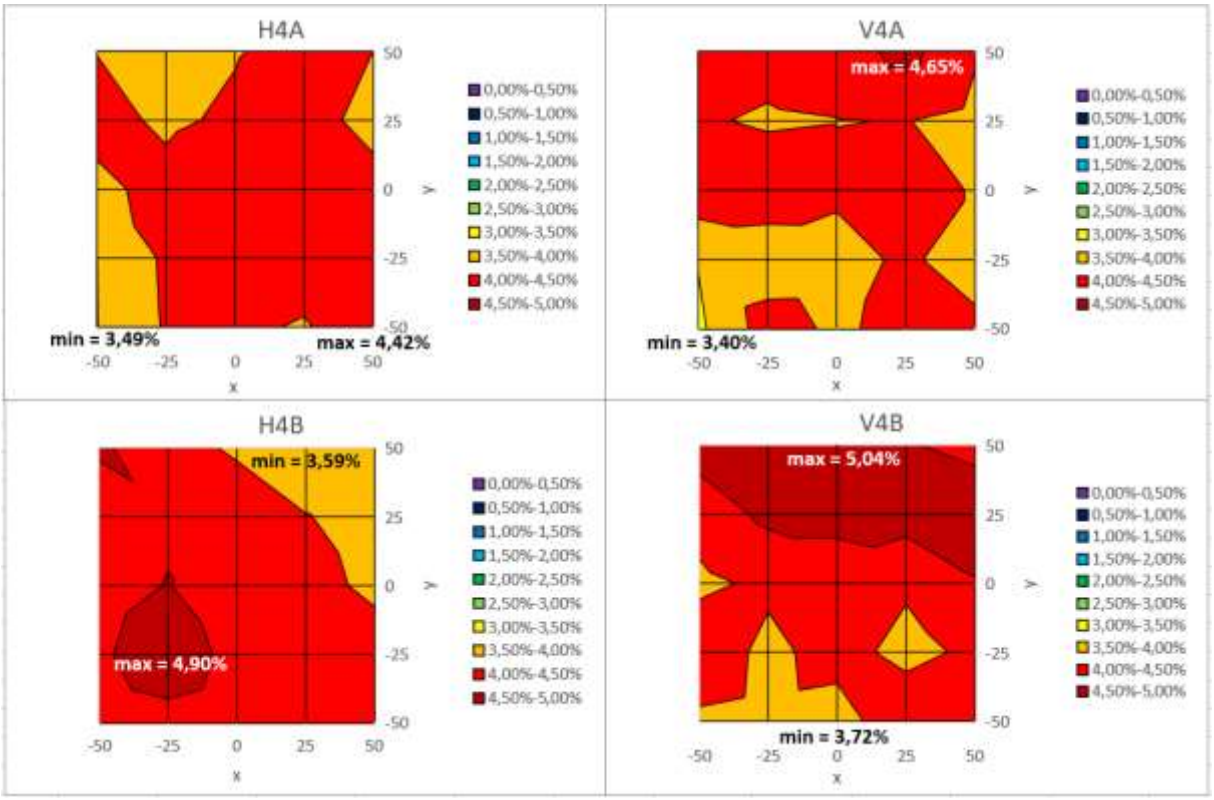
H4A
min = 3,49%
max = 4,42%
V4A
max = 4,65%
min = 3,40%
H4B
min = 3,59%
max = 4,90%
V4B
max = 5,04%
min = 3,72%
0,00%-0,50%
0,50%-1,00%
1,00%-1,50%
1,50%-2,00%
2,00%-2,50%
2,50%-3,00%
3,00%-3,50%
3,50%-4,00%
4,00%-4,50%
4,50%-5,00%
x
y

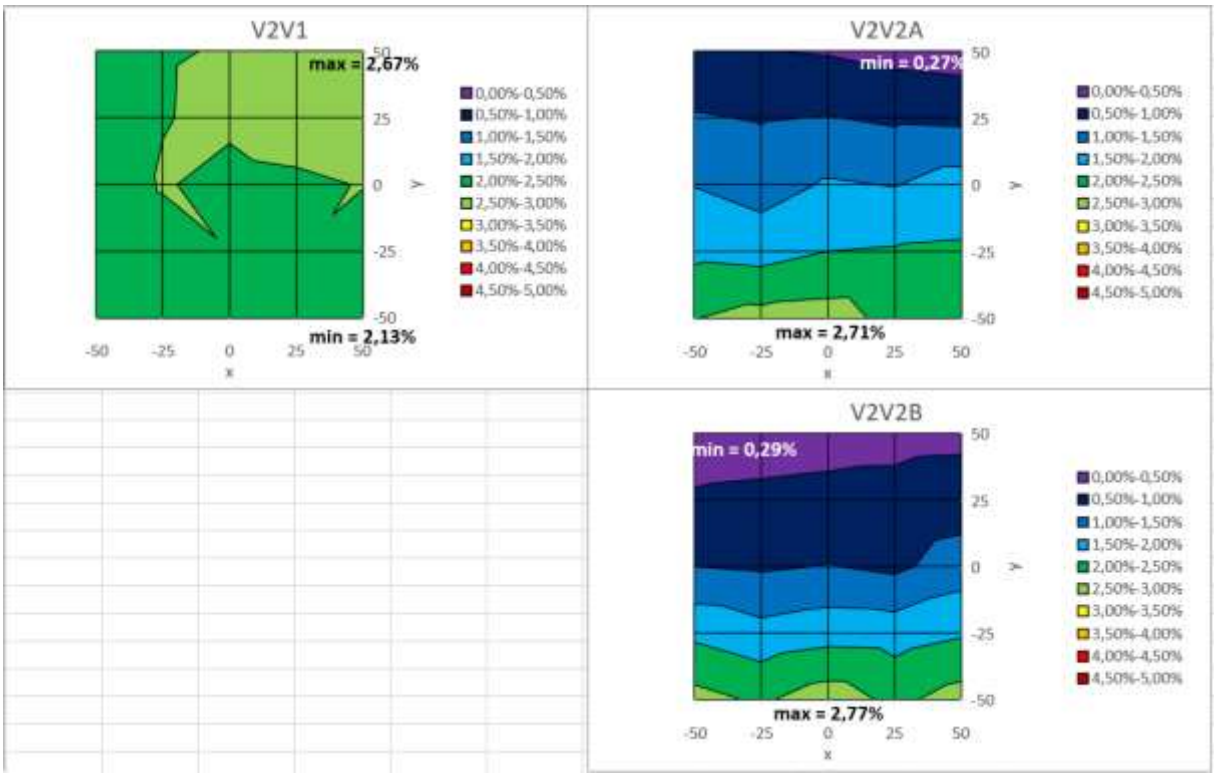
V2V1
max = 2,67%
min = 2,13%
V2V2A
min = 0,27%
max = 2,71%
V2V2B
min = 0,29%
max = 2,77%
0,00%-0,50%
0,50%-1,00%
1,00%-1,50%
1,50%-2,00%
2,00%-2,50%
2,50%-3,00%
3,00%-3,50%
3,50%-4,00%
4,00%-4,50%
4,50%-5,00%

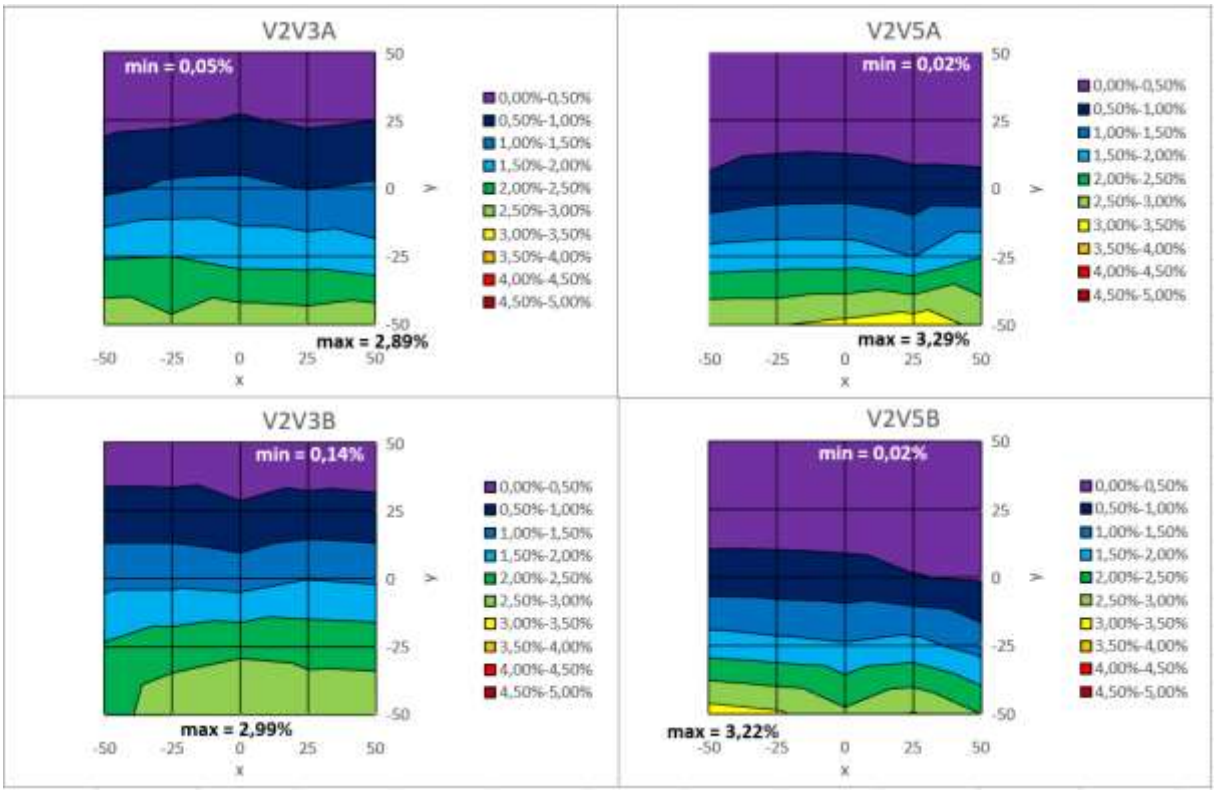
V2V3A
min = 0,05%
max = 2,89%
V2V5A
min = 0,02%
max = 3,29%
V2V3B
min = 0,14%
max = 2,99%
V2V5B
min = 0,02%
max = 3,22%
0,00%-0,50%
0,50%-1,00%
1,00%-1,50%
1,50%-2,00%
2,00%-2,50%
2,50%-3,00%
3,00%-3,50%
3,50%-4,00%
4,00%-4,50%
4,50%-5,00%

1% fiber content plates

Lair =	372,2	kv =	2,5933							
LUHPFRC		H1a_smooth	Perp.	H1b_smooth	Perp.	V1a_side1	Perp.	V1b_side1	Perp.	
[mH]	x = -50, y = 50	383,3	382,7	383,1	382,7	379,7	379,4	384,3	383,9	
	x = -25, y = 50	384,2	384,0	381,9	381,6	381,1	380,8	383,4	382,9	
	x = 0, y = 50	383,9	383,6	382,6	382,3	380,6	380,4	382,9	382,4	
	x = 25, y = 50	382,7	382,7	383,2	383,1	380,2	380,0	381,6	381,4	
	x = 50, y = 50	382,6	382,4	383,9	383,7	381,3	381,1	383,0	381,9	
	x = -50, y = 25	382,7	382,7	383,1	382,9	381,6	381,1	383,7	383,5	
	x = -25, y = 25	383,3	383,4	382,7	382,6	381,6	381,3	384,0	383,7	
	x = 0, y = 25	382,9	382,6	383,6	383,4	381,2	380,8	383,0	382,7	
	x = 25, y = 25	383,0	382,8	383,1	383,0	379,8	379,5	381,3	381,1	
	x = 50, y = 25	383,2	382,7	384,0	383,7	381,5	381,3	383,3	383,0	
	x = -50, y = 0	381,9	381,8	382,1	382,1	381,3	380,9	381,6	381,3	
	x = -25, y = 0	383,0	382,9	382,7	382,7	381,9	381,5	384,0	383,6	
	x = 0, y = 0	383,2	382,6	383,1	382,9	382,2	381,8	381,7	381,8	
	x = 25, y = 0	383,0	382,7	383,0	382,9	380,2	379,8	380,6	380,5	
	x = 50, y = 0	383,3	383,0	384,7	384,7	379,9	379,5	380,7	380,3	
	x = -50, y = -25	382,0	381,7	382,6	382,6	381,5	381,3	380,0	380,1	
	x = -25, y = -25	382,2	382,2	383,6	383,5	382,9	382,6	380,9	380,9	
	x = 0, y = -25	382,9	382,4	383,5	383,1	381,1	381,0	380,3	380,3	
	x = 25, y = -25	381,8	381,7	382,9	382,8	380,5	380,1	380,0	380,1	
	x = 50, y = -25	382,0	381,9	384,2	384,0	379,2	378,9	380,0	380,0	
	x = -50, y = -50	381,9	381,8	381,2	381,0	382,3	382,0	380,5	380,8	
	x = -25, y = -50	382,9	382,9	382,1	382,0	381,7	381,4	379,4	378,7	
	x = 0, y = -50	384,2	383,9	382,3	382,3	382,5	382,3	379,8	379,8	
	x = 25, y = -50	382,8	382,8	382,3	382,5	381,2	380,8	379,9	379,8	
	x = 50, y = -50	382,3	382,1	383,3	383,2	381,3	380,8	379,9	379,6	

H1a_smooth	1,09%	-100	-75	-50	-25	0	25	50	75	100
V_f	100									
	75									
	50			1,12%	1,23%	1,19%	1,08%	1,06%		
	25			1,08%	1,15%	1,09%	1,10%	1,11%		
	0			1,00%	1,11%	1,10%	1,10%	1,13%		
	-25			1,00%	1,03%	1,08%	0,99%	1,01%		
	-50			1,00%	1,10%	1,22%	1,09%	1,03%		
	-75									
	-100									

H1b_smooth	1,11%	-100	-75	-50	-25	0	25	50	75	100
V_f	100									
	75									
	50			1,10%	0,99%	1,06%	1,13%	1,20%		
	25			1,12%	1,08%	1,17%	1,12%	1,20%		
	0			1,02%	1,08%	1,12%	1,11%	1,29%		
	-25			1,07%	1,17%	1,15%	1,10%	1,23%		
	-50			0,92%	1,02%	1,04%	1,05%	1,14%		
	-75									
	-100									

V1a_side1	0,91%	-100	-75	-50	-25	0	25	50	75	100
V_f	100									
	75									
	50			0,76%	0,90%	0,86%	0,81%	0,93%		
	25			0,94%	0,95%	0,91%	0,77%	0,95%		
	0			0,92%	0,98%	1,01%	0,80%	0,77%		
	-25			0,95%	1,09%	0,91%	0,84%	0,71%		
	-50			1,03%	0,97%	1,05%	0,91%	0,91%		
	-75									
	-100									

V1b_side1	0,96%	-100	-75	-50	-25	0	25	50	75	100
V_f	100									
	75									
	50			1,23%	1,13%	1,08%	0,96%	1,06%		
	25			1,18%	1,20%	1,10%	0,93%	1,13%		
	0			0,95%	1,20%	0,99%	0,86%	0,86%		
	-25			0,81%	0,90%	0,84%	0,81%	0,80%		
	-50			0,87%	0,71%	0,78%	0,79%	0,78%		
	-75									
	-100									

2% fiber content plates

Lair =	372,2		kv =	2,5933					
LUHPFRC		H2a_smooth	Perp.	H2b_smoot	Perp.	V2a_side1	Perp.	V2b_side1	Perp.
[mH]	x = -50, y = 50	391,6	391,4	391,6	391,3	391,8	391,6	400,4	400,2
	x = -25, y = 50	391,1	390,8	392,2	391,8	391,0	390,6	401,0	401,3
	x = 0, y = 50	391,3	391,2	392,1	391,7	390,5	390,1	403,0	403,1
	x = 25, y = 50	389,7	389,6	392,5	392,5	389,5	389,2	404,2	404,0
	x = 50, y = 50	389,0	388,6	392,9	392,7	390,5	390,4	400,8	400,5
	x = -50, y = 25	392,3	392,1	390,9	391,3	391,2	391,0	401,0	400,8
	x = -25, y = 25	392,6	392,3	391,1	391,1	389,0	388,6	401,0	400,5
	x = 0, y = 25	392,3	391,9	392,6	392,8	390,9	390,4	401,4	400,7
	x = 25, y = 25	390,9	390,5	392,0	392,3	388,7	388,2	401,1	400,3
	x = 50, y = 25	390,6	390,3	392,9	393,2	390,0	389,6	398,5	398,3
	x = -50, y = 0	391,4	391,1	389,1	389,5	392,1	392,0	397,7	397,3
	x = -25, y = 0	392,7	392,2	391,4	391,4	392,4	391,9	400,2	399,9
	x = 0, y = 0	391,7	391,4	392,3	392,4	394,9	393,9	397,0	396,5
	x = 25, y = 0	390,5	390,0	392,4	393,1	390,7	389,9	398,9	398,4
	x = 50, y = 0	391,1	390,7	392,5	392,6	392,8	392,4	394,6	394,9
	x = -50, y = -25	392,1	392,0	388,7	389,1	391,7	391,7	393,8	393,1
	x = -25, y = -25	392,0	391,5	391,5	391,2	394,6	394,4	394,6	394,6
	x = 0, y = -25	391,6	391,1	391,9	391,6	397,6	397,2	394,6	394,1
	x = 25, y = -25	390,5	390,0	393,0	393,1	396,1	395,8	394,1	393,8
	x = 50, y = -25	389,8	389,6	390,2	390,2	397,2	396,9	393,1	392,4
	x = -50, y = -50	391,8	391,2	388,6	388,9	391,9	390,9	393,3	392,5
	x = -25, y = -50	390,2	389,6	388,7	388,4	391,4	390,9	393,2	392,5
	x = 0, y = -50	390,8	390,3	391,5	391,5	394,8	394,2	393,9	393,3
	x = 25, y = -50	390,8	389,9	390,0	390,0	394,5	393,6	393,5	393,1
	x = 50, y = -50	388,9	388,4	389,3	389,2	392,6	391,9	394,2	393,5

H2a_smooth	1,94%	-100	-75	-50	-25	0	25	50	75	100
V_f	100									
	75									
	50			2,00%	1,94%	1,97%	1,81%	1,72%		
	25			2,07%	2,10%	2,06%	1,92%	1,89%		
	0			1,97%	2,10%	2,00%	1,87%	1,94%		
	-25			2,06%	2,03%	1,98%	1,87%	1,81%		
	-50			2,00%	1,83%	1,90%	1,88%	1,70%		
	-75									
	-100									

H2b_smooth	1,98%	-100	-75	-50	-25	0	25	50	75	100
V_f	100									
	75									
	50			1,99%	2,05%	2,04%	2,10%	2,13%		
	25			1,96%	1,96%	2,12%	2,07%	2,16%		
	0			1,77%	1,99%	2,09%	2,13%	2,11%		
	-25			1,73%	1,98%	2,03%	2,16%	1,86%		
	-50			1,71%	1,69%	2,00%	1,84%	1,77%		
	-75									
	-100									

V2a_side1	2,06%	-100	-75	-50	-25	0	25	50	75	100
V_f	100									
	75									
	50			2,02%	1,93%	1,88%	1,78%	1,89%		
	25			1,96%	1,72%	1,91%	1,68%	1,82%		
	0			2,06%	2,07%	2,30%	1,88%	2,11%		
	-25			2,02%	2,31%	2,61%	2,46%	2,57%		
	-50			1,99%	1,96%	2,31%	2,26%	2,08%		
	-75									
	-100									

V2b_side1	2,61%	-100	-75	-50	-25	0	25	50	75	100
V_f	100									
	75									
	50			2,91%	3,00%	3,20%	3,30%	2,95%		
	25			2,97%	2,96%	2,99%	2,95%	2,71%		
	0			2,62%	2,89%	2,54%	2,74%	2,34%		
	-25			2,20%	2,32%	2,29%	2,25%	2,13%		
	-50			2,14%	2,14%	2,22%	2,19%	2,24%		
	-75									
	-100									

2% fiber content plates B

L_{air} =	372,2	k_V =	2,5933						
Luhpfrc		H2a2_smooth	Perp.	H2b2_smo	Perp.	V2a2_side1	Perp.	V2b2_side1	Perp.
[mH]	x = -50, y = 50	395,8	395,5	390,0	389,8	385,0	385,1	389,4	389,2
	x = -25, y = 50	396,1	395,9	390,0	389,9	383,7	383,4	390,4	389,9
	x = 0, y = 50	393,7	393,4	388,9	388,4	386,0	385,1	389,5	389,0
	x = 25, y = 50	394,5	394,8	389,2	388,9	385,7	385,5	391,2	390,8
	x = 50, y = 50	394,5	394,6	389,6	389,6	384,5	384,4	389,9	389,9
	x = -50, y = 25	393,8	393,6	393,9	393,3	386,9	386,8	391,7	391,3
	x = -25, y = 25	398,5	398,3	392,8	392,7	385,4	385,0	391,1	391,1
	x = 0, y = 25	397,7	397,4	390,7	390,3	387,3	387,1	390,0	389,8
	x = 25, y = 25	395,6	395,3	392,0	391,8	389,0	389,0	392,6	392,1
	x = 50, y = 25	393,6	394,2	390,4	390,4	388,8	388,4	390,4	390,1
	x = -50, y = 0	393,5	393,0	393,2	393,0	387,4	387,4	391,5	391,1
	x = -25, y = 0	393,8	393,5	392,3	392,2	387,6	387,4	391,8	391,7
	x = 0, y = 0	395,8	395,4	391,0	390,9	386,9	386,9	389,6	389,1
	x = 25, y = 0	393,8	393,5	392,4	392,3	389,9	389,8	392,3	391,9
	x = 50, y = 0	394,1	394,2	390,8	390,8	388,6	388,4	388,0	387,8
	x = -50, y = -25	393,1	392,9	393,4	393,2	386,7	386,6	392,5	392,2
	x = -25, y = -25	390,1	391,6	393,0	392,9	388,9	389,0	392,7	392,5
	x = 0, y = -25	393,1	393,0	392,1	392,0	387,5	387,5	391,9	391,7
	x = 25, y = -25	391,7	391,5	391,8	391,9	387,0	387,9	394,0	394,1
	x = 50, y = -25	392,6	392,6	391,0	391,0	387,2	386,9	388,5	388,4
	x = -50, y = -50	391,0	390,8	393,0	392,6	384,7	384,3	392,5	391,9
	x = -25, y = -50	389,8	389,9	391,9	391,8	386,5	385,9	392,2	391,7
	x = 0, y = -50	390,7	390,2	390,0	390,0	385,3	385,0	392,1	391,8
	x = 25, y = -50	389,9	389,6	390,4	390,3	383,8	383,7	393,4	393,5
	x = 50, y = -50	391,4	391,1	391,0	391,0	384,0	383,8	392,9	392,7

H2a2_smooth	2,20%	-100	-75	-50	-25	0	25	50	75	100
V_f	100									
	75									
	50			2,43%	2,47%	2,21%	2,33%	2,32%		
	25			2,23%	2,71%	2,63%	2,41%	2,25%		
	0			2,18%	2,22%	2,42%	2,22%	2,27%		
	-25			2,15%	1,93%	2,16%	2,01%	2,11%		
	-50			1,94%	1,83%	1,89%	1,82%	1,97%		
	-75									
	-100									

H2b2_smooth	1,98%	-100	-75	-50	-25	0	25	50	75	100
V_f	100									
	75									
	50			1,83%	1,84%	1,70%	1,75%	1,80%		
	25			2,22%	2,13%	1,90%	2,04%	1,89%		
	0			2,17%	2,08%	1,94%	2,09%	1,93%		
	-25			2,19%	2,15%	2,06%	2,04%	1,95%		
	-50			2,13%	2,04%	1,84%	1,88%	1,95%		
	-75									
	-100									

V2a2_side1	1,48%	-100	-75	-50	-25	0	25	50	75	100
V_f	100									
	75									
	50			1,33%	1,18%	1,38%	1,39%	1,27%		
	25			1,52%	1,35%	1,55%	1,74%	1,70%		
	0			1,57%	1,59%	1,52%	1,83%	1,69%		
	-25			1,50%	1,74%	1,59%	1,58%	1,54%		
	-50			1,27%	1,45%	1,34%	1,20%	1,21%		
	-75									
	-100									

V2b2_side1	1,96%	-100	-75	-50	-25	0	25	50	75	100
V_f	100									
	75									
	50			1,77%	1,86%	1,77%	1,95%	1,83%		
	25			2,00%	1,96%	1,83%	2,09%	1,87%		
	0			1,98%	2,03%	1,78%	2,06%	1,63%		
	-25			2,09%	2,11%	2,03%	2,26%	1,68%		
	-50			2,07%	2,05%	2,05%	2,20%	2,13%		
	-75									
	-100									

3% fiber content plates

L_{air} =	372,2	k_V =	2,6082						
Luhpfrc		H3a_smooth	Perp.	H3b_smoot	Perp.	V3a_side1	Perp.	V3b_side1	Perp.
[mH]	x = -50, y = 50	397,7	397,3	394,8	394,9	408,7	408,4	403,6	403,2
	x = -25, y = 50	402,4	402,1	394,0	393,6	405,3	405,3	403,6	403,9
	x = 0, y = 50	408,6	408,0	396,4	396,3	412,3	412,1	403,9	403,3
	x = 25, y = 50	406,1	405,5	393,9	393,8	412,9	412,9	403,5	403,5
	x = 50, y = 50	405,8	405,7	396,2	396,3	408,1	407,7	401,4	402,3
	x = -50, y = 25	399,6	400,0	394,8	394,8	408,4	408,5	402,4	402,6
	x = -25, y = 25	403,2	403,0	395,4	395,0	406,2	406,2	407,2	407,3
	x = 0, y = 25	404,3	403,9	399,0	398,8	408,6	408,9	406,2	405,8
	x = 25, y = 25	404,3	404,6	397,2	397,3	411,3	411,3	408,8	408,3
	x = 50, y = 25	406,0	405,5	395,0	395,1	409,5	409,2	406,4	405,8
	x = -50, y = 0	397,8	398,1	395,9	396,0	396,4	396,3	400,6	400,3
	x = -25, y = 0	399,5	400,0	394,9	394,7	400,1	400,0	403,2	403,4
	x = 0, y = 0	403,9	404,2	397,0	396,7	401,3	401,2	403,6	403,5
	x = 25, y = 0	403,4	404,1	394,8	394,5	398,4	398,3	406,8	406,5
	x = 50, y = 0	403,0	403,4	396,2	396,3	402,6	403,2	405,4	405,2
	x = -50, y = -25	396,2	396,3	396,8	396,9	390,7	390,5	401,3	400,9
	x = -25, y = -25	398,4	398,5	395,6	395,7	391,6	391,6	403,0	402,7
	x = 0, y = -25	401,8	401,8	395,8	395,9	394,6	394,8	403,1	402,8
	x = 25, y = -25	402,4	402,6	397,4	397,9	396,9	397,0	402,5	402,1
	x = 50, y = -25	401,8	401,8	396,2	396,1	398,2	397,9	399,9	399,3
	x = -50, y = -50	396,8	396,4	396,8	396,5	388,0	387,8	398,7	398,2
	x = -25, y = -50	398,3	398,3	396,1	396,0	389,4	388,6	400,3	399,7
	x = 0, y = -50	401,0	401,0	396,9	396,8	388,5	388,7	397,6	397,0
	x = 25, y = -50	401,5	401,2	396,4	396,4	397,6	396,8	398,1	397,5
	x = 50, y = -50	401,2	400,9	395,0	395,0	400,9	400,2	395,4	395,0

H3a_smooth	3,04%	-100	-75	-50	-25	0	25	50	75	100
V_f	100									
	75									
	50			2,60%	3,09%	3,72%	3,46%	3,45%		
	25			2,84%	3,18%	3,28%	3,32%	3,45%		
	0			2,65%	2,84%	3,28%	3,25%	3,19%		
	-25			2,47%	2,70%	3,05%	3,12%	3,05%		
	-50			2,51%	2,69%	2,96%	3,00%	2,97%		
	-75									
	-100									

H3b_smooth	2,44%	-100	-75	-50	-25	0	25	50	75	100
V_f	100									
	75									
	50			2,33%	2,22%	2,48%	2,23%	2,47%		
	25			2,33%	2,37%	2,75%	2,58%	2,35%		
	0			2,44%	2,33%	2,54%	2,31%	2,47%		
	-25			2,54%	2,41%	2,43%	2,62%	2,46%		
	-50			2,52%	2,45%	2,54%	2,49%	2,35%		
	-75									
	-100									

V3a_side1	2,96%	-100	-75	-50	-25	0	25	50	75	100
V_f	100									
	75									
	50			3,74%	3,41%	4,12%	4,19%	3,67%		
	25			3,73%	3,50%	3,76%	4,02%	3,82%		
	0			2,48%	2,87%	2,99%	2,69%	3,16%		
	-25			1,89%	2,00%	2,32%	2,55%	2,66%		
	-50			1,61%	1,73%	1,69%	2,57%	2,92%		
	-75									
	-100									

V3b_side1	3,12%	-100	-75	-50	-25	0	25	50	75	100
V_f	100									
	75									
	50			3,21%	3,25%	3,23%	3,22%	3,05%		
	25			3,12%	3,61%	3,48%	3,74%	3,49%		
	0			2,91%	3,20%	3,23%	3,55%	3,41%		
	-25			2,97%	3,15%	3,16%	3,10%	2,82%		
	-50			2,70%	2,86%	2,58%	2,63%	2,37%		
	-75									
	-100									

4% fiber content plates

L_{air} =	372,2		k_v =	2,6082					
Luhpfrc		H4a_smooth	Perp.	H4b_smooth	Perp.	V4a_side1	Perp.	V4b_side1	Perp.
[mH]	x = -50, y = 50	410,9	411,0	416,9	416,5	413,8	413,2	418,0	417,9
	x = -25, y = 50	406,6	406,7	412,8	412,9	412,7	412,4	420,2	419,7
	x = 0, y = 50	410,9	410,7	410,2	410,5	413,7	413,7	421,4	420,8
	x = 25, y = 50	412,0	412,3	406,9	407,2	417,3	417,4	416,7	416,2
	x = 50, y = 50	411,2	410,8	407,9	408,4	412,0	411,1	413,7	414,3
	x = -50, y = 25	412,3	412,2	412,1	412,6	411,6	411,4	413,1	413,0
	x = -25, y = 25	410,4	410,4	414,9	415,2	410,8	410,2	417,1	416,8
	x = 0, y = 25	411,6	411,7	414,0	413,8	411,3	410,5	417,1	416,9
	x = 25, y = 25	414,0	413,8	411,1	411,3	410,8	411,5	417,9	417,7
	x = 50, y = 25	408,6	408,7	409,2	409,7	410,5	408,9	420,3	420,3
	x = -50, y = 0	410,2	410,1	413,1	413,4	414,4	414,2	410,1	409,8
	x = -25, y = 0	412,1	412,3	416,1	416,1	414,0	413,7	411,6	412,5
	x = 0, y = 0	414,5	414,1	412,1	411,1	412,6	412,0	414,0	413,6
	x = 25, y = 0	413,0	413,4	412,8	412,1	412,2	412,4	411,7	412,0
	x = 50, y = 0	413,7	413,6	410,2	410,1	411,1	410,5	415,8	415,1
	x = -50, y = -25	406,5	405,8	414,9	414,8	406,4	406,4	414,6	414,5
	x = -25, y = -25	411,7	411,9	419,8	419,8	408,2	408,0	409,7	409,5
	x = 0, y = -25	414,6	414,3	413,9	413,7	408,6	407,9	413,3	413,3
	x = 25, y = -25	413,8	413,6	413,9	413,7	412,4	412,2	409,2	409,2
	x = 50, y = -25	413,3	413,3	412,9	413,1	407,5	406,9	412,5	412,0
	x = -50, y = -50	405,8	406,4	412,0	412,5	405,5	404,9	410,0	410,2
	x = -25, y = -50	411,3	411,7	413,6	413,8	413,4	413,1	409,5	408,9
	x = 0, y = -50	412,0	412,1	412,0	412,1	410,7	409,6	408,7	407,9
	x = 25, y = -50	410,6	410,5	415,1	415,3	412,9	412,6	415,9	415,3
	x = 50, y = -50	415,1	415,1	414,7	415,2	413,3	412,9	412,6	411,6

H4a_smooth	4,04%	-100	-75	-50	-25	0	25	50	75	100
V_f	100									
	75									
	50			3,99%	3,55%	3,98%	4,12%	4,00%		
	25			4,13%	3,94%	4,06%	4,30%	3,75%		
	0			3,91%	4,12%	4,34%	4,22%	4,27%		
	-25			3,50%	4,08%	4,35%	4,27%	4,23%		
	-50			3,49%	4,05%	4,10%	3,95%	4,42%		
	-75									
	-100									

H4b_smooth	4,20%	-100	-75	-50	-25	0	25	50	75	100
V_f	100									
	75									
	50			4,58%	4,19%	3,93%	3,59%	3,70%		
	25			4,14%	4,41%	4,30%	4,02%	3,84%		
	0			4,23%	4,52%	4,06%	4,15%	3,91%		
	-25			4,39%	4,90%	4,29%	4,29%	4,20%		
	-50			4,13%	4,27%	4,10%	4,43%	4,40%		
	-75									
	-100									

V4a_side1	4,03%	-100	-75	-50	-25	0	25	50	75	100
V_f	100									
	75									
	50			4,25%	4,16%	4,27%	4,65%	4,05%		
	25			4,05%	3,95%	3,99%	4,01%	3,86%		
	0			4,34%	4,29%	4,13%	4,13%	3,98%		
	-25			3,52%	3,70%	3,71%	4,13%	3,61%		
	-50			3,40%	4,23%	3,91%	4,18%	4,21%		
	-75									
	-100									

V4b_side1	4,31%	-100	-75	-50	-25	0	25	50	75	100
V_f	100									
	75									
	50			4,71%	4,92%	5,04%	4,56%	4,31%		
	25			4,21%	4,61%	4,61%	4,70%	4,95%		
	0			3,89%	4,10%	4,29%	4,08%	4,46%		
	-25			4,36%	3,85%	4,23%	3,81%	4,13%		
	-50			3,90%	3,81%	3,72%	4,47%	4,11%		
	-75									
	-100									

2% fiber content vibration plates

L_{air} =	372,2		k_V =	2,5933												
LUHPFRC		V2V1_side1	Perp.	V2V5A_sid	Perp.	V2V5B_sid	Perp.	V2V2A_side	Perp.	V2V2B_sid	Perp.	V2V3A_side	Perp.	V2V3B_sid	Perp.	L_{air}
[mH]	x = -50, y = 50	395,8	396,0	372,6	372,6	372,7	372,7	377,1	377,1	374,9	375,0	373,1	373,3	373,9	373,8	372,3
	x = -25, y = 50	396,2	396,2	372,4	372,4	372,8	372,7	377,0	377,4	375,6	375,6	372,5	372,8	373,6	373,6	372,3
	x = 0, y = 50	396,8	396,5	372,4	372,5	372,5	372,4	376,7	376,6	375,8	375,8	373,0	373,0	374,2	374,1	372
	x = 25, y = 50	398,1	397,5	372,3	372,4	372,4	372,4	375,5	375,4	375,9	375,8	372,9	372,9	373,6	373,4	372,2
	x = 50, y = 50	398,2	398,0	372,5	372,5	372,5	372,5	374,7	374,9	376,0	376,0	373,1	373,2	374,1	373,9	372,1
	x = -50, y = 25	393,3	393,8	374,2	374,2	374,0	374,1	382,4	382,2	377,5	377,5	375,9	375,7	378,8	378,7	
	x = -25, y = 25	396,4	396,1	374,6	374,5	374,1	374,2	381,5	381,6	377,8	377,6	376,2	376,3	378,8	378,7	
	x = 0, y = 25	397,3	397,4	374,3	374,2	374,0	374,0	382,2	381,9	377,9	378,0	377,5	377,3	377,6	377,4	
	x = 25, y = 25	399,1	399,0	374,0	373,8	373,7	373,5	381,2	381,1	378,5	378,1	376,5	376,2	378,5	378,4	
	x = 50, y = 25	397,3	397,4	374,1	373,9	373,7	373,7	380,7	380,9	379,3	379,2	377,1	376,9	378,2	378,0	
	x = -50, y = 0	392,7	392,7	378,0	378,0	379,3	379,0	386,6	386,5	381,9	381,8	380,8	380,8	385,3	385,3	
	x = -25, y = 0	396,8	396,9	379,7	379,5	378,9	379,1	384,4	384,8	381,4	381,1	382,9	382,7	385,4	385,2	
	x = 0, y = 0	395,1	394,9	380,0	379,8	378,6	378,8	387,2	387,3	381,9	382,2	382,9	383,1	384,6	384,5	
	x = 25, y = 0	395,5	395,6	378,8	378,6	377,1	377,4	386,6	386,5	380,9	380,8	381,6	381,9	386,5	386,7	
	x = 50, y = 0	396,7	396,6	378,3	378,5	376,4	376,4	389,0	388,7	384,2	384,3	382,7	382,4	385,9	386,1	
	x = -50, y = -25	392,8	392,7	388,7	388,5	388,9	389,1	390,3	390,5	390,6	390,5	391,2	391,3	392,1	392,0	
	x = -25, y = -25	394,0	394,1	389,3	389,0	388,0	388,1	389,6	389,8	388,2	388,5	391,6	391,6	394,2	394,3	
	x = 0, y = -25	396,4	396,3	389,1	389,1	387,2	387,2	391,5	391,7	389,7	389,6	389,7	389,9	395,3	395,6	
	x = 25, y = -25	396,3	396,1	387,0	386,4	388,4	388,1	391,9	392,0	389,3	389,6	389,5	389,9	394,7	395,2	
	x = 50, y = -25	393,5	393,7	391,2	391,4	384,8	384,5	392,1	392,3	391,1	391,0	388,2	388,3	394,7	394,6	
	x = -50, y = -50	394,1	394,2	400,8	401,4	403,3	403,6	396,1	396,5	398,2	398,0	399,7	399,9	393,8	393,7	
	x = -25, y = -50	394,4	394,2	401,2	400,9	402,3	401,8	398,1	398,0	396,1	395,4	397,3	397,4	400,0	399,9	
	x = 0, y = -50	393,1	393,1	402,4	402,6	397,4	397,5	398,4	398,6	399,2	398,9	399,6	399,7	401,3	401,2	
	x = 25, y = -50	394,0	394,0	404,0	404,2	401,8	401,5	395,1	394,9	395,2	395,4	399,1	399,0	399,4	399,4	
	x = 50, y = -50	393,0	392,8	400,0	400,4	396,4	396,3	395,8	395,6	398,5	398,4	400,2	400,3	399,9	399,4	

V_f										
V2V1_side	2,41%	-100	-75	-50	-25	0	25	50	75	100
V_f	100									
	75									
	50			2,46%	2,49%	2,54%	2,65%	2,69%		
	25			2,21%	2,49%	2,61%	2,78%	2,61%		
	0			2,13%	2,56%	2,36%	2,42%	2,54%		
	-25			2,13%	2,27%	2,50%	2,49%	2,22%		
	-50			2,28%	2,29%	2,17%	2,26%	2,15%		
	-75									
	-100									
V2V5A_sid	1,15%	-100	-75	-50	-25	0	25	50	75	100
V_f	100									
	75									
	50			0,04%	0,02%	0,03%	0,02%	0,03%		
	25			0,21%	0,25%	0,21%	0,18%	0,19%		
	0			0,60%	0,77%	0,80%	0,68%	0,64%		
	-25			1,70%	1,76%	1,75%	1,50%	1,98%		
	-50			3,00%	2,99%	3,14%	3,31%	2,90%		
	-75									
	-100									
V2V5B_sid	1,06%	-100	-75	-50	-25	0	25	50	75	100
V_f	100									
	75									
	50			0,05%	0,06%	0,03%	0,02%	0,03%		
	25			0,19%	0,20%	0,19%	0,15%	0,16%		
	0			0,72%	0,71%	0,68%	0,53%	0,44%		
	-25			1,74%	1,64%	1,56%	1,66%	1,29%		
	-50			3,24%	3,09%	2,62%	3,05%	2,50%		
	-75									
	-100									
V2V2A_sid	1,48%	-100	-75	-50	-25	0	25	50	75	100
V_f	100									
	75									
	50			0,51%	0,52%	0,46%	0,34%	0,27%		
	25			1,05%	0,97%	1,02%	0,93%	0,89%		
	0			1,49%	1,29%	1,56%	1,49%	1,73%		
	-25			1,89%	1,82%	2,01%	2,05%	2,07%		
	-50			2,50%	2,68%	2,73%	2,36%	2,44%		
	-75									
	-100									
V2V2B_sid	1,29%	1,29%	-75	-50	-25	0	25	50	75	100
V_f	100									
	75									
	50			0,29%	0,35%	0,38%	0,38%	0,40%		
	25			0,55%	0,57%	0,60%	0,63%	0,73%		
	0			1,00%	0,94%	1,02%	0,90%	1,25%		
	-25			1,90%	1,68%	1,81%	1,79%	1,96%		
	-50			2,69%	2,44%	2,78%	2,40%	2,72%		
	-75									
	-100									
V2V3A_sid	1,25%	-100	-75	-50	-25	0	25	50	75	100
V_f	100									
	75									
	50			0,11%	0,05%	0,08%	0,07%	0,10%		
	25			0,38%	0,42%	0,54%	0,43%	0,50%		
	0			0,89%	1,10%	1,12%	0,99%	1,07%		
	-25			1,98%	2,01%	1,83%	1,82%	1,66%		
	-50			2,86%	2,61%	2,85%	2,78%	2,91%		
	-75									
	-100									
V2V3B_sid	1,45%	-100	-75	-50	-25	0	25	50	75	100
V_f	100									
	75									
	50			0,17%	0,15%	0,20%	0,14%	0,19%		
	25			0,68%	0,68%	0,55%	0,65%	0,61%		
	0			1,36%	1,36%	1,28%	1,49%	1,43%		
	-25			2,06%	2,29%	2,41%	2,36%	2,33%		
	-50			2,23%	2,88%	3,01%	2,82%	2,85%		
	-75									
	-100									

Appendix 3: Fiber orientation results small plates

1% fiber content plates

LUHPFRC	dir.[°]	H1a_rough	H1a_smooth	H1b_rough	H1b_smooth	V1a_side1	V1a_side2	V1b_side1	V1b_side2
[H]	0	1,388	1,419	1,391	1,421	1,414	1,411	1,413	1,412
	15	1,389	1,419	1,389	1,424	1,414	1,410	1,413	1,415
	30	1,387	1,418	1,388	1,425	1,412	1,410	1,412	1,417
	45	1,387	1,417	1,388	1,423	1,410	1,409	1,410	1,420
	60	1,388	1,416	1,389	1,420	1,409	1,409	1,409	1,423
	75	1,387	1,416	1,390	1,419	1,408	1,409	1,411	1,424
	90	1,388	1,416	1,390	1,420	1,408	1,408	1,414	1,421
	105	1,387	1,417	1,389	1,422	1,409	1,408	1,416	1,416
	120	1,386	1,414	1,389	1,422	1,411	1,409	1,414	1,413
	135	1,386	1,414	1,390	1,419	1,412	1,409	1,412	1,410
	150	1,387	1,416	1,391	1,419	1,414	1,410	1,410	1,408
	165	1,388	1,418	1,392	1,420	1,415	1,411	1,411	1,410
	180	1,388	1,419	1,391	1,421	1,414	1,411	1,412	1,411
	195	1,388	1,419	1,389	1,424	1,414	1,410	1,413	1,415
	210	1,388	1,418	1,388	1,426	1,413	1,410	1,412	1,417
	225	1,388	1,417	1,388	1,423	1,411	1,410	1,410	1,420
	240	1,388	1,416	1,389	1,420	1,410	1,409	1,410	1,424
	255	1,389	1,416	1,390	1,419	1,409	1,409	1,411	1,424
	270	1,389	1,416	1,389	1,420	1,408	1,409	1,415	1,421
	285	1,388	1,417	1,389	1,422	1,410	1,408	1,416	1,417
	300	1,387	1,414	1,390	1,422	1,412	1,409	1,416	1,414
	315	1,386	1,414	1,391	1,420	1,413	1,410	1,412	1,411
	330	1,387	1,415	1,392	1,420	1,415	1,411	1,410	1,409
	345	1,388	1,417	1,392	1,419	1,415	1,412	1,411	1,411
	360	1,389	1,419	1,391	1,421	1,414	1,411	1,413	1,412

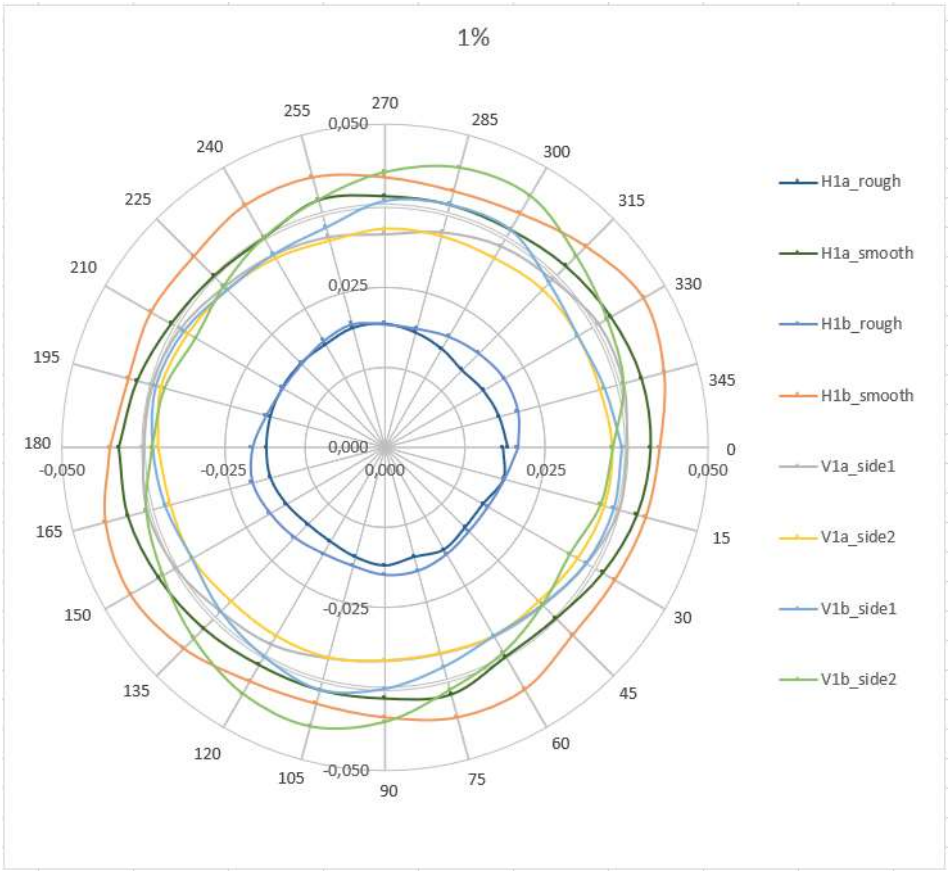

2% fiber content plates

LUHPFRC	dir.[°]	H2a_rough	H2a_smooth	H2b_rough	H2b_smooth	V2a_side1	V2a_side2	V2b_side1	V2b_side2
[H]	0	1,438	1,481	1,430	1,473	1,481	1,483	1,525	1,529
	15	1,439	1,479	1,441	1,475	1,478	1,477	1,524	1,523
	30	1,432	1,475	1,442	1,477	1,477	1,472	1,518	1,516
	45	1,433	1,470	1,442	1,480	1,477	1,468	1,506	1,509
	60	1,431	1,467	1,440	1,484	1,475	1,465	1,494	1,505
	75	1,425	1,465	1,445	1,485	1,473	1,465	1,490	1,498
	90	1,421	1,465	1,448	1,476	1,470	1,469	1,489	1,499
	105	1,422	1,466	1,451	1,468	1,468	1,470	1,491	1,496
	120	1,431	1,467	1,437	1,466	1,468	1,474	1,495	1,499
	135	1,430	1,473	1,428	1,468	1,470	1,477	1,501	1,512
	150	1,434	1,477	1,423	1,472	1,475	1,478	1,511	1,523
	165	1,437	1,479	1,420	1,473	1,482	1,482	1,522	1,529
	180	1,438	1,482	1,424	1,473	1,483	1,484	1,524	1,531
	195	1,445	1,479	1,441	1,475	1,483	1,477	1,523	1,524
	210	1,438	1,475	1,441	1,477	1,482	1,472	1,517	1,517
	225	1,436	1,470	1,435	1,481	1,481	1,467	1,507	1,509
	240	1,428	1,466	1,441	1,484	1,475	1,464	1,494	1,505
	255	1,424	1,464	1,448	1,486	1,472	1,464	1,489	1,499
	270	1,420	1,465	1,445	1,476	1,469	1,469	1,488	1,498
	285	1,423	1,466	1,445	1,468	1,466	1,470	1,490	1,498
	300	1,430	1,468	1,431	1,466	1,466	1,474	1,494	1,499
	315	1,430	1,474	1,423	1,469	1,470	1,477	1,501	1,511
	330	1,435	1,476	1,419	1,472	1,475	1,478	1,511	1,523
	345	1,437	1,479	1,420	1,472	1,481	1,482	1,522	1,529
	360	1,432	1,482	1,425	1,473	1,481	1,484	1,525	1,531

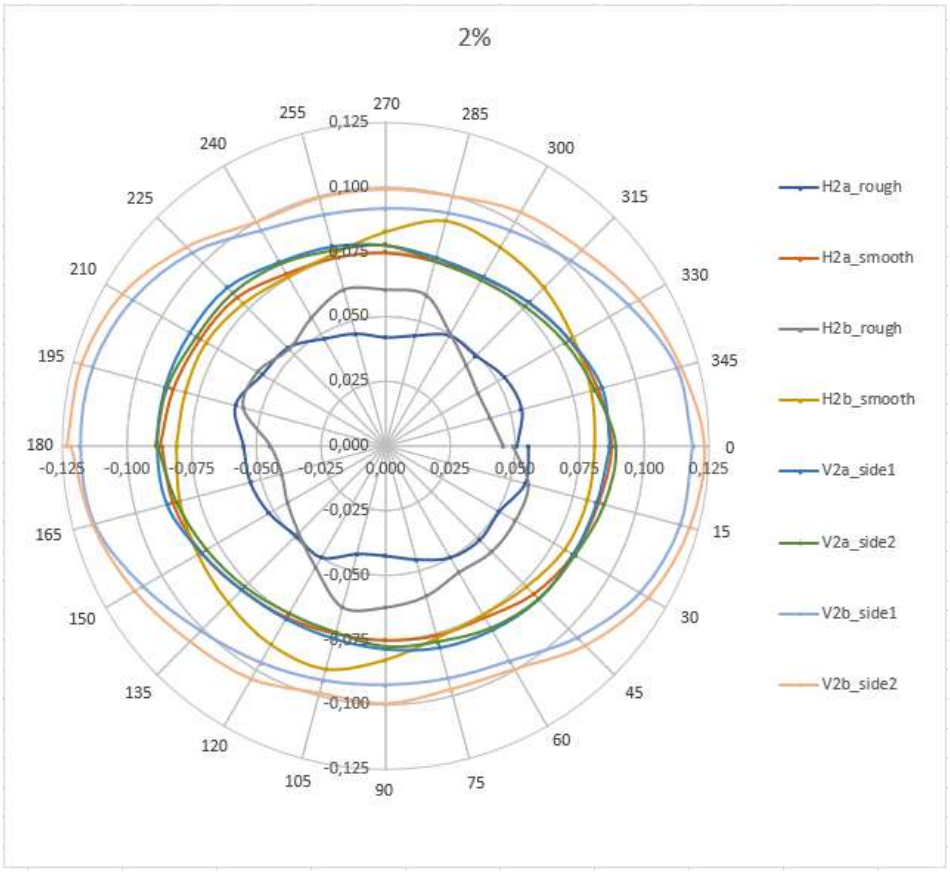

2% fiber content plates B

LUHPFRC	dir.[°]	H2a2_rou	H2a2_smoo	H2b2_rou	H2b2_smoc	V2a2_sid	V2a2_sid	V2b2_side	V2b2_side
[H]	0	1,429	1,485	1,441	1,479	1,456	1,457	1,481	1,472
	15	1,428	1,490	1,436	1,480	1,452	1,458	1,483	1,473
	30	1,424	1,493	1,435	1,479	1,447	1,457	1,484	1,474
	45	1,420	1,494	1,433	1,476	1,442	1,455	1,479	1,467
	60	1,418	1,492	1,430	1,470	1,439	1,453	1,472	1,461
	75	1,419	1,483	1,427	1,466	1,442	1,449	1,464	1,453
	90	1,421	1,478	1,427	1,463	1,446	1,444	1,459	1,453
	105	1,425	1,477	1,430	1,462	1,450	1,441	1,459	1,458
	120	1,430	1,477	1,437	1,463	1,455	1,442	1,469	1,466
	135	1,434	1,477	1,443	1,468	1,458	1,446	1,475	1,470
	150	1,432	1,479	1,446	1,472	1,460	1,450	1,479	1,472
	165	1,430	1,482	1,448	1,475	1,462	1,456	1,480	1,474
	180	1,429	1,486	1,441	1,478	1,456	1,457	1,481	1,472
	195	1,427	1,492	1,437	1,480	1,453	1,460	1,483	1,472
	210	1,423	1,494	1,435	1,478	1,447	1,458	1,482	1,472
	225	1,420	1,494	1,432	1,477	1,441	1,455	1,479	1,469
	240	1,418	1,491	1,429	1,471	1,438	1,453	1,472	1,461
	255	1,418	1,483	1,427	1,467	1,441	1,449	1,463	1,453
	270	1,420	1,479	1,427	1,464	1,445	1,444	1,459	1,453
	285	1,424	1,478	1,430	1,461	1,450	1,441	1,460	1,458
	300	1,432	1,477	1,437	1,463	1,455	1,442	1,468	1,466
	315	1,435	1,478	1,442	1,468	1,457	1,446	1,475	1,471
	330	1,432	1,479	1,446	1,473	1,459	1,451	1,479	1,472
	345	1,430	1,481	1,447	1,476	1,461	1,456	1,479	1,473
	360	1,429	1,486	1,441	1,478	1,456	1,458	1,481	1,472

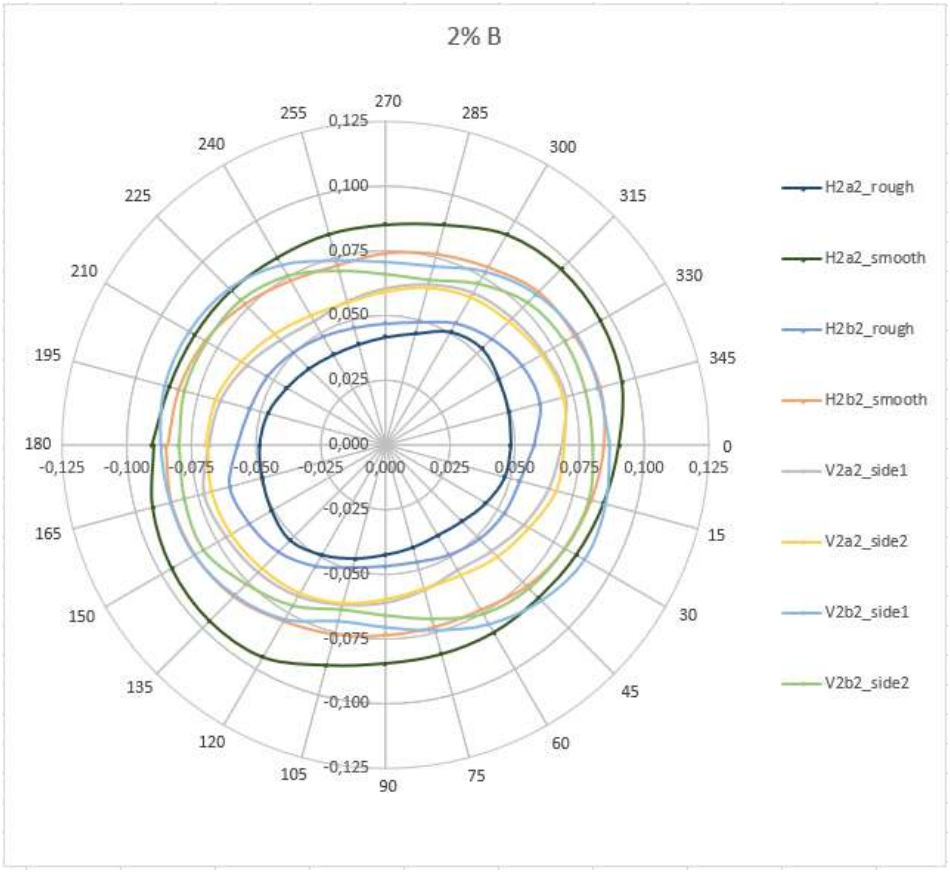

3% fiber content plates

LUHPFRC	dir.[°]	H3a_rough	H3a_smooth	H3b_rough	H3b_smooth	V3a_side1	V3a_side2	V3b_side1	V3b_side2
[H]	0	1,473	1,528	1,456	1,496	1,525	1,524	1,565	1,564
	15	1,470	1,531	1,460	1,497	1,530	1,520	1,570	1,555
	30	1,467	1,540	1,461	1,501	1,536	1,519	1,567	1,550
	45	1,467	1,552	1,462	1,506	1,528	1,522	1,564	1,542
	60	1,468	1,555	1,459	1,505	1,511	1,528	1,557	1,536
	75	1,473	1,550	1,455	1,502	1,508	1,524	1,549	1,531
	90	1,479	1,538	1,455	1,499	1,516	1,514	1,540	1,532
	105	1,483	1,529	1,456	1,495	1,528	1,511	1,541	1,543
	120	1,487	1,522	1,458	1,491	1,532	1,520	1,543	1,552
	135	1,488	1,518	1,455	1,493	1,534	1,534	1,553	1,558
	150	1,484	1,517	1,456	1,496	1,530	1,536	1,563	1,566
	165	1,479	1,521	1,454	1,500	1,526	1,530	1,563	1,572
	180	1,472	1,525	1,457	1,497	1,525	1,522	1,566	1,563
	195	1,469	1,529	1,461	1,498	1,531	1,515	1,569	1,555
	210	1,463	1,535	1,462	1,502	1,537	1,515	1,564	1,549
	225	1,462	1,545	1,458	1,506	1,528	1,520	1,561	1,543
	240	1,465	1,551	1,457	1,503	1,511	1,529	1,555	1,535
	255	1,470	1,548	1,454	1,499	1,508	1,525	1,549	1,531
	270	1,475	1,542	1,452	1,497	1,517	1,515	1,540	1,532
	285	1,481	1,528	1,455	1,494	1,528	1,513	1,539	1,541
	300	1,487	1,519	1,458	1,491	1,532	1,521	1,543	1,553
	315	1,487	1,517	1,455	1,494	1,528	1,535	1,552	1,559
	330	1,482	1,520	1,452	1,497	1,529	1,542	1,562	1,567
	345	1,478	1,525	1,454	1,500	1,528	1,532	1,563	1,572
	360	1,472	1,529	1,457	1,497	1,525	1,524	1,567	1,564

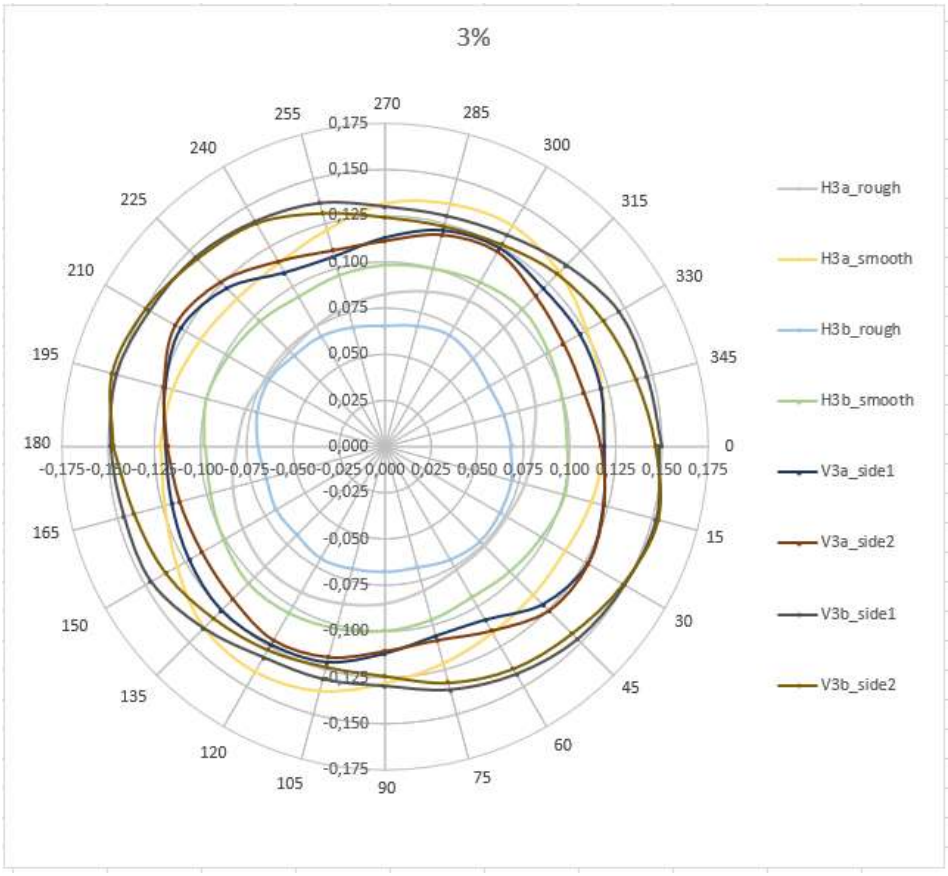

4% fiber content plates

LUHPFRC	dir.[°]	H4a_rougl	H4a_smoot	H4b_rougl	H4b_smoot	V4a_side:	V4a_side:	V4b_side1	V4b_side2
[H]	0	1,585	1,592	1,617	1,621	1,596	1,597		
	15	1,588	1,595	1,619	1,606	1,593	1,601		
	30	1,588	1,601	1,609	1,587	1,587	1,604		
	45	1,594	1,603	1,587	1,575	1,591	1,605		
	60	1,597	1,602	1,569	1,572	1,595	1,603		
	75	1,598	1,600	1,560	1,570	1,593	1,597		
	90	1,597	1,596	1,563	1,568	1,594	1,592		
	105	1,593	1,599	1,567	1,562	1,596	1,589		
	120	1,593	1,600	1,568	1,570	1,598	1,591		
	135	1,592	1,596	1,571	1,585	1,601	1,586		
	150	1,586	1,594	1,581	1,603	1,602	1,584		
	165	1,583	1,593	1,597	1,620	1,600	1,589		
	180	1,585	1,592	1,617	1,620	1,596	1,595		
	195	1,588	1,596	1,619	1,606	1,591	1,600		
	210	1,588	1,599	1,608	1,588	1,587	1,603		
	225	1,593	1,601	1,588	1,575	1,592	1,604		
	240	1,596	1,602	1,569	1,572	1,595	1,604		
	255	1,598	1,597	1,560	1,571	1,592	1,598		
	270	1,597	1,598	1,564	1,567	1,593	1,592		
	285	1,591	1,600	1,567	1,561	1,597	1,589		
	300	1,589	1,601	1,568	1,569	1,599	1,590		
	315	1,589	1,597	1,572	1,585	1,601	1,585		
	330	1,586	1,595	1,582	1,605	1,603	1,584		
	345	1,583	1,593	1,597	1,621	1,601	1,588		
	360	1,585	1,592	1,617	1,621	1,596	1,595		

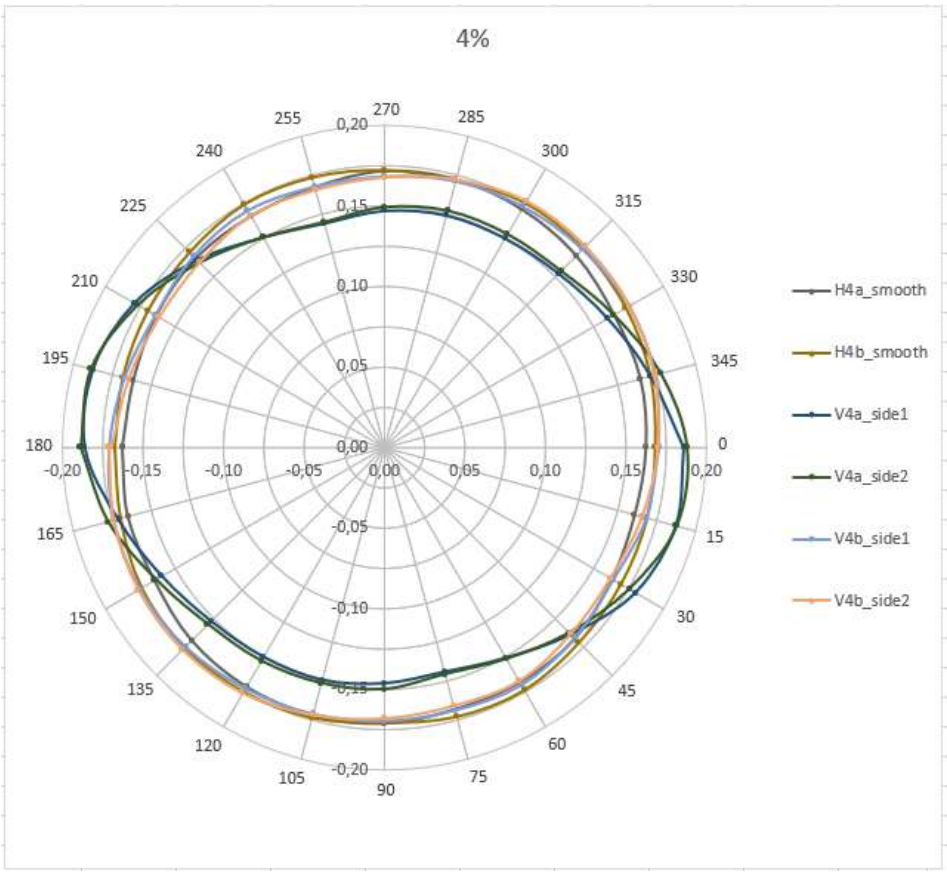

2% vibration plates

LUHPFRC	dir.[°]	V2V1	V2V5A	V2V5B	V2V2A	V2V2B	V2V3A	V2V3B
[H]	0	1,503	1,396	1,394	1,440	1,401	1,416	1,442
	15	1,504	1,396	1,396	1,442	1,400	1,414	1,443
	30	1,506	1,398	1,400	1,443	1,403	1,418	1,443
	45	1,506	1,402	1,406	1,445	1,409	1,421	1,444
	60	1,508	1,406	1,412	1,447	1,409	1,422	1,446
	75	1,508	1,411	1,412	1,447	1,412	1,424	1,448
	90	1,503	1,413	1,409	1,449	1,416	1,426	1,448
	105	1,502	1,411	1,407	1,450	1,420	1,426	1,444
	120	1,501	1,408	1,406	1,451	1,418	1,425	1,442
	135	1,500	1,406	1,404	1,451	1,413	1,425	1,441
	150	1,502	1,404	1,398	1,447	1,409	1,423	1,440
	165	1,503	1,401	1,393	1,443	1,404	1,419	1,441
	180	1,503	1,397	1,393	1,441	1,401	1,416	1,441
	195	1,505	1,398	1,394	1,443	1,400	1,413	1,442
	210	1,505	1,400	1,399	1,444	1,404	1,418	1,444
	225	1,506	1,405	1,404	1,446	1,409	1,421	1,444
	240	1,508	1,412	1,409	1,448	1,409	1,422	1,447
	255	1,508	1,413	1,412	1,448	1,412	1,424	1,449
	270	1,503	1,414	1,408	1,448	1,417	1,426	1,450
	285	1,502	1,412	1,407	1,450	1,421	1,427	1,444
	300	1,502	1,410	1,406	1,449	1,418	1,426	1,441
	315	1,500	1,407	1,404	1,449	1,413	1,425	1,442
	330	1,502	1,405	1,399	1,447	1,410	1,424	1,442
	345	1,502	1,400	1,395	1,442	1,405	1,420	1,442
	360	1,503	1,396	1,394	1,440	1,401	1,416	1,442

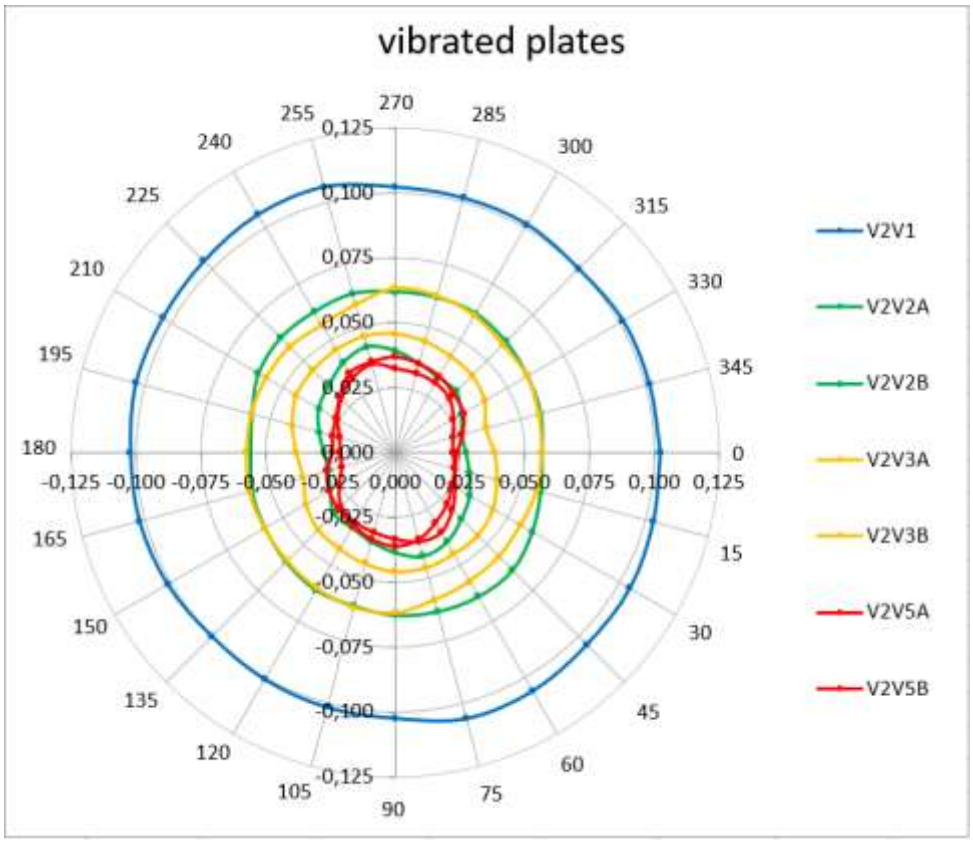

Appendix 4: Results other effects

Edge distance

Plate	V2B				V4B			
Probe	Single		C-shape		Single		C-shape	
d / angle	0	90	0	90	0	90	0	90
100	397,6	397,1	1,53	1,5	409	409,4	1,598	1,605
90	397,5	397	1,528	1,498	408,9	409,2	1,597	1,603
80	397,3	396,9	1,526	1,495	408,8	408,8	1,596	1,601
70	397	396,7	1,524	1,491	408,7	408,7	1,593	1,596
60	396,8	396,6	1,517	1,486	408,6	408,5	1,584	1,591
50	396,3	396,1	1,502	1,467	407,9	407,8	1,563	1,57
40	394,2	393,9	1,472	1,438	405	405,3	1,53	1,53

μR,mean	V2B		V4B	
	Single	C-shape	Single	C-shape
100	1,068	1,112	1,100	1,175
90	1,068	1,110	1,099	1,174
80	1,067	1,108	1,099	1,173
70	1,067	1,106	1,098	1,170
60	1,066	1,102	1,098	1,165
50	1,065	1,089	1,096	1,149
40	1,059	1,067	1,089	1,123

	V2B		V4B	
	Single	C-shape	Single	C-shape
kv	2,6082	4,1405	2,6082	4,1405

Vf	V2B		V4B	
	Single	C-shape	Single	C-shape
100	2,61%	2,69%	3,83%	4,23%
90	2,60%	2,66%	3,81%	4,20%
80	2,58%	2,61%	3,79%	4,17%
70	2,55%	2,56%	3,78%	4,10%
60	2,54%	2,45%	3,76%	3,98%
50	2,49%	2,15%	3,69%	3,61%
40	2,27%	1,63%	3,41%	2,96%

Vf / Vf,0	V2B		V4B	
	Single	C-shape	Single	C-shape
100	100,00%	100,00%	100,00%	100,00%
90	99,60%	98,68%	99,60%	99,37%
80	99,01%	97,04%	98,92%	98,74%
70	98,02%	95,07%	98,65%	97,06%
60	97,43%	91,12%	98,25%	94,13%
50	95,45%	79,93%	96,37%	85,32%
40	86,95%	60,53%	89,10%	70,02%

μR,mean / ΔL	V2B		V4B	
	Single	C-shape	Single	C-shape
100	0,00E+00	0,00E+00	0,00E+00	0,00E+00
90	1,34E-05	7,34E-05	2,02E-05	5,50E-05
80	2,02E-05	9,17E-05	3,36E-05	5,50E-05
70	3,36E-05	1,10E-04	1,34E-05	1,47E-04
60	2,02E-05	2,20E-04	2,02E-05	2,57E-04
50	6,72E-05	6,24E-04	9,41E-05	7,70E-04
40	2,89E-04	1,08E-03	3,63E-04	1,34E-03

White paint

Lair =	1,363		kv =	4,1405											
	WHITE PAINT					NO PAINT					DEV				
LUHPFRC		V1b_side1	V2a_side1	V3a_side1	V4a_side1	V1b_side2	V2a_side1	V3a_side1	V4a_side2		V1b_side1	V2a_side1	V3a_side1	V4a_side1	
	0	1,410	1,480	1,518	1,613	1,412	1,483	1,524	1,621		0,20%	0,30%	0,60%	0,80%	
	45	1,418	1,463	1,514	1,569	1,420	1,468	1,522	1,575		0,20%	0,50%	0,80%	0,60%	
	90	1,420	1,467	1,508	1,558	1,421	1,469	1,514	1,568		0,10%	0,20%	0,60%	1,00%	
	135	1,409	1,475	1,528	1,579	1,410	1,477	1,534	1,585		0,10%	0,20%	0,80%	0,60%	
	180	1,410	1,479	1,518	1,613	1,411	1,484	1,522	1,620		0,10%	0,50%	0,40%	0,70%	
	225	1,418	1,464	1,514	1,568	1,420	1,467	1,520	1,575		0,20%	0,30%	0,60%	0,70%	
	270	1,419	1,466	1,508	1,558	1,421	1,469	1,515	1,567		0,20%	0,30%	0,70%	0,90%	
	315	1,410	1,474	1,529	1,580	1,411	1,477	1,535	1,585		0,10%	0,30%	0,60%	0,50%	
	360	1,410	1,480	1,518	1,613	1,412	1,484	1,524	1,621		0,20%	0,40%	0,60%	0,80%	
										Av dev	0,16%	0,33%	0,61%	0,73%	
μR		V1b_side1	V2a_side1	V3a_side1	V4a_side2	V1b_side2	V2a_side2	V3a_side2	V4a_side2						
	0	1,034	1,086	1,113	1,183	1,036	1,088	1,118	1,189						
	45	1,040	1,073	1,111	1,151	1,042	1,077	1,116	1,155						
	90	1,042	1,076	1,106	1,143	1,042	1,078	1,111	1,150						
	135	1,033	1,082	1,121	1,158	1,034	1,083	1,125	1,163						
	180	1,034	1,085	1,113	1,183	1,035	1,089	1,116	1,188						
	225	1,040	1,074	1,111	1,150	1,042	1,076	1,115	1,155						
	270	1,041	1,075	1,106	1,143	1,042	1,078	1,111	1,149						
	315	1,034	1,081	1,122	1,159	1,035	1,083	1,126	1,163						
	360	1,034	1,086	1,113	1,183	1,036	1,089	1,118	1,189						
μR,mean		V1b_side1	V2a_side1	V3a_side1	V4a_side1	V1b_side2	V2a_side1	V3a_side1	V4a_side2						
	0 / 90	1,038	1,081	1,110	1,163	1,039	1,083	1,114	1,170						
	45 / 135	1,037	1,078	1,116	1,155	1,038	1,080	1,121	1,159						
	90 / 180	1,038	1,080	1,110	1,163	1,039	1,083	1,113	1,169						
	135 / 225	1,037	1,078	1,116	1,154	1,038	1,080	1,120	1,159						
	180 / 270	1,038	1,080	1,110	1,163	1,039	1,083	1,114	1,169						
	225 / 315	1,037	1,078	1,116	1,155	1,038	1,080	1,120	1,159						
	270 / 360	1,038	1,080	1,110	1,163	1,039	1,083	1,115	1,169						
	315 / 45	1,037	1,077	1,116	1,155	1,038	1,080	1,121	1,159						
	360 / 90	1,038	1,081	1,110	1,163	1,039	1,083	1,114	1,170						
											DEV				
Vf		V1b_side1	V2a_side1	V3a_side1	V4a_side1	V1b_side2	V2a_side1	V3a_side1	V4a_side2		V1b_side1	V2a_side1	V3a_side1	V4a_side1	
	0 / 90	0,92%	1,95%	2,65%	3,94%	0,94%	2,00%	2,76%	4,10%		0,03%	0,04%	0,11%	0,16%	
	45 / 135	0,89%	1,87%	2,79%	3,73%	0,92%	1,93%	2,92%	3,84%		0,03%	0,06%	0,12%	0,11%	
	90 / 180	0,92%	1,94%	2,65%	3,94%	0,93%	2,00%	2,74%	4,09%		0,02%	0,06%	0,09%	0,15%	
	135 / 225	0,89%	1,88%	2,79%	3,72%	0,92%	1,93%	2,90%	3,84%		0,03%	0,04%	0,11%	0,12%	
	180 / 270	0,91%	1,93%	2,65%	3,94%	0,93%	2,00%	2,75%	4,08%		0,03%	0,07%	0,10%	0,14%	
	225 / 315	0,90%	1,87%	2,80%	3,73%	0,92%	1,93%	2,91%	3,84%		0,03%	0,05%	0,11%	0,11%	
	270 / 360	0,91%	1,94%	2,65%	3,94%	0,94%	2,00%	2,77%	4,09%		0,04%	0,06%	0,12%	0,15%	
	315 / 45	0,90%	1,86%	2,80%	3,74%	0,92%	1,93%	2,93%	3,84%		0,03%	0,07%	0,12%	0,10%	
	360 / 90	0,92%	1,95%	2,65%	3,94%	0,94%	2,00%	2,76%	4,10%		0,03%	0,05%	0,11%	0,16%	
Av Vf		0,90%	1,91%	2,72%	3,85%	0,93%	1,97%	2,82%	3,98%	Av dev	0,03%	0,06%	0,11%	0,13%	

Surface roughness

L_{UHPFRC} [H]	H1b_rough	H1b_sanded	H1b_smooth	H3b_rough	H3b_sanded	H3b_smooth
0	1,391	1,392	1,421	1,456	1,457	1,496
45	1,388	1,388	1,423	1,462	1,462	1,506
90	1,390	1,390	1,420	1,455	1,455	1,499
135	1,390	1,392	1,419	1,455	1,457	1,493
180	1,391	1,391	1,421	1,457	1,457	1,497
225	1,388	1,389	1,423	1,458	1,459	1,506
270	1,389	1,390	1,420	1,452	1,454	1,497
315	1,391	1,391	1,420	1,455	1,457	1,494
360	1,391	1,392	1,421	1,457	1,457	1,497

L_{UHPFRC} [H]	H1b_rough	H1b_sanded	H1b_smooth	H3b_rough	H3b_sanded	H3b_smooth	H1b	H3b
0	1,391	1,392	1,421	1,456	1,457	1,497	3%	2%
45	1,388	1,388	1,419	1,462	1,462	1,493	0%	0%
90	1,390	1,390	1,420	1,455	1,455	1,499	0%	0%
135	1,390	1,392	1,423	1,455	1,457	1,506	6%	4%
180	1,391	1,391	1,421	1,457	1,457	1,496	0%	0%
225	1,388	1,389	1,420	1,458	1,459	1,494	3%	3%
270	1,389	1,390	1,420	1,452	1,454	1,497	3%	4%
315	1,391	1,391	1,423	1,455	1,457	1,506	0%	4%
360	1,391	1,392	1,421	1,457	1,457	1,497	3%	0%
							2,1%	1,9%

Appendix 5: Inductance results shear panels

Horizontal panel 1

Fiber distribution

Epoxy horizontal Panel 1	1,46%	50	150	250	350	450	550	650	750	850	950	1.050	1.150	1.250	1.350
100															
50		1,63%	1,75%	1,37%	1,60%	1,79%	1,51%	1,42%	1,74%	1,19%	1,27%	1,40%	1,19%	1,24%	1,38%
0		1,69%	1,29%	1,36%	1,49%	1,81%	1,45%	1,24%	1,25%	1,21%	1,43%	1,20%	1,40%	1,35%	1,64%
-50		1,54%	1,29%	1,39%	1,80%	1,80%	1,25%	1,91%	1,37%	1,46%	1,56%	1,41%	1,45%	1,46%	1,71%
-100															

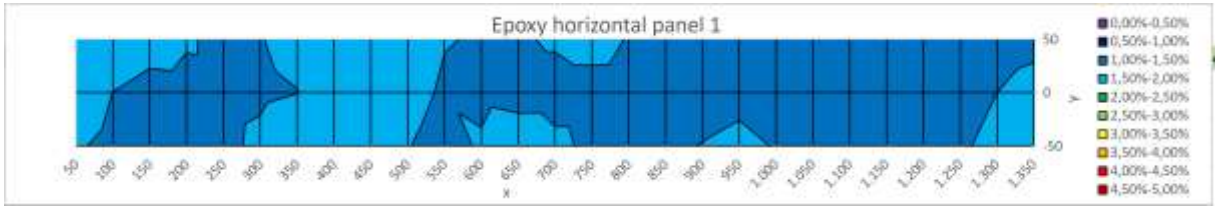

Epoxy horizontal Panel 1	-650	-550	-450	-350	-250	-150	-50	50	150	250	350	450	550	650		
50	1,63%	1,75%	1,37%	1,60%	1,79%	1,51%	1,42%	1,74%	1,19%	1,27%	1,40%	1,19%	1,24%	1,38%	1,46%	0,73
0	1,69%	1,29%	1,36%	1,49%	1,81%	1,45%	1,24%	1,25%	1,21%	1,43%	1,20%	1,40%	1,35%	1,64%	1,42%	0,00
-50	1,54%	1,29%	1,39%	1,80%	1,80%	1,25%	1,91%	1,37%	1,46%	1,56%	1,41%	1,45%	1,46%	1,71%	1,53%	-0,76
	1,62%	1,44%	1,37%	1,63%	1,80%	1,40%	1,52%	1,45%	1,29%	1,42%	1,34%	1,34%	1,35%	1,58%		-1,05
	-10,54	-7,93	-6,17	-5,70	-4,50	-2,10	-0,76	0,73	1,93	3,55	4,68	6,05	7,42	10,25	-1,70	1,70

Fiber orientation

Epoxy horizontal Panel 1							L_{UHPFRC} [H]
A	B	C	D	E	F	G	
1,483	1,461	1,477	1,474	1,465	1,463	1,476	
1,502	1,482	1,485	1,492	1,472	1,468	1,485	
1,48	1,5	1,491	1,486	1,481	1,47	1,488	
1,471	1,48	1,484	1,477	1,477	1,468	1,473	
1,485	1,46	1,478	1,475	1,468	1,462	1,476	
1,489	1,481	1,483	1,492	1,47	1,468	1,484	
1,484	1,498	1,491	1,487	1,483	1,47	1,483	
1,476	1,477	1,485	1,478	1,476	1,468	1,473	
1,484	1,46	1,476	1,474	1,466	1,463	1,475	

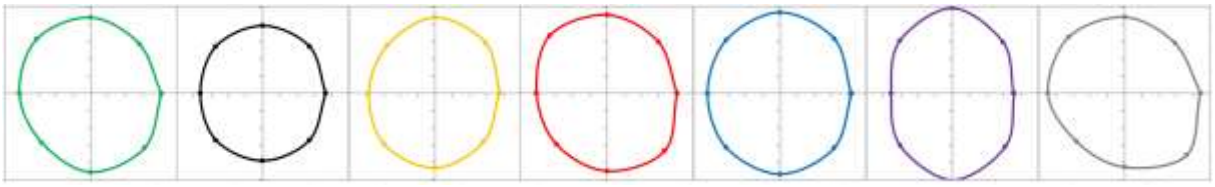

Horizontal panel 2

Fiber distribution

Epoxy horizontal Panel 2	1,51%	50	150	250	350	450	550	650	750	850	950	1.050	1.150	1.250	1.350
	100														
	50	1,60%	1,53%	1,72%	1,70%	1,67%	1,78%	1,45%	1,95%	1,91%	1,63%	1,10%	1,42%	1,72%	1,64%
	0	1,58%	1,69%	1,98%	1,62%	1,63%	1,51%	1,24%	1,20%	1,38%	1,21%	1,22%	1,28%	1,25%	1,42%
	-50	1,47%	1,49%	1,49%	1,50%	1,31%	1,41%	1,33%	1,25%	1,62%	1,28%	1,58%	1,62%	1,61%	1,36%
	-100														

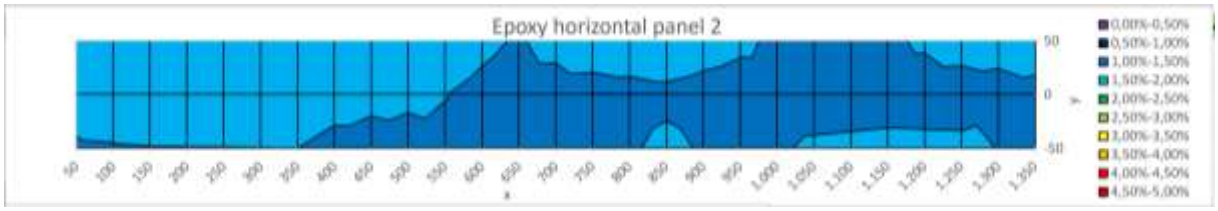

Epoxy horizontal Panel 2	-650	-550	-450	-350	-250	-150	-50	50	150	250	350	450	550	650		
50	1,60%	1,53%	1,72%	1,70%	1,67%	1,78%	1,45%	1,95%	1,91%	1,63%	1,10%	1,42%	1,72%	1,64%	1,63%	0,81
0	1,58%	1,69%	1,98%	1,62%	1,63%	1,51%	1,24%	1,20%	1,38%	1,21%	1,22%	1,28%	1,25%	1,42%	1,44%	0,00
-50	1,47%	1,49%	1,49%	1,50%	1,31%	1,41%	1,33%	1,25%	1,62%	1,28%	1,58%	1,62%	1,61%	1,36%	1,45%	-0,73
	1,55%	1,57%	1,73%	1,61%	1,54%	1,57%	1,34%	1,46%	1,63%	1,37%	1,30%	1,44%	1,53%	1,47%		2,94
	-10,07	-8,64	-7,77	-5,63	-3,84	-2,35	-0,67	0,73	2,45	3,43	4,54	6,48	8,40	9,57	-1,85	2,94

Fiber orientation

L_{UHPFRC} **[H]**

Epoxy horizontal Panel 2						
A	B	C	D	E	F	G
1,478	1,478	1,465	1,467	1,473	1,467	1,469
1,462	1,487	1,459	1,466	1,479	1,465	1,467
1,472	1,470	1,456	1,466	1,466	1,472	1,469
1,479	1,473	1,459	1,460	1,461	1,469	1,473
1,476	1,478	1,464	1,468	1,472	1,467	1,469
1,458	1,487	1,460	1,466	1,480	1,465	1,467
1,463	1,471	1,456	1,465	1,466	1,472	1,468
1,482	1,471	1,458	1,460	1,461	1,469	1,473
1,477	1,479	1,464	1,468	1,472	1,467	1,469

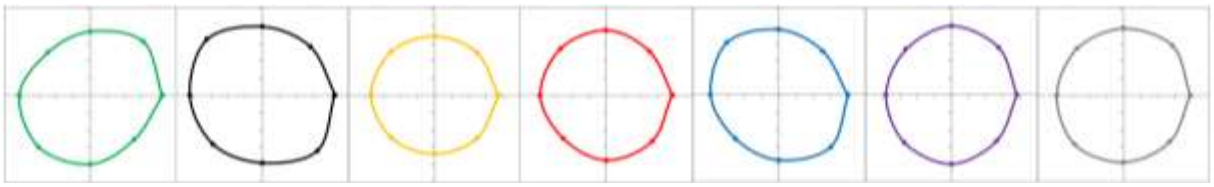

Vertical panel 1

Fiber distribution

Epoxy vertical Panel 1	1,53%	50	150	250	350	450	550	650	750	850	950	1050	1150	1250	1350
	100														
	50	0,36%	0,20%	0,23%	0,22%	0,16%	0,37%	0,19%	0,12%	0,22%	0,20%	0,18%	0,22%	0,19%	0,33%
	0	0,33%	0,20%	0,18%	0,73%	1,55%	1,18%	1,02%	0,68%	0,27%	0,26%	0,24%	0,19%	0,05%	0,19%
	-50	0,69%	2,58%	3,14%	4,68%	4,78%	5,37%	5,08%	3,97%	4,68%	4,06%	3,81%	4,16%	3,74%	3,20%
	-100														

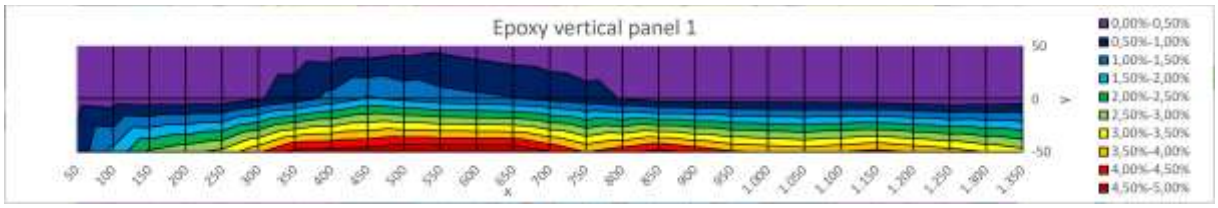

Epoxy vertical Panel 1	-650	-550	-450	-350	-250	-150	-50	50	150	250	350	450	550	650		
50	0,36%	0,20%	0,23%	0,22%	0,16%	0,37%	0,19%	0,12%	0,22%	0,20%	0,18%	0,22%	0,19%	0,33%	0,23%	0,11
0	0,33%	0,20%	0,18%	0,73%	1,55%	1,18%	1,02%	0,68%	0,27%	0,26%	0,24%	0,19%	0,05%	0,19%	0,51%	0,00
-50	0,69%	2,58%	3,14%	4,68%	4,78%	5,37%	5,08%	3,97%	4,68%	4,06%	3,81%	4,16%	3,74%	3,20%	3,85%	-1,93
	0,46%	1,00%	1,19%	1,88%	2,17%	2,31%	2,10%	1,59%	1,72%	1,51%	1,41%	1,52%	1,33%	1,24%		-60,37
	-2,99	-5,48	-5,34	-6,56	-5,41	-3,46	-1,05	0,80	2,58	3,77	4,93	6,86	7,30	8,07	2,21	60,37

Fiber orientation

Epoxy vertical Panel 1						L_{UHPFRC} [H]
A	B	C	D	E	F	G
1,372	1,384	1,444	1,483	1,495	1,376	1,369
1,386	1,405	1,463	1,492	1,489	1,395	1,385
1,399	1,419	1,465	1,489	1,474	1,424	1,418
1,381	1,406	1,456	1,478	1,488	1,405	1,39
1,371	1,385	1,444	1,483	1,493	1,378	1,37
1,385	1,404	1,463	1,492	1,49	1,396	1,387
1,399	1,419	1,465	1,49	1,474	1,425	1,418
1,38	1,408	1,454	1,478	1,489	1,406	1,391
1,372	1,384	1,444	1,483	1,495	1,376	1,369

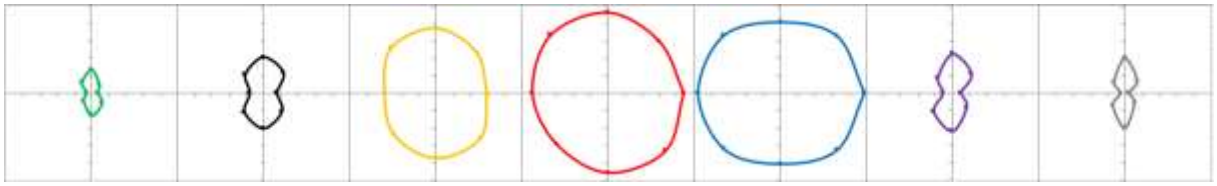

Vertical panel 2

Fiber distribution

Epoxy vertical Panel 2	1,83%	50	150	250	350	450	550	650	750	850	950	1.050	1.150	1.250	1.350
	100														
	50	0,28%	0,18%	0,21%	0,21%	0,19%	0,25%	0,35%	0,40%	0,38%	0,28%	0,24%	0,17%	0,33%	0,38%
	0	0,35%	0,16%	0,12%	0,26%	0,93%	1,65%	2,20%	2,49%	2,43%	1,93%	1,21%	0,11%	0,07%	0,31%
	-50	4,32%	3,66%	5,24%	4,97%	5,99%	4,77%	4,50%	5,52%	4,97%	5,40%	4,75%	2,90%	0,74%	1,01%
	-100														

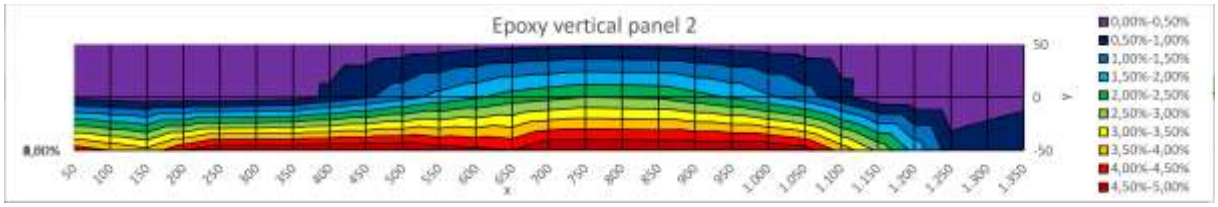

Epoxy vertical Panel 2	-650	-550	-450	-350	-250	-150	-50	50	150	250	350	450	550	650		
50	0,28%	0,18%	0,21%	0,21%	0,19%	0,25%	0,35%	0,40%	0,38%	0,28%	0,24%	0,17%	0,33%	0,38%	0,27%	0,14
0	0,35%	0,16%	0,12%	0,26%	0,93%	1,65%	2,20%	2,49%	2,43%	1,93%	1,21%	0,11%	0,07%	0,31%	1,02%	0,00
-50	4,32%	3,66%	5,24%	4,97%	5,99%	4,77%	4,50%	5,52%	4,97%	5,40%	4,75%	2,90%	0,74%	1,01%	4,20%	-2,10
	1,65%	1,33%	1,86%	1,81%	2,37%	2,22%	2,35%	2,80%	2,59%	2,54%	2,07%	1,06%	0,38%	0,57%		-65,35
	-10,73	-7,33	-8,35	-6,35	-5,92	-3,34	-1,17	1,40	3,88	6,34	7,24	4,77	2,09	3,68	-7,58	65,35

Fiber orientation

L_{UHPFRC} **[H]**

Epoxy vertical Panel 2						
A	B	C	D	E	F	G
1,378	1,38	1,441	1,406	1,38	1,381	1,371
1,406	1,402	1,447	1,419	1,413	1,411	1,377
1,44	1,443	1,463	1,444	1,428	1,422	1,396
1,403	1,404	1,442	1,434	1,415	1,386	1,383
1,379	1,381	1,442	1,407	1,379	1,382	1,371
1,405	1,402	1,448	1,421	1,413	1,41	1,377
1,441	1,443	1,464	1,444	1,429	1,421	1,395
1,402	1,403	1,442	1,434	1,416	1,386	1,383
1,378	1,38	1,441	1,406	1,38	1,381	1,371

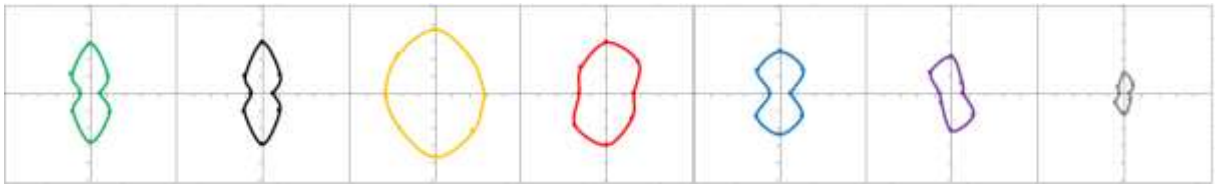

Appendix 6: CT-scan

CT scans of full plates

H1A

H1B

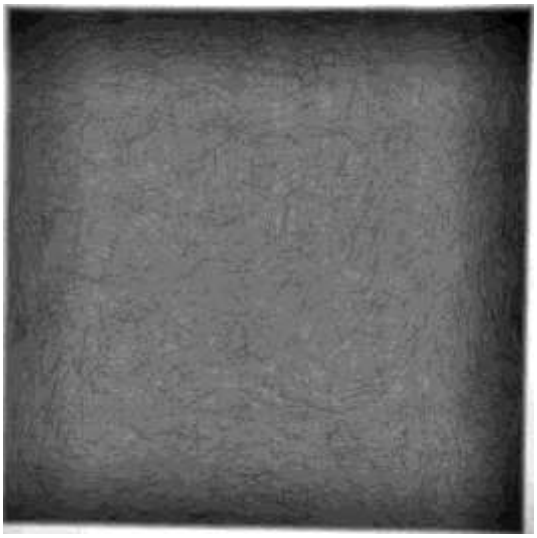

V1A

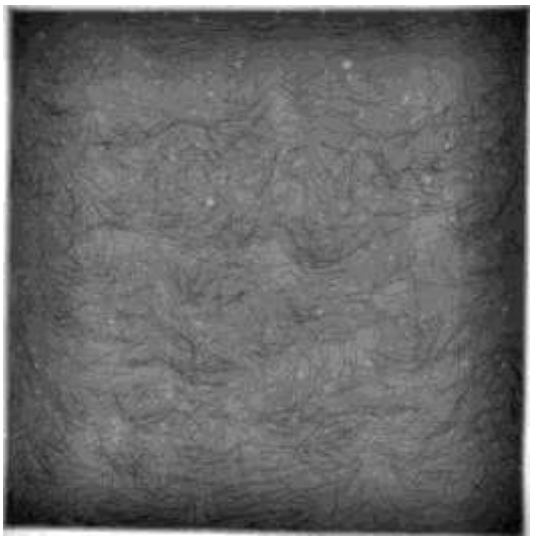

H2A2

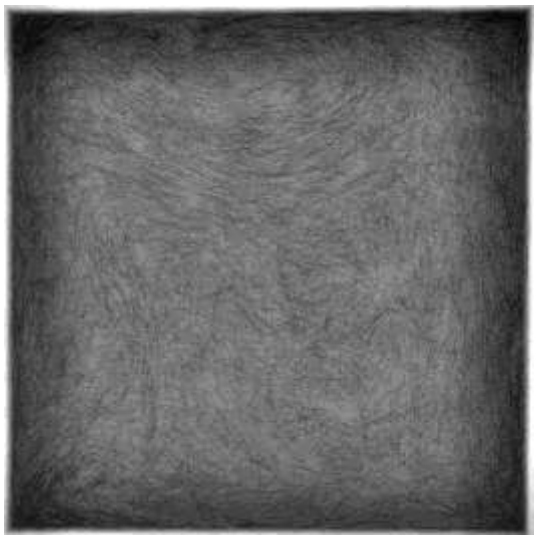

H2B2

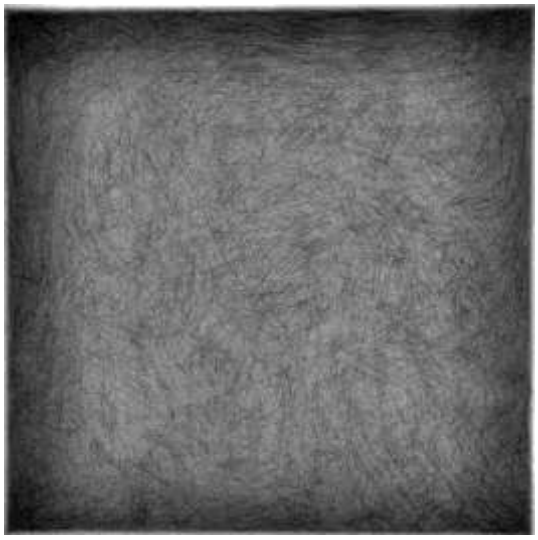

V2A2

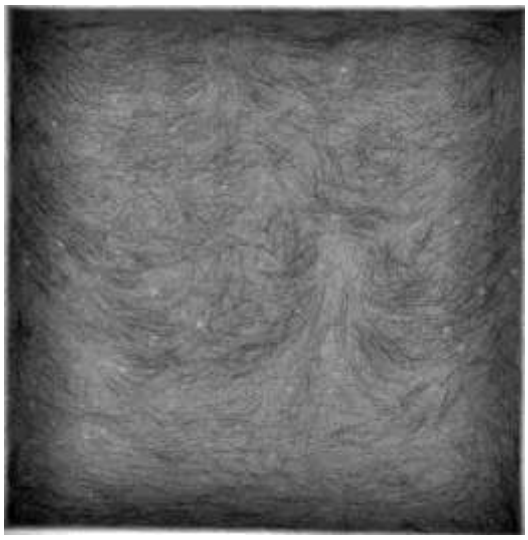

V2B2

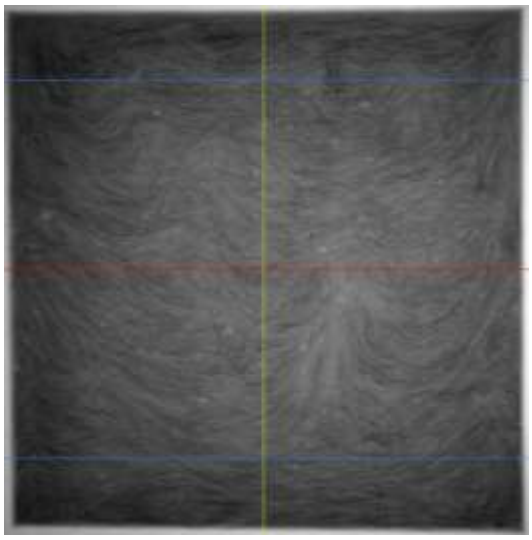

H3A

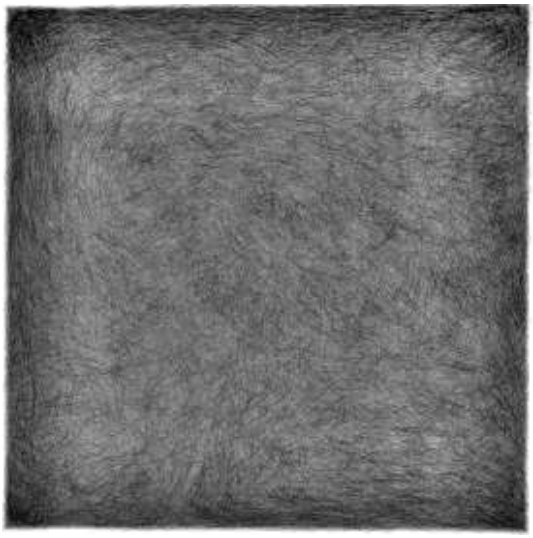

V3B

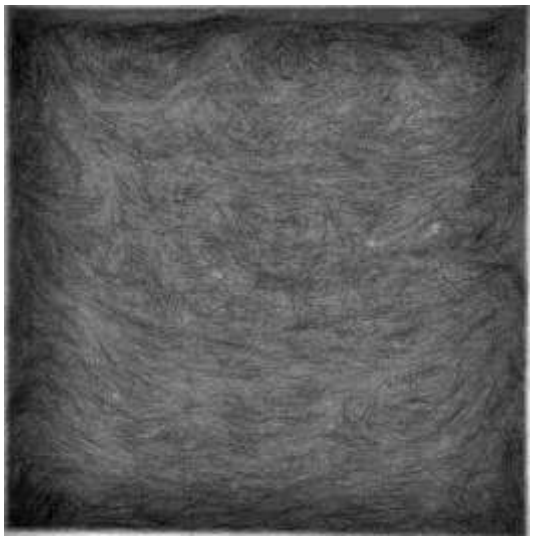

V2V5A

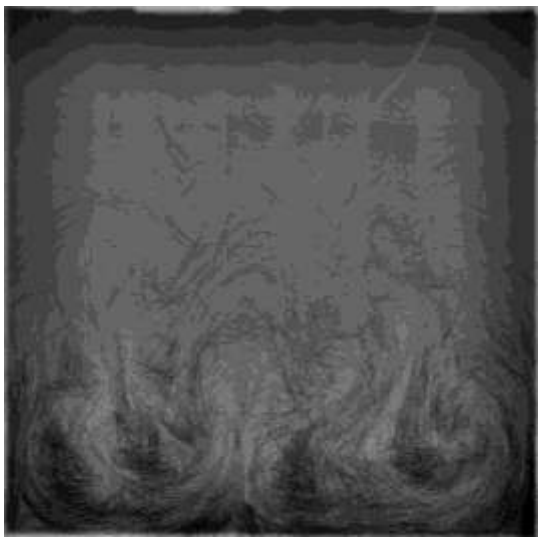

Data all plates

H1A	No. of particles	Total Area	Average Size	%Area
top	12945	585888	45,3	33,2%
center	11566	600145	51,9	30,9%
bottom	11483	495382	43,1	28,6%
H1B				
top	11678	535588	45,9	32,8%
center	14523	599252	41,3	31,5%
bottom	11904	527229	44,3	33,6%
V1A				
top	1365	398888	292,2	26,6%
center	2053	563356	274,4	32,0%
bottom	1945	509143	261,8	31,5%
H2A2				
top	7335	841495	115	49,6%
center	13936	836265	60,0	41,0%
bottom	9599	634693	66,1	38,5%
H2B2				
top	9021	704906	78,1	42,8%
center	10629	850796	80,0	41,7%
bottom	10359	696219	67,2	40,2%
V2A2				
top	10121	637578	63,0	36,4%
center	11582	724082	62,5	37,1%
bottom	10972	514592	46,9	31,4%
V2B2				
top	8455	683834	81	40,9%
center	11127	842137	76	41,3%
bottom	7884	713222	90,5	42,1%
H3A				
top	7644	887280	116	51,4%
center	8200	939167	115	46,1%
bottom	6407	786843	123	47,0%
V3B				
top	5776	818468	142	50,1%
center	8191	994982	121	48,8%
bottom	7890	763953	97	45,7%
V2V5A				
top	6098	20160	3,3	1,5%
center	13327	284724	21,4	15,1%
bottom	19481	1185150	60,8	61,0%

CT scan processing

1) Plate H3A CT scan

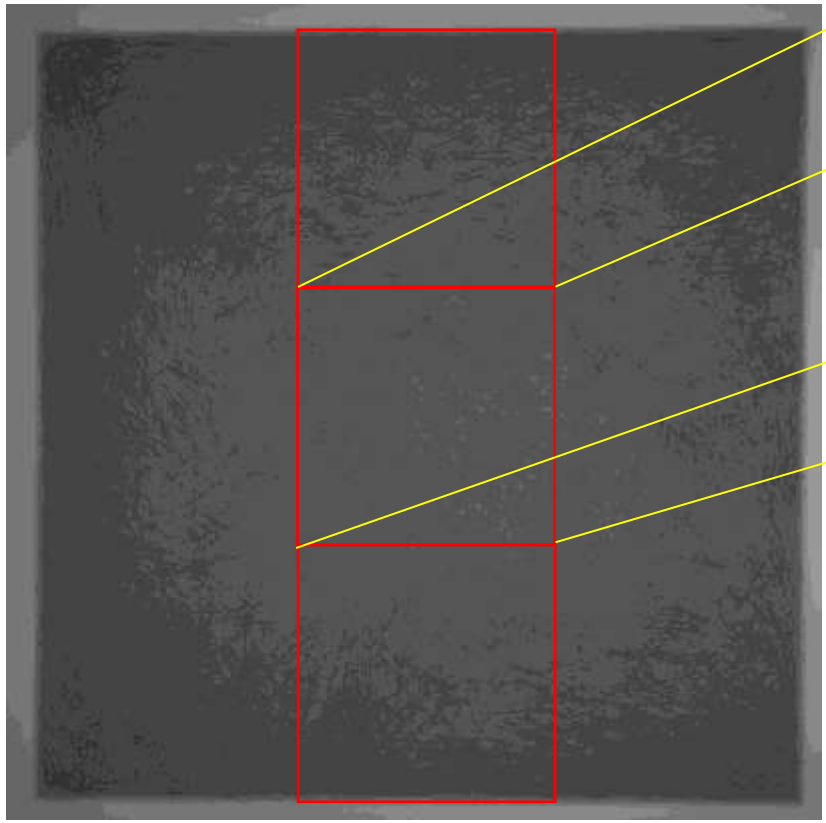

2) Individual scans center top, center middle and center bottom for better quality

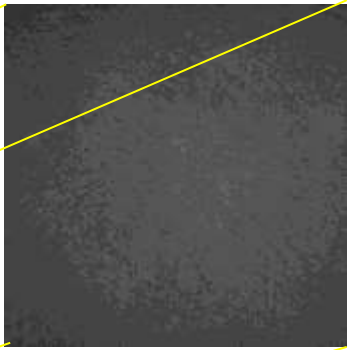

3) Using vignetting filter in Mathlab in order to have a more homogeneous hue / less shading (see next page)

4) Using ImageJ tool to enhance contrast, brightness and sharpness

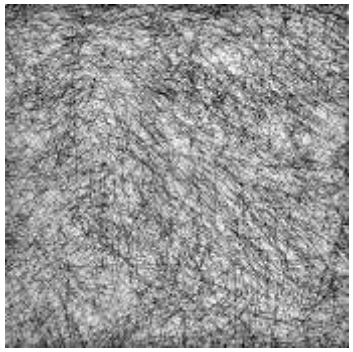

5) Using ImageJ tool to distinguish fiber from matrix using greyscale treshold

6) Using ImageJ tool to analyse particles and calculate the area percentage of fibers

Vignetting code Mathlab

```
clc;
close all;
clear all;
%Assigning standard deviation value of Guassian kernel
sigma=120;
%reading input images
A1=imread("H1-zt.tif");
A2=imread("H1-zm.tif");
A3=imread("H1-zb.tif");
%output(images which are free of vignette effect) of input images
output1=guassianfilt(A1,sigma);
output2=guassianfilt(A2,sigma);
output3=guassianfilt(A3,sigma);
%figure of input and output images
figure
subplot(3,1,1)
imshowpair(A1,output1,"montage")
title("Input image(left) and Output image(right) with sigma=120")
subplot(3,1,2)
imshowpair(A2,output2,"montage")
title("Input image(left) and Output image(right) with sigma=120")
subplot(3,1,3)
imshowpair(A3,output3,"montage")
title("Input image(left) and Output image(right) with sigma=120")

% Save processed images to files
imwrite(output1, 'outputtop_processed.tif');
imwrite(output2, 'outputcenter_processed.tif');
imwrite(output3, 'outputbottom_processed.tif');

%Applying Guassian Filter to remove the effect of vignette in images
function output=guassianfilt(A,sigma)
% non-double images are converted to single
A=im2single(A);
% Symmetric image padding is used over here
blurredimg = imgaussfilt(A,sigma,'padding','symmetric','filtersize',2*ceil(2*sigma)+1);
output=A*mean(A(:),'omitnan')./blurredimg; % mean of A, not of blurred image
output=im2uint8(output);
end
```

References

Abrishambaf, A., Pimentel, M., & Nunes, S. (2017). *Influence of fibre orientation on the tensile behaviour of ultra-high performance fibre reinforced cementitious composites.* Porto, Portugal: Elsevier Ltd.

Abrishambaf, A., Pimentel, M., & Nunes, S. (2019). *A meso-mechanical model to simulate the tensile behaviour of ultra-high performance fibre-reinforced cementitious composites.* Porto, Portugal: Elsevier Ltd.

Acker, P., & Behloul, M. (2004). *Ductal® Technology: A Large Spectrum of Properties, A Wide Range of Applications.* Paris, France: Kassel University.

AFNOR. (2016). *National addition to Eurocode 2 — Design of concrete structures: specific rules for Ultra-High Performance Fibre-Reinforced Concrete (UHPFRC).* La Plaine Saint-Denis Cedex, France: AFNOR - French standard institute.

Ahlborn, T., & Kollmorgen, G. (2004). *Impact of Age and Size on the Mechanical Behavior of Ductal®.* Houghton, USA: Michigan Technological University.

Akeed, M., Qaidi, S., Ahmed, H., Emad, W., Faraj, R., Mohammed, A., . . . Azevedo, A. (2022). *Ultra-high-performance fiber-reinforced concrete. Part 3: Fresh and hardened properties.* Kurdistan, Iraq: Elsevier Ltd.

Akhnoukh, A., & Buckhalter, C. (2021). *Ultra-high-performance concrete: Constituents, mechanical properties, applications and current challenges.* Greenville, USA: Elsevier Ltd.

Alsomiri, M., Jiang, X., & Liu, Z. (2021). *Elastic Restraint Effect of Concrete Circular Columns with Ultrahigh-Performance Concrete Jackets: An Analytical and Experimental Study.* Nanjing: MDPI.

Amoorezaei, K., & Dabbagh, H. (2022). *Flexural Toughness of Steel Fiber Reinforced Lightweight Aggregate Concrete.* Isfahan, Iran: ResearchGate.

Amran, M., Huang, S., Onaizi, A., Makul, N., Abdelgader, H., & Ozbakkaloglu, T. (2022). *Recent trends in ultra-high performance concrete (UHPC): Current status, challenges and future prospects.* Constr. Build. Mater.

Arafa, M., Shihada, S., & Karmout, M. (2010). *Mechanical Properties of Ultra High Performance Concrete Produced in the Gaza Strip.* Gaza, Palestine: Knowledgia Review.

Aziz, O., & Ahmed, G. (2012). *Mechanical Properties of Ultra High Performance Concrete (UHPC).* Prague, Czech Republic: ResearchGate.

Barbos, A. (2015). *Long-term Behavior of Ultra – High Performance Concrete (UHPC) Bended Beams.* Cluj-Napoca, Romania: Elsevier Ltd.

Barnett, S., Lataste, J.-F., Parry, T., Millard, S., & Soutsos, M. (2009). *Assessment of fibre orientation in ultra high performance fibre reinforced concrete and its effect on flexural strength.* RILEM.

Berendsen, P. (2014). *Application of UHPFRC in the building engineering.* Delft: Technische Universiteit Delft.

Bertola, N., Schiltz, P., Denarié, E., & Brühwiler, E. (2021). *A Review of the Use of UHPFRC in Bridge Rehabilitation and New Construction in Switzerland.* Lausanne, Switzerland: Frontiers in Built Environment.

Betonhuis. (n.d.). *balkon- en galerijplaten, loggia's.* Betonhuis.

Bhandari, S., & Babar, N. (2018). *Abnormal Activity Recognition Using Saliency and Spatio-Temporal Interest Point Detector: Second International Conference, ICSCS 2018, Kollam, India, April 19-20, 2018, Revised Selected Papers.* Kollam, India: ResearchGate.

Boulekbache, B., Hamrat, M., Chemrouk, M., & Amziane, S. (2010). *Flowability of fibre-reinforced concrete and its effect on the mechanical properties of the material.* Bretagne, France: Elsevier Ltd.

Brühwiler, E. (2017, December 14). Accelerated Bridge Strengthening using UHPFRC. Lausanne, Switzerland.

Brühwiler, E. (2022). *UHPFRC is ready to revolutionize existing and new structures.* Lussy-sur-Morges, Switzerland: IABSE Symposium Prague 2022.

Brühwiler, E., Bastien-Masse, M., Mühlberg, H., Houriet, B., Fleury, B., Cuennet, S., . . . Maurer, M. (2015). *Strengthening the Chillon viaducts deck slabs with reinforced UHPFRC.* Lausanne, Switzerland: ResearchGate.

Buitelaar, P. (2018). *35 years of HPC and UHPC toppings for industrial floors.* ResearchGate.

Cao, W.-J. (2021, March). *Getting it straight: bridges are becoming circular*. Retrieved from tudelft.nl: https://www.tudelft.nl/en/ceg/research/stories-of-science/getting-it-straight-bridges-are-becoming-circular

Cement. (2010, October 27). *Eerste betonnen sluisdeuren ter wereld*. Retrieved from Cement: https://www.cementonline.nl/eerste-betonnen-sluisdeuren-ter-wereld

Cement. (2013). *Ontwerp sluisdeur in vvUHSB.* Cement.

Chu, S., Jiang, Y., & Kwan, A. (2019). *Effect of rigid fibres on aggregate packing.* Hong Kong, China: ResearchGate.

Denarié, E. (2005). *Full Scale Application of UHPFRC for the Rehabilitation of Bridges - from the lab to the field.* Brussels, Belgium: Samaris.

Du, J., Meng, W., Khayat, K., Bao, Y., Guo, P., Lyu, Z., . . . Wang, H. (2021). *New development of ultra-high-performance concrete (UHPC).* Hoboken, USA: Elsevier Ltd.

EPFL. (2023). *UHPFRC Map Switzerland*. Retrieved from epfl.ch: https://www.epfl.ch/labs/mcs/mcs-laboratory-for-maintenance-and-safety-of-structures/uhpfrc-map-switzerland/

EPFL-Swiss Federal Institute of Technology. (2016). *Recommendation: Ultra-High Performance Fibre Reinfroced Cement-based composites (UHPFRC): Construction material, dimensioning and application.* Lausanne: EPFL-Swiss Federal Institute of Technology.

Faifer, M., Ottoboni, R., Toscani, S., & Ferrara, L. (2010). *Nondestructive Testing of Steel-Fiber-Reinforced Concrete Using a Magnetic Approach.* Milan, Italy: IEEE.

Garas, V., Kahn, L., & Kurtis, K. (2009). *Short-term tensile creep and shrinkage of ultra-high performance concrete.* Atlanta, USA: Elsevier Ltd.

Garner, A. (2011). *Strengthening reinforced concrete slabs using a combination of CFRP and UHPC.* Albuquerque, New Mexico: University of Mexico.

Graybeal, B. (2017). Emerging UHPC-based bridge construction and preservation solutions. *International Symposium on Ultra-High Performance Fibre-Reinforced Concrete* (pp. 2-4). Montpellier, France: International Symposium on Ultra-High Performance Fibre-Reinforced Concrete.

Guo, Y.-Q., Wang, J.-Y., & Gu, J.-B. (2022). *Nonlinear Inverse Analysis for Predicting the Tensile Properties of Strain-Softening and Strain-Hardening UHPFRC.* Basel, Switzerland: MDPI.

GWW. (2019, Oktober 22). *Hoe ultrahogesterktebeton constructieve problemen kan oplossen*. Retrieved from gww-bouw.nl: https://www.gww-bouw.nl/artikel/hoe-ultrahogesterktebeton-constructieve-problemen-kan-oplossen/

Hi-Con. (2023, Januari). *Ultra high performance concrete: our work*. Retrieved from Hi-Con.com: https://www.hi-con.com/cases/?filterValues=The%20Netherlands

Huang, Y., & Luković, M. (2022). *Effect of freeze-thaw cycles on shear resistance of reinforced concrete beams strengthened with UHPFRC.* Delft: ResearchGate.

Huang, Y., Grünewald, S., Schlangen, E., & Luković, M. (2022). *Strengthening of concrete structures with ultra high performance fiber reinforced concrete (UHPFRC): A critical review.* Delft: Elsevier Ltd.

Huang, Y., Schlangen, E., & Lukovic, M. (2023). *Strengthening of Reinforced Concrete Beams with Ultra-High Performance Fiber-Reinforced Concrete in Shear.* Delft: Delft University of Technology.

ImageJ. (2024, January). *ImageJ*. Retrieved from imagej.net: https://imagej.net/ij/

Islam, M., Zhang, Q., & Jin, Q. (2022). *A review of existing codes and standards on design factors for UHPC placement and fiber orientation.* Tallahassee, USA: Elsevier Ltd.

Jiao, C., Ta, J., Niu, Y., Meng, S., Chen, X.-F., He, S., & Ma, R. (2022). *Analysis of the flexural properties of ultra-high-performance concrete consisting of hybrid straight steel fibers.* Guangzhou, China: Elsevier Ltd.

Kang, S.-T., & Kim, J.-K. (2011). *Investigation on the flexural behavior of UHPCC considering the effect of fiber orientation distribution.* Gyeongbuk, South Korea: Elsevier Ltd.

Kennedy, D., Habel, K., & Fraser, G. (2015). Ultra High-Performance Concrete Column Jacket Retrofit for the Mission Bridge. *11th Canadian Conference on Earthquake Engineering.* Victoria, Canada: 11th Canadian Conference on Earthquake Engineering.

Kloft, Ledderose, L., & Stümmler, A. (2021). *Magnetic alignment of steel fibers*. Retrieved from TU Braunschweig: https://www.tu-braunschweig.de/ite/research/magnetic-alignment-of-steel-fibres

Kusumawardaningsih, Y., Fehling, E., & Ismail, M. (2015). *UHPC compressive strength test specimens: Cylinder or cube?* Kassel, Germany: ScienceDirect.

Lataste, J., Behloul, M., & Breysse, D. (2008). *Characterisation of fibres distribution in a steel fibre reinforced concrete with electrical resistivity measurements.* Paris, France: Elsevier Ltd.

Li, J., Wu, Z., Shi, C., Yuan, Q., & Zhang, Z. (2020). *Durability of ultra-high performance concrete – A review.* Changsha, China: Elsevier Ltd.

Li, L., Xia, J., & Galobardes, I. (2018). *Magnetic Probe to Test Spatial Distribution of Steel fibres in UHPFRC Prisms.* Melbourne, Australia: ResearchGate.

Li, L., Xia, J., Chin, C., & Jones, S. (2020). *Fibre Distribution Characterization of Ultra-High Performance Fibre-Reinforced Concrete (UHPFRC) Plates Using Magnetic Probes.* Suzhou, China: MDPI.

Liu, C.-T., & Huang, J.-S. (2008). *Fire performance of highly flowable reactive powder concrete.* Tainan, Taiwan: Elsevier Ltd.

Memon, I., Jhatial, A., Sohu, S., Lakhiar, M., & Hussain, Z. (2018). *Influence of Fibre Length on the Behaviour of Polypropylene Fibre Reinforced Cement Concrete.* Johor, Malaysia: ResearchGate.

Mokhberdoran, P. (2020). *An Assessment of Key Factor for Implementing Magnetic NDT Method on UHPFRC Structures.* Porto, Portugal: University of Porto.

Moreillon, L., & Menétrey, P. (2013). *Rehabilitation and strengthening of existing RC structures with UHPFRC: various applications.* Marseille, France: RILEM-fib-AFGC.

Mu, R., Li, H., Qing, L., Lin, J., & Zhao, Q. (2016). *Aligning steel fibers in cement mortar using electro-magnetic field.* Tianjin, China: Elsevier Ltd.

Naaman, A., & Wille, K. (2012). The Path to Ultra-High Performance Fiber Reinforced Concrete (UHP-FRC): Five Decades of Progress. *Proceedings of HiperMat 2012*, (pp. 3-15). Kassel, Germany.

NEN. (2020, February 5). *NEN-EN 1992-1-1+C2:2011/NB:2016+A1:2020.* Retrieved from nen.nl: https://www.nen.nl/nen-en-1992-1-1-c2-2011-nb-2016-a1-2020-nl-267151

Nunes, S. (2017, March 20). Presentation UHPFRC. Leuven, Belgium: KU Leuven.

Nunes, S., Pimentel, M., & Carvalho, A. (2016). *Non-destructive assessment of fibre content and orientation in UHPFRC layers based on a magnetic method.* Porto, Portugal: Elsevier Ltd.

Nunes, S., Pimentel, M., Ribeiro, F., Milheiro-Oliveira, P., & Carvalho, A. (2017). *Estimation of the tensile strength of UHPFRC layers based on non-destructive assessment of the fibre content and orientation.* Porto, Portugal: Elsevier Ltd.

Nunes, S., Pimentel, M., Sine, A., & Mokhberdoran, P. (2021). *Key Factors for Implementing Magnetic NDT Method on Thin UHPFRC Bridge Elements.* Basel: MDPI.

Reitsema, A. (2012). *Ontwerpen van een vvUHSB sluisdeur m.b.v. optimalisatie algoritmen.* Eindhoven: Technische Universiteit Eindhoven.

Riciotti, R., Pastor, F., Hajar, Z., & Bernardi, S. (2017). *La Republique Bridge in Montpellier.* Montpellier: AFGC-ACI-fib-RILEM Int.

Rijkswaterstaat. (2023, January). *Vernieuwen van bruggen, tunnels, sluizen en viaducten*. Retrieved from Rijkswaterstaat: https://www.rijkswaterstaat.nl/over-ons/onze-organisatie/vervanging-en-renovatie

Ruan, T., & Poursaee, A. (2019). *Fiber-Distribution Assessment in Steel Fiber-Reinforced UHPC Using Conventional Imaging, X-Ray CT Scan, and Concrete Electrical Conductivity.* Clemson, USA: American Society of Civil Engineers.

Sawicki, B., Brühwiler, E., & Denarié, E. (2022). *Inverse Analysis of R-UHPFRC Beams to Determine the Flexural Response under Service Loading and at Ultimate Resistance.* ASCE.

Schlangen, E. (2021, December 2). Properties of Hardened Concrete Fiber Reinforced Concrete High Strength Concrete. Delft, Zuid-Holland, Nederland.

Schmidt, M., Fehling, E., Glotzbach, C., Fröhlich, S., & Piotrowski, S. (2012). *Ultra-High Performance Concrete and Nanotechnology in Construction.* Kassel: Hipermat.

Sedran, T., Durand, C., & de Larrard, F. (2009). *An example of UHPFRC recycling.* Marseille, France: AFGC.

Shen, X., & Brühwiler, E. (2020). *Influence of local fiber distribution on tensile behavior of strain hardening UHPFRC using NDT and DIC.* Lausanne, Switzerland: Elsevier Ltd.

Sine, A. (2021). *Strengthening of reinforced concrete elements with UHPFRC.* Porto: University of Porto.

Sine, A., Pimentel, M., Nunes, S., & Mokhberdoran, P. (2020). *Non-destructive evaluation of the fiber content and anisometry in thin UHPFRC elements.* Porto, Portugal: ResearchGate.

South Dakota Department of Transportation. (n.d.). *Bridge Rehabilitation.* Retrieved from dot.sd.gov: https://dot.sd.gov/media/documents/Chapter16BridgeRehab.pdf

Spasojevic, A., Redaelli, D., & Muttoni, A. (2009). *Thin UHPFRC slabs without conventional reinforcement as light-weight structural elements.* Genève: ResearchGate.

Tayeh, B., Aadi, A., Hilal, N., & Bakar, B. (2019). *Properties of Ultra-High-Performance Fiber-Reinforced Concrete (UHPFRC) - A Review Paper.* ResearchGate.

Torrents, J., Juan-García, P., Patau, O., & Aguado, A. (2009). *Surveillance of steel fibre reinforced concrete slabs measured with an open-ended coaxial probe.* Barcelona, Spain: XIX IMEKO World Congress.

Tosec. (2023). *Plaatgewicht berekenen*. Retrieved from Tosec: https://tosec.nl/nl/wiki/gewicht-berekenen-van-metaalplaat/#:~:text=Staal%20%2D%207.850%20kg%2Fm%C2%B3

Toutlemonde, F., & Resplendino, J. (2014). *The UHPFRC revolution in structural design and construction.* Marseille, France: ResearchGate.

Toutlemonde, F., Bernardi, S., Brugeaud, Y., & Simon, A. (2004). *Twenty years-long French experience in UHPFRC application and paths opened from the completion of the standards for UHPFRC.* France.

Tran, D., Shen, X., Sorelli, L., Ftima, M., & Brühwiler, E. (2023). *Predicting the effect of non-uniform fiber distribution on the tensile response of ultra-high-performance fiber reinforced concrete by magnetic inductance-based finite element analysis.* Montreal, Canada: Elsevier Ltd.

TU Delft CIE4100. (2020). *Case study Portfolio task 1: ECI calculation Prefab concrete bridge deck.* Delft: TU Delft CIE4100.

U.S. Department of Transportation. (2013, June). *Ultra-High Performance Concrete: A State-Of-The-Art Report for The Bridge Community*. Retrieved from Federal Highway Administration: https://www.fhwa.dot.gov/publications/research/infrastructure/structures/hpc/13060/index.cfm

U.S. Department of Transportation. (2014, Oktober). *Design and Construction of Field-Cast UHPC Connections*. Retrieved from Federal Highway Administration: https://www.fhwa.dot.gov/publications/research/infrastructure/structures/14084/index.cfm

Uchida, Y., Niwa, J., Yoshihiro, T., & Katagiri, M. (2005). *Outlines of JSCE "Recommendations for Design and Construction of Ultra High Strength Fiber Reinforced Concrete Structures (Draft)".* Tokyo, Japan: ResearchGate.

Vastmans Frank betonvloeren. (2019, November 16). *Wat is het verschil tussen staalvezel en wapeningsnetten?* Retrieved from vastmansfrank.com: https://www.vastmansfrank.com/2019/11/verschil-staalvezel-wapeningsnetten.html#:~:text=Bij%20staalvezel%20zijn%20de%20stukjes,en%20kunnen%20het%20nascheuren%20opvangen.

Vergoossen, R. (1999). *Ontwerp van een ophaalbrug in (zeer) hoge strekte beton, voor verkeersklasse 600.* Delft: Bouwdienst Rijkswaterstaat / TU Delft.

Wu, C., Oehlers, D., Rebentrost, M., & Whittaker, A. (2009). *Blast testing of ultra-high performance fibre and FRP-retrofitted concrete slabs.* Adelaide, Australia: Elsevier Ltd.

Yang, H., Joh, C., & Kim, B.-S. (2010). *Structural behavior of ultra high performance concrete beams subjected to bending.* South Korea: Elsevier Ltd.

Yazici, S., Inan, G., & Tabak, V. (2006). *Effect of aspect ratio and volume fraction of steel fiber on the mechanical properties of SFRC.* Izmir, Turkey: Elsevier Ltd.

Yoo, D.-Y., Kang, S.-T., & Yoon, Y.-S. (2014). *Effect of fiber length and placement method on flexural behavior, tension-softening curve, and fiber distribution characteristics of UHPFRC.* Republic of Korea: Elsevier Ltd.

Yu, R. (2015). *Development of sustainable protective ultra-high performance fibre reinforced concrete (UHPFRC) : design, assessment and modeling.* Eindhoven: Technische Universiteit Eindhoven.

Yu, R., Spiesz, P., & Brouwers, H. (2014). *Static properties and impact resistance of a green Ultra-High Performance Hybrid Fibre Reinforced Concrete (UHPHFRC): Experiments and modeling.* Eindhoven, the Netherlands: Elsevier Ltd.

Zheng, Y., Zhou, Y., Nie, F., Luo, H., & Huang, X. (2022). *Effect of a Novel Vibration Mixing on the Fiber Distribution and Mechanical Properties of Ultra-High Performance Concrete.* Nanjing, China: MDPI.